Fall 12-15-2017

In-Vitro and In-Vivo Models of Bile Acid Metabolism and Transport

Rhishikesh Thakare
University of Nebraska Medical Center

IN-VITRO AND IN-VIVO MODELS OF BILE ACID METABOLISM AND TRANSPORT

By

Rhishikesh Thakare

A DISSERTATION

Presented to the Faculty of

The Graduate College in the University of Nebraska

In Partial Fulfillment of the Requirements

For the Degree of Doctor of Philosophy

Department of Pharmaceutical Sciences

Under the Supervision of Professor Yazen Alnouti

University of Nebraska Medical Center

Omaha, Nebraska

September, 2017

ACKNOWLEDGEMENTS

I would like to express my sincere gratitude to many people who have been continuously supporting and encouraging me throughout my graduate studies. First and foremost, I am deeply indebted to my mentor Dr. Yazen Alnouti for providing me the opportunity to work in his lab. Dr. Alnouti has been very instrumental in my research career. He has been a great influence in my personal and professional life and has educated me on numerous qualities that are required for becoming a good scientist. I would specially thank him for allowing me to gain hands-on experience in an industrial setting through a summer internship at Pfizer Inc, Groton.

I would like to thank my committee members Dr. Rakesh Singh, Dr. Jonathan Vennerstrom, Dr. Jered Garrison for their valuable inputs, suggestions, and guidance during my training here at UNMC. I am indebted to Dr. Nagsen Gautam for nurturing my research skills and for all the suggestions and inputs during my studies. I thank the UNMC Graduate studies office and Pharmaceutical Sciences department for providing me the financial support for my graduate studies.

I will cherish all the wonderful moments that I had with my friends over the last five years. I would like to especially thank my friends Prathamesh, Shrey, Pravin, Aniruddha, Shrabasti, Aditya, Rohan, Sugandha, and Kruti for all their constant support and encouragement throughout my Ph.D. program. I also thank all my friends from Omaha Cricket Club and the rest of my friends in Omaha for the wonderful company during the last five years. I would like to thank our department secretaries Elaine, Jamie, Michelle, and Katina for all the administrative help during my studies here at UNMC.

Finally, I would like to thank my family including my dad- Mr. Narayan Thakare, my mom- Mrs. Jyoti Thakare, my brother- Abhishek, and my sister Mrs. Suverna for their love, prayers, support and encouragement throughout the years. I would like to thank my wife- Mrs. Rashmi for her support and commitment towards my success in graduate

school. Finally, I appreciate all the teachers and friends from my school who played a significant role all in my life.

IN-VITRO AND IN-VIVO MODELS OF BILE ACID METABOLISM AND TRANSPORT

Rhishikesh Thakare

University of Nebraska Medical Center, 2017

Supervisor: Yazen Alnouti, Ph.D.

All biomedical research is conducted in animal models first. In addition, the Food and Drug Administration requires extrapolation from animal data to predict human responses. There are ongoing scientific and regulatory challenges translating interspecies comparisons and predictions. Metabolic pathways are a cornerstone to understanding drug metabolism and toxicities and the liver is a key organ in this process. Bile acids (BAs) play a central role in the hepatobiliary toxicities of chemicals, toxins, and biological reagents. BAs have many physiological functions including regulation of genes involved in cholesterol and glucose metabolism and BA homeostasis. However, BAs also have several pathological effects including carcinogenicity and liver toxicity. Maintenance of bile acid (BA) homeostasis is essential to achieve their physiologic functions and avoid their toxic effects. Several metabolic pathways including sulfation by sulfotransferase (SULT), glucuronidation by UDP-glucuronosyltransferases (UGTs), and oxidation by Cytochrome-P450 (CYP450) enzymes participate in the direct detoxification, enhance the elimination of BAs, and help maintain their homeostasis. In addition, influx and efflux transporters at both the sinusoidal and basolateral membranes play an important role in determining intracellular BA concentration, and therefore their hepatotoxicity. There are known species differences in BA metabolism and transporter. There are known species differences in the composition of the BA pool, the toxicity of BAs, and drug-induced hepatotoxicity related to BAs. These species differences can

prevent extrapolation of toxicity profiles of xenobiotics between species causing a serious disconnect between preclinical safety findings in rodent and canine animal models and safety finding at clinical stages. In this thesis, we compare the metabolic profile of representative BAs between several species including humans, chimpanzee, monkeys, minipigs, hamster, rabbits, dogs, rats, and mice. The metabolic profile was characterized by the identification of BA metabolites and by quantifying the kinetics of their formation in hepatocyte S9 in-vitro system. The relative contributions of individual metabolic pathways were determined. LC-MS/MS was used for the qualitative and quantitative analysis of BAs and their metabolites. A mixture of stable-isotope labeled ($^{2}H_{4}$) and unlabeled BAs were used to facilitate the identification of all minor and major metabolites. Major species differences were found in the metabolism of BAs. Amidation with taurine and glycine was the major pathway in all species. Sulfation was predominant in humans, whereas oxidation and glucuronidation were predominant in rodents and dogs, respectively. Glucuronidation and amidation of BAs are exclusive, where glucuronidation only takes place for unamidated BAs. In vitro-In vivo extrapolation (IVIVE) is performed to establish the correlation of the in vitro results and the bile acid profile in vivo. These results explain, at least in part, the dissociation between preclinical toxicity data in various in vitro and in vivo models and toxicities observed in humans. Furthermore, more relevant species are suggested based on the similarity to the human BA metabolism. In addition, we also screened different bile acids as a potential biomarker for transporter activity using cynomolgus monkey as preclinical model. This resulted in identification of key bile acid sulfates as biomarker for transporter mediated drug-drug interactions.

TABLE OF CONTENTS

ACKNOWLEDGEMENTS i

ABSTRACT iii

TABLE OF CONTENTS V

LIST OF FIGURES IX

LIST OF TABLES XII

LIST OF ABBREVIATIONS XIV

CHAPTER 1: SPECIES DIFFERENCES IN BILE ACID METABOLISM 1

1.1 Introduction 1

1.2 Materials and Method 13

1.2.1 Chemicals and Reagents 13

1.2.2 Hepatocyte S9 fractions Incubation Condition 14

1.2.3 Identification of Metabolites Generated by Hepatocyte S9 fractions 15

1.2.4 Biosynthesis and NMR-based Quantification of UDCA Metabolites 16

1.2.5 BAs Quantification by LC-MS/MS 18

1.2.6 Calculation of BA Indices 19

1.3 Results 20

1.3.1 BA Profiles in Plasma 20

1.3.1 BA Profiles in Urine 21

1.3.3 Identification of Ursodeoxycholic acid (UDCA) Metabolites Generated by Hepatocyte S9 fractions 23

1.3.4 Biosynthesis and NMR-quantification of UDCA Metabolites 27

1.3.5 Species Differences of BA Metabolism by Hepatocyte S9 fractions 28

1.4 Discussion 31

1.4.1 In-vivo BA Profile 31

1.4.2 Literature Summary of BA Profiles in Different Species 36

1.4.3 Biosynthesis of UDCA Metabolites and Quantification Using NMR 38

1.4.4 Optimization of Hepatocyte S9 Incubation Conditions 41

1.4.5 Species Differences in BA Metabolism by Hepatocyte S9 fractions 42

1.4.6 In-vivo and In-vitro Correlation 46

1.5 Conclusions 46

1.6 References 74

CHAPTER 2: BILE ACIDS AS POTENTIAL NOVEL BIOMARKERS FOR ORGANIC ANION-TRANSPORTING POLYPEPTIDE 91

2.1 Introduction 91

2.2 Materials and Methods 93

2.2.1 Chemicals and Reagents 93

2.2.2 Animal Handling, Dosing, Plasma Draws, and Urine Collection 94

2.2.3 Liquid Chromatography-Tandem Mass Spectrometry (LC-MS/MS) Analysis 96

2.2.4 Determination of Uptake Clearance in the Presence of Cynomolgus Monkey Plated Primary Hepatocytes 98

2.2.5 Pharmacokinetics Analysis 99

2.2.6 Statistical Analysis of RIF Dose Response 100

2.3 Results 101

2.3.1 Pharmacokinetics of RIF in Cynomolgus Monkeys 101

2.3.2 Impact of RIF on 2H4-Pitavastatin Pharmacokinetics 101

2.3.3 Profiling of Plasma BAs at Different Doses of RIF 102

2.3.4 Assessment of RIF Dose Response 103

2.3.5 Impact of RIF on BA Renal Clearance 104

2.3.6 Incubation of GCDCA-S, GDCA-S, DCA-S, TDCA-S, TCA and Pitavastatin with Cynomolgus Monkey Plated Hepatocytes 105

2.4 Discussionand Conclusion 106

2.5 References 138

CHAPTER 3: QUANTITATIVE ANALYSIS OF ENDOGENOUS COMPOUNDS 142

3.1 Introduction 142

3.2 Quantitative Liquid Chromatography-Tandem Mass Spectrometry (LC-MS/MS) Analysis 143

3.3 Approaches for Quantification of Endogenous Analytes 146

3.3.1 Method of Background Subtraction 146

3.3.2 Method of Standard Addition 148

3.3.3 Surrogate Matrices 150

3.3.4 Surrogate Analytes 152

3.4 Regulatory Guidelines 154

3.5 Conclusions 155

3.6 References 169

CHAPTER 4: SIMULTANEOUS LC-MS/MS ANALYSIS OF EICOSANOIDS AND RELATED METABOLITES IN HUMAN SERUM, SPUTUM, AND BALF 177

4.1 Introduction 177

4.2 Experimental 179

4.2.1 Chemicals and Reagents 179

4.2.2 Instrumentation 180

4.2.3 Liquid chromatographic and Mass spectrometric Conditions 180

4.2.4. Preparation of Charcoal-stripped Serum for Calibration Curves 181

4.2.5 Preparation of Standard Solutions and Calibration Curves 182

4.2.6 Sample preparation 182

4.2.7 Extraction Recovery 183

4.2.8 Method Validation 183

4.2.9 Stability Studies 183

4.2.10 Human Subjects 184

4.3 Results 184

4.3.1 LC-MS/MS Method Development 184

4.3.2 Method Validation 185

4.3.3 Recovery 186

4.3.4 Stability Studies 187

4.3.5 Human eicosanoids profiles 187

4.4 Discussion 188

4.5 Conclusions 192

4.6 References 209

LIST OF FIGURES

Figure 1.1 Chemical structures of major BAs and their glycine (G), taurine (T), and sulfate (S) conjugates. 48

Figure 1.2 Individual BA contributions to the overall composition of plasma BA pools in humans and in various animal species. 49

Figure 1.3 Individual BA contributions to the overall composition of urine BA pools in humans and in various animal species. 50

Figure 1.4 Extracted ion chromatograms (EIC) of detected metabolites obtained after incubation of UDCA with hepatocyte S9 fractions from different species for 60 min. A) parent-UDCA (m/z 391), B) M1 to M3: glucuronide conjugates (m/z 567), C) M4 and M5: sulfate conjugates (m/z 471), D) M6: glutathione conjugate (m/z 680), E) M7 to M10: hydroxylation into tri-OH BA metabolites (m/z 407), F) M11: glycine (G) amidate (m/z 448), G) M12: taurine (T) amidate (m/z 498), and H) M13: combination of hydroxylation and taurine amidation into T-MCA (m/z 514). 51

Figure 1.5 Representative enhanced product ion (EPI) spectra of UDCA metabolites. A) M1 and M2: O- glucuronide conjugate, B) M3: acyl-glucuronide conjugate, C) M4: 3-O-sulfate conjugate, D) M5: 7-O-sulfate conjugate, E) M6: glutathione conjugate, F) M7 to M10: hydroxylation into tri-OH BA metabolites G) M11: glycine (G) amidate H) M12: taurine (T) amidate, and I) M13: combination of hydroxylation and taurine amidation into T-MCA. 53

Figure 1.6 Proposed structures of MS/MS fragments produced by HRMS analyses of various BA standards. 54

Figure 1.7 Identification of a unique proton signal by comparing 1H NMR spectrum of 1) blank hepatocyte S9 fraction incubation and B) UDCA neat standard. 55

Figure 1.8 Uniform 1H NMR responses of the 0.6 ppm proton for A) 0.2 mM LCA, B) 0.2 mM T-UDCA, and C) 0.2 mM UDCA 56

Figure 1.9 Quantification of UDCA-3S by 1H NMR using UDCA calibration curve: (A) UDCA-3-S 1H NMR spectrum showing the AUC of the unique 0.6 ppm proton obtained from hepatocyte S9 fractions incubation, (b) a UDCA calibration curve using the same proton. 57

Figure 1.10 (A) LC-MS Chromatogram of equal concentrations of UDCA and its representative metabolites (UDCA-3-S, β-MCA, and G-UDCA) at 0.5 μM. RF is calculated from the ratio of metabolite: parent peak areas at equal concentrations, (B) comparison of metabolite concentrations calculated using the RF approach vs. direct analysis using authentic standards. 58

Figure 2.1 Plasma concentration-time profile of (A) GDCA-S, (B) TDCA-S, (C) GCDCA-S, (D) TCDCA-S, (E) GLCA-S and (F) TLCA-S in male cynomolgus monkeys after oral administration of vehicle alone (open squares), and RIF 1 mg/kg (open circles), 3 mg/kg (closed triangles), 10 mg/kg (closed circles) and 30 mg/kg (closed squares). Data are presented as mean ± SD of n = 4 animals. 111

Figure 2.2 Fold change in $AUC_{0\text{-}24,plasma}$ of (A) un-sulfated bile acids and (B) bile acid 3-O-sulfates at increasing doses of RIF in male cynomolgus monkeys. 112

Figure 2.3 Fold change in plasma C_{max} of (A) un-sulfated bile acids and (B) bile acid 3-O-sulfates at increasing doses of RIF in male cynomolgus monkeys. 113

Figure 2.4 Linear regression of plasma AUC ratio ($AUCR_{plasma}$) between pitavastatin and bile acid 3-O-sulfates for (A) GDCA-S, (B) TDCA-S, (C) GCDCA-S, (D) TCDCA-S, (E) GLCA-S and (F) TLCA-S. For pitavastatin and bile acids, $AUCR_{plasma}$ is calculated by dividing $AUC_{0\text{-}24,plasma}$ obtained with RIF (1, 3, 10 and 30 mg/kg) by the $AUC_{0\text{-}24,plasma}$ for vehicle control. 114

Figure 2.5 Linear regression between free RIF plasma C_{max} (μM) at 1, 3, 10 and 30 mg/kg and bile acid 3-O-sulfate $AUCR_{plasma}$ for (A) GDCA-S, (B) TDCA-S, (C) GCDCA-S, (D) TCDCA-S, (E) GLCA-S, (F) TLCA-S, and (G) pitavastatin. $AUCR_{plasma}$ as defined in the legend to Figure 2.4. 115

Figure 2.6 Fold change in CL_{renal} of (A) un-sulfated bile acids and (B) bile acid 3-O-sulfates at increasing doses of RIF in male cynomolgus monkeys. 116

Figure 2.7 Impact of RIF and RIFsv (A) and sodium removal (B) on the uptake of $^{2}H_{5}$-GCDCA-S (0.5 mM), $^{2}H_{4}$-GDCA-S (0.5 mM), $^{2}H_{4}$-TCA (0.5 mM), and non-labeled pitavastatin (0.1 mM) by plated cynomolgus monkey primary hepatocytes. RIF and RIFsv were added at a final concentration of 5 mM and 1 mM, respectively. Data for individual duplicates are shown. The mean % decrease is shown also and calculated as (VDMSO-Vi/ VDMSO)*100. VDMSO and Vi is the mean uptake rate in the presence of DMSO alone (plus sodium) and inhibitor (or minus sodium) respectively. 117

Figure 2.8 Impact of RIF on the uptake of $^{2}H_{5}$-GCDCA-S (0.1 mM), $^{2}H_{4}$-GDCA-S (0.1 mM), $^{2}H_{4}$-TCA (0.1 mM), $^{2}H_{4}$-TDCA-S (0.1 mM), $^{2}H_{4}$-DCA-S (0.1 mM), and nonlabeled pitavastatin (0.1 mM) by plated cynomolgus monkey primary hepatocytes. RIF was added at a final concentration of 5 mM. Data for individual duplicates are shown. The mean % decrease is shown and was calculated as described in the legend to Figure 2.7. 118

Figure 3.1. A LC-MS/MS chromatograms showing differences in MS response of one analyte spiked pre- extraction (A) and post-extraction (B) into plasma, liver, as well as neat matrices at the same concentration. 157

Figure 3.2 LC-MS/MS chromatograms showing (A) background peak of endogenous analyte in blank matrix, (B) a neat standard with known concentration of the same analyte, (C) the same matrix after spiking with a standard of a known concentration (method of background subtraction), (D) one study sample is split into several aliquots, each spiked with a standard (Std.) of different concentration (method of standard addition), (E) analyte standard spiked into a surrogate matrix that contains no

background (surrogate matrix method), (F) a standard of a surrogate analyte spiked into the same original matrix (surrogate analyte method). 158

Figure 3.3 A LC-MS/MS chromatogram showing the subtraction of the background (blank) peak area of endogenous compound (A) from the peak area of the same compound after spiking with a 500 ng/ml standard. (B) is an exogenous compound and no background exists in the blank matrix. 159

Figure 4.1 Representative chromatograms of all eicosanoid standards at 10 ng/ml under final chromatography and detection conditions in negative ESI mode. Peaks are labeled with analytes IDs and retention time as given in table 5.1 194

Figure 4.2 Isobaric compounds that also share fragmentation patterns as well as retention times were distinguished via specific MRMs. LC-MS/MS chromatograms of various HETEs after the injection of a 5-HETE standard at 500 ng/ml. Isobaric HETEs including 5-HETE (13), 8-HETE (12), 11-HETE (11), and, 12-HETE (10), were not resolved chromatographically, and they produced both common and selective fragments in MS/MS. The 319/301 transition was the most sensitive but was shared by all HETEs (a, c, e, g). In contrast, the less sensitive but more selective transitions of HETEs were used including 319/114.7 for 5-HETE (b), 319/154.8 for 8-HETE (d), 319/167.2 for 11-HETE (f) and 319/179 for 12-HETE (h). 195

Figure 4.3 Isobaric and that undergo in-source fragmentation eicosanoids were separated chromatographically. (a) The isobaric compounds PGE2 (7), PGD2 (6), and 13, 14-dihydro-15-k-PGE2 (18) share the same MRM transition of 351→333 and had to be separated chromatographically (retention time (RT) = 11.58, 11.77, and, 12.5 min, respectively). (b) PGJ2 (333.1→315.2) and (c) 15-dexoxy-delta 12, 14-PGJ2 (315.2→271.2) have different precursor as well as fragment masses. However, PGJ2 produces an in-source fragment (315.2) with the same mass as the parent 15-dexoxy-delta 12, 14-PGJ2. Therefore, the two compounds had to be separated chromatographically. 196

LIST OF TABLES

Table 1.1 Plasma BA profiles in humans and in various animal species. 59

Table 1.2 Urine BA profiles in humans and in various animal species. 60

Table 1.3 Exact mass analyses of various BA standards and their fragments using Orbitrap high resolution mass spectrometry (HRMS). 61

Table 1.4 HRMS analysis of UDCA metabolites and their fragments. Each biotransformation product is described by molecular formula [M-H]-, exact m/z shift (compared to the parent), and MS/MS fragments. 63

Table 1.5 Physiological concentrations of biotransformation cofactors for various metabolic pathways in human liver and biological fluids, and in previously and currently used in vitro metabolism systems. 64

Table 1.6 LCA, UDCA, CDCA, and CA metabolism by hepatocyte S9 fractions from humans and various animal species 65

Table 1.7 BA oxidation into hydroxylated metabolites by hepatocytes S9 fractions.67

Table 1.8 Literature summary of plasma BA profiles in different species. 68

Table 1.9 Literature summary of biliary BA profiles in different species. 70

Table 1.10 Literature summary of liver BA profiles in different species. 72

Table 2.1 Pharmacokinetic parameters of pitavastatin in male cynomolgus monkeys after i.v. administration (0.2 mg/kg) with increasing doses of RIF 119

Table 2.2 Pharmacokinetic parameters of RIF after oral administration to male cynomolgus monkeys 120

Table 2.3 The p-value for the linear trend with RIF dose and false discovery rate (FDR) estimates for area under the plasma concentration-time curve ($AUC_{0\text{-}24,plasma}$), maximum plasma concentration ($C_{max,plasma}$) and renal clearance (CL_{renal}) for various bile acids and their respective 3-O-sulfate conjugates. 121

Table 3.1 Applications of the background subtraction method 160

Table 3.2 Applications of the method of standard addition. 161

Table 3.3 Applications of the use of neat solutions as surrogate matrices. 162

Table 3.4 Typical composition of commonly used artificial matricesa. 163

Table 3.5 Applications of the use of artificial matrices as surrogate matrices. 164

Table 3.6 Applications of the use of stripped matrices as surrogate matrices. 166

Table 3.7 Applications of the surrogate analytes method. 168

Table 4.1 Summary of SRM, precursor and product ions (Q1, Q3), internal standard (IS), declustering potential (DP), collision energy (CE), and retention time (RT) used for eicosanoids in negative ESI mode. 197

Table 4.2 Dynamic range, linearity, accuracy, and precision of eicosanoids in human serum. 199

Table 4.3 Unstable eicosanoids in different matrices under various storage conditions*. 201

Table 4.4 Concentrations (ng/ml) of eicosanoids in serum (n=5), sputum (n =2), bronchial and alveolar fluids (n =5) of healthy human subjects. 202

LIST OF ABBREVIATIONS

UPLC: ultra-performance liquid chromatography

LC-MS/MS: liquid chromatography-tandem mass spectrometry

BAs: bile acids

G-BAs: glycine-amidated bile acids

T-BAs: taurine-amidated bile acids

MCA: muricholic acid

CA: cholic acid

HCA: hyocholic acid

MDCA: murideoxycholic acid

UDCA: ursodeoxycholic acid

HDCA: hyodeoxycholic acid

DCA: deoxycholic acid

CDCA: chenodeoxycholic acid

LCA: lithocholic acid

CA-S: cholic acid-sulfate

UDCA-S: ursodeoxycholic acid-sulfate

DCA-S: deoxycholic acid-sulfate

CDCA-S: chenodeoxycholic acid-sulfate

LCA-S: lithocholic acid-sulfate

IS: internal standard

MeOH: methanol

ACN: acetonitrile

QC: quality control

U: unamidated

G: glycine

T: taurine

SULT2A1: sulfotransferase 2A1

BAT: bile acid-coenzyme A : amino acid N-acyltransferase

AUC: Area under the ROC curve

OAT3: organic anion transporter 3

$AUCR_{plasma}$: AUC (area under the plasma concentration-time curve) ratio determined by dividing the $AUC_{0\text{-}24,plasma}$ after RIF treatment by the $AUC_{0\text{-}24,plasma}$ after vehicle alone

FDR: false discover rate

CL_{renal} ratio: renal clearance (CL_{renal}) after RIF treatment divided by the CL_{renal} following vehicle alone

RIF: rifampicin

RIFsv: rifamycin SV

PAPS, 3'-phosphoadenosine-5'-phosphosulfate;

SLC: solute carrier

DDI: drug-drug interaction

OATP: organic anion-transporting polypeptide

NTCP: sodium-taurocholate co-transporting polypeptide

CHAPTER 1

Species Differences in Bile Acid Metabolism

1.1 Introduction

1.1.1 History of Bile Acids

Bile acids (BAs), the end products of cholesterol metabolism, are synthesized in the liver and excreted into bile, which flows to the small intestine via the bile duct. Most of BAs are reabsorbed from the intestine into the portal circulation and they undergo enterohepatic recirculation. Bile was known as early as the Greek-Roman medicine as part of the humorism concept. Bear bile and gallbladders were also used in traditional Chinese medicine to treat diseases in the 1st-2nd century BC [1], but It was only in 1827 when L. Gamlin first succeeded in isolating the 1st BA, glycocholic acid (G-CA) [2]. The term “bile acid ” was first coined in 1838 by H. Demarcay [3]. Subsequent studies in 1848-1911 identified additional BAs including lithocholic acid (LCA), chenodeoxycholic acid (CDCA), ursodeoxycholic acid (UDCA), and muricholic acid (MCA) from ox, goose, bear, and rodents, respectively [4]. BAs were first commercially synthesized in 1917 when the pharmaceutical company Ingelheim (Germany) isolated cholic acid (CA) from ox bile [5]. **Figure 1.1** shows chemical structures of major BAs in humans and various animal species.

1.1.2 BA Synthesis

BA synthesis occurs in hepatocytes via cytochrome P450-mediated oxidation of cholesterol in a multi-step process [6]. The major pathway of BA synthesis is initiated via the hydroxylation of cholesterol at the 7α position by CYP7A1 [7]. This pathway of BA synthesis is called the "classic" or "neutral" pathway. Next steps include the oxidation of the 3β-OH and isomerization of the C5-C6 double bond by the microsomal C27-3β-hydroxysteroid dehydrogenase (C27-3β-HSD). The resulting intermediate is

either, hydroxylated at the 12α position by the microsomal CYP8B1 or passed on directly to the next step. The 12α-OH intermediates and those that escaped 12α-hydroxylation are then subjected to reduction of the C4-C5 double bond by the enzyme oxosteroid 5β reductase. This is followed by reduction of the C3-oxo group by the enzyme 3α-HSD to yield 3α-OH intermediates [7, 8]. The 12α-hydroxylated intermediates ultimately produce CA, whereas the intermediates that were not hydroxylated, ultimately produce CDCA. CDCA and CA are the primary BAs in humans. Next steps in BA synthesis introduce a hydroxyl group at C27, followed by its oxidation into a carboxylic acid by the mitochondrial CYP27A1. This is followed by ligation to coenzyme A by the bile acid coenzyme-A synthetase (BAS) [9]. The side chain of these C27 intermediates are then shortened to C24 BAs by series of β-oxidation reactions catalyzed by various enzymes in the peroxisomes including bile acid CoA ligase, CoA racemase, acyl-CoA oxidase, and peroxisomal thiolase. The last step in BA synthesis is the amidation of the bile acid-CoA with an amino acid (glycine (G) or taurine (T)), by the bile acid-CoA:amino acid N-acyltransferase (BAT) [10].

There are minor pathways for BA synthesis, which do not require the initiation by CYP7A1 [11]. These pathways are initiated via the hydroxylation of the cholesterol side chain at the different positions (C24, C25, or C27) by various enzymes including, CYP46A1, cholesterol 25-hydroxylase, and CYP27A1. The resulting oxysterols are then hydroxylated at the 7α position by CYP7B1 or CYP39A1. These pathways of BA synthesis are called the "alternative" or "acidic" pathways. In contrast to the classical pathway, these alternative pathways predominantly produce CDCA [12]. Alternative BA pathways are important in conditions associated with a deficiency in CYP7A1 activity [13].

1.1.3 Enterohepatic Recirculation of BAs

BAs synthesized in the liver are secreted into bile, which flows through the bile duct to the duodenum. BAs are efficiently absorbed from the terminal ileum and returned to the liver where they are once again secreted into bile. This cycle is called the enterohepatic recirculation of BAs [6]. Enterohepatic cycling of BAs is efficiently controlled by various transporters in the hepatocytes and enterocytes [6, 14, 15]. BAs are actively absorbed in the ileum by the Na+-dependent bile salt transporter (ASBT) located on the apical side of enterocytes. Organic solute transporters (OST-α/β) and multidrug resistance-associated protein 3 (MRP3), located on the basolateral side of enterocytes, transport BAs from the intestinal lumen to blood [15, 16]. Absorbed BAs are carried in the portal vein and extracted by the liver via the Na+-taurocholate co-transporting polypeptide (NTCP) and members of the organic anion transporting polypeptide (OATP) family (OATP1B1, 1B3, and 2B1) [6, 17]. BAs spill-over across the basolateral side of hepatocytes into systemic circulation takes place via MRP1, MRP3, MRP4, MRP6, and OST-α/β transporters [18, 19].

At the canalicular membrane of hepatocytes, BAs are excreted into bile via the canalicular bile salt export pump (BSEP), MRP2, and multi-drug resistance protein 1 (MDR1) [20]. In species that have gallbladders such as humans, chimpanzees, monkeys, dogs, and mice, secreted bile is stored in the gallbladder, which contracts to empty its content into the duodenum under the influence of cholycystokinin secretion after meal ingestion [14]. In species without a gallbladder such as rat, deer, elephant, and horse, and in patients who have undergone surgical removal of the gallbladder, bile acids also have an enterohepatic circulation, but presumably the bile acid pool is stored in the small intestine during overnight fasting [14]. In the small intestine, most conjugated BAs are actively absorbed in the ileum, while unconjugated BAs are passively absorbed throughout the intestinal tract [21, 22]. Partial deconjugation takes place by the bacteria in the distal parts of the small intestine, and the liberated

unconjugated BAs are passively absorbed [21, 23]. Unabsorbed BAs are passed along the intestinal tract. In the large intestine, BAs undergo bacterial transformations, including deamidation, desulfation, deglucuronidation, dehydroxylation, epimerization, and/or dehydrogenation to produce secondary BAs [6, 24]. DCA and LCA are secondary BAs produced from the dehydroxylation of CA and CDCA, respectively, in the intestine. Unabsorbed BAs are excreted in feces. Ninety-five percent of BAs excreted in bile are reabsorbed throughout the intestinal tract and less than 5% are excreted in feces [6]. Absorbed BAs are carried in the portal vein and extracted by the liver via active or passive diffusion. In hepatocytes, most BAs undergoes amidation, but other metabolic pathways also take place including, hydroxylation and sulfate or glucuronide conjugation. The reabsorbed and newly synthesized BAs are then excreted into bile to complete the enterohepatic cycle.

1.1.4 Physiological Functions of BAs

BAs are essential for the formation of mixed micelles in the small intestine, which facilitates the solubilization, digestion, and absorption of cholesterol, dietary lipids, and fat-soluble vitamins [25]. Hepatic conversion of cholesterol to BAs and subsequent excretion in feces represent the only significant mechanism for the elimination of excess cholesterol from the body [26]. Micelles present in the gallbladder solubilize cholesterol in bile and prevent cholesterol crystallization and gallstone formation. BAs also induce the BA-dependent bile flow from hepatocytes through bile canaliculi to the gallbladder [27]. This eventually helps in the excretion of some substances like bilirubin and some drugs and toxins [27]. BAs also have bacteriostatic effects that maintain sterility in the biliary tract and control the normal flora composition in the intestine [28, 29].

Over the last two decades, new insights have been introduced about the biological activities of BAs. Recent findings have demonstrated that BAs are involved in their own homeostasis, regulation of energy expenditure, glucose and lipid metabolism,

thyroid hormone signaling, and cellular immunity. Specific BAs differentially activate various nuclear and surface receptors, namely farnesoid X receptor (FXR), pregnane X receptor (PXR), vitamin D receptor (VDR), and G protein-coupled receptor (TGR5), which mediate their various hormonal functions [30-33].

1.1.5 Pathological Effects of BAs

Despite their physiological roles, BAs are also cytotoxic when present at high concentrations. BAs exhibit pathological effects due to their direct detergent effects on biological membranes, apoptotic and necrotic effects via mitochondria and endoplasmic reticulum-mediated toxicities, and cancer promoting effects [25].

Due to their detergent activity, BAs can bind to lipid bilayers and solubilize plasma membranes, causing cell lysis [34]. In addition, elevated intracellular levels of BAs can deteriorate mitochondrion integrity, causing permeabilization of mitochondrial membranes, which provokes depolarization of the organelle, uncoupling of oxidative phosphorylation, and mitochondrial swelling [35, 36]. Ultimately this leads to mitochondrial collapse, cytochrome c release, and activation of apoptosis [37, 38]. BAs can also induce apoptosis by causing endoplasmic reticulum (ER) stress [39]. BAs can also cause cell necrosis through various mechanisms including generation of hydroperoxides, ATP depletion, and sustained rise in cytosolic free Ca^{2+} [40]. Furthermore, BAs act as cancer promoters by stimulating cell invasion and migration through activation of multiple oncogenic signaling pathways [41, 42].

Hepatotoxicity is a well-characterized toxicity of BAs. Cholestatic diseases are hepatobiliary diseases associated with reduction in bile flow due to defects in bile production or impairment of bile flow through the canaliculi into bile duct [43]. Several studies in animal models including mice, rats, cats, and dogs clearly showed that various hepatobiliary diseases result in the accumulation of BAs in the liver, systemic blood, and extrahepatic tissues [44]. Accumulation of toxic BAs during cholestasis induces

hepatotoxicity, extrahepatic toxicity such as encephalopathy, and contributes to the unfavorable prognosis of these diseases such as liver failure [44-46]. Furthermore, several studies in animals indicate that the accumulation of toxic BAs in the liver is associated with the incidence and severity of complications after liver transplant [45, 47, 48], where patients with lower secretion of biliary BAs are less likely to develop bile duct complications after liver transplant [49, 50]. The cholestatic activity of BAs is attributed to their water insolubility because BAs with low solubility may form insoluble BA salts, such as Ca^{+2}salts, which precipitate in and damage the canaliculi [51-53]. Another mechanism of liver injury by BAs, is increasing the biliary secretion of phospholipids causing their depletion and allowing BAs to solubilize membrane phospholipids, which disturbs the integrity of the canalicular membranes [6].

1.1.6 Differences between Individual BAs

Individual BAs vary widely in their physicochemical properties, physiological functions, and toxicities. BA hydrophobicity is influenced by both the BA nucleus and the side chain structures [54]. There is an inverse relationship between the number of OH groups present on steroid nucleus and lipophilicity. The Mono-hydroxy (mono-OH) BA (LCA) is more hydrophobic than di-hydroxy (di-OH) BAs (CDCA and DCA), which in turn are more hydrophobic than tri-hydroxy (tri-OH) BAs (CA, MCA, and HCA). Hydrophobicity is also determined by the position and stereochemistry of hydroxyl groups. For example the 7β, 6α, and 6β- OH substitutions result in the formation of more hydrophilic BAs. BAs possess two distinct hydrocarbon surfaces, the convex hydrophobic side and the concave hydrophilic side. 7β, 6α, and 6β- OH groups are located above the steroid nucleus and are equatorial to the plane of steroid nucleus, while 7α and 12α- OH groups are located below the steroid nucleus and are axial to the plane of the steroid nucleus. The equatorial location of hydroxyl groups confers polarity to the hydrophobic concave side of the steroid nucleus and they are more resistant to

the loss of associated water [15, 55, 56]. Therefore, UDCA (7β- OH) is more hydrophilic than CDCA (7α- OH) and DCA (12α- OH). Similarly, MCAs, containing both 6α and 7β-orientated hydroxyl groups, is more hydrophilic than HCA (6α and 7α- OH), which in turn is more hydrophilic than CA (7α and 12α- OH).

Amidation increases the acidity of unconjugated BAs, where pKa is reduced from about 5.5 for the unamidated BAs to 4.5 and 1.5 for those with G- and T-amidation, respectively [51]. This increase BA ionization and solubility at physiological pH. Conjugation of the BA backbone with sulfate or glucuronide groups also increases BA ionization and solubility. This result in complete ionization of BAs at physiological pH, which markedly reduces their lipophilicity, increases their solubility, decreases membrane permeability, and increases their urinary and biliary excretion [51, 57].

The term hydrophobicity index (HI) was introduced to describe the hydrophilic-hydrophobic balance of BAs based on their relative retention time and capacity factor in C18 reversed-phase HPLC. HI of BAs ranges from +1.46 for the most hydrophobic BA (LCA) to -0.94 for the most hydrophilic BA (T-UDCA) [58, 59]. A composite HI index can be calculated for any BA pool based on the HI of individual BAs normalized with their concentrations, which describes the overall hydrophobicity of the BA pool [58, 59].

As amphipathic molecules with hydrophobic and hydrophilic regions BAs form micelles. The concentration at which BAs start forming micelles is called the critical micelle concentration (CMC). The lower the CMC, the more stable is the micelle and the more efficient micelle former is the BA. The CMC values of mono-OH BAs are lower than Di-OH BAs, which in turn are lower than tri-OH BAs. CMC values (in mM) for the various BAs are LCA (0.5) < DCA (3) < CDCA (4) < UDCA (7) < CA (11) < HDCA (16) < HCA (20) <α-MCA (32) < ωMCA (35) <β-MCA (50) [60-62]. In addition, amidation with G or T lowers the CMC [61, 62], while conjugation with sulfate or glucuronide increases the CMC of BAs [6, 63].

Individual BAs also differ in their physiological effects. As mentioned above, the more hydrophilic BAs have higher CMC values and are less efficient micellar formers; therefore, less efficient in cholesterol solubilization and absorption [64]. In addition, the effects of BAs on bile flow vary according to their hydrophilicity. Hydrophilic BAs such as UDCA, MCA, HCA, and CA induce bile flow (cholaresis), whereas hydrophobic BAs such LCA, DCA, and CDCA decrease or block bile flow (cholestasis) [65-69]. Individual BAs also have marked differences in their affinities to their various receptors. For example, the various BAs affinities for TGR5 are in the order of LCA>DCA>CDCA>CA>UDCA [32, 70]. In contrast, the various BAs affinities for FXR are in the order of CDCA>DCA>LCA>UDCA, CA [71, 72], while MCA acts as FXR antagonist [73].

BA cytotoxicity has been extensively characterized in several cell lines including hepatocytes [74], HepG2 cell [75], erythrocytes [76], mast cells [77], and intestinal cells [78]. In general, BA cytotoxicity increases with hydrophobicity, where the tri-OH BAs are less toxic than the di-OH BAs, which in turn are less toxic than the mono-OH BAs. In addition, G- and T- amidation, as well as glucuronide and sulfate conjugation decrease BA cytotoxicity [79-81]. Also, LCA and DCA are potent inducers of apoptosis compared with CA and UDCA [79, 82].

1.1.7 Species Differences in BA Homoeostasis

There are known species differences in BA metabolism and transport. BAs are metabolized via amidation (glycine or taurine), hydroxylation by CYP3A, or conjugation (sulfation by SULT2A1 and glucuronidation by UGTs). Amidation with glycine is predominant in humans [43, 83], rabbits [84], and pigs [85], whereas taurine amidation is predominant in rats [86], mice [87, 88], dog [89], cats [90], and horses [91]. Hydroxylation, on the 6-α, 6-β, and 7-β positions [92, 93] is a primary pathway that produces the most hydrophilic and least toxic HCA (pigs), MCA (rats and mice), and

UDCA (bears), respectively [94]. Equivalent to hydroxylation in rodents, sulfation is the major pathway of BA metabolism and detoxification in humans [6] and chimpanzees [95].

Species differences in intestinal flora and anatomy of large intestine also affect the composition of bile acids [96]. For example, compared with other animals rabbit has unusually large cecum (10 times the capacity of stomach), where large quantity of anaerobic bacteria reside, which results into formation of higher secondary BAs (DCA) in rabbit compared with other species [84].

In addition to BA metabolism, influx and efflux transporters at both the sinusoidal and basolateral membranes play an important role in determining intracellular BA concentration, and therefore their hepatotoxicity. Similar to BA metabolism, major species differences were reported in BA transport [97-101]. The contribution of basolateral efflux via MRP transporters to ameliorate drug-induced toxicity was 5-fold higher in rats than humans [97]. Rodent Mrp3 transports BAs with high affinity, but human MRP3 with relatively low affinity [100, 101]. BAs uptake by NTCP and OATP transporters was 3-15 higher in rats compared to human hepatocyte [98]. Furthermore, OATP1B1 and OATP1B3 are poorly conserved in humans, rodents, and dogs [99].

1.1.8 BAs and Drug Induced Liver Injury (DILI)

DILI is the most common cause of acute liver failure in USA [102, 103]. An online database (http://www.livertox.nih.gov/) provides detailed information on more than 600 drugs and herbal products associated with DILI. DILI has an unpredictable and heterogeneous course, ranging from an asymptomatic rise in liver enzymes to acute liver failure. DILI is one of the primary reasons for the failure of pharmaceutical agents during drug development as well as the withdrawal of approved drugs from the market [104]. The mechanisms underlying DILI are not fully understood, but one of the established mechanisms is the alteration of BA homeostasis. The relationship of altered BA

homeostasis and the pathogenesis of cholestatic liver diseases has been demonstrated in animal models of cholestasis, where the interruption of bile flow leads to BA retention in the liver and the biliary tree [105]. Because of their hepatotoxicity, intrahepatic accumulation of BAs itself can worsen and contribute to the pathogenesis of liver diseases [106, 107]. Similar to liver diseases, BA accumulation due to alterations of various aspects of their homeostasis caused by some drugs is proposed to be one of the major mechanisms underlying DILI [108, 109]. For example, total BAs concentrations were shown to correlate with the progression of liver and bile duct damage in bile-duct ligated and thioacitamide-induced cholestatic rats [105, 110].

A variety of in vitro models including membrane vesicles expressing BA transporters, primary hepatocytes, micropatterned hepatocytes culture, and sandwich culture hepatocytes were developed and applied for high-throughput assessment of DILI risk [111]. However, such exercises have rendered mixed results with many false negative and positive predictions [112, 113]. For example, drugs that inhibit transporters involved in BA excretion from hepatocytes into bile such as BSEP and/or transporters involved in the basolateral efflux of BAs from hepatocytes into systemic blood such as members of the MRP family was shown to lead to intrahepatic accumulation of BAs and DILI [114, 115]. However, inhibition of BA transporters, by itself, is not always a predictor for DILI. For example, telmisartan is a potent BSEP inhibitor, but is not associated with DILI in the clinic [116]. Similarly, rifabutin is known to cause DILI in humans, but it is a weak BSEP inhibitor [112]. Therefore, current DILI in-vitro models address one aspect of BA homeostasis, that is transport via one or a limited combination of transporters (BSEP and MRPs), but do not account for other transporters such as OATPs and NTCP. Also, these in-vitro models do not account for other aspects of perturbation of BA homeostasis such as BA metabolism, synthesis, and excretion.

In general, in vivo preclinical safety studies are conducted in two species, one rodent and one non-rodent [117, 118]. Preclinical safety studies in animals can capture various toxicities including carcinogenicity, teratogenicity, genotoxicity, and adverse effects of compounds on the cardiovascular, nervous, and respiratory systems, but they are not as predictive of DILI in humans [119]. Toxicology studies using rodent and non-rodent species failed to detect DILI in approximately 45 % of cases [119]. For example, bosentan was not hepatotoxic in rats but it causes DILI in humans [104, 120]. In contrast, primidone was hepatotoxic in dogs, but was not in the clinic [121]. The marked differences in BA composition and homeostasis between preclinical safety models and humans may play a major role in the poor prediction of DILI using preclinical in vivo models. Major species differences in the susceptibility to BA-induced hepatotoxicity were previously reported and were explained by species differences in BA metabolism. For example, CDCA and LCA produced severe hepatic toxicity, in species that lack BA sulfation capabilities including rhesus monkeys [122, 123], rabbits [124], guinea pigs [125], and dogs [126]. However, in humans and chimpanzees, where sulfation is a primary metabolic pathway of BAs, CDCA and LCA are not associated with hepatic injury [122, 127-130]. In addition, mice [131] and rats [132] are more resistant to LCA and CDCA hepatotoxicity because their BAs are more hydrophilic than humans due to efficient hydroxylation and taurine amidation [97, 133-135]. Collectively, strong evidence exists that species susceptibility to BA toxicity and therefore DILI, may be determined by their capability to efficiently metabolize BAs.

Overall, DILI remains to be one of the most poorly predicted side effects in humans due to the shortcomings of the currently used preclinical in vivo and in vitro toxicity models.

1.1.9 Objectives

There are major inter-species differences in BA homeostasis, which may play a major role in the poor predictability of DILI using the currently available preclinical in vitro and in vivo models. In particular, there is a major gap in our knowledge regarding the differences in BA metabolism between preclinical species used in drug safety testing and humans. Therefore, this work aims to i) quantify the in-vivo BA profile in plasma from various species, (ii) quantify the contribution of the various pathways involved in BA metabolism in-vitro using hepatocytes S9 fractions from various species, (iii) assess the in vitro-in vivo extrapolation of BA metabolism using our in vitro model in the various species, (iv) quantify the species differences in BA metabolism, composition, hydrophilicity, and toxicity (v) identify preclinical species that are most similar to humans in regards to BA metabolism. Overall, this knowledge will facilitate the development of in vitro models more predictive of DILI as well as the identification of preclinical species that metabolize BAs in a similar fashion to humans and therefore are more relevant to in vivo testing of DILI.

1.2 Materials and Method

1.2.1 Chemicals and Reagents

Human, rhesus monkeys, cynomolgus monkeys, gottingen minipigs, begal dogs, new zealand rabbits, golden syrian hamsters, sprague dawley rats, and CD-1 mice hepatocyte S9 fractions were purchased from Sekisui XenoTech, LLC (Kansas City, KS). Chimpanzees and C57BL/6 mice hepatocyte S9 fractions were purchased from BioreclamationIVT (Westbury, NY). Plasma from Chimpanzees, Rhesus monkeys, Cynomolgus monkeys, Gottingen minipigs, Begal dogs, New Zealand rabbits, Sprague Dawley rats, CD-1 mice, C57BL/6 mice, and Golden Syrian hamsters were obtained from BioreclamationIVT (NY, USA). Nicotinamide adenine dinucleotide phosphate (NADPH), uridine diphosphate glucuronic acid (UDPGA), D-Saccharic acid 1,4-lactone, 3'-phosphoadenosine-5'-phosphosulfate (PAPS), glutathione (GSH), glycine, taurine, adenosine triphosphate (ATP), Coenzyme A (CoA) were purchased from Sigma-Aldrich (St. Louis, MO). Cholic acid (CA), chenodeoxycholic acid (CDCA), deoxycholicacid (DCA), lithocholic acid (LCA), ursodeoxycholic acid (UDCA), tauro-cholic acid (T-CA), tauro-chenodeoxycholic acid (T-CDCA), tauro-deoxycholic acid (T-DCA), tauro-lithocholic acid (T-LCA),tauro-ursodeoxycholic acid (T-UDCA), glyco-cholic acid (G-CA),glyco-chenodeoxycholic acid (G-CDCA), glyco-deoxycholic acid (G-DCA), glyco-lithocholic acid (G-LCA), glyco-ursodeoxycholicacid (G-UDCA), LCA-sulfate and activated charcoal (DARCO®G-60, 100 mesh powder) were purchased from Sigma-Aldrich (St Louis, MO). β-muricholic acid (β-MCA), tauro-β-muricholicacid (T- β-MCA), hyocholic acid (HCA), glyco-hyocholic acid (G-HCA), tauro-hyocholic acid (T-HCA), hyodeoxycholic acid (HDCA), glyco-hyodeoxycholic acid (G-HDCA), tauro-hyodeoxycholic acid (T-HDCA), murideoxycholic acid (MDCA), isolithocholic acid (isoLCA), isodeoxycholic acid (isoDCA), 7-oxoLCA, 12-oxoLCA,12-oxoCDCA, 3-dehydroCA, and norDCA were purchased from Steraloids, Inc. (Newport, Rhode Island).

UDCA-sulfate, CDCA-sulfate, DCA-sulfate, CA-sulfate, their G- and T-amidates, as well as G-LCA-sulfate and T-LCA-sulfate were generously provided by Dr.Junichi Goto, Tohoku University, Aoba-ku, Japan. $^{2}H_4$-G-CDCA, $^{2}H_4$-T-CDCA, $^{2}H_4$--CDCA, $^{2}H_4$-G-UDCA, $^{2}H_4$-CA, and $^{2}H_4$-LCA were purchased from C/D/N isotopes, Inc. (Pointe-Claire, Quebec,Canada). HPLC-grade methanols, acetonitrile, water, ammonium acetate, ammonium hydroxide, formic acid, acetic acid, hydrochloric acid (HCl) were obtained from Fisher Scientific (Fair Lawn, NJ).

1.2.2 Hepatocyte S9 Fractions Incubation Condition

Hepatocyte S9 fractions from male humans, chimpanzees (23.3 mg/ml protein), rhesus monkeys (20 mg/ml protein), cynomolgus monkeys (20 mg/ml protein), beagle dogs (20 mg/ml protein), gottingen minipigs (20 mg/ml protein), new zealand rabbits (20 mg/ml protein), sprague dawley rats (20 mg/ml protein), golden syrian hamster (20 mg/ml protein), CD-1 mice (20 mg/ml protein), and C57BL/6 mice (21.3 mg/ml protein) were thawed carefully on ice and divided into aliquots for further experiments. Prior to incubation, stock solutions of 200 mM GSH, 250 mM glycine, 250 mM taurine, 50mM ATP, 200 mM CoA, 500 mM D-saccharic acid 1,4-lactone, 10.1 mg/ml 3'-Phosphoadenosine-5'-phosphosulfate (PAPS), 25 mM uridine 5’-diphospho-glucuronic acid (UDPGA), and 125 µg/ml alamethicin were prepared in potassium phosphate buffer (pH 7.4, 100 mM) containing 5 mM $MgCl_2$. BA substrate stock solutions of 20 mM unlabeled:labeled (1:1) substrate were prepared in MeOH. Final MeOH concentration in the incubation mixture did not exceed 0.2%. Cofactors and hepatocyte S9 protein were 10-x diluted with 100 mM potassium phosphate buffer (pH 7.4), and biotransformation reaction was initiated by adding a 50-µl mixture of cofactors and substrate to 50 µl of S9 protein at a final concentration of 1 mg protein/ml and a final volume of 100 µl. The reaction mixture was incubated for 60 min at 37°C and the reaction was terminated by adding a 100 µl of ice-cold methanol, followed by vortex-mixing and centrifugation at

16,000 g for 10 min. Ten µl of supernatant was directly subjected to LC-MS/MS analysis. For zero-min incubations, a 100 µl of ice-cold methanol was added to the 50 µl mixture of cofactors before the addition of 50 µl of S9 protein. Final concentration of reagents were 1 mM NADPH, 0.1 mM PAPS, 5 mM GSH, 5 mM glycine, 5 mM taurine, 1 mM ATP, 0.4 mM CoA, 0.4 mM UDPGA, 25 µg/mL alamethicin, and 40 µM unlabeled:labeled substrate (1:1) in a final volume of a 100 µl.

1.2.3 Identification of Metabolites Generated by Hepatocyte S9 fractions

1.2.3.1 Liquid chromatography tandem mass spectrometry (LC-MS/MS) analysis

A Waters ACQUITY ultra performance liquid chromatography (UPLC) system (Waters, Milford, MA) coupled to a 4000 Q TRAP® quadrupole linear ion trap hybrid mass spectrometer (MS) with an electrospray ionization (ESI) source (Applied Biosystems, MDS Sciex, Foster City, CA) was used. Metabolite identification was performed by enhanced MS-information dependent acquisition-enhanced product ion scan (EMS-IDA-EPI) in negative ionization mode. The EMS survey scan was conducted in the mass range from 160 to 750 Da, at a 1000 Da/s scan rate followed by an enhanced resolution (ER) scan at 250 Da/s. The IDA threshold was set at 5000 counts per second (cps), above which enhanced product ion (EPI) spectrum collection is triggered from the precursor mass of that particular channel. The EPI scan rate was 4000 Da/s and the scan range was 70–750 Da. The IDA method was also employed to trigger EPI scans by analyzing MRM signals. The pMRM–IDA-EPI (predicted MRM-enhanced production scan) method used pMRM (predicted MRM) as a survey scan. The pMRM channels were generated by an Analyst script from mass-to-charge ratio of the deprotonated molecules based on predicted biotransformation pathways. A total of 114 MRM channels for predicted metabolites were created for every compound, with dwell times of 5 msec/channel and pause times of 5 msec. The same declustering potential (DP), collision energy (CE), and cell exit potential (CXP) values for every parent

compound were used for the MRM transitions of their predicted metabolites. The IDA threshold was set at a 1000 counts per second (cps), above which EPI spectra were collected from the parent mass of that particular channel. The EPI scan was operated from m/z 100 to 700 at a scan rate of 4000 amu/s with dynamic fill and CE spread of 15 eV. The total cycle time for the MRM-IDA-EPI was 2.2 sec/cycle. Metabolite identification was performed using LightSight 2.2 software by comparing MS spectrums obtained from samples after 60 min incubation with those obtained at zero-min incubations. Mixtures of 1:1 unlabeled: stable-isotopically labeled parent BA substrates were used in all incubations. Therefore, total ion chromatograms (TIC), obtained from the screening scans mentioned above, were filtered for the isotopic pattern of 1:1 abundance of ion pairs with a mass difference of 4 Da, using the elemental targeting feature in Analyst software (AB Sciex, Framingham, MA).

1.2.3.2 High resolution mass spectrometry (HRMS) analysis

HRMS analyses were performed using a LTQ-Orbitrap Elite (ThermoFisher Scientific) fitted with an electrospray ionization (ESI) source in a continuous infusion mode. Both sheath and auxiliary gases were high purity nitrogen, and the collision gas was ultra-high purity helium. Parent mass range was set at m/z 100–1000; sheath gas, 30 arbitrary units; auxiliary gas, 5 units; spray voltage, 4.5 kV; capillary temperature, 300 °C; capillary voltage, 18 V; and energy for collision-induced dissociation (CID) was set at 35 eV. MS resolution was set at 60,000 FWHM for full MS scans. Authentic parent BA standards and biosynthesized metabolites (1 µg/ml in MeOH: H_2O) were injected into the instrument via a syringe pump at 10 µl/min. The instrument was controlled by Xcalibur 1.4™ software (Thermo Fisher Scientific, CA, USA).

1.2.4 Biosynthesis and NMR-based Quantification of UDCA Metabolites

UDCA (100 µM) was incubated with the hepatocyte S9 fractions as describe above. For the biosynthesis of oxidation and sulfation metabolites, cynomolgus and

rabbit hepatocyte S9s were used, respectively. For the biosynthesis of glucuronidation and glutathione conjugates, dog hepatocyte S9 fractions were used. Reactions were performed in final volumes of 500 µl and were allowed to proceed for 60 min at 37°C. At the end of each incubation, reactions were terminated by adding 500 µl MeOH, followed by vortex-mixing and centrifugation at 16,000 g for 10 min. Supernatants were aspirated and dried down by vacuum centrifugation. Residues were dissolved in a 100 µl of MeOH:H_2O. Metabolites were separated using chromatographic conditions similar to the analytical-scale conditions described above, but the separation was carried out on HPLC column (XBridge BEH C18 5 µm, 150 × 4.6 mm) at a flow rate of one ml/min. Metabolites were fraction-collected from the HPLC column effluent, in a time-slice mode, into 12-mm test tubes. Fractions containing metabolite of interest were pooled from multiple injections, vacuum centrifuged to remove the mobile phase solvents, reconstituted in 0.4 mL of $^2H_6$-DMSO, and subsequently transferred to 5-mm NMR tubes.

Proton spectra of biosynthesized metabolites were acquired using a Burker-600 spectrometer (Billerica, MA) equipped with 5-mm CyroProbe operating at 600 MHz. Three hundred forty scans with an acquisition time of 4.5 S were collected for each spectrum. A pre-acquisition delay of 60 S was used during the data acquisition. ^{1}H NMR spectra were acquired at 30°C. The signal of the protonated portion of the deuterated solvent was arbitrarily set to 100 and used as an internal reference to normalize the integral values within each spectrum. NMR integral of a common proton, which was neither affected metabolically nor coincided with any endogenous signals, was obtained. NMR spectra of UDCA were obtained at five different concentrations (5-200 µM) and a calibration curve was constructed by plotting proton integral values against nominal concentrations. Concentrations of metabolites in collected fractions were determined using the UDCA calibration curve.

1.2.5 BAs Quantification by LC-MS/MS

BAs concentrations were measured by LC-MS/MS, as we described previously with some modifications [83, 87]. Briefly, a Waters ACQUITY ultra performance liquid chromatography (UPLC) system (Waters, Milford, MA) coupled to a 4000 Q TRAP® quadrupole linear ion trap hybrid mass spectrometer (MS) with an electrospray ionization (ESI) source (Applied Biosystems, MDS Sciex, Foster City, CA) was used. The following MS source settings were used: ion spray voltage, -4000V; temperature, 500 °C; curtain gas, 20; gas-1, 35; gas-2 35 (arbitrary units); collision gas pressure, high; Q1/Q3 resolution, unit; and interface heater, on. Mobile phase consisted of 7.5 mM ammonium bicarbonate, adjusted to pH 9.0 using ammonium hydroxide (mobile phase A), and 30% acetonitrile in methanol (mobile phase B), at a total flow rate of 0.2 ml/min. The gradient profile was held at 52.5% mobile phase B for 12.75 min, increased linearly to 68% in 0.25 min, held at 68% for 8.75 min, increased linearly to 90% in 0.25 min, held at 90% 12 for 1 min, and finally brought back to 52.5% in 0.25 min followed by 4.75 min re-equilibration (total run time of 28 min per sample). For the preparation of calibration curves, blank matrices were obtained by charcoal stripping as described previously [83, 87]. Eleven -point calibration curves were prepared by spiking 10 µl of appropriate standard solution into 100 µl stripped matrices at final concentrations ranging from 1 to 1000 ng/ml.

For preparation of plasma samples, 100 µl of plasma samples were spiked with 10 µl of IS, 1 mL of ice-cold alkaline ACN (5% NH4OH) was added, and samples were vortexed. Samples were then centrifuged at 16,000 x g for 10 min and the supernatants were aspirated, evaporated under vacuum and reconstituted in 100 µl of 50% MeOH solution. For urine, 100 µl of samples were spiked with 10 µl of IS, vortexed, and loaded onto SPE cartridges pre-conditioned with 4 ml MeOH and 4 ml H_2O and eluted with 4 ml MeOH. Eluates were then evaporated under vacuum at room temperature and

reconstituted in 100 µl of 50% MeOH solution. Ten µl of reconstituted samples were injected for analysis.

1.2.6 Calculation of BA Indices

BA profiles in plasma and urine were characterized using BA "indices" that describe the composition, hydrophobicity, metabolism of total and individual BAs as we described previously [43, 44, 136]. Briefly, the composition of individual BAs was calculated as the ratio of the concentration of individual BAs in all of their forms (amidated, unamidated, sulfated, and unsulfated) to the total concentration of BAs. The percentage of sulfation of individual BAs was calculated as the ratio of the concentration of sulfated BAs, in both the amidated and unamidated forms, to the total concentration of individual BAs in all of their forms (sulfated, unsulfated, amidated, and unamidated). The percentage of amidation of individual BAs was calculated as the ratio of the concentration of amidated BAs, in both the sulfated and unsulfated forms, to the total concentration of individual BAs in all of their forms (sulfated, unsulfated, amidated, and unamidated). In addition, percentages of amidation were divided into the percentages of BAs existing as glycine (G) vs. taurine-(T) amidates. The percentages of mono-OH BA (LCA), di-OH BAs (MDCA, UDCA, HDCA, CDCA, and DCA), and tri-OH BAs (CA, HCA, and MCA) were calculated as the ratio of the concentration of the sum of the respective BAs in all their forms to the total concentration of BAs. The ratio of primary to secondary BAs was calculated as the ratio of the sum of the concentrations of CDCA, CA, MCA, and HCA to the sum of the concentrations of DCA, LCA, UDCA, HDCA, and MDCA in all their forms. Similarly, ratio of 12α-OH: non-12α-OH was calculated as the ratio of the sum of the concentrations of DCA and CA to the sum of the concentrations of CDCA, HDCA, MCA, LCA, UDCA, HCA, and MCA in all their forms. The Hydrophobicity index (HI) of the BA pool was calculated according to the Heuman index, based on the relative contributions of the individual BAs to the total BA pool and their hydrophobicity indices [58].

1.3 Results

1.3.1 BA Profiles in Plasma

Table 1.1 shows plasma BA profiles in humans and in various animal species. The total plasma BA pool was highest in pig (31 μM) followed by rat (12 μM) and lowest (0.07 μM) in chimpanzee. In all other species, the BA pool ranged from 1-5 μM. The highest sulfation of BAs was 30-50% in human and chimpanzee followed by 5% in rabbit and it was less than 2% in all other species. Also, tri-OH BAs (CA, MCA, and HCA) were the least sulfated (for example, <5% in human), mono-OH BAs (LCA) was the most sulfated (for example, 93% in human), while di-OH BAs (UDCA, CDCA, and DCA) had an intermediate sulfation (for example, 30-60% in human) across all species studied in this manuscript. Amidation was highest (50-80%) in dog, chimpanzee, human, and CD-1 and C57/BL6 mice, while it was 10-20% in all other species. G-amidation was predominant in human, minipig, hamster, and rabbit, while it was lowest in dog and both strains of mice (<1%). In contrast, T-amidation was predominant in both strains of mice, rat, dogs, while it was lowest in minipig and rabbit (<1%). Glucuronidation was low (< 0.5%) in all species across all BAs, with dog being the highest. Also, similar to sulfation, glucuronidation was inversely proportional to the number of OH groups, with tri-OH BAs (CA, MCA, and HCA) being the lowest and mono-OH BA (LCA) being the highest glucuronidated BAs.

The percentage of mono-OH BAs (LCA) was highest in chimpanzee (52%) and rhesus monkey (26%), followed by human, cynomolgus monkey, dog, and rabbit (5-10%), while it was less than 1% in all other species. The percentage of Di-OH BAs was highest (50-75%) in human, rabbit, minipig, and both strains of monkeys and lowest (25-35%) in hamster, rat and both strains of mice. The percentage of Tri-OH BAs was highest in hamster, rat, dog and both strains of mice (50-75%), followed by monkey (25-35%), and lowest in human, chimpanzee and rabbit (5-10%). The contribution of

individual BAs to the overall composition of the plasma BA pools in the various species is shown in **Figure 1.2**. The most abundant BAs were CA (37%) in cynomolgus monkey, dog (54%), hamster (56%), and SD rat (30%); LCA (26%), DCA (23%), and CA (22%) in rhesus monkey; HCA (33%) and HDCA (57%) in minipig; CA (41-46%) and MCA (28-36%) in mice; CDCA (33%) and DCA (27%) in human; DCA in rabbit (43%); and LCA (51%) in chimpanzee.

The ratio of primary (sum of CDCA, CA, MCA and HCA) to secondary (sum of DCA, LCA, UDCA, HDCA, and MDCA) BAs was lowest in rabbit (0.05), followed by the chimpanzee (0.18) and minipig (0.59) because these species have the highest concentrations of the secondary BAs DCA, LCA, and HDCA, respectively **(Table 1.1)**. In contrast, this ratio was highest in mice (4.5) and cynomolgus monkey (3.84) because of the high concentrations of the primary BAs, CA, and MCA, respectively. CA: CDCA ratio was highest (6-15) in mice, dog, and hamster, and it was lowest in minipig and human (0.04 and 0.3). Similarly, the ratio of 12α-OH (sum of DCA and CA): non-12α-OH (sum of CDCA, HDCA, MCA, LCA, UDCA, HCA, and MCA) BAs was highest (2-4.4) in dog, hamster, and mice, while it was lowest in minipig, chimpanzee and human (0.002, 0.2, and 0.7).

HI was lowest (-0.1 to -0.2) in minipig and in both strains of mice because these species have the lowest concentrations of LCA (the most hydrophobic BA) and they have the highest concentrations of the hydrophilic BAs, MCA and HCA, respectively. In contrast, highest HI values were found in the rabbit (0.6) and rhesus monkey (0.55) because of the high concentrations of the secondary BAs, DCA, and LCA, respectively.

1.3.2 BA Profiles in Urine

Table 1.2 shows urine BA profiles in humans and in the various species**.** The total urine BA pool was highest in pig (205 μM) followed by rat and CD-1 mouse (21 μM) and was lowest (0.2-0.7 μM) in chimpanzee, monkeys, hamster, and rabbit. In all other

species, the BA pool ranged from 5 to 21 μM. The highest sulfation of BAs was 85% in human followed by 50-70% in chimpanzee, rabbit, and mice, while it was 25% in monkey and less than 10% in all other species. Amidation was highest (85%) in human and rabbit followed by 55-70% in chimpanzee, dog and mice, while it was 30% in monkey and lowest in hamster (3%). BA amidation in minipig, human, chimpanzee, rhesus monkey, and rabbit was primarily with glycine (50-80%), whereas it was primarily with taurine (55-75%) in rat, mice, and dog. Glucuronidation was low (< 0.5%) in all species across all BAs, with dogs being the highest.

The percentage of mono-OH BA (LCA) was highest in chimpanzee (30%), followed by human and rhesus monkey (10-12%), while it was less than 5% in all other species. The percentage of Di-OH BAs was highest (50-75%) in human, monkey, rabbit, and minipig and was lowest (3-7%) in dog, and mice. The percentage of Tri-OH BAs was highest in hamster, rat, dog and mice (70-95%) and was lowest in human and monkey (12-29%). The contribution of individual BAs to the overall composition of the urine BA pool is shown in **Figure 1.3**. The most abundant BAs were CA in chimpanzee (36%) and mice (66-76%); MCA (56%) in rat; MCA and CA in hamster (41 and 37%) and dog (49 and 40%); HCA (32%) and HDCA (28%) in minipig; CA (33%) and CDCA (29%) in rabbit; DCA (36%) in rhesus monkey; DCA (30%) and CA (22%) in cynomolgus monkey; and CDCA (28%) and DCA (27%) in human.

The ratio of primary to secondary BAs was lowest in monkey and human (0.5-0.8) because they have the highest concentration of the secondary BAs, DCA **(Table 1.2)**. In contrast, this ratio was highest in mice (15-18) and dog (10) because of the high concentrations of the primary BAs, CA and MCA. CA: CDCA ratio was highest (> 100) in mice followed by dog (35), rat (30), and hamster (29), while it was lowest in minipig and human (0.3-1). Similarly, the ratio of 12α-OH: non-12α-OH BAs was highest (2.2-

3.8) in hamster, and mice, while it was lowest in minipig, rat, and human (0.11, 0.15, and 0.55).

HI was lowest (-0.2 to -0.6) in mice, rat, minipig, and dog because these species have the lowest concentrations of LCA (the most hydrophobic BA) and they have the highest concentrations of the hydrophilic BAs, CA, MCA, and HCA, respectively. In contrast, highest HI values were found in the rhesus monkey (0.52) because of the high concentrations of the secondary BAs, DCA.

1.3.3 Identification of Ursodeoxycholic acid (UDCA) Metabolites Generated by Hepatocyte S9 fractions

1.3.3.1 Triple quadrupole tandem mass spectrometry

For metabolite identification, incubations of 1:1 unlabeled:stable isotopically labeled ($^2H_4$) UDCA were carried out with hepatocyte S9 fractions from 12 different species. **Table 1.4** shows optimized cofactor concentrations in our S9 fraction in vitro system to maximize assay sensitivity at relevant physiological concentrations. Thirteen metabolites of UDCA were formed and detected in the hepatocyte S9 fractions from these species **(Figure 1.4)**. Detected metabolites were assigned based on the following criteria: 1) Mass shifts of metabolites relative to parent compound, 2) metabolites should not be detected in the control sample (0 min), 3) by matching the retention times of metabolites with available authentic standards, 4) by characterizing the MS/MS fragmentation patterns from the enhanced product ion (EPI) spectra of metabolites, and 5) detections of pairs of isotopic peaks with mass difference of 4 Da due to the use of the mixture of 1:1 unlabeled:stable isotopically labeled UDCA ($^2H_4$) in the incubations. Representative EPI spectra of the UDCA metabolites generated by S9 fractions and their fragmentation patterns are shown in **Figure 1.5**.

UDCA produced three metabolites (M1, M2, and M3) at *m/z* 567 corresponding to glucuronide conjugation **(Figure 1.4 B)**. UDCA has three possible sites for

glucuronidation, two hydroxyl group at C3 and C7 (O-glucuronide) and one free carboxyl group on side chain (acyl glucuronide). Fragmentation patterns of M1 and M2 metabolites **(Figure 1.5 A)** showed sequential loss of two H_2O and one carbonate (-H_2CO_3) moieties. They also showed a fragment corresponding to the intact parent molecule at 391 m/z. Characteristic fragments (*m/z* 175 and 113) of the glucuronide moiety were also observed. In contrast, the fragmentation pattern of M3 metabolite **(Figure 1.5 B)** did not show sequential loss of two H_2O moieties or a carbonate (-H_2CO_3) moiety. However, it showed a characteristic fragment of glucuronide anion at *m/z* 193, which was not present in the EPI spectra of M1 and M2 metabolites. Collectively, these data suggest that M1 and M2 are O-glucuronide, whereas M3 is an acyl-glucuronide conjugate of UDCA. This is also supported by the longer retention time for acyl-glucuronide (M3 at 7.4 min) compared to O-glucuronides (M1:3.5 and M2:4.3 min). O-glucuronides are more polar than acyl glucuronides due to the presence of one extra free carboxyl group, which cause them to elute earlier than acyl glucuronides. However, the exact position of the O-glucuronidation, i.e. C3 vs. C7 could not be confirmed due to the identical MS/MS spectra of both metabolites and the lack of authentic standards.

Two metabolites, M4 and M5, corresponding to sulfate conjugates were observed for UDCA at retention times of 4.1 and 7.4 min, respectively **(Figure 1.4 C)**. There are two possible sites for sulfate conjugation at the hydroxyl groups at C3 and C7. Fragmentation of the deuterated ($^2H_4$) sulfate conjugates showed major fragments at *m/z* 98 and 97 for M4 and M5, respectively **(Figure 1.5 C and 1.4 E)**. The sulfate ion (*m/z* 97) is generated when the proton from the β carbon is transferred to the sulfate moiety, and the C-O bond is broken **(Figure 1.5 D)**. For the 3-O-sulfate metabolites, the proton from the β carbon is deuterated; and therefore, forms a *m/z* 98 rather than the *m/z* 97 fragment resulting from the 7-O-sulfates. These data suggest that M5 is a UDCA sulfate conjugate at the C3 position and M6 is a sulfate conjugate at the C7 position.

UDCA produced one metabolite (M6) at *m/z* 680 corresponding to a glutathione conjugate **(Figure 1.4 D)**. EPI spectra of the glutathione conjugate **(Figure 1.5 E)** showed characteristic fragments of glutathione at *m/z* 306, 272, 254, 210, 179, and 128.

Four metabolites representing single-step hydroxylation into tri-OH metabolites, (M7, M8, M9, and M10; *m/z* 407) at retention times 2.5, 4.3, 5.2 and 7.4 min, respectively, were detected **(Figure 1.4 E)**. M10 was assigned as β-muricholic acid (β-MCA) because its retention time and fragmentation pattern matched with the authentic standard of β-MCA. EPI spectra were similar between all hydroxylated metabolites (M7-M10), with a common feature of loss of two consecutive H_2O molecules **(Figure 1.5 F)**. Due to the lack of authentic standards, the positions of the hydroxyl groups of M7, M8 and M9 were not assigned at this stage.

Glycine (G) and taurine (T) amidates of UDCA were observed at *m/z* 448 (M11) and 498 (M12), respectively **(Figure 1.4 F and G)**. EPI spectra of G-UDCA **(Figure 1.5 G)** produced intact G (*m/z* 74) and [M-H-COO^-] (m/z 404) fragments. EPI spectra of T-UDCA **(Figure 1.5 H)** produced intact T (*m/z* 124) and two T fragments (m/z107 [$C_2H_3SO_3^-$] and 80 [SO_3-]). G-UDCA and T-UDCA metabolite assignments were confirmed by matching their retention times with authentic standards.

One metabolite at *m/z* 514 (M13), corresponding to the combination of mono-hydroxylation and T amidation, was observed **(Figure 4 H)**. EPI spectrum of M13 **(Figure 5 I)** showed the loss of H_2O and the production of intact T (*m/z* 124) and two T fragments at m/z of 107 [$C_2H_3SO_3^-$] and 80 [SO_3^-]. M13 was confirmed as T-MCA by matching the retention time with authentic standard.

1.3.3.2 High resolution mass spectrometry (HRMS) analysis

High resolution MS/MS was used to confirm the structural identification of the in-vitro UDCA metabolites to confirm the low-resolution triple quadrapole MS/MS data by matching the MS/MS fragmentation patterns of metabolites with BA standards. First, the

fragmentation patterns of the available authentic BA standards were characterized. Exact mass analyses of parent BA standards and their MS/MS fragments are shown in **Table 1.3**. Proposed structures of MS/MS fragments are given in **Figure 1.6**.

Tri-OH BAs (CA, HCA, α-MCA, β-MCA and ω-MCA) produced common fragments at *m/z* 405.2636, 389.2684, 387.2530, and 371.2585. However, CA can be identified among all isomeric tri-OH BAs by the presence of unique MS/MS fragments at *m/z* 363.2894, 353.2479, 345.2788, 327.2684, 325.2528, 289.2166 and, 251.2010. MCA isomers (α-MCA, β-MCA and ω-MCA) can be identified by the presence of one unique MS/MS fragment at *m/z* 369.2429. In addition, for the MCA isomers, α-MCA, and ω-MCA showed similar MS/MS spectra characterized by unique fragments at *m/z* 377.2687 and 375.2530, which were not produced by β-MCA. In contrast, HCA did not produce any unique MS/MS fragments that allow its distinction from the other tri-OH BAs.

For the di-OH isomers (UDCA, CDCA, MDCA, HDCA, DCA, and isoDCA), UDCA, CDCA, MDCA, and HDCA produced common fragments at *m/z* 389.2688, 373.2739 and 371.2583, whereas DCA and isoDCA produced different fragments at *m/z* 355.2637, 347.2950, 345.2796, 329.2846, and 327.2690. The two mono-OH BAs isomers (LCA and isoLCA) could not be distinguished and produced common fragments at *m/z* 357.2789 and 355.2635.

All G- and T-amidates produced G (*m/z* 74.2048) and T (m/z 124.0074, 106.9808, 79.9574) fragments, respectively. All S-conjugates produced a common fragment (SO_3^-) at *m/z* 96.9602.

After determining the fragmentation patterns of authentic BA standards, they were compared with the fragmentation patterns of in-vitro UDCA metabolites. The metabolites of interest were isolated from UDCA incubation with hepatocyte S9 fractions

for 60 min. Fractions collected from several injections were pooled to produce about 10 µg quantity of metabolites before MS/MS analyses. Exact mass analyses of the isolated metabolites and their MS/MS fragments are shown in **Table 1.4**. In general, the fragmentation patterns of glucuronide, sulfate, glutathione conjugates (M1-M6), and G and T-amidates (M11-M13) of UDCA were similar in both the low-resolution triple quad **(Figure 1.4)** and HRMS Orbitrap MS systems **(Table 1.4)**. In addition, M10 was assigned as β-MCA because it shared the same retention time and fragmentation pattern with the authentic standard **(Table 1.3 and Figure 1.6)**. However, fragmentation patterns of other oxidative (M7-M9) metabolites did not match with any of the available authentic standards of tri-OH BAs. Therefore, the positions of hydroxylation of M7-M9 were not assigned but they could be excluded from being CA, HCA, α-MCA, β-MCA, or ω-MCA, because their retention times did not match with that from any of these authentic standards.

1.3.4 Biosynthesis and NMR-quantification of UDCA Metabolites

Authentic standards are required for the absolute quantification of analytes using ESI-LC-MS. When authentic standards are not available, the parent drug standards are used to quantify the metabolites after adjusting their MS responses with a MS response factor (RF) from a global detector with a uniform response detector that accounts for the ratio of the metabolite/parent MS sensitivity. We used NMR to establish this MS-RF. First, metabolites are biosynthesized, separated, and isolated. UDCA metabolites were isolated from hepatocyte S9 fraction incubations by collecting fractions that contain individual chromatographic peaks from the HPLC column. Fractions collected from several injections were pooled to produce about 10 µg quantities of individual metabolites. To generate a UDCA NMR calibration curve, a unique proton signal is needed. To identify this unique proton, the ^{1}H NMR spectra of fractions collected from blank versus UDCA incubations were compared. Proton signal at 0.6 ppm was not

observed in the blank incubation and was selected as a unique proton for UDCA quantification **(Figure 1.7)**. To confirm the response uniformity between parent UDCA and its metabolites and since metabolite standards were not available, we used structural analogs of UDCA including LCA and T-UCDA to prove that various structural modifications of UDCA did not change its NMR response **(Figure 1.8)**. Therefore, it can be concluded that structural modifications due to metabolism will also not affect the signal of this proton, i.e. a uniform NMR response for parents and their metabolites. Accordingly, concentrations of metabolites in the fractions isolated from S9 fraction incubations were determined by NMR using UDCA calibration curves. **Figure 1.9** shows an example for the determination of UDCA-3-S concentration in a HPLC fraction collected from UDCA hepatocyte S9 fraction incubation. After determining their concentrations by NMR, metabolite and parent LC fractions were diluted to equal concentrations and were analyzed by LC-MS/MS. A response factor (RF), calculated as the ratio of the metabolite/parent MS signal at equal concentrations was determined. A metabolite concentration can be calculated in any in vivo or in vitro sample using a parent calibration carve after adjusting the metabolite peak area with RF. This RF approach for LC-MS/MS quantification was validated by comparing UDCA metabolite concentrations measured by this approach versus direct LC-MS/MS quantification using metabolites authentic standards for representative UDCA metabolites, for which authentic standards were available **(Figure 1.10)**. Results from both approaches were < 15% different.

1.3.5 Species Differences of BA Metabolism by Hepatocyte S9 fractions

The species differences of BA metabolism was studied for four representative BAs (LCA, UDCA, CDCA, and CA) using the optimized S9 fractions in vitro system **(Table 1.5).**

1.3.6.1 LCA

Table 1.6 shows the various metabolic pathways of LCA, UDCA, CDCA, and CA in hepatocyte S9 fractions obtained from different species. The highest sulfation of LCA was observed in chimpanzee (52%) and human (18%) and it was < 5% in all other species. Amidation was higher than 70% in all species except in dog and chimpanzee, where it was 9% and 36%, respectively. BA amidation in minipig (89%) and rabbit (65%) was primarily with G, whereas it was primarily with T in mice (70%), hamster (52%), chimpanzee (25%), rat (15%), and dog (9%). The rest of the species had similar G- vs. T- amidation rates. Oxidation was highest in rat (80%) followed by mice, hamster and rabbit (~30%), while it was 5-10% in all other species. **Table 1.7** shows the relative formation of various hydroxylated metabolites as a result of LCA oxidation. In general, and for all species, except in dog, LCA oxidation occurs at the C6 position resulting in the formation of HDCA (C6-α-OH) and MDCA (C6-β-OH). Among the hydroxylated metabolites, MDCA was predominant in rabbit, rat and mice, while HDCA was predominant in human, chimpanzee, monkey, pig, and hamster. Glucuronidation was highest in dog (75%) followed by rhesus monkey (11%), while it was < 5% in all other species. Glutathione conjugation (< 5%) was a minor pathway in all species.

1.3.6.2 UDCA

The highest sulfation of UDCA was observed in chimpanzee and human (20-27%) followed by hamster and rabbit (9-12%), while it was < 1% in all other species. Amidation was highest (95%) in minipig, while it was lowest in the dog (20%). BA amidation in minipig (91%) and rabbit (62%) was primarily with G, whereas it was primarily with T in CD-1 and C57/BL6 mouse (>70%), rat (~40%), hamster (50%), dog (19%), and chimpanzee (44%). The rest of the species had similar G- vs. T- amidation rates. Oxidation was highest in rat (60%), while it was lowest (5-10%) in human and minipig. In general, UDCA oxidation occurs primarily at the C6-β position in chimpanzee, pig, hamster, rat, and mice, which lead to the formation of β-MCA (**Table**

1.7). The remaining species hydroxylation primarily occurs on other positions that we did not identify. Glucuronidation was highest in dog (56%), while it was < 5% in all other species. Glutathione conjugation (< 5%) was a minor pathway in all species.

1.3.6.3 CDCA

The highest sulfation of CDCA was observed in human, chimpanzee, and rabbit (14-22%) followed by hamster, minipig, and rhesus monkey (5-8%), while it was < 3% in all other species. Amidation was highest (70-75%) in minipig and cynomolgus monkey, and it was lowest in the dog and rat (22-25%). BA amidation in minipig (65%) and rabbit (62%) was primarily with G, whereas it was primarily with T in mice (50-60%), chimpanzee (44%), rat (25%), and dog (19%). The rest of the species had similar G- vs. T- amidation rates. The highest oxidation was observed in rat (70%) followed by mice and dog (40-50%), while it was lowest (12%) in human. CDCA oxidation occurred primarily at the C12-α position (CA) for human, chimpanzee, monkey, and dog, while it was primarily at the C6-β position (α-MCA) for rat and mice and at the C6-α position (HCA) in pig (**Table 1.7**). Glucuronidation was highest in the dog (27%), while it was < 3% in all other species. Glutathione conjugation (< 5%) was a minor pathway in all species.

1.3.6.4 CA

The highest sulfation of CA was observed in human (5%) and it was < 5% in all other species. Amidation was 90-95% in all species except in dog, rat, and mice it was 80%. BA amidation in minipig (94%) and rabbit (95%) was primarily with G, whereas it was primarily with T in mice (80%), dog (80%), human (60%), and chimpanzee (62%). The rest of the species had similar G- vs. T- amidation rates. Oxidation was highest in rat, mice, and hamster (10-20%), while it was <5% in all other species. Oxidation of CA results in the formation of unidentified tetra-OH BAs. Glucuronidation was highest in dog

(10%), while it was < 2% in all other species. Glutathione conjugation (< 5%) was a minor pathway in all species.

1.4 Discussion

Because of their hepatotoxicity, intrahepatic accumulation of BAs can worsen and contribute to the pathogenesis of liver diseases [106, 107]. Similar to liver diseases, BA accumulation due to alterations of various aspects of their homeostasis by some drugs, is proposed to be one of the major mechanisms underlying DILI [108, 109]. However, currently used in vitro and in vivo preclinical models of BA homeostasis fail to predict DILI in humans [137]. The marked differences in BA composition and homeostasis between preclinical safety models and humans may play a major role in the poor prediction of DILI at earlier stages of drug discovery and development. Major species differences in the susceptibility to BA-induced hepatotoxicity were previously reported, which may be explained by species differences in BA homeostasis. For example, CDCA produces severe hepatic toxicity in species that lack BA sulfation capabilities including rhesus monkeys [122, 123], rabbits [124], guinea pigs [125], and dogs [126]. However, in humans and chimpanzees, where sulfation is a primary metabolic pathway of BAs, CDCA administration is not associated with hepatic injury [122, 127-130]. Collectively, strong evidence exists that species susceptibility to BA toxicity may be determined by their capability to efficiently metabolize BAs. Therefore, this work aimed to quantify the species differences in BA metabolism in vitro and in vivo to identify preclinical species that are most similar to humans in regards to BA metabolism and therefore are more relevant to in vivo testing of DILI. Furthermore, we developed an in vitro model that represents the in vivo metabolism of BAs in humans and in various animal species.

1.4.1 In-vivo BA Profile

We observed major species differences in multiple aspects of the plasma BA profiles. Similar to previous data our data showed that highest total concentrations of plasma BAs were observed in rat and pig [86, 138-140] and that G-amidation was predominant in human and pig [86, 139, 141, 142], while T-amidation was predominant in rat, mice, and dog [91, 135, 138, 142-146]. Furthermore, in-line with previous data we found that the BA pool in plasma was primarily composed of Di-OH BAs in human, while tri-OH BAs were the main components in rat, mice, and hamster **(Table 1.1)**.

BA hydrophobicity is influenced by both the BA nucleus and the side chain structures [54]. Amidation increases the acidity of unconjugated BAs, where pKa is reduced from about 5.5 for the unamidated BAs to 4.5 and 1.5 for those with G- and T-amidation, respectively [51]. This increases BA ionization and solubility at physiological pH. There is an inverse relationship between the number of OH groups present on steroid nucleus and lipophilicity. The mono-OH BA (LCA) is more hydrophobic than di-OH BAs (CDCA, and DCA), which in turn are more hydrophobic than tri-OH BAs (CA, MCA, and HCA). Hydrophobicity is also determined by the position and stereochemistry of hydroxyl groups. For example, the 7β, 6α, and 6β- OH substitutions result in the formation of more hydrophilic BAs. These hydroxyl groups are equatorial to the plane of the steroid ring system and they are more resistant to the loss of associated water than is a 7α-hydroxyl group, causing these hydroxyl groups to be intrinsically more hydrophilic [55, 56]. Therefore, UDCA (contains 7β-OH) is the most hydrophilic among all other di-OH BAs, and MCA (contains 6β-OH) and HCA (contains 6α-OH) are more hydrophilic than other tri-OH BAs such as CA (contains 12α-OH) [56, 58]. The term hydrophobicity index (HI) was introduced to describe the hydrophilic- hydrophobic balance of BAs based on their relative retention time and capacity factor in C18 reversed-phase HPLC. HI of BAs ranges from +1.46 for the most hydrophobic BA (LCA) to -0.94 for the most hydrophilic BA (T-UDCA) [58, 59, 147]. HI of individual BAs ranged from +1.46 for the

hydrophobic BA (LCA) to -0.94 for the hydrophilic BA (T-UDCA). The lower the composite HI value of the overall BA pool in any species, the higher the concentrations of the more hydrophilic BAs and the less cytotoxic is the BA pool [94, 148, 149].

We observed that HI was lowest in minipig and mice because more than 90% of the plasma BA pool in minipig was consisted of hydrophilic BAs (HDCA and HCA), while the hydrophobic BA, LCA, comprised less than 1% of the plasma BA pool **(Figure 1.2)**. Similarly, in mice, the hydrophilic BAs (MCA and CA) constituted 75% of the total BA pool, while LCA comprised less than 1% **(Figure 1.2)**. Furthermore, in mice 70-85% of the total BA pool was conjugated with taurine, which is more hydrophilic than G-amidated or unamidated BAs **(Table 1.1)**. In contrast, higher HI values were observed for rhesus monkey and rabbit, primarily due to higher LCA composition (26%) in rhesus monkey and higher DCA composition (43%) in rabbit **(Figure 1.2)**. This is in accordance with previous reports, where composite HI for mice and pigs ranged from -0.37 to -0.05 in different matrices including plasma [86, 139, 141, 150], liver [139, 151], and bile [135, 152-154], while it was 0.45 for rabbit [155-157].

In general, BA toxicity is highly correlated with hydrophobicity, where the most hydrophobic BAs, LCA and DCA, are more cytotoxic than the more hydrophilic BAs, CA, UDCA, MCA, and HCA [158-160]. Therefore, mice [131] and rats [132] are more resistant to LCA and CDCA hepatotoxicity due to efficient BA hydroxylation and taurine amidation compared to humans [97, 133-135]. LCA is also hepatotoxic in rabbits, a species in which the toxic BA, DCA, is dominant and it lacks both BA sulfation and hydroxylation capabilities [84, 124, 152].

Most of the previous reports on BA profiling in various species did not include sulfated BAs because of the challenges associated with their analysis. In accordance with previous reports, we found sulfation to be a minor pathway of BA metabolism in rats and mice **(Table 1.1)**. No to very small percentages of exogenous doses of LCA [132,

161], DCA [162], CDCA, or CA [163, 164] were sulfated in rats and mice. Furthermore, less than 5% of plasma BAs were detected in the sulfated form in rats and mice [87, 151, 165]. In baboons [129, 166] and rabbits [124] less than 10% of CDCA and LCA exogenous doses were sulfated, and 15% was sulfated in rhesus monkey [95, 122]. Also, less than 1% of plasma BAs are present in the sulfate form in cat [90] and hamster [167]. In contrast, we found sulfation to be the highest in human and chimpanzee. Similarly, it was previously reported that 63% of administered LCA was sulfated in chimpanzee and human [95, 168]. Among the individual BAs, sulfation was highest in LCA, followed by di-OH-BAs, and lowest in CA, which is consistent with previous data [169-175].

Lowest ratios of primary to secondary BAs were observed in rabbit followed by chimpanzee and minipig **(Table 1.1)**. Secondary BAs are produced in the intestine as a result of bacterial biotransformation of primary BAs, including deamidation, dehydroxylation, epimerization, dehydrogenation, and desulfation [6, 24]. Rabbit has a large intestinal lumen, full of anaerobic bacteria, and the prolonged retention of colonic contents provide ample opportunity for secondary BAs to be formed and absorbed [84] which results in extensive conversion into secondary BAs [155]. Furthermore, coprophagy causes recirculation of secondary BAs, which increases their systemic concentrations [176, 177] in minpig and chimpanzee. This is in agreement with previous reports where lowest primary: secondary BA ratios were observed in rabbit (1.1 fold [155]) and pig (1.2 fold [139, 141]), while it was highest in mice (2.6-8.6 fold [86, 145, 150]), rat (2.1-7 fold [86, 138, 146]), and hamster (5.4 fold [155]).

CYP8B1 catalyzes 12α-hydroxylation of CDCA to CA and the CA: CDCA ratio or the ratio 12α-BAs (sum of DCA and CA) to non-12α BAs (sum of CDCA, HDCA, MDCA, LCA, UDCA, HCA, and MCA) are used as probes for CYP8B1 activity [178, 179]. We observed that both ratios were highest in mice, dog, and hamster, and were lowest in

human, chimpanzee, and pig. This is in line with previous reports, where CA: CDCA ratio was in the range of 9 to 28 in mice [86, 135, 145, 150], 5.1 to 6.2 in dog [91, 144] and 5.9 in hamster [155]. Similarly, 12α: non-12α BAs ratio were high (6 - 7.6) in dog [91, 144] and hamster [155]. In contrast, CA: CDCA ratio was low (0.3 - 0.6) in human [86, 91, 142, 180-185] and 0.024 in pig [139, 141]. Similarly, 12α-OH: non-12α-OH BAs ratio was 0.7, 0.4, and 0.004 in human [86, 91, 142, 180-185], pig [139, 141], and rat [86, 138, 141, 143, 146], respectively.

In general, the absolute total concentration of BAs in urine was higher than plasma in all species except monkeys, hamster, and rabbit. However, urine BAs showed similar patterns to these in plasma. For example, and similar to plasma, highest total BA concentration in urine was observed in minipig, while it was lowest in chimpanzee. In addition, amidation with glycine in urine was predominant over taurine in minipig, human, chimpanzee, rhesus monkey, and rabbit, whereas it was primarily with taurine in rat, mice, and dog. This is in agreement with previous reports [163, 186, 187], which showed 65-95% of urinary BAs are conjugated with glycine in human, while it was conjugated with taurine in mice and rat. However, in urine percentage amidation in urine was higher compared to plasma.

The percentage of BAs excreted in the sulfated form in urine was more than that in plasma across all species. For example, in human, 85% of urinary BAs and were sulfated, compared to 32% in plasma, indicating the role of sulfation in enhancing the urinary excretion of BAs. However, species that do not sulfate BA efficiently, had <5% of their urinary BAs in the sulfated form, which was also shown previously [135, 188-190]. Similar to plasma, the percentage of BAs present in the sulfated form was inversely proportional to the number of OH group, where 99% of LCA, 97-98% of UDCA, CDCA and DCA, and 55% of CA were sulfated in human urine. Previous reports for the % sulfation of BAs varied markedly, where 50–100% for LCA, 13–100% for UDCA, 86–

100% for CDCA, 56–100% for DCA, and 1.2–59% for CA in human urine were reported [169-171, 191, 192].

Similar to plasma the highest percentage of mono-OH BAs was observed in chimpanzee, the percentage of Di-OH BAs was highest in human, monkey, rabbit, and minipig, while the percentage of Tri-OH BA was highest in hamster, rat, dog, and mice. In general, the percentage of tri-OH BAs in urine (12-94%) was higher than that in plasma (4-75%) across all species **(Table 1.1 and 1.2)**, while the percentage of mono-OH BAs was lower in urine (0.01 to 19%) compared to plasma (0.06 to 52%), also indicating the role of hydroxylation in enhancing the urinary excretion of BAs.

The ratios of primary to secondary BAs, CA: CDCA, and 12α-OH-BAs: non-12α-OH-BAs were higher in urine compared to plasma due to the higher concentrations of primary and 12α-OH-BAs in urine compared to plasma across all species except human and monkey. For example, 95% and 86% of plasma BAs were secondary BAs in rabbits and chimpanzees, respectively, while in urine it was BAs were 36% and 51% in the same species. This is expected due to the relatively higher hydrophilicity and therefore urinary excretion of these BAs [151, 159, 193, 194].

Collectively, the urinary BA pool was more hydrophilic than the plasma BA pool across all species. This was due to the presence of more tri-OH, amidated, sulfated, and primary BAs, in urine compared to plasma. This can also be demonstrated using the HI values, where it was 5-10 folds lower in urine than plasma across all species except in minipig, hamster, and rhesus monkey where HI was similar in both urine and plasma.

1.4.2 Literature Summary of BA Profiles in Different Species

Table 1.8 shows a literature summary of plasma BA profiles in different species. Data reported from different laboratories are extremely variable for the same species, which is expected due to the variability in the analytical techniques and more

importantly due to the high inter-and intra-variability of BAs associated with feeding status, gender, age, etc. [43]. However, trends can be depicted regarding the species differences of the plasma BA profiles and the contributions of the various metabolic pathways. Total plasma BA pool was highest in cow (93 μM) followed by rat (3.6-38 μM) and pig (6.6-31 μM). In all other species, the BA pool ranged from 1-10 μM. BA amidation in pig and human was primarily with glycine whereas it was primarily with taurine in rat, mice, dog, and horse. Cow plasma showed similar glycine to taurine amidation. LCA is a minor BA (~1%) in the plasma of all species except in humans, where it ranged between 0.5 and 8%. The BA pool in plasma was primarily composed of di-OH BAs in human and horse (65-85%), while tri-OH BAs were the main components in rat, mice, hamster, and cow (50-90%). The most abundant BAs were CDCA in human (29-75%) and horse (68%), DCA (44%) and CA (45%) in rabbit, HDCA (57%) in pig, and CA (60-84%) in dog, hamster, and cow. Also, CA (14-63%) and MCA (13-59%) were the major BAs in rat and mouse. The ratio of primary to secondary BAs was highest in horse (15 fold), cow (6.5 fold), hamster (5.4 fold), mice (2.6-8.6 fold), and rat (2.1-17 fold), while it was lowest in rabbit (1.1 fold), human (0.74-1.9 fold), and pig (1.26 fold). CA: CDCA ratio was highest (9-31) in mice and cow followed by dog (5.1-6.2), rabbit (6.3), and hamster (5.9), and it was lowest in pig (0.024) and human (0.3-0.6). Similarly, 12α: non-12α BAs ratio was highest (27) in cow followed by dog (6-7) and hamster (7.6) and it was lowest in pig (0.004). HI was low in mice, pig and rat, while it was high in human, cow, and horse.

Table 1.9 shows a literature summary of biliary BA profiles of different species. Total BA pool in bile was highest in rabbit (72-358 mM) followed by pig (35-208 mM) and hamster (52-133 mM), while it was lowest in rat (16-25 mM). Similar to plasma, BA amidation in pig, human, hamster, and rabbit was primarily with glycine whereas it was primarily with taurine in rat and mice. The percentage of mono-OH BAs (LCA) was

highest 22% in cat, while it was less than 5% in all other species except in hamster it was 1-15%. The percentage of Di-OH BA was highest (82-91%) in rabbit followed by 50-84% in pig, while it was lowest in mouse (2.5%) and cat (15%). Tri-OH BAs was highest (72-86%) in rat and mice, while it was lowest (3-10%) in rabbit. The most abundant BAs were CDCA in human (46%), while it was CA (40-70%) in mouse, rat, hamster, and cat; it was DCA (80-89%) in rabbit and HDCA (55%) in pig. The ratio of primary to secondary BAs was lowest in rabbit (0.03-0.1) and human (0.5-0.8), while it was highest in mice (8-45) and rat (5-9). CA: CDCA ratio was highest (80) in mice followed by cat (14), rat (5.3-10), and rabbit (6.7), while it was lowest in human (0.75). 12α: non-12α BAs ratio was highest (50-250) in rabbit and it was lowest in human (0.91). HI was low in mice, pig and rat, while it was high in human and hamster.

Table 1.10 shows a literature summary of liver BA profiles of different species. Total BA pool in liver was highest (150-226 μM) in mice and hamster, while it was lowest in bovine (2.54 μM). The percentage of mono-OH BAs (LCA) was highest 7% in pig, while it was less than 2% in all other species. The percentage of Di-OH BA was highest (89%) in pig followed by rat (50-64%) and hamster (32%), while it was lowest (6-11%) in mouse and bovine. Tri-OH BAs was highest (90%) in mice and bovine followed by hamster (68%) and rat (35-49%), while it was lowest (6.4%) in pig. The most abundant BAs were MCA (50%) in mice, CA in bovine (94%), hamster (67%), and rat (50%) and HDCA in pig (47%). The ratio of primary to secondary BAs was highest (10-30) in mice, hamster and bovine, while it was lowest (0.5-1.5) in pig and rat. CA:CDCA ratio was highest (20-40) in mice and bovine, while it was lowest (0.29) in pig. 12α: non-12α BAs ratio was highest (46) in bovine and it was lowest in pig (0.22). HI was low in mice and rat, while it was high in hamster, pig, and bovine.

1.4.3 Biosynthesis of UDCA Metabolites and Quantification Using NMR

LC-MS is the method of choice for quantitative analysis due to its superior sensitivity, selectivity, and speed. In LC-MS, analytes are ionized in the ion source, before mass-separation by the MS analyzer. Atmospheric pressure ionization (API) is one of the most common ionization sources in mass spectrometry because it allows direct coupling of the LC flow into the MS system. Electrospray ionization is a subtype of API that utilizes a high-electric field and high temperature to evaporate and produce charged droplets from sprayed solution. However, due to differences in ionization efficiencies, analytes at equal concentrations can produce different MS responses [195-197]. Therefore, authentic standards are required for the absolute quantification of analytes using ESI-LC-MS. Although reference standards are available for the parent drugs, it is usually difficult, time consuming, and expensive to produce authentic standards for the metabolites. Hence, it is unlikely to have authentic standards for metabolites available in early stages of drug discovery and development to facilitate their absolute quantification.

When authentic standards are not available, the parent drug standards are used to quantify the metabolites after adjusting with a response factor (RF) that accounts for the ratio of the metabolite/parent MS sensitivity. To establish this RF without metabolite authentic standards, a universal detector, which response is independent of chemical structure is needed. Several universal detection techniques such as nanospray ionization-mass spectrometry (NSI-MS) [198, 199], chemiluminescence nitrogen detection (CLND) [200-202], evaporative light scattering detection (ELSD) [203, 204], accelerator mass spectrometry (AMS) [205], charged aerosol detector (CAD) [206], radiometric detection [207], and ultraviolet detection (UV) [208] and nuclear magnetic resonance (NMR) detection [209-211] can be used for this purpose. NSI-MS is a sensitive technique and it utilizes low LC flow rates and small sample volume. However, because of the complexity of operation and lack of reproducibility, NSI has not been

used extensively [199]. CLND is coupled with LC flow for high throughput analysis to produce a uniform response for most analytes, regardless of their physical and chemical properties. However, CLND is limited to nitrogen-containing compounds and all LC mobile-phase components must be free of nitrogen to keep baseline noise to a minimum. Furthermore, it requires longer method run time because endogenous nitrogen containing compounds should be separated from analytes [200-202]. ELSD is used as an alternative to UV detection for non-UV absorbing compounds and it is compatible with gradient elution. However, this technique is less sensitive than UV and it does not have robust linear responses [204, 212]. Advantages of AMS are the much greater sensitivity of the measurement and sample size is thus typically 1000 times smaller. The major limitation of AMS is the cost of instrumentation, which makes it of limited availability [205]. CAD offers a universal response for diverse structures with low nanograms sensitivity. However, changes in the solvent composition in gradient elution used for the separation of metabolites affect the uniform CAD response [206]. UV and fluorescence are widely available detection techniques. However they can only be used if the metabolites maintain the parent chromophore intact, i.e. no modification of the parent chromophore as a result of metabolism [208].

Among all the universal detectors, NMR is the most commonly used for metabolite quantification, when authentic standards are not available [209-211]. NMR requires the separation and isolation of metabolites, which was accomplished by the fraction collection of metabolites, generated by hepatocyte biosynthesis, after their chromatographic separation. Concentrations of biosynthesized metabolites in these collected fractions were determined by NMR analyses using parent drug calibration curves. Metabolites and parent drugs are then injected in LC-MS to calculate RF that accounts for the ratio of the metabolite/parent MS sensitivity.

To quantify UDCA metabolites, we isolated these metabolites from hepatocyte S9 fraction incubations using fraction collections of the HPLC column effluents. To generate a UDCA NMR calibration curve, a unique proton signal, which does not exist in any of the endogenous components of the samples and is not modified by metabolism is needed. Therefore, this unique proton should have a uniform response for the parent and its metabolites should not produce any response in blank S9 fraction incubations, and it should not be affected by metabolism. Proton signal at 0.6 ppm **(Figure 1.8)** was identified as unique proton for quantification and its response for structurally different compounds was uniform **(Figure 1.9)**. The concentrations of metabolites in the fractions isolated from S9 incubations were determined using UDCA calibration curves. After determining their concentrations by NMR, the metabolites and parent LC fractions were diluted to equal concentrations and were injected in LC-MS/MS. A response factor (RF), calculated as the ratio of the metabolite/parent MS signal at equal concentration was determined. A metabolite concentration can be calculated in any in vivo or in vitro sample using a parent calibration curve after adjusting the metabolite peak area with RF **(Figure 1.10)**. This RF approach for LC-MS/MS quantification was validated by comparing UDCA metabolite concentrations measured by this approach versus direct LC-MS/MS quantification using metabolites authentic standards for representative UDCA metabolites, for which authentic standards were available. Using this combination of NMR and LC-MS/MS, we were able to detect and quantify BA metabolites from all major and minor pathways known to be involved in BA metabolism in the various species including sulfation, amidation, glucuronidation, and hydroxylation.

1.4.4 Optimization of Hepatocyte S9 Incubation Conditions

Various in vitro systems including hepatocyte microsomes, cytosol fractions, S9 fractions, intact hepatocytes, and recombinant metabolizing enzymes are used to characterize biotransformation of compounds [213]. Hepatocyte S9 fractions offer

unique advantages among these systems including capability to study both phase I and phase II metabolism, feasibility to study individual, gender-, and species-specific biotransformation, and affordability. Hepatocyte S9 fractions often require supplementation with exogenous cofactors for the various metabolic pathways including oxidation, glucuronidation, sulfation, glutathione conjugation, and amidation at physiological concentrations. Previous in vitro systems were always supplemented with cofactors at more than 10-fold higher than physiological concentrations. Therefore, we optimized cofactor concentrations in our S9 fraction in vitro system to maximize assay sensitivity at relevant physiological concentrations **(Table 1.5).** This optimized S9 in vitro system was subsequently used to study the species differences in metabolism of BAs metabolism.

1.4.5 Species Differences in BA Metabolism by Hepatocyte S9 fractions

Species differences in BA metabolism was studied for four BAs (LCA, UDCA, CDCA, and CA) using optimized hepatocyte S9 fractions in vitro system. Overall data from our in-vitro system showed that sulfation of BAs was highest in human and chimpanzee followed by rabbit and hamster, and it was lowest in all other species, for all four BAs (LCA, UDCA, CDCA, and CA). Previous in-vitro studies also showed low sulfation affinity in rodents. In rat primary hepatocytes, very low [214, 215] or no [216] BA sulfation activity was detected. Furthermore, sulfation of LCA by rat liver was shown to be more than a 100-fold less than that of humans [217]. In addition, rat and hamster sulfotransferase has lower affinity for BAs compared with human [218, 219]. Also, our current data showed that the tri-OH BA (CA) had the lowest sulfation, while LCA had the highest sulfation among all tested BAs, which agreed with previous reports, where K_m for LCA, CDCA and CA sulfation by human liver sulfotransferase was 2.5, 25, 71 μM [218] and sulfation activity for G/T-LCA was 4-5 times higher than G/T-CDCA by rat sulfotransferase [219]. Similarly, we have also previously reported that the K_m of LCA,

DCA, UDCA, and CDCA sulfation by SULT2A1 were 2.0, 8.9, 12.9, and 15.7 μM, respectively, whereas, the K_m of CA could not be determined as no CA-S formation was detected [174]. A common observation among all these studies is that the extent of sulfation is inversely related to the hydrophobicity or the number of hydroxyl groups of BA species, with mono-OH BA species (LCA) being almost 100% sulfated, and tri-OH BAs showing the lowest sulfation. These results indicate that sulfation acts as a protective mechanism for detoxifying the more toxic BAs such as LCA [6]. We also found species differences in the position of BA sulfation, where sulfation was primarily at C3 in human, chimpanzee, monkey, pig, and rabbit, while it was primarily at C7 in mice and hamster.

Amidation was the major pathway of all four BAs and across all species, but with different preferences toward G vs. T amidation. Amidation was primarily with glycine in minipig and rabbit, primarily with taurine in human, chimpanzee, dog, hamster, rat, and mice, while it was similar all other species. Also, CA had the highest G or T amidation across all species.

Overall, oxidation was highest in rat and mice followed by hamster, while it was lowest in human, chimpanzee, and minipig. Also, CA had the lowest oxidation among all BAs across all species. In general, oxidation was predominant at the 6-β position in rat and mice, while it was at the 6-α position in pig, and at the 12-α position in human, chimpanzee, monkey, and dog. Previous reports showed 6-β hydroxylation of LCA and CDCA to MDCA and α-MCA, respectively, by rat liver microsomes and hepatocytes [220, 221]. Also 6-α hydroxylation of LCA and T-LCA to HDCA [222] and T-HDCA [223, 224] was minimal compared to12-α hydroxylation of CDCA into CA [225].

Glucuronidation was highest in dog, while it was minor pathway in all other species. Acyl glucuronidation was predominant in all species except in pig and rabbit, where it was primarily hydroxyl glucuronidation. Also, similar to sulfation,

glucuronidation was inversely proportional to the number of OH groups, with CA being the lowest and LCA being the highest glucuronidated BAs across all species. This is in-line with previous reports which showed glucuronidation of LCA was 8-9 times higher than CDCA and 2 times higher than DCA and UDCA by rat liver glucuronyltransferase. Furthermore, affinity (k_m) for glucuronidation by human liver microsomes was highest for LCA (0.019 μM) followed by DCA (0.11 μM) and UDCA (0.29 μM) [226, 227]. Glutathione conjugation was minor for all BAs across all species. This is in-line with previous in-vivo reports where only 0.02% of GSH conjugates was observed in rat bile [228, 229].

1.4.6 In-vivo and In-vitro Correlation

We compared data obtained from our in vitro system vs. in vivo plasma BA profiles on the contributions of the different metabolic pathways across various species. For sulfation, the extent of in-vivo sulfation was higher than that in-vitro across all species for all BAs. For example, in-vivo sulfation of LCA in plasma was 91-93%, whereas it was 18-52% in our in-vitro system for both human and chimpanzee. However, both in-vivo and in-vitro data showed that sulfation of BAs was highest in human and chimpanzee followed by rabbit, and hamster, while it was very low for all other species across all BAs. In addition, both sets of data showed that the extent of sulfation of individual BAs was inversely proportional to the number of OH groups, with the tri-OH BA (CA) is the least sulfated vs. the mono OH BA (LCA) is the most sulfated.

There was a dissociation between the extent of amidation in vivo vs. in vitro of total and individual BAs for both monkey species, minipig, hamster, rabbit, and rat, where extent of amidation was markedly higher in vitro (75-95%) vs. in vivo (10-30%). In contrast, extent of amidation was lower in vitro compared to in vivo for dog, chimpanzee, and mice. The rate determining step in determining extent of amidation by G and T is not solely determined by the affinity of BAs to the bile acid-coenzyme A: amino acid N-

acyltransferase (BAT) enzyme, but it is also depended on the intracellular availability of G and T in peroxisomes [7, 10, 230, 231]. Amidation of BAs with T and G via BAT takes place in the peroxisomes. There are known species differences in the intra-peroxisomal concentrations of T and G, possibly due to species differences in the peroxisomal synthesis of glycine catalyzed by alanine:glyoxylate aminotransferase (AGT), which convert glyoxylate to glycine [10, 232]. Since this is not a cellular system, our S9 fraction in vitro system is not expected to capture the effects of intra-peroxisome concentrations of G and T. However, this in-vitro system was still predictive of in vivo data in terms of comparing the contribution of amidation to BA metabolism between the various species, where amidation was the highest in human, chimpanzee, and mice, and lowest in rats in both in vitro and in vivo systems. In addition, both sets of data showed G-amidation was predominant in minipig and rabbit, while T-amidation was predominant in dog, rat, and mice across all BAs.

Among the different in-vitro oxidative metabolites C6-β oxidation was highest in rat and mice and it was lowest in human and chimpanzee. In agreement with the in vitro data, MCA, a BA with a C6-β OH group, was highest in rat and mice (22-36%) and lowest in human and chimpanzee (<1%). In-vitro, oxidation at the C6-α position was predominant in pig. Similarly, HCA, a C6-α-OH BA, and its metabolite (HDCA) constituted 90% of the BA pool in pig plasma. In-vitro, oxidation at the C12-α position was predominant in hamster and rabbit. Similarly, CA and DCA, both are BAs with an OH group on the C12-α position, represent 70% and 50% of the BA pool in hamster and rabbit plasma, respectively. Therefore, both in vitro and in vivo data showed that hydroxylation on the C6-α and C6-β positions are primary pathways that produce the most hydrophilic and least toxic BAs, HCA in pig and MCA in rat and mice, respectively.

For glucuronidation, both sets of data showed glucuronidation was a minor pathway in all species across all BAs, except in dog where glucuronidation was

detectable in vivo and it was also the highest in-vitro. In addition, similar to sulfation, both sets of data showed that the extent of glucuronidation of individual BAs is inversely proportional to the number of OH groups, with the tri-OH BA (CA) is the least glucuronidated, while the mono OH BA (LCA) is the most glucuronidated.

1.5 Conclusions

There is a major gap in our knowledge regarding the differences in BA metabolism between preclinical species used in drug safety testing and humans, which prevents extrapolation of preclinical safety data from the various in-vivo and in-vitro hepatotoxicity models. In this study, we filled this gap by quantifying and comparing the in-vivo plasma BA profiles and of the in-vitro BA metabolism across various species.

In summary, plasma BA profiles showed that only two species (human and chimpanzee) could efficiently sulfate BAs. BAs were preferentially amidated with glycine in human, minipig, hamster, and rabbit, while it was primarily amidated with taurine in mice, rat, and dogs. Composition of BAs consisted primarily of tri-OH BAs in hamster, rat, dog, and mice, di-OH BAs in human, rabbit, and minipig. While it primarily consisted of mono-OH BA (LCA) in chimpanzee. As a results, plasma BA profiles comprised primarily hydrophilic and less toxic BAs (CA, MCA, HCA, and HDCA) in mice, rat, pig, and hamster, while it primarily comprised hydrophobic and more toxic BAs (DCA, CDCA) in human, and rabbit, and chimpanzee. Glucuronidation and amidation were minor pathways in all species

In-vitro, sulfation predominated in human and chimpanzee, while oxidation predominated in rat, mice, rabbit, and hamster. Species differences were also observed in the position of sulfation and oxidation, where C6-β oxidation was predominant in rat and mice, while it was at C6-α position in pig. For sulfation 3-O-sulfate was predominant in human and chimpanzee, while rodents and monkeys showed 3-O- and 7-O- sulfates. Amidation was the major metabolic pathway in all species. G-amidation was

predominant in minipig and rabbit, while T-amidation was predominant in dog, rat, and mice. Glucuronidation and glutathione conjugation were minor pathways in all species, except dog.

The absolute extent of metabolism by the various pathways was different between the in-vitro and in-vivo data. For example, sulfation and oxidation were lower in in-vitro vs. in-vivo across all species for all BAs whereas, extent of amidation was higher in monkeys, minipig, hamster, rabbit, and rat and lower in dog, chimpanzee, and mice in-vitro compared to in-vivo. However, the trends and the patterns of relative contributions of the various metabolic pathways in vivo were preserved using our in vitro system. For sulfation, both in-vivo and in-vitro data showed that human and chimpanzee were the only species that efficiently sulfate BAs. Amidation was the highest in human, chimpanzee, and mice and lowest in rats in both in vitro and in vivo systems. In addition, both sets of data showed G-amidation was predominant in minipig and rabbit, while T-amidation was predominant in dog, rat, and mice across all BAs. Similarly, both sets of data showed C6-α and C6-β positions were the primary position of oxidation that produces the most hydrophilic and least toxic HCA in pig and MCA in rat and mice, respectively. Finally, both sets of data showed that glucuronidation and glutathione conjugation were minor pathways in all species across all BAs. Therefore, our hepatocyte S9 fraction in vitro system can reliability predict the in vivo metabolism of BAs, and could be used for the early screening of the effect of compounds on BA homeostasis as a part of the screening for DILI.

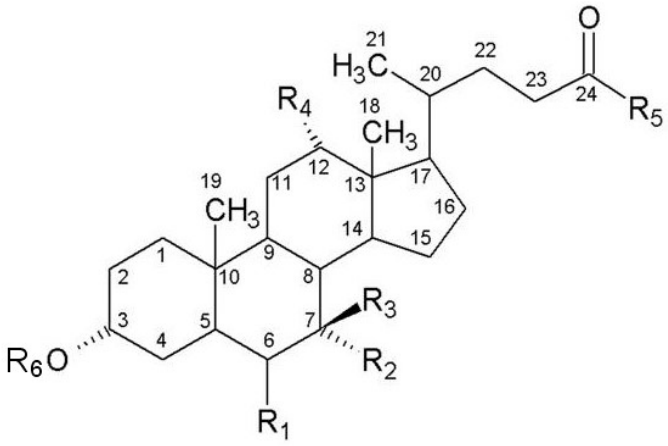

Bile acid	R1	R2	R3	R4
Tri-OH BAs				
Cholic acid (CA)	H	OH	H	OH
α-Muricholic acid (α-MCA)	β-OH	OH	H	H
β-Muricholic acid (β-MCA)	β-OH	H	OH	H
ω- Muricholic acid (ω-MCA)	α-OH	H	OH	
Hyocholic acid (HCA)	α-OH	OH	H	H
Di-OH BAs				
Chenodeoxycholic acid (CDCA)	H	OH	H	H
Deoxycholic acid (DCA)	H	H	H	OH
Ursodeoxycholic acid (UDCA)	H	H	OH	H
Mono-OH BAs				
Lithocholic acid (LCA)	H	H	H	H
	R5			
Unamidated BAs	OH			
Glycine-amidated BAs (G-BAs)	NH_2CH_2COOH			
Taurine-amidated BAs (T-BAs)	$NH_2CH_2CH_2SO_3H$			
	R6			
Unsulfated BAs	H			
Sulfated BAs (S-BAs)	SO_3H			

Figure 1.1 Chemical structures of major BAs and their glycine (G), taurine (T), and sulfate (S) conjugates.

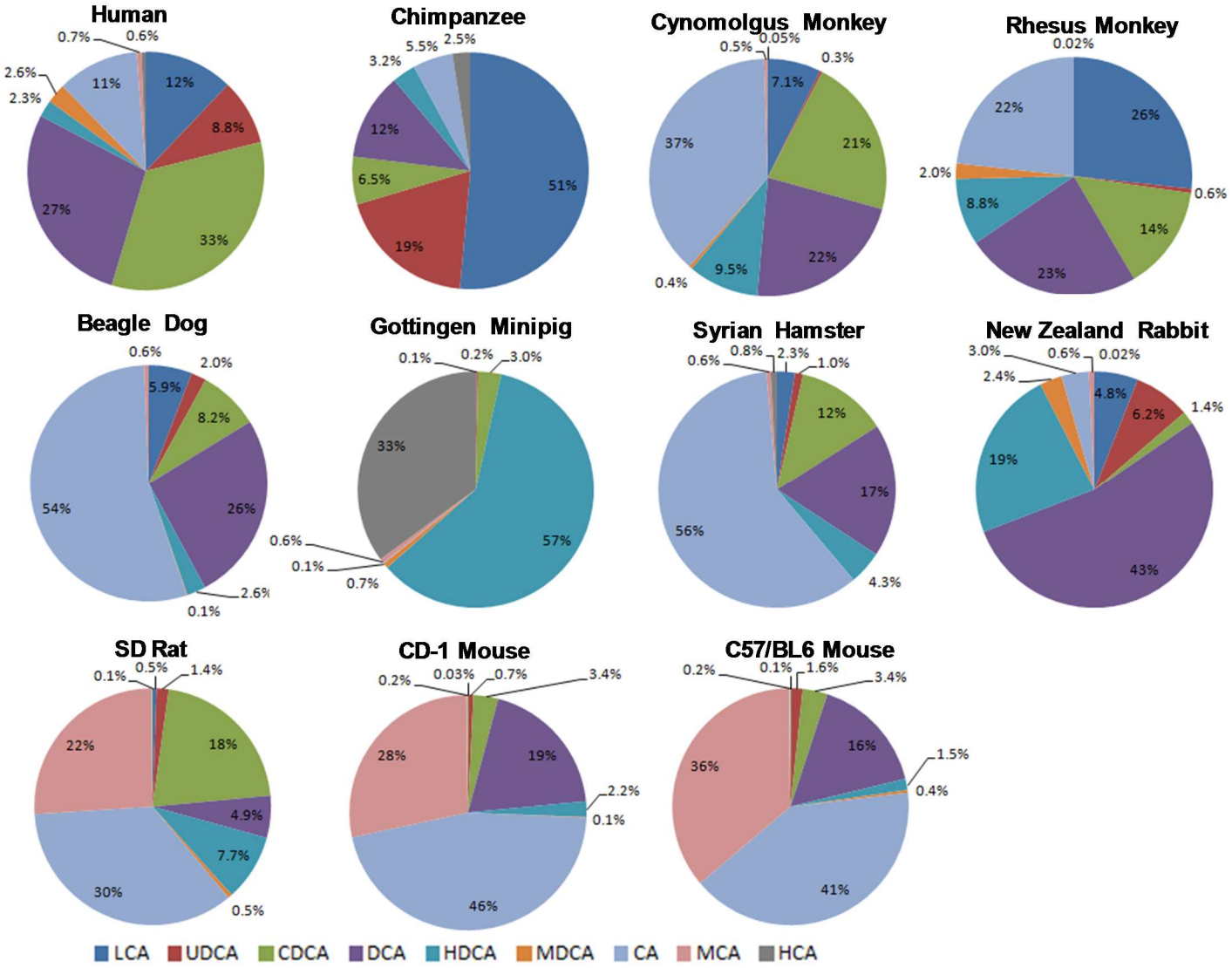

Figure 1.2 Individual BA contributions to the overall composition of plasma BA pools in humans and in various animal species.

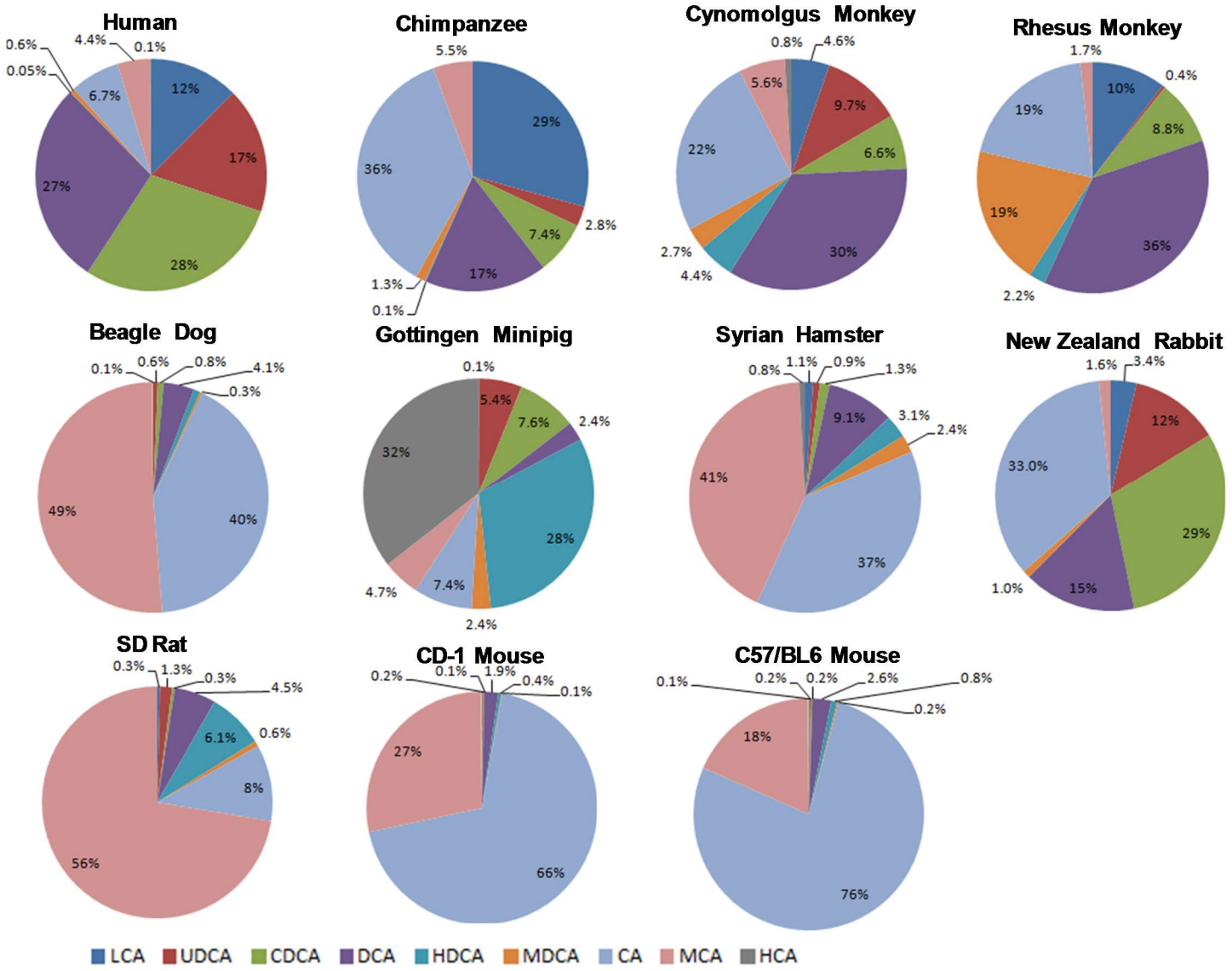

Figure 1.3 Individual BA contributions to the overall composition of urine BA pools in humans and in various animal species.

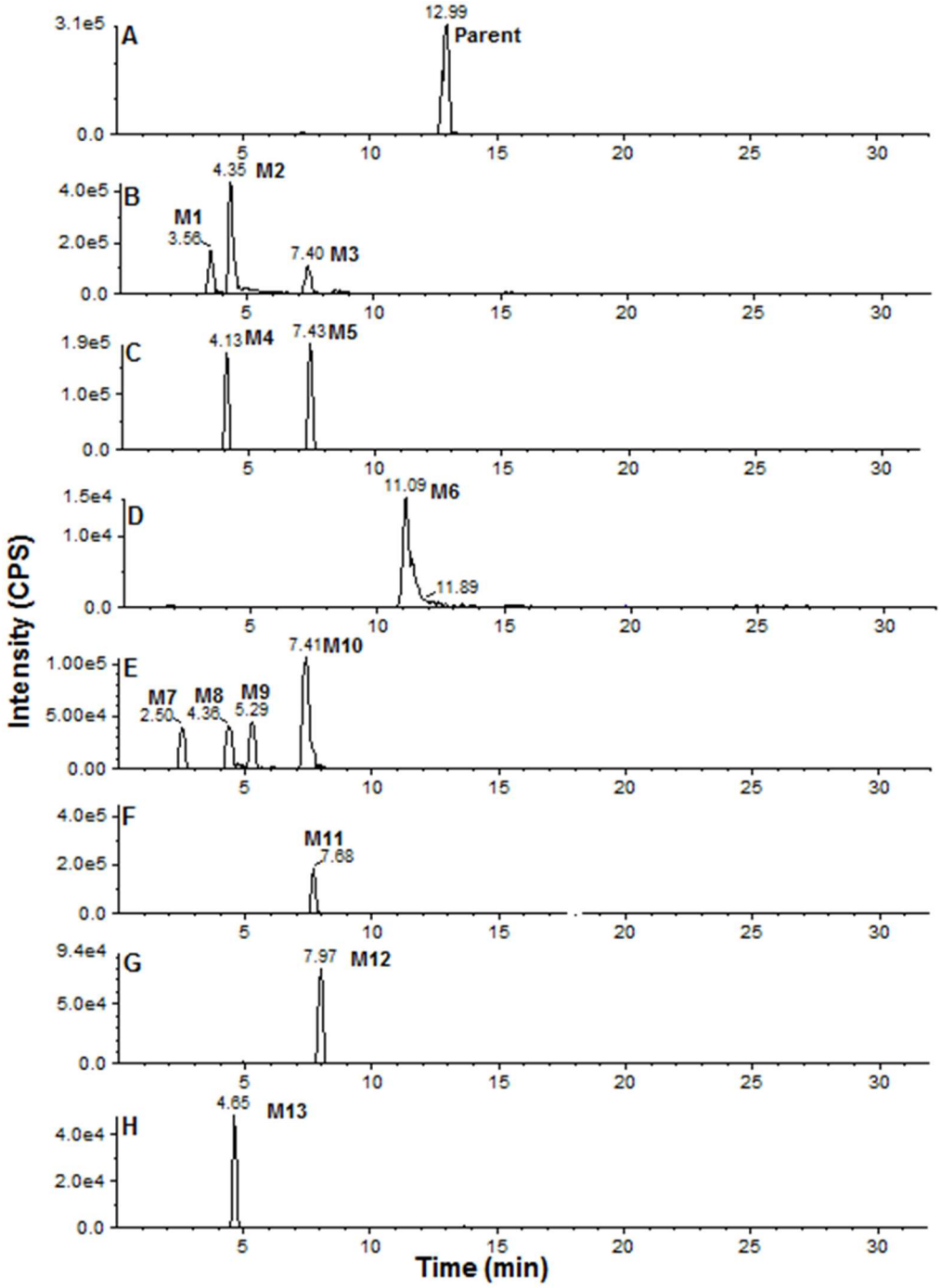

Figure 1.4 Extracted ion chromatograms (EIC) of detected metabolites obtained after incubation of UDCA with hepatocyte S9 fractions from different species for 60 min. A) parent-UDCA (*m/z* 391), B) M1 to M3: glucuronide conjugates (*m/z* 567), C) M4 and M5: sulfate conjugates (*m/z* 471), D) M6: glutathione conjugate (*m/z* 680), E) M7 to M10: hydroxylation into tri-OH BA metabolites (*m/z* 407), F) M11: glycine (G) amidate (*m/z* 448), G) M12: taurine (T) amidate (*m/z* 498), and H) M13: combination of hydroxylation and taurine amidation into T-MCA (*m/z* 514).

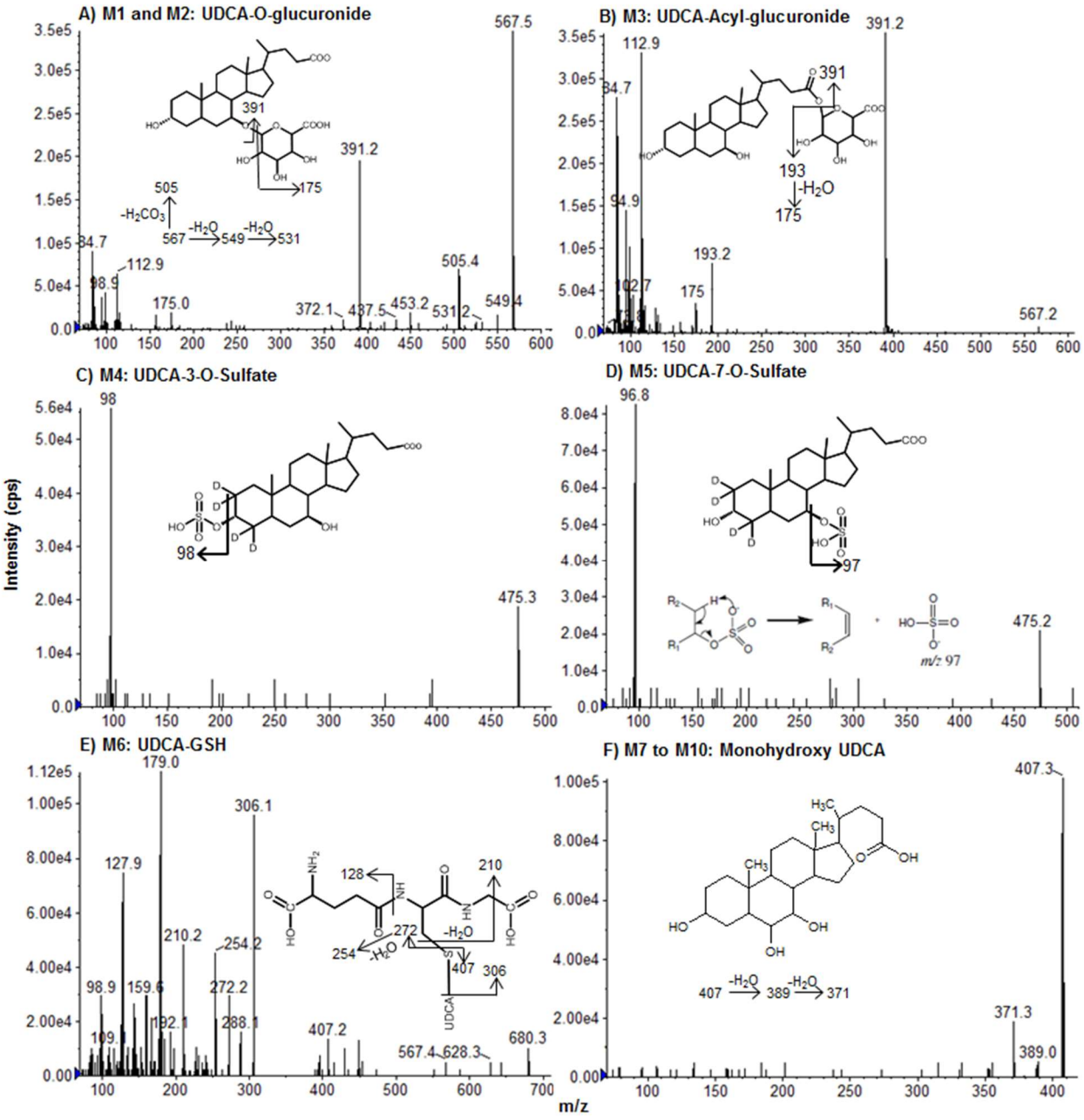
A) M1 and M2: UDCA-O-glucuronide
B) M3: UDCA-Acyl-glucuronide
C) M4: UDCA-3-O-Sulfate
D) M5: UDCA-7-O-Sulfate
E) M6: UDCA-GSH
F) M7 to M10: Monohydroxy UDCA
Intensity (cps)
m/z
567.5
391.2
505.4
549.4
453.2
531.2
372.1
437.5
175.0
112.9
98.9
84.7
505
391
175
567
549
531
-H2CO3
-H2O
-H2O
-H2O
391.2
112.9
84.7
94.9
193.2
175
102.7
567.2
391
193
-H2O
175
98
475.3
98
96.8
475.2
97
m/z 97
179.0
306.1
127.9
210.2
254.2
272.2
98.9
159.6
192.1
288.1
109.1
407.2
567.4
628.3
680.3
128
210
272
-H2O
254
-H2O
407
306
UDCA
407.3
371.3
389.0
407
389
371
-H2O
-H2O

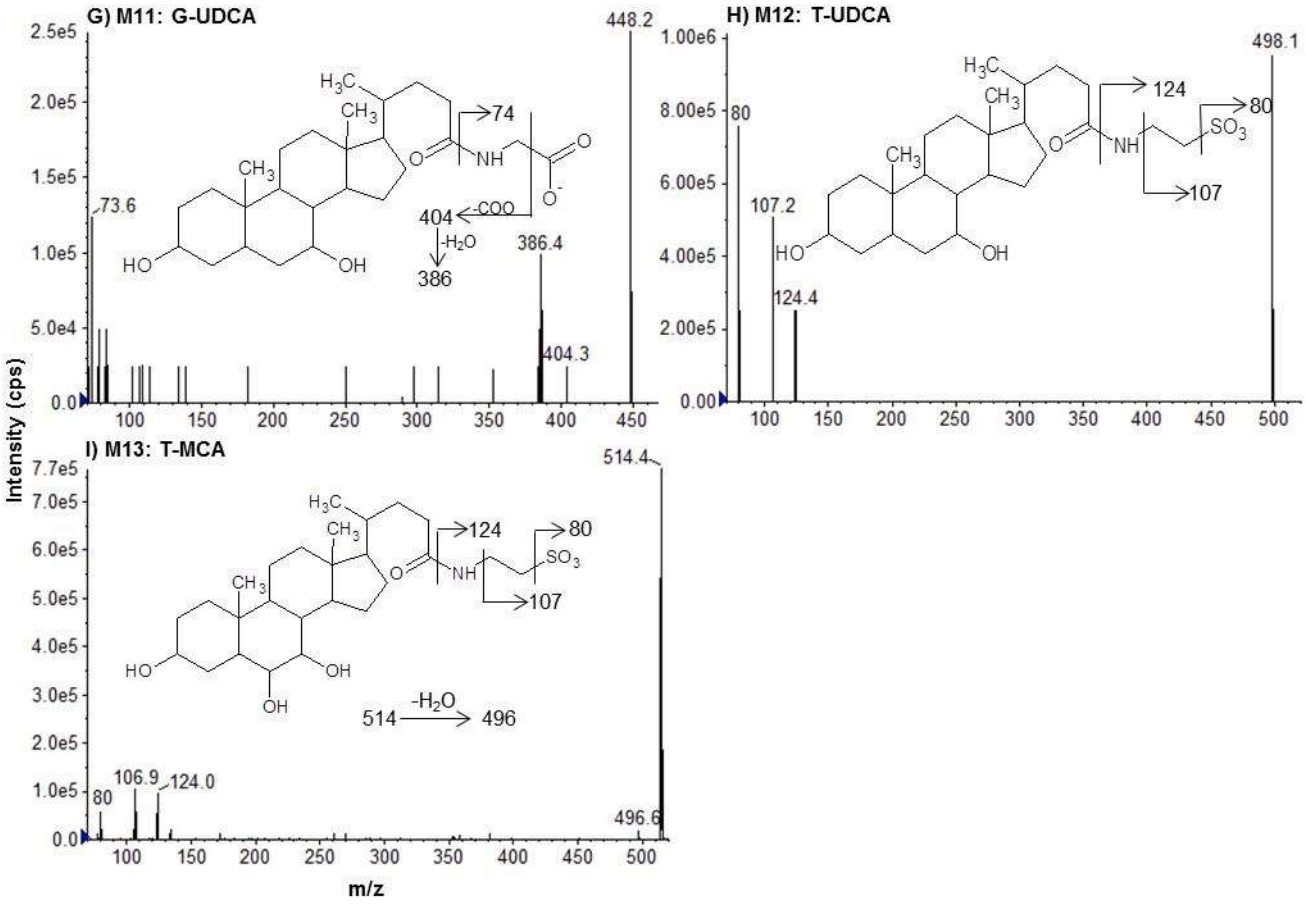

Figure 1.5 Representative enhanced product ion (EPI) spectra of UDCA metabolites. A) M1 and M2: O- glucuronide conjugate, B) M3: acyl-glucuronide conjugate, C) M4: 3-O-sulfate conjugate, D) M5: 7-O-sulfate conjugate, E) M6: glutathione conjugate, F) M7 to M10: hydroxylation into tri-OH BA metabolites G) M11: glycine (G) amidate H) M12: taurine (T) amidate, and I) M13: combination of hydroxylation and taurine amidation into T-MCA.

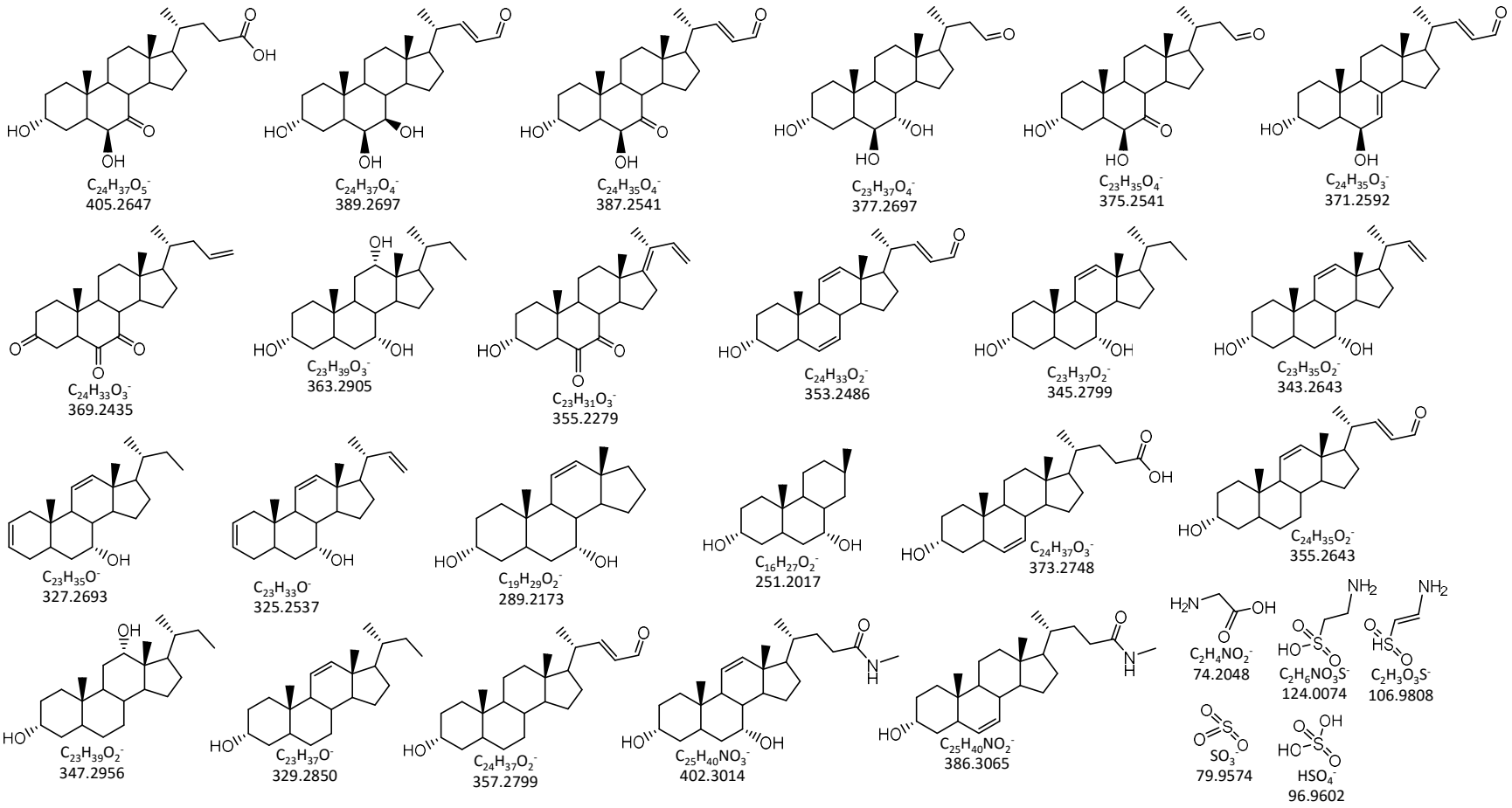

Figure 1.6 Proposed structures of MS/MS fragments produced by HRMS analyses of various BA standards.

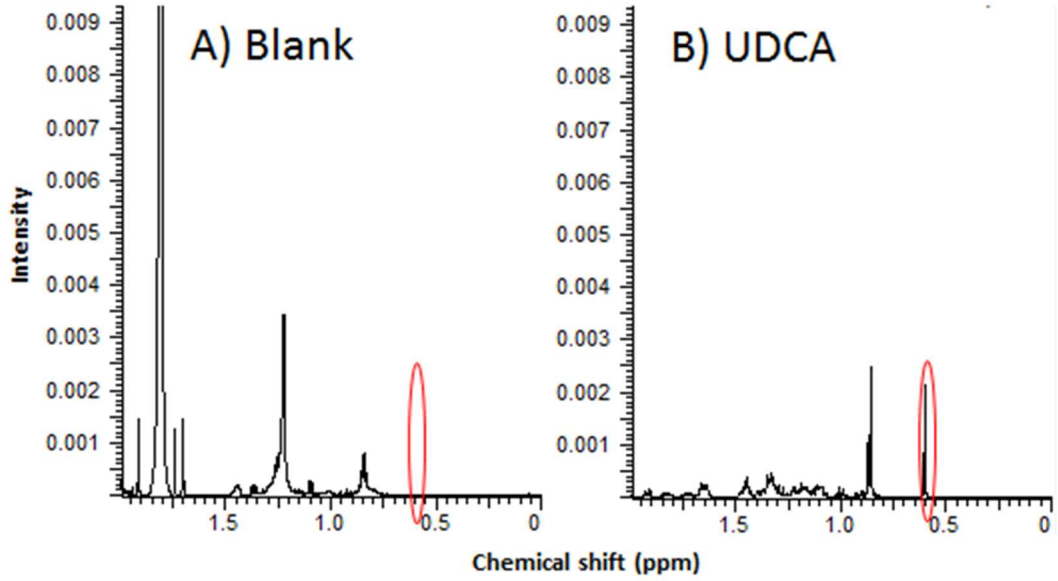

Figure 1.7 Identification of a unique proton signal by comparing ^{1}H NMR spectrum of 1) blank hepatocyte S9 fraction incubation and B) UDCA neat standard.

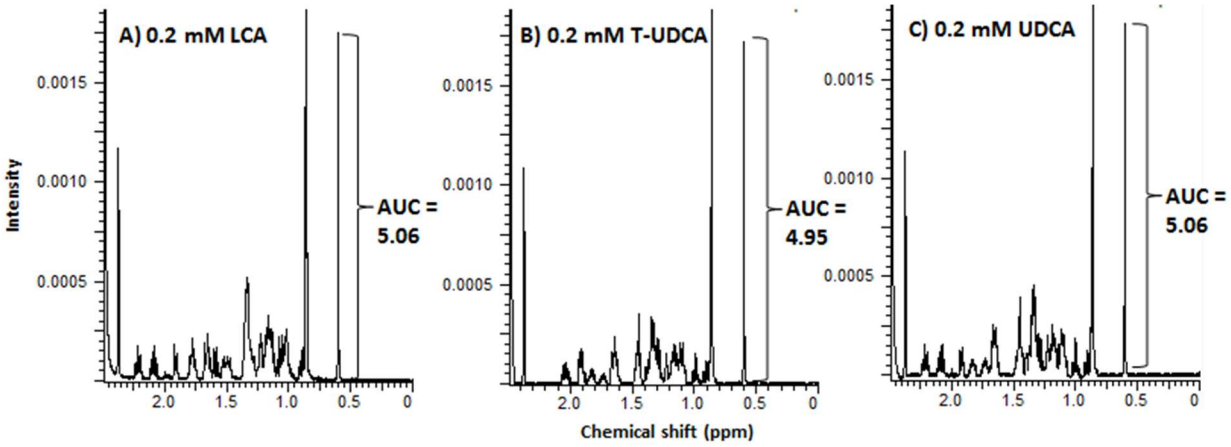

Figure 1.8 Uniform ^{1}H NMR responses of the 0.6 ppm proton for A) 0.2 mM LCA, B) 0.2 mM T-UDCA, and C) 0.2 mM UDCA

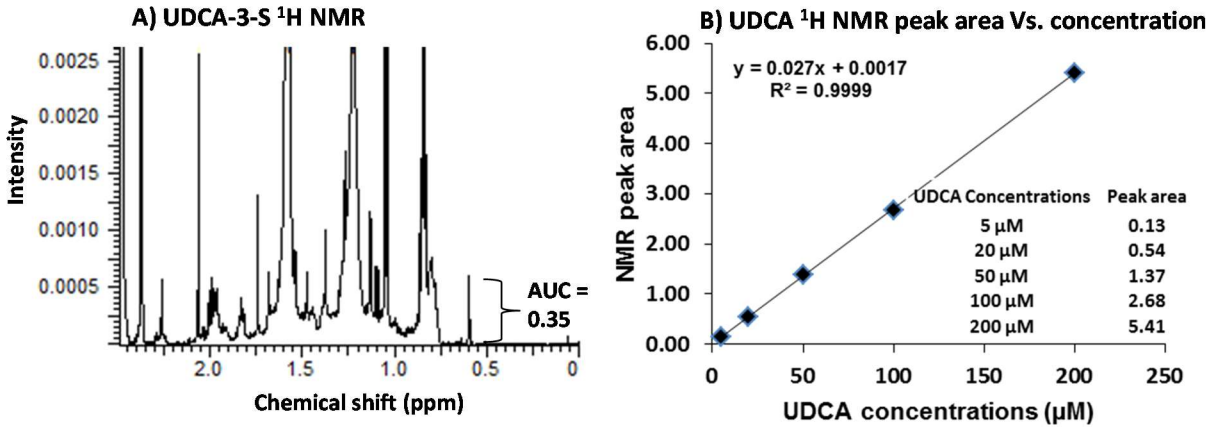

Figure 1.9 Quantification of UDCA-3S by ^{1}H NMR using UDCA calibration curve: (A) UDCA-3-S ^{1}H NMR spectrum showing the AUC of the unique 0.6 ppm proton obtained from hepatocyte S9 fractions incubation, (b) a UDCA calibration curve using the same proton.

(A)

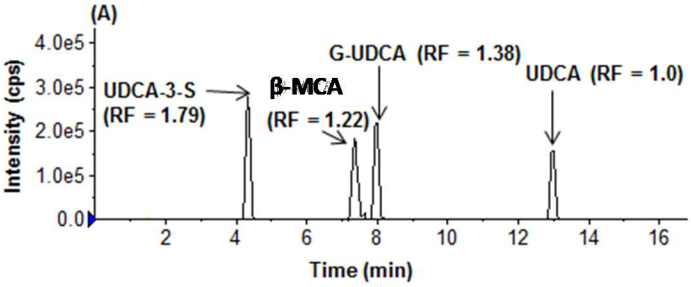

(B)

	Concentrations (μM)		
Metabolites	RF LC-MS/MS	Direct LC-MS/MS	% Difference
G-UDCA	1.25	1.45	14
MCA	1.16	1.25	7
UDCA-3-S	0.81	0.72	-13

Figure 1.10 (A) LC-MS Chromatogram of equal concentrations of UDCA and its representative metabolites (UDCA-3-S, β-MCA, and G-UDCA) at 0.5 μM. RF is calculated from the ratio of metabolite: parent peak areas at equal concentrations, (B) comparison of metabolite concentrations calculated using the RF approach vs. direct analysis using authentic standards.

Table 1.1 Plasma BA profiles in humans and in various animal species.

	Human	Chimpanzee	Cynomolgus Monkey	Rhesus Monkey	Beagle Dog	Gottingen Minipig	Syrian Hamster	New Zealand Rabbit	SD Rat	CD-1 Mouse	C57/BL6 Mouse
Total BA (μM)	3.9	0.074	3.5	5.3	1.4	31.0	1.6	2.9	12	2.2	3.1
Total LCA (μM)	0.36	0.034	0.22	0.63	0.029	0.016	0.038	0.083	0.051	0.001	0.004
Total UDCA (μM)	0.34	0.013	0.009	0.024	0.022	0.024	0.014	0.16	0.17	0.019	0.06
Total CDCA (μM)	1.4	0.003	0.78	1.2	0.08	1.1	0.21	0.032	2.2	0.093	0.12
Total DCA (μM)	0.99	0.015	0.75	0.72	0.254	0.000	0.24	1.4	0.55	0.415	0.52
Total HDCA (μM)	0.069	0.005	0.28	0.17	0.021	16.2	0.066	0.504	0.84	0.071	0.053
Total MDCA (μM)	0.093	0.000	0.015	0.057	0.003	0.16	0.000	0.047	0.059	0.003	0.016
Total CA (μM)	0.56	0.003	1.3	2.4	0.95	0.022	0.90	0.055	3.5	0.99	1.2
Total MCA (μM)	0.025	0.000	0.016	0.000	0.011	0.075	0.008	0.014	2.8	0.60	1.2
Total HCA (μM)	0.02	0.001	0.002	0.003	0.000	11.2	0.011	0.001	0.019	0.002	0.003
Total Unamidated BA (μM)	1.4	0.037	3.0	4.8	1.1	26.0	1.3	2.7	9.5	0.38	1.1
Total G-BA (μM)	2.1	0.019	0.16	0.23	0.001	4.8	0.19	0.21	0.76	0.007	0.009
Total T-BA (μM)	0.43	0.018	0.33	0.21	0.34	0.13	0.055	0.000	1.9	1.8	2.1
Total Unsulfated BA (μM)	2.8	0.043	3.4	5.2	1.4	30.9	1.6	2.8	12.2	2.2	3.1
Total Sulfated BA (μM)	1.1	0.031	0.046	0.031	0.000	0.077	0.026	0.078	0.021	0.000	0.003
%Sulfation of total BA	32%	50%	1.4%	0.9%	0.01%	0.5%	1.6%	4.8%	0.2%	0.0%	0.2%
%Amidation of total BA	65%	62%	15%	13%	52%	20%	12%	11%	22%	86%	71%
%G-amidation of total BA	54%	33%	5.4%	7.6%	0.03%	20%	8.5%	11%	7%	0.3%	0.3%
%T-amidation of total BA	12%	29%	10%	5.6%	52%	0.5%	3.1%	0.00%	15%	86%	71%
% Glucuronidation of total BA	0.01%	0.2%	0.0%	0.0%	0.5%	0.0%	0.0%	0.1%	0.1%	0.1%	0.2%
%Mono-OH BA	12%	52%	7.1%	26%	5.9%	0.06%	2.3%	4.8%	0.5%	0.03%	0.1%
%Di-OH BA	74%	41%	53%	48%	39%	61%	34%	72%	33%	26%	23%
%Tri-OH BA	12%	8%	38%	23%	55%	34%	58%	3.6%	52%	74 %	77%
Total Primary BA (μM)	2.0	0.010	2.1	3.6	1.1	12.4	1.1	0.10	8.5	1.7	2.5
Total Secondary BA (μM)	1.9	0.070	1.3	1.7	0.36	18.6	0.45	2.8	3.7	0.51	0.67
% Primary BA	45%	14%	59%	36%	63%	37%	69%	5%	7%	78%	80%
% Secondary BA	55%	86%	41%	64%	37%	63%	31%	95%	30%	22%	20%
Primary/secondary	1.1	0.18	3.8	2.0	2.0	0.59	2.5	0.050	2.3	4.2	4.5
Total 12α-OH BA (μM)	1.6	0.020	2.1	3.1	1.2	0.060	1.2	1.7	4.1	1.4	1.7
Total non-12α-OH BA (μM)	2.3	0.060	1.4	2.2	0.20	31.0	0.42	1.2	8.1	0.80	1.5
% 12α-OH BA	38%	17%	59%	46%	80%	0.2%	75%	56%	35%	65%	57%
% non-12α-OH BA	62%	83%	41%	54%	20%	99%	25%	44%	65%	35%	43%
12α-OH/ non-12α-OH BA	0.69	0.23	1.6	1.1	4.4	0.002	3.2	1.4	0.55	2.0	1.4
CA/CDCA	0.34	0.87	1.7	1.2	8.5	0.040	6.1	1.9	1.7	17.8	13.7
HI	0.45	0.10	0.41	0.55	0.30	-0.19	0.29	0.60	0.24	-0.06	-0.09

Table 1.2 Urine BA profiles in humans and in various animal species.

	Human	Chimpanzee	Cynomolgus Monkey	Rhesus Monkey	Beagle Dog	Gottingen Minipig	Syrian hamster	New Zealand Rabbit	SD Rat	CD-1 Mouse	C57/BL6 Mouse
Total BA (μM)	9.2	0.3	0.7	0.2	11.6	205	0.4	0.3	20.6	21.4	4.3
Total LCA (μM)	1.2	0.080	0.031	0.009	0.002	0.29	0.004	0.010	0.062	0.003	0.005
Total UDCA (μM)	1.4	0.008	0.069	0.002	0.078	6.8	0.004	0.035	0.28	0.039	0.008
Total CDCA (μM)	2.7	0.030	0.059	0.013	0.18	15.3	0.005	0.11	0.058	0.016	0.008
Total DCA (μM)	2.6	0.047	0.23	0.10	1.23	6.9	0.029	0.055	0.94	0.44	0.11
Total HDCA (μM)	0.004	0.000	0.030	0.011	0.14	80.3	0.012	0.000	1.2	0.089	0.037
Total MDCA (μM)	0.047	0.004	0.021	0.020	0.023	6.8	0.008	0.004	0.11	0.011	0.009
Total CA (μM)	0.61	0.15	0.18	0.063	7.7	19.6	0.13	0.092	1.8	14.0	3.3
Total MCA (μM)	0.36	0.015	0.034	0.003	1.0	9.9	0.17	0.004	11.5	5.9	0.78
Total HCA (μM)	0.033	0.000	0.006	0.000	0.007	39.2	0.000	0.000	0.19	0.026	0.005
Total Unamidated BA (μM)	1.1	0.072	0.52	0.19	10.1	85.2	0.37	0.03	9.1	5.6	1.2
Total G-BA (μM)	7.5	0.17	0.10	0.04	0.01	109.8	0.007	0.25	0.12	0.039	0.011
Total T-BA (μM)	0.60	0.092	0.13	0.005	1.53	9.9	0.006	0.036	11.4	15.8	3.08
Total Unsulfated BA (μM)	1.2	0.16	0.53	0.21	11.6	202.5	0.38	0.12	20.5	8.1	1.2
Total Sulfated BA (μM)	8.0	0.17	0.22	0.03	0.00	2.4	0.00	0.19	0.14	13.2	3.1
%Sulfation of total BA	85%	52%	27%	24%	0.0%	7.3%	2.1%	55%	0.7%	63%	72%
%Amidation of total BA	86%	69%	30%	31%	53%	49%	3%	88%	56%	73%	72%
%G-amidation of total BA	80%	47%	14%	26%	0.0%	45%	2.0%	78%	0.6%	0.2%	0.3%
%T-amidation of total BA	6.6%	22%	16%	5.4%	53%	3.6%	1.4%	10%	56%	73%	72%
% Glucuronidation of total	0.01%	0.16%	0.01%	0.03%	0.54%	0.0%	0.01%	0.09%	0.06%	0.13%	0.28%
%Mono-OH BA	12%	29%	4.6%	10%	0.0%	0.1%	1.1%	3%	0.27%	0.02%	0.12%
%Di-OH BA	73%	28%	54%	67%	7%	46%	17%	57%	13%	2.6%	4.0%
%Tri-OH BA	12%	42%	29%	21%	89%	44%	78%	35%	65%	94%	94%
Total Primary BA (μM)	3.7	0.20	0.30	0.10	8.9	84	0.30	0.20	13.5	19.9	4.1
Total Secondary BA (μM)	5.5	0.10	0.50	0.20	2.7	121	0.10	0.10	7.1	1.5	0.26
% Primary BA	40%	49%	35%	30%	90%	51%	80%	64%	66%	94%	94%
% Secondary BA	60%	51%	65%	70%	10%	49%	20%	36%	34%	6.4%	6.0%
Primary/secondary BA	0.80	1.7	0.57	0.44	10.1	1.3	3.9	2.0	1.9	18.0	16.5
Total 12α-OH BA (μM)	3.3	0.20	0.41	0.16	8.9	26.5	0.16	0.16	2.7	14.5	3.4
Total non-12α-OH BA (μM)	5.9	0.14	0.34	0.07	2.7	178.4	0.23	0.16	17.9	6.9	0.94
% 12α-OH BA	34%	54%	53%	55%	44%	9.8%	46%	53%	13%	68%	78%
% non-12α-OH BA	66%	46%	47%	45%	56%	90%	54%	47%	87%	32%	22%
12α-OH/ non-12α-OH BA	0.55	1.6	1.2	2.0	1.6	0.11	0.97	1.3	0.15	2.2	3.8
CA/CDCA	0.3	5.0	3.5	4.4	35	0.99	29	2.1	30	1019	434
HI	0.04	0.24	0.29	0.52	-0.28	-0.19	0.23	0.09	-0.57	-0.60	-0.49

Table 1.3 Exact mass analyses of various BA standards and their fragments using Orbitrap high resolution mass spectrometry (HRMS).

Experimental mass	Theoretical mass	Mass difference (ppm)	Formula	Parent BAs that produce the fragment
Tri-OH BAs (CA, HCA, α-MCA, β-MCA and ω-MCA)				
407.2795	407.2803	1.96	$C_{24}H_{39}O_5^-$	CA, HCA, α-MCA, β-MCA and ω-MCA
405.2636	405.2647	2.59	$C_{24}H_{37}O_5^-$	CA, HCA, α-MCA, β-MCA, and ω-MCA
389.2684	389.2697	3.40	$C_{24}H_{37}O_4^-$	CA, HCA, α-MCA, β-MCA, and ω-MCA
387.2530	387.2541	2.79	$C_{24}H_{35}O_4^-$	CA, HCA, α-MCA, β-MCA, and ω-MCA
377.2687	377.2697	2.76	$C_{23}H_{37}O_4^-$	α-MCA and ω-MCA
375.2530	375.2541	2.80	$C_{23}H_{35}O_4^-$	α-MCA and ω-MCA
371.2585	371.2592	1.80	$C_{24}H_{35}O_3^-$	CA, HCA, α-MCA, β-MCA, and ω-MCA
369.2429	369.2435	1.68	$C_{24}H_{33}O_3^-$	α-MCA, β-MCA, and ω-MCA
363.2894	363.2905	2.95	$C_{23}H_{39}O_3^-$	CA
355.2269	355.2279	2.70	$C_{23}H_{31}O_3^-$	α-MCA and β-MCA
353.2479	353.2486	1.98	$C_{24}H_{33}O_2^-$	CA
345.2788	345.2799	3.19	$C_{23}H_{37}O_2^-$	CA
343.2638	343.2643	1.31	$C_{23}H_{35}O_2^-$	CA and ω-MCA
327.2684	327.2693	2.87	$C_{23}H_{35}O^-$	CA
325.2528	325.2537	2.64	$C_{23}H_{33}O^-$	CA
289.2166	289.2173	2.59	$C_{19}H_{29}O_2^-$	CA
251.2010	251.2017	2.55	$C_{16}H_{27}O_2^-$	CA
Di-OH BAs (UDCA, CDCA, MDCA, HDCA, DCA, and isoDCA)				
391.2847	391.2854	1.79	$C_{24}H_{39}O_4^-$	UDCA, CDCA, MDCA, HDCA, DCA, and isoDCA
389.2688	389.2697	2.31	$C_{24}H_{37}O_4^-$	UDCA, CDCA, MDCA, HDCA and DCA
373.2739	373.2748	2.41	$C_{24}H_{37}O_3^-$	UDCA, CDCA, MDCA, HDCA and DCA
371.2583	371.2592	2.42	$C_{24}H_{35}O_3^-$	UDCA, CDCA, MDCA, HDCA and DCA
355.2637	355.2643	1.69	$C_{24}H_{35}O_2^-$	DCA, and isoDCA
347.2950	347.2956	1.73	$C_{23}H_{39}O_2^-$	DCA, and isoDCA
345.2796	345.2799	0.87	$C_{23}H_{37}O_2^-$	DCA, and isoDCA
329.2846	329.2850	1.21	$C_{23}H_{37}O^-$	DCA, and isoDCA
327.2690	327.2693	0.92	$C_{23}H_{35}O^-$	DCA, and isoDCA
Mono-OH BAs (LCA and isoLCA)				
375.2902	375.2905	0.80	$C_{24}H_{39}O_3^-$	LCA and isoLCA
357.2789	357.2799	2.80	$C_{24}H_{37}O_2^-$	LCA and isoLCA
355.2635	355.2643	2.25	$C_{24}H_{35}O_2^-$	LCA and isoLCA
BA G-amidates (G-LCA, G-UDCA, G-CDCA, G-DCA, G-MDCA, G-CA, and G-HCA)				
432.3109	432.2119	2.32	$C_{26}H_{42}NO_4^-$	G-LCA

448.3056	448.3068	2.68	$C_{26}H_{42}NO_5^-$	G-UDCA, G-CDCA, G-DCA, and G-HDCA
464.3017	464.3018	0.22	$C_{26}H_{42}NO_6^-$	G-CA and G-HCA
402.3001	402.3014	3.23	$C_{25}H_{40}NO_3^-$	G-CA and G-HCA
386.3054	386.3065	2.85	$C_{25}H_{40}NO_2^-$	G-UDCA, G-CDCA, G-DCA, and G-HDCA
74.2050	74.2048	1.35	$C_2H_4NO_2^-$	G-CA, G-HCA, G-UDCA, G-CDCA, G-DCA, and G-HDCA, and G-LCA
BA T-amidates (T-LCA, T-UDCA, T-CDCA, T-DCA, T-HDCA, T-CA, T-MCA, and T-HCA)				
482.2940	482.2946	1.2	$C_{26}H_{44}NO_5S^-$	T-LCA
498.2882	498.2895	2.61	$C_{26}H_{45}NO_6S^-$	T-UDCA, T-CDCA, T-DCA, and T-HDCA
514.2797	514.2797	0.00	$C_{26}H_{45}NO_7S^-$	T-CA , T-MCA, and T-HCA
124.0075	124.0074	-0.81	$C_2H_6NO_3S^-$	T-CA, T-MCA, T-HCA, T-UDCA, T-CDCA, T-DCA, and T-HDCA
106.9809	106.9808	-0.93	$C_2H_3O_3S^-$	T-CA, T-MCA, T-HCA, T-UDCA, T-CDCA, T-DCA, and T-HDCA
79.9576	79.9574	-2.50	SO_3^-	T-CA, T-MCA, T-HCA, T-UDCA, T-CDCA, T-DCA, and T-HDCA
BA S-conjugates (CA-S, G-CA-S, T-CA-S, UDCA-S, CDCA-S, DCA-S, G-CDCA-S, T-CDCA-S, T-UDCA-S, T-CDCA-S, T-DCA-S, G-LCA-S, and TLCA-S				
594.2422	594.2412	-1.68	$C_{26}H_{44}NO_{10}S_2^-$	T-CA-S
544.2575	544.2586	2.02	$C_{26}H_{42}NO_9S$-	G-CA-S
487.2374	487.2371	-0.62	$C_{24}H_{39}O_8S^-$	CA-S
578.2464	578.2463	-0.17	$C_{26}H_{44}NO_9S_2^-$	T-UDCA-S, T-CDCA-S, and T-DCA-S
528.2637	528.2642	0.95	$C_{26}H_{42}NO_8S^-$	G-CDCA-S, and G-DCA-S
471.2418	471.2422	0.82	$C_{24}H_{39}O_7S^-$	UDCA-S, CDCA-S, and DCA-S
96.9601	96.9602	1.03	HSO_4^-	CA-S, G-CA-S, T-CA-S, UDCA-S, CDCA-S, DCA-S, G-CDCA-S, T-CDCA-S, T-UDCA-S, and T-CDCA-S, T-DCA-S

Table 1.4 HRMS analysis of UDCA metabolites and their fragments. Each biotransformation product is described by molecular formula $[M-H]^-$, exact *m/z* shift (compared to the parent), and MS/MS fragments.

Modification	Exact m/z shift	Formula $[M-H]^-$	Experimental mass	Theoretical mass	Mass difference (ppm)	Fragment of
UDCA (Parent)	-	$C_{24}H_{39}O_4^-$	391.2849	391.2854	1.28	-
UDCA-Glucuronide (M1-M3)	176.0325 (+$C_6H_8O_6$)	$C_{30}H_{47}O_{10}^-$	567.3174	567.3175	0.18	M1-M3
		$C_{30}H_{45}O_9^-$	549.3063	549.3069	1.09	M1 and M2
		$C_{29}H_{47}O_8^-$	523.3271	523.3276	0.96	M1 and M2
		$C_{29}H_{45}O_7^-$	505.3166	505.3171	0.99	M1-M3
		$C_{24}H_{39}O_4^-$	391.2849	391.2854	1.28	M1-M3
		$C_6H_9O_7^-$	193.0354	193.0354	0.00	M3
		$C_6H_7O_6^-$	175.0245	175.0248	1.71	M1-M3
UDCA-Sulfate (M4-M5)	79.9562 (+SO_3)	$C_{24}H_{39}O_7S^-$	471.2422	471.2416	1.27	M4-M5
		HO_4S^-	96.9601	96.9602	1.03	M4-M5
UDCA-Glutathione conjugate (M6)	289.0733 (+$C_{10}H_{15}N_3O_5S$)	$C_{34}H_{54}N_3O_9S^-$	680.3582	680.3586	0.59	M6
		$C_{34}H_{52}N_3O_8S^-$	662.3461	662.3481	3.02	M6
		$C_{10}H_{16}N_3O_6S^-$	306.0764	306.0765	0.33	M6
		$C_{10}H_{14}N_3O_6^-$	272.0887	272.0888	0.37	M6
		$C_{10}H_{14}N_3O_5^-$	254.0781	254.0782	0.39	M6
		$C_9H_{12}N_3O_3^-$	210.0885	210.0884	-0.48	M6
		$C_5H_6NO_3^-$	128.0353	128.0353	0.00	M6
Oxidation (M7-M10)	15.9946 (+O)	$C_{24}H_{39}O_5^-$	407.2795	407.2803	1.96	M7-M10
		$C_{24}H_{37}O_5^-$	405.2639	405.2647	1.85	M7 and M10
		$C_{24}H_{37}O_4^-$	389.2689	389.2697	2.13	M7-M10
		$C_{24}H_{35}O_4^-$	387.2533	387.2541	2.01	M7-M10
		$C_{23}H_{35}O_4^-$	375.2533	375.2541	2.08	M7
		$C_{24}H_{35}O_3^-$	371.2584	371.2592	2.07	M7-M10
		$C_{24}H_{33}O_3^-$	369.2424	369.2435	2.98	M10
		$C_{23}H_{39}O_3^-$	363.2896	363.2905	2.39	M7
		$C_{22}H_{33}O_4^-$	361.2377	361.2384	1.94	M7 and M8
		$C_{23}H_{31}O_3^-$	355.2272	355.2279	1.89	M8 and M10
		$C_{24}H_{33}O_2^-$	353.2480	353.2486	1.70	M8
		$C_{22}H_{35}O_3^-$	347.2586	347.2592	1.73	M7-M9
		$C_{23}H_{37}O_2^-$	345.2792	345.2799	2.03	M9
		$C_{23}H_{35}O_2^-$	343.2637	343.2643	1.60	M7-M9
		$C_{20}H_{31}O_4^-$	335.2222	335.2280	1.79	M7-M9
		$C_{21}H_{31}O_3^-$	331.2273	331.2279	1.72	M8 and M9
		$C_{22}H_{33}O_2^-$	329.2481	329.2486	1.52	M8 and M9
		$C_{20}H_{29}O_3^-$	317.2117	317.2122	1.58	M7-M9
G-UDCA (M11)	57.0211 (+$C_2H_3NO_1$)	$C_{26}H_{42}NO_5^-$	448.3060	448.3068	1.78	M11
		$C_{25}H_{40}NO_2^-$	386.3055	386.3065	2.59	M11
		$C_2H_4NO_2^-$	74.2049	74.2048	-1.35	M11
T-UDCA (M12)	107.0042 (+$C_2H_5NO_2S$)	$C_{26}H_{44}NO_6S^-$	498.2891	498.2895	0.80	M12
T-UDCA+Oxidation (T-MCA; M13)	122.9987(+O+$C_2H_5NO_2S$)	$C_{26}H_{45}NO_7S^-$	514.2800	514.2794	-0.58	M13
		$C_2H_6NO_3S^-$	124.0076	124.0074	-1.61	M12 and M 13
		$C_2H_3O_3S^-$	106.9809	106.9808	-0.93	M12 and M 13
		SO_3^-	79.9575	79.9574	-1.25	M12 and M 13

Table 1.5 Physiological concentrations of biotransformation cofactors for various metabolic pathways in human liver and biological fluids, and in previously and currently used *in vitro* metabolism systems.

Cofactors	Metabolic Pathway	Human liver	Human biological fluids	Previous in vitro systems	Current in vitro system
Taurine	T-amidation	0.3-3.6 mM [233-236]	Bile: 0.2 mM [233]; WBC: 0.02-0.035 mM [233]; Plasma: 0.068 mM [235]	20-30 mM [10, 237]	5 mM
Glycine	G-amidation	1.5-3.8 mM [235, 236]	Plasma: 0.23 mM [235]	20-30 mM [10, 237]	5 mM
GSH	Glutathione conjugation	1 mM [238]	Plasma: 0.0034-0.026 mM [239, 240], blood: 0.85-1.8 mM [239, 241]; Lymp 11 -21.5 nmol/mg protein [242]	1.5-10 mM [243-245]	5 mM
PAPS	Sulfation	0.023 mM [246]	-	0.04-1 mM [174, 244, 247-250]	0.1 mM
UDPGA	Glucuronidation	0.29 mM [251]	-	1-5 mM [250, 252-255]	0.4 mM
CoA	G and T Amidation	0.065-0.1 mM [256]	-	0.4-2 mM [10, 237]	0.4 mM
ATP	G and T Amidation	1-10 mM [257]	Plasma: 0.000028 mM [258]	5-7 mM [10, 237]	1 mM
NADPH	Oxidation	0.2-0.3 mM [259]	RBC:0.02 mM [241]	1 mM [260-262]	1 mM

Table 1.6 LCA, UDCA, CDCA, and CA metabolism by hepatocyte S9 fractions from humans and various animal species

Species	% Metabolized	% Sulfation	% Amidation	% G-Amidation	% T-Amidation	% Oxidation	% Glucuronidation	% Glutathione conjugation
LCA								
Human	25%	18 %	76 %	23 %	53 %	4.6 %	0.8 %	0.0 %
Chimpanzee	19%	52 %	36 %	10%	25%	9.6%	2.7%	0.2 %
Cynomolgus Monkey	25%	1.3 %	86 %	44%	42%	8.0%	4.4%	0.2 %
Rhesus Monkey	26%	2.1 %	75 %	40%	35%	11%	11.3%	0.5 %
Beagle Dog	21%	0.1 %	9 %	0%	8.8%	13%	75%	2.9 %
Gottingen Minipig	54%	0.2 %	96 %	89%	7.2%	3.7%	0.1%	0.0%
Syrian Hamster	33%	0.7 %	71 %	19%	52%	25%	3.2%	0.2%
New Zealand Rabbit	27%	2.1 %	70 %	65%	4.2%	27%	1.0%	0.1%
SD Rat	46%	0.2 %	16 %	1.1%	15%	80%	3.8%	0.1%
CD-1 Mouse	47%	0.0 %	72 %	0.4%	71%	28%	0.1%	0.1%
C57/BL6 Mouse	33%	0.1 %	70 %	0.4%	69%	30%	0.2%	0.1%
UDCA								
Human	23%	19%	70%	28%	43%	9.5%	0.3%	0.7%
Chimpanzee	11%	27%	55%	11%	44%	15%	2%	0.4%
Cynomolgus Monkey	30%	0.4%	77%	39%	37%	22%	0.8%	0.2%
Rhesus Monkey	21%	0.15%	79%	42%	37%	19%	1.3%	0.2%
Beagle Dog	8%	0.01%	19%	0.0%	19%	25%	56%	0.4%
Gottingen Minipig	62%	0.04%	96%	91 %	5.3%	3.6%	0.0%	0.15%
Syrian Hamster	16%	9%	70%	20%	50%	20%	1.0%	0.01%
New Zealand Rabbit	16%	12%	64%	62%	2.3%	20%	0.5%	0.05%
SD Rat	23%	0.0%	40%	0.9%	39%	59%	0.5%	0.02%
CD-1 Mouse	39%	0.0%	76%	0.32%	75%	24%	0.03%	0.1%
C57/BL6 Mouse	20%	0.0%	72%	0.42%	71%	28%	0.12%	0.02%
CDCA								
Human	25%	22%	64%	24%	40%	12%	1.1%	0.6%
Chimpanzee	9%	14%	61%	17%	44%	22%	1.9%	1%
Cynomolgus Monkey	31%	2.1%	73%	35%	38%	24%	0.8%	0.4%
Rhesus Monkey	21%	5.4%	65%	31%	34%	26%	1.5%	1.4%
Beagle Dog	12%	0.0%	22%	2.7%	19%	48%	27%	3.3%
Gottingen Minipig	80%	5.7%	68%	65%	3.1%	25%	0.5%	0.2%
Syrian Hamster	28%	7.5%	60%	32%	28%	31%	1.5%	0.8%
New Zealand Rabbit	15%	14%	64%	62%	2.4%	20%	2.9%	0.0%
SD Rat	22%	1.3%	26%	1.0%	25%	70%	1.6%	0.6%
CD-1 Mouse	34%	0.0%	50%	0.5%	50%	49%	0.7%	0.4%
C57/BL6 Mouse	26%	0.0%	60%	0.5%	59%	39%	0.8%	0.4%
CA								
Human	16 %	4.8%	93%	26%	66%	2.1%	0.1%	0.5%
Chimpanzee	2.0%	0.5%	90%	29%	62%	7.6%	0.3%	1.2%
Cynomolgus Monkey	17%	0.04%	98%	61%	36%	2.1%	0.2%	0.1%
Rhesus Monkey	9.0%	0.06%	97%	61%	36%	2.1%	0.6%	0.3%
Beagle Dog	2.0%	0.00%	81%	0.0%	81%	4.8%	9.7%	4.3%
Gottingen Minipig	68%	0.02%	98%	94%	4%	1.6%	0.0%	0.0%
Syrian Hamster	20%	0.3%	89%	42%	48%	10%	0.5%	0.0%
New Zealand Rabbit	6.0%	1.4%	98%	95%	3%	0.6%	0.2%	0.2%

SD Rat	6.0%	0.04%	81%	33%	48%	18%	0.6%	0.4%
CD-1 Mouse	19%	3.5%	81%	0.5%	81%	13%	1.0%	1.2%
C57/BL6 Mouse	7.0%	2.0%	80%	0.7%	79%	16%	1.1%	1.3%

Table 1.7 BA oxidation into hydroxylated metabolites by hepatocytes S9 fractions.

	LCA			UDCA		CDCA			
	6-β-OH (MDCA)	6-α-OH (HDCA)	Other*	6-β-OH (MCA)	Other	6-β-OH (MCA)	12-α-OH (CA)	6-α-OH (HCA)	Other
Human	12%	59%	29%	44%	56%	7%	73%	7%	12%
Chimpanzee	7%	68%	25%	55%	45%	12%	56%	6%	27%
Cynomolgus Monkey	13%	38%	49%	4.8%	95%	11%	63%	12%	14%
Rhesus Monkey	13%	41%	47%	16%	84%	10%	58%	14%	18%
Beagle Dog	3%	4%	93%	9.2%	91%	20%	57%	7%	16%
Gottingen Minipig	3%	36%	61%	64%	36%	1%	0.7%	97%	1.6%
Syrian Hamster	6%	71%	23%	89%	11%	10%	69%	3%	18%
New Zealand Rabbit	93%	2%	5%	8.9%	91%	0%	65%	15%	19%
SD Rat	94%	3%	2%	94%	5.5%	95%	1.2%	1.7%	2.1%
CD-1 Mouse	65%	3%	32%	94%	6.4%	93%	2.9%	1.3%	2.5%
C57/BL6 Mouse	67%	2%	31%	89%	11%	92%	3.3%	1.5%	2.7%

*Other: Sum of metabolites resulting from hydroxylation of various overlapping position excluding 6-α, 6-β, and 12-α position.

Table 1.8 Literature summary of plasma BA profiles in different species.

	Human [86, 91, 142, 180-185]	Mouse [86, 135, 142, 145]	Rat [86, 138, 141, 143, 146]	Beagle dog [91, 144]	Syrian Hamster [155]	New Zealand Rabbit [155]	Pig [139, 141]	Cow [91]	Horse [91]
Total BA (μM)	0.9 - 4.4	1.3-9.0	3.6-38	2.4-5.0	-	-	6.6-31	93	3.64
Total LCA (μM)	0.01 - 0.3	0.004-0.02	0.01-0.11	0.0-0.02	-	-	0.02-0.04	0.84	0.00
Total UDCA (μM)	0.02 - 0.51	0.01-0.5	0.04-0.73	0.04-0.12	-	-	0.02-2.9	0.00	0.23
Total CDCA (μM)	0.15 - 4.2	0.008-0.4	0.3-2.8	0.28-0.51	-	-	1.0-1.1	2.5	2.5
Total DCA (μM)	0.13 - 0.96	0.09-1.0	0.3-4.1	0.66-1.24	-	-		11.6	0.00
Total HDCA (μM)	0.002-0.18	0.02-0.1	0.2-4.8	-	-	-	16.2	-	-
Total MDCA (μM)	0.0 - 0.0001	0-0.5	0.0-0.05	-	-	-	0.16	-	-
Total CA (μM)	0.09-1.26	0.44-4.5	1-19	1.4-3.1	-	-	0.02-0.03	78	0.92
Total MCA (μM)	0.003-0.026	0.65-4.5	0.4-7.6	0	-	-	0.07	-	-
Total HCA (μM)	0.004-0.032	0-0.02	0.0-0.08	-	-	-	2.7-11.2	-	-
Total G-BA (μM)	0.7 - 2.7	0.02-0.04	0.03-0.9	-	-	-	3.0	29	0.25
Total T-BA (μM)	0.06 - 0.57	1-5.3	0.6-10	2.3-4.8	-	-	0.0	23	3.1
Total Unsulfated BA (μM)	0.7 - 4.4	1.3-9.0	3.6-24	2.4-5.0	-	-	-	-	-
Total Sulfated BA (μM)	-	-	-	-	-	-	-	-	-
%Sulfation of Total BA	-	-	-	-	-	-	-	-	-
%Amidation of Total BA	36%-72%	18%-82%	9%-73%	94-95%	-	-	45%	56%	92%
%G-amidation of Total BA	31%-66%	0%-0.2%	0.7%-4%	0%	-	-	42%	31%	7.0%
%T-amidation of Total BA	2.7%-12%	18%-82%	5%-72%	94-95%	-	-	2.7%	25%	85%
%Mono-OH BA	0.5%-8%	0%-0.4%	0.15%-1.5%	0-1%	1.40%	3.1%	0.1-0.5%	0.9%	0.0%
%Di-OH BA	65%-85%	1%-40%	12%-50%	37-40%	25%	52%	59%	15%	75%
%Tri-OH BA	12%-28%	50-90%	50%-87%	58-62%	73%	45%	40%	84%	25%
%LCA	0.5%-8%	0%-0.4%	0.15%-1.5%	0-1%	1.40%	3.1%	0.1-0.5%	0.9%	0.0%
%UDCA	1.8%-20%	1%-7%	0.7%-10%	1.7-2.3	2.10%	1.4%	0.2-44%	0.0%	6.3%
%CDCA	29%-75%	0.8%-5%	5%-29%	10-12%	11%	7.0%	3-15%	2.7%	68%
%DCA	9.2%-36%	0.5-26%	0.8%-11%	25-27%	12%	44%	0.00%	12.5%	0.0%
%HDCA	0.09%-5.5%	0%-2.6%	1%-27%	-	-	-	57%	-	-
%MDCA	0%	0-1%	0.0-0.2%	-	-	-	-	-	-
%CA	9%-28%	14%-63%	27%-56%	58-63%	73%	45%	0.38%	84%	25%
%MCA	0.12%-0.8%	13%-59%	18%-42%	0%			0.6	-	-
%HCA	0.2%-5.7%	0%-0.32%	0.0%-0.4%	0%			33-40%		
Total Primary BAs (μM)	0.23-2.85	1.1%-4.9%	2.7-28	1.7-3.7	-	-	3.70	81	3.4
Total Secondary BAs (μM)	0.13-1.53	0.13%-2.3%	1-9.2	0.7-1.35	-	-	2.94	12	0.23
% Primary BAs	40%-65%	58%-90%	68-95%	70-73%	-	-	56%	87%	94%
% Secondary BAs	9.2%-56%	10%-40%	5.5-32%	27-30%	-	-	44%	13%	6.3%
Primary/secondary	0.74-1.9	2.6-8.6	2.1-17	2.3-2.7	5.4	1.1	1.3	6.5	14.9
Total 12α-OH BAs (μM)	0.22-1.81	0.5-5.5	1-24	2.1-4.4			0.03	90	0.92
Total non-12α-OH BAs (μM)	0.22-2.5	0.7-3.6	2.6-14	0.3-0.6	-	-	6.61	3.4	2.7
% 12α-OH BAs	21%-49%	35%-78%	28-59%	85-88%	-	-	0.38%	96%	25%

% non-12α-OH BAs	29%-61%	23%-65%	37-72%	12-14%	-	-	99%	3.6%	75%
12α-OH/ non-12α-OH BAs	0.7-1.7	0.8-2.1	0.4-1.4	6.0-7.0	7.6	1.1	0.004	27	0.34
CA/CDCA	0.3-0.6	9-28	1.7-9	5.1-6.2	5.9	6.3	0.024	31	0.37
HI	0.3-0.54	-0.32- -0.1	-0.09-0.22	0.19-0.22	-	-	-0.18	0.17	0.30

Table 1.9 Literature summary of biliary BA profiles in different species.

	Human [263-265]	Mouse [88, 135, 266]	Rat [153, 155, 267]	Syrian Hamster [268-270]	Pig [140, 153, 154, 157]	New Zealand Rabbit [90, 155-157]	Cat [90]
Total BA (μM)	14,000-99,000	57,100-64,000	16,000-25,700	52,076-133,000	35,759-208,000	72,824-358,000	52,131
Total LCA (μM)	2172	0	3.2-8.2	1414	25	244-269	11,344
Total UDCA (μM)	8554	571	1400-3500	-	176-255	-	-
Total CDCA (μM)	76,144	0	1100-2700	7844	19,278-20,379	-	2258
Total DCA (μM)	22,022	856.5	750-1150	7060	241-595	60,204-64,640	5711
Total HDCA (μM)	-	-	-	-	4825-41005	-	-
Total MDCA (μM)	-	-	-	-	-	-	-
Total CA (μM)	56,883	35,230	14,800-11,198	35,758	242	2222-7333	14,003
Total MCA (μM)	-	13,532	1,500-3,900	-	-	-	
Total HCA (μM)	-	286	-	-	11,612-26,112	-	-
Total G-BA (μM)	-	26	-	-	42,820	-	-
Total T-BA (μM)	-	63,737	-	-	7395	-	
Total Unsulfated BA (μM)	-	-	-	-	-	-	-
Total Sulfated BA (μM)	-	-	-	-	-	-	-
%Sulfation of Total BA	-	-	-	-	-	-	-
%Amidation of Total BA	-	-	96-99%	-		-	-
%G-amidation of Total BA	80%	0.04%	5-14%	64-82%	73-82%	92%	-
%T-amidation of Total BA	20%	99%	86-95%	17-35%	15-27%	8%	-
%Mono-OH BA	1-1.3%	0.00-0.01%	0.01-0.05%	1.1-15%	2.1%	0.4-1.2%	22%
%Di-OH BA	64-67%	2.5-4.4%	19-27%	29-57%	50-84%	82-91%	15%
%Tri-OH BA	34-35%	86-95%	72-80%	38-69%	20-52%	3-10%	60%
%LCA	1-1.3%	0-0.01%	0.01-0.05%	1.1-15%	2.1%	0.4-1.2%	22%
%UDCA	5.2-6.0%	1-2.5%	6-14%	8.0-13%	0.35-14%	-	-
%CDCA	46-48%	0.6-2.3%	6-11%	15-38%	14-38%	0.7-1.2%	4%
%DCA	13%	0.9-3.5%	3.0-6.0%	5-15%	0.33%	80-89%	11%
%HDCA	-	-	-	0%	55%	-	-
%MDCA	-	-	-	-	-	-	-
%CA	34-35%	46-62%	57-70%	38-68%	20%	3-10%	60%
%MCA	-	24-49%	09-15%	-	-	-	-
%HCA	-	0.50%	-	0%	16%	-	-
Total Primary BAs (μM)	133,028	49,049-62,626	13,770-21,507	43602	31,990-45,390	2222-7333	16261
Total Secondary BAs (μM)	32,748	1372-1428	2300-4256	8475	4825-41,501	60,449-64,909	17,056
% Primary BAs	80-83%	50-86%	83-90%	68-83%	43-90%	8-10%	64%
% Secondary BAs	20%	3-6%	10-16%	16-30%	55-65%	82-90%	33%
Primary/secondary	4.1-4.3	8.1-45	5-8.6	2.2-9.2	0.55-0.77	0.03-0.1	1.96
Total 12α-OH BAs (μM)	78,906	30,265-36,087	12,094-17,389	42,818	241-837	66,882-67,538	19,714
Total non-12α-OH BAs (μM)	86,871	14,389-33,732	3984-10205	9259	50212-73250	244-269	13,602
% 12α-OH BAs	48%	47-63%	60-75%	51-82%	0-0.3%	92-97%	71%
% non-12α-OH BAs	52%	25-52%	24-40%	18-49%	99%	0.33-2.1%	26%

12α-OH/ non-12α-OH BAs	0.87-0.91	0.9-1.4	1.5-3.04	1.1-4.6	2.25	50-250	2.7
CA/CDCA	0.73-0.75	20-80	5.3-10	1.25-4.56	1.43	6.7	14
HI	0.27-0.4	-0.28 - -0.37	-0.03-0.11	0.23	-0.05	-	-

Table 1.10 Literature summary of liver BA profiles in different species.

Species	Human [271]	Mice [151]	Rat [271, 272]	Hamster [273]	Pig [139]	Bovine [139]
Total BA (μM)	62	170-226	9-70	151	6.5	2.54
Total LCA (μM)	1.5	0.4-0.7	0.1-6.8	1	0.6	0
Total UDCA (μM)	2	3.9-4.1	2.0-2.7	1.9	0.8	0
Total CDCA (μM)	31	4.1-4.6	0.6-2.5	36	1.4	0.06
Total DCA (μM)	6.2	7.4-8.1	1.3-7	10.3	0.92	0.1
Total HDCA (μM)		1.9-2.8	0.02-0.11	-	2.24	0
Total MDCA (μM)		2.2-2.3	-	-	-	-
Total CA (μM)	21	70-91	5-23	102	0.63	2.4
Total MCA (μM)		80-112	0.05-5.9	-	-	-
Total HCA (μM)		0.3-0.4	7.2	-	-	-
Total G-BA (μM)		0.1	0.65-0.69	-	-	-
Total T-BA (μM)		135-163	6.4-8.5	-	-	-
Total Unsulfated BA (μM)		170-226	7.3-9.4	-	6.5	2.54
Total Sulfated BA (μM)		-	-	-	-	-
%Sulfation of Total BA		-	-	-	-	-
%Amidation of Total BA		73-80%	96-98%	-	-	-
%G-amidation of Total BA		0.04-0.06%	7.3-8.9%	-	-	-
%T-amidation of Total BA		72-79%	87-91%	-	-	-
%Mono-OH BA	4.5%	0.2-0.3%	1-13%	0.7%	6.8%	0%
%Di-OH BA	67%	9.5-11%	50-64%	32%	89%	6%
%Tri-OH BA	28%	88-90%	35-49%	68%	6.4%	94%
%LCA	4.5%	0.2-0.3%	1-13%	0.7%	6.8%	0%
%UDCA	4.6%	1.7-2.4%	3.8-36%	1.3%	8.5%	0%
%CDCA	46%	2.0-4.0%	4.7-10%	24%	21%	2.3%
%DCA	16%	3.5-4.5%	14-18%	6.8%	10%	3.7%
%HDCA		1.1-1.3%	0.2-13%	-	47%	0%
%MDCA		1-1.3%	-	-	-	-
%CA	29%	40-41%	35-49%	67%	6.4%	94%
%MCA		47-49%	0.1-11%	-	-	-
%HCA		0.2%	-	-	-	-
Total Primary BAs (μM)	52	155-208	3.2-30	138	2.0	2.44
Total Secondary BAs (μM)	9.7	15-17	3.8-23	13	4.5	0.1
% Primary BAs	75%	90-92%	43-59%	91%	28%	96%
% Secondary BAs	25%	7.5-8.6%	41-57%	9%	72%	4%

Primary/secondary	3.03	11-12	0.8-1.5	11	0.4	33
Total 12α-OH BAs (μM)	27	77-99	3.8-29	112	1.6	2.5
Total non-12α-OH BAs (μM)	35	92-125	3.5-24	39	4.9	0.06
% 12α-OH BAs	44%	44-45%	52-63%	74%	17%	98%
% non-12α-OH BAs	56%	54-56%	37-48%	26%	83%	2%
12α-OH/ non-12α-OH BAs	0.80	0.8	1.1-1.7	2.89	0.22	46
CA/CDCA	0.62	17-19	4.4-8.7	2.83	0.29	45
HI		-0.24	-0.02	0.28	0.41	0.16

1.6 References

[1] D.Q. Wang, M.C. Carey, Therapeutic uses of animal biles in traditional Chinese medicine: an ethnopharmacological, biophysical chemical and medicinal review, World J Gastroenterol, 20 (2014) 9952-9975.
[2] D. Kritchevsky, P.P. Nair, Chemistry of the Bile Acids, in: P.P. Nair, D. Kritchevsky (Eds.) The Bile Acids Chemistry, Physiology, and Metabolism, Springer Science & Business Media2013, pp. 1-10.
[3] L.B. Agellon, Metabolism and function of bile acids, in: J.E. Vance, D. Vance (Eds.) Biochemistry of Lipids, Lipoproteins and Membranes, Elsevier Science2002, pp. 433-448.
[4] H.O. Wieland, Nobel Prize Lecture (1928): the chemistry of the bile acids, In Nobel Lectures, Chemistry, Elsevier Publishing Company, Amsterdam, 1966.
[5] A.F. Hofmann, L.R. Hagey, Key discoveries in bile acid chemistry and biology and their clinical applications: history of the last eight decades, J Lipid Res, 55 (2014) 1553-1595.
[6] Y. Alnouti, Bile Acid sulfation: a pathway of bile acid elimination and detoxification, Toxicol Sci, 108 (2009) 225-246.
[7] D.W. Russell, The enzymes, regulation, and genetics of bile acid synthesis, Annu Rev Biochem, 72 (2003) 137-174.
[8] T.M. Penning, Y. Jin, S. Steckelbroeck, T. Lanisnik Rizner, M. Lewis, Structure-function of human 3 alpha-hydroxysteroid dehydrogenases: genes and proteins, Mol Cell Endocrinol, 215 (2004) 63-72.
[9] S.J. Mihalik, S.J. Steinberg, Z. Pei, J. Park, D.G. Kim, A.K. Heinzer, G. Dacremont, R.J. Wanders, D.A. Cuebas, K.D. Smith, P.A. Watkins, Participation of two members of the very long-chain acyl-CoA synthetase family in bile acid synthesis and recycling, J Biol Chem, 277 (2002) 24771-24779.
[10] K. Solaas, A. Ulvestad, O. Soreide, B.F. Kase, Subcellular organization of bile acid amidation in human liver: a key issue in regulating the biosynthesis of bile salts, J Lipid Res, 41 (2000) 1154-1162.
[11] M. Axelson, J. Sjovall, Potential bile acid precursors in plasma--possible indicators of biosynthetic pathways to cholic and chenodeoxycholic acids in man, J Steroid Biochem, 36 (1990) 631-640.
[12] Z.R. Vlahcevic, W.M. Pandak, R.T. Stravitz, Regulation of bile acid biosynthesis, Gastroenterol Clin North Am, 28 (1999) 1-25, v.
[13] M. Axelson, B. Mork, A. Aly, O. Wisen, J. Sjovall, Concentrations of cholestenoic acids in plasma from patients with liver disease, J Lipid Res, 30 (1989) 1877-1882.
[14] A.F. Hofmann, L.R. Hagey, Bile acids: chemistry, pathochemistry, biology, pathobiology, and therapeutics, Cell Mol Life Sci, 65 (2008) 2461-2483.
[15] C. Thomas, R. Pellicciari, M. Pruzanski, J. Auwerx, K. Schoonjans, Targeting bile-acid signalling for metabolic diseases, Nat Rev Drug Discov, 7 (2008) 678-693.
[16] M. Trauner, J.L. Boyer, Bile salt transporters: molecular characterization, function, and regulation, Physiol Rev, 83 (2003) 633-671.
[17] P.J. Meier, B. Stieger, Bile salt transporters, Annu Rev Physiol, 64 (2002) 635-661.
[18] M. Trauner, M. Wagner, P. Fickert, G. Zollner, Molecular regulation of hepatobiliary transport systems: clinical implications for understanding and treating cholestasis, J Clin Gastroenterol, 39 (2005) S111-124.
[19] N. Ballatori, W.V. Christian, J.Y. Lee, P.A. Dawson, C.J. Soroka, J.L. Boyer, M.S. Madejczyk, N. Li, OSTalpha-OSTbeta: a major basolateral bile acid and steroid transporter in human intestinal, renal, and biliary epithelia, Hepatology, 42 (2005) 1270-1279.

[20] J.A. Byrne, S.S. Strautnieks, G. Mieli-Vergani, C.F. Higgins, K.J. Linton, R.J. Thompson, The human bile salt export pump: characterization of substrate specificity and identification of inhibitors, Gastroenterology, 123 (2002) 1649-1658.
[21] R. Aldini, M. Montagnani, A. Roda, S. Hrelia, P.L. Biagi, E. Roda, Intestinal absorption of bile acids in the rabbit: different transport rates in jejunum and ileum, Gastroenterology, 110 (1996) 459-468.
[22] F. Kuipers, M. Enserink, R. Havinga, A.B. van der Steen, M.J. Hardonk, J. Fevery, R.J. Vonk, Separate transport systems for biliary secretion of sulfated and unsulfated bile acids in the rat, J Clin Invest, 81 (1988) 1593-1599.
[23] H. Takikawa, M. Yokote, N. Sano, Y. Kuyama, M. Yamanaka, Absorption of unconjugated bile acids and tauroursodeoxycholate in the rat intestine, J Gastroenterol Hepatol, 12 (1997) 815-821.
[24] B. Philipp, Bacterial degradation of bile salts, Appl Microbiol Biotechnol, 89 (2011) 903-915.
[25] L. Maillette de Buy Wenniger, U. Beuers, Bile salts and cholestasis, Dig Liver Dis, 42 (2010) 409-418.
[26] S.M. Post, R. de Crom, R. van Haperen, A. van Tol, H.M. Princen, Increased fecal bile acid excretion in transgenic mice with elevated expression of human phospholipid transfer protein, Arterioscler Thromb Vasc Biol, 23 (2003) 892-897.
[27] T.Q. de Aguiar Vallim, E.J. Tarling, P.A. Edwards, Pleiotropic roles of bile acids in metabolism, Cell Metab, 17 (2013) 657-669.
[28] A.F. Hofmann, The continuing importance of bile acids in liver and intestinal disease, Arch Intern Med, 159 (1999) 2647-2658.
[29] M.J. Monte, J.J. Marin, A. Antelo, J. Vazquez-Tato, Bile acids: chemistry, physiology, and pathophysiology, World J Gastroenterol, 15 (2009) 804-816.
[30] A. Bajor, P.G. Gillberg, H. Abrahamsson, Bile acids: short and long term effects in the intestine, Scand J Gastroenterol, 45 (2010) 645-664.
[31] D.J. Parks, S.G. Blanchard, R.K. Bledsoe, G. Chandra, T.G. Consler, S.A. Kliewer, J.B. Stimmel, T.M. Willson, A.M. Zavacki, D.D. Moore, J.M. Lehmann, Bile acids: natural ligands for an orphan nuclear receptor, Science, 284 (1999) 1365-1368.
[32] H. Sato, A. Macchiarulo, C. Thomas, A. Gioiello, M. Une, A.F. Hofmann, R. Saladin, K. Schoonjans, R. Pellicciari, J. Auwerx, Novel potent and selective bile acid derivatives as TGR5 agonists: biological screening, structure-activity relationships, and molecular modeling studies, J Med Chem, 51 (2008) 1831-1841.
[33] I. Pineda Torra, T. Claudel, C. Duval, V. Kosykh, J.C. Fruchart, B. Staels, Bile acids induce the expression of the human peroxisome proliferator-activated receptor alpha gene via activation of the farnesoid X receptor, Mol Endocrinol, 17 (2003) 259-272.
[34] M.J. Perez, O. Briz, Bile-acid-induced cell injury and protection, World J Gastroenterol, 15 (2009) 1677-1689.
[35] M. Ferreira, P.M. Coxito, V.A. Sardao, C.M. Palmeira, P.J. Oliveira, Bile acids are toxic for isolated cardiac mitochondria: a possible cause for hepatic-derived cardiomyopathies?, Cardiovasc Toxicol, 5 (2005) 63-73.
[36] M.S. Gachet, P. Rhyn, O.G. Bosch, B.B. Quednow, J. Gertsch, A quantitiative LC-MS/MS method for the measurement of arachidonic acid, prostanoids, endocannabinoids, N-acylethanolamines and steroids in human plasma, J Chromatogr B Analyt Technol Biomed Life Sci, 976-977 (2015) 6-18.
[37] H. Higuchi, S.F. Bronk, Y. Takikawa, N. Werneburg, R. Takimoto, W. El-Deiry, G.J. Gores, The bile acid glycochenodeoxycholate induces trail-receptor 2/DR5 expression and apoptosis, J Biol Chem, 276 (2001) 38610-38618.
[38] C.M. Rodrigues, X. Ma, C. Linehan-Stieers, G. Fan, B.T. Kren, C.J. Steer, Ursodeoxycholic acid prevents cytochrome c release in apoptosis by inhibiting

mitochondrial membrane depolarization and channel formation, Cell Death Differ, 6 (1999) 842-854.
[39] A.A. Gafar, H.M. Draz, A.A. Goldberg, M.A. Bashandy, S. Bakry, M.A. Khalifa, W. AbuShair, V.I. Titorenko, J.T. Sanderson, Lithocholic acid induces endoplasmic reticulum stress, autophagy and mitochondrial dysfunction in human prostate cancer cells, PeerJ, 4 (2016) e2445.
[40] J.R. Spivey, S.F. Bronk, G.J. Gores, Glycochenodeoxycholate-induced lethal hepatocellular injury in rat hepatocytes. Role of ATP depletion and cytosolic free calcium, J Clin Invest, 92 (1993) 17-24.
[41] R.W. Owen, M. Dodo, M.H. Thompson, M.J. Hill, Fecal steroids and colorectal cancer, Nutr Cancer, 9 (1987) 73-80.
[42] B.S. Reddy, K. Watanabe, J.H. Weisburger, E.L. Wynder, Promoting effect of bile acids in colon carcinogenesis in germ-free and conventional F344 rats, Cancer Res, 37 (1977) 3238-3242.
[43] S.P. Bathena, R. Thakare, N. Gautam, S. Mukherjee, M. Olivera, J. Meza, Y. Alnouti, Urinary bile acids as biomarkers for liver diseases I. Stability of the baseline profile in healthy subjects, Toxicol Sci, 143 (2015) 296-307.
[44] S.P. Bathena, R. Thakare, N. Gautam, S. Mukherjee, M. Olivera, J. Meza, Y. Alnouti, Urinary bile acids as biomarkers for liver diseases II. Signature profiles in patients, Toxicol Sci, 143 (2015) 308-318.
[45] G. Chen, S. Wang, P. Bie, X. Li, J. Dong, Endogenous bile salts are associated with bile duct injury in the rat liver transplantation model, Transplantation, 87 (2009) 330-339.
[46] N.F. LaRusso, B.L. Shneider, D. Black, G.J. Gores, S.P. James, E. Doo, J.H. Hoofnagle, Primary sclerosing cholangitis: summary of a workshop, Hepatology, 44 (2006) 746-764.
[47] H. Hoekstra, R.J. Porte, Y. Tian, W. Jochum, B. Stieger, W. Moritz, M.J. Slooff, R. Graf, P.A. Clavien, Bile salt toxicity aggravates cold ischemic injury of bile ducts after liver transplantation in Mdr2+/- mice, Hepatology, 43 (2006) 1022-1031.
[48] M.J. Yska, C.I. Buis, D. Monbaliu, T.A. Schuurs, A.S. Gouw, O.N. Kahmann, D.S. Visser, J. Pirenne, R.J. Porte, The role of bile salt toxicity in the pathogenesis of bile duct injury after non-heart-beating porcine liver transplantation, Transplantation, 85 (2008) 1625-1631.
[49] C.I. Buis, E. Geuken, D.S. Visser, F. Kuipers, E.B. Haagsma, H.J. Verkade, R.J. Porte, Altered bile composition after liver transplantation is associated with the development of nonanastomotic biliary strictures, J Hepatol, 50 (2009) 69-79.
[50] E. Geuken, D. Visser, F. Kuipers, H. Blokzijl, H.G. Leuvenink, K.P. de Jong, P.M. Peeters, P.L. Jansen, M.J. Slooff, A.S. Gouw, R.J. Porte, Rapid increase of bile salt secretion is associated with bile duct injury after human liver transplantation, J Hepatol, 41 (2004) 1017-1025.
[51] A.F. Hofmann, K.J. Mysels, Bile acid solubility and precipitation in vitro and in vivo: the role of conjugation, pH, and Ca2+ ions, J Lipid Res, 33 (1992) 617-626.
[52] P. Fickert, A. Fuchsbichler, H.U. Marschall, M. Wagner, G. Zollner, R. Krause, K. Zatloukal, H. Jaeschke, H. Denk, M. Trauner, Lithocholic acid feeding induces segmental bile duct obstruction and destructive cholangitis in mice, Am J Pathol, 168 (2006) 410-422.
[53] I.M. Yousef, G. Bouchard, B. Tuchweber, G.L. Plaa, Monohydroxy bile acid induced cholestasis: role of biotransformation, Drug Metab Rev, 29 (1997) 167-181.
[54] A. Roda, A. Minutello, M.A. Angellotti, A. Fini, Bile acid structure-activity relationship: evaluation of bile acid lipophilicity using 1-octanol/water partition coefficient and reverse phase HPLC, J Lipid Res, 31 (1990) 1433-1443.

[55] M.C. Carey, J.C. Montet, M.C. Phillips, M.J. Armstrong, N.A. Mazer, Thermodynamic and molecular basis for dissimilar cholesterol-solubilizing capacities by micellar solutions of bile salts: cases of sodium chenodeoxycholate and sodium ursodeoxycholate and their glycine and taurine conjugates, Biochemistry, 20 (1981) 3637-3648.
[56] M.J. Armstrong, M.C. Carey, The hydrophobic-hydrophilic balance of bile salts. Inverse correlation between reverse-phase high performance liquid chromatographic mobilities and micellar cholesterol-solubilizing capacities, J Lipid Res, 23 (1982) 70-80.
[57] J.J. Gu, A.F. Hofmann, H.T. Ton-Nu, C.D. Schteingart, K.J. Mysels, Solubility of calcium salts of unconjugated and conjugated natural bile acids, J Lipid Res, 33 (1992) 635-646.
[58] D.M. Heuman, Quantitative estimation of the hydrophilic-hydrophobic balance of mixed bile salt solutions, J Lipid Res, 30 (1989) 719-730.
[59] D.M. Heuman, P.B. Hylemon, Z.R. Vlahcevic, Regulation of bile acid synthesis. III. Correlation between biliary bile salt hydrophobicity index and the activities of enzymes regulating cholesterol and bile acid synthesis in the rat, J Lipid Res, 30 (1989) 1161-1171.
[60] M. Posa, K. Popovic, Structure-Property Relationships in Sodium Muricholate Derivative (Bile Salts) Micellization: The Effect of Conformation of Steroid Skeleton on Hydrophobicity and Micelle Formation-Pattern Recognition and Potential Membranoprotective Properties, Mol Pharm, DOI 10.1021/acs.molpharmaceut.7b00375(2017).
[61] A.F. Hofmann, A. Roda, Physicochemical properties of bile acids and their relationship to biological properties: an overview of the problem, J Lipid Res, 25 (1984) 1477-1489.
[62] A. Roda, A.F. Hofmann, K.J. Mysels, The influence of bile salt structure on self-association in aqueous solutions, J Biol Chem, 258 (1983) 6362-6370.
[63] Y. Alnouti, I.L. Csanaky, C.D. Klaassen, Quantitative-profiling of bile acids and their conjugates in mouse liver, bile, plasma, and urine using LC–MS/MS, Journal of Chromatography B, 873 (2008) 209-217.
[64] M.O. Reynier, J.C. Montet, A. Gerolami, C. Marteau, C. Crotte, A.M. Montet, S. Mathieu, Comparative effects of cholic, chenodeoxycholic, and ursodeoxycholic acids on micellar solubilization and intestinal absorption of cholesterol, J Lipid Res, 22 (1981) 467-473.
[65] D.L. Schmucker, M. Ohta, S. Kanai, Y. Sato, K. Kitani, Hepatic injury induced by bile salts: correlation between biochemical and morphological events, Hepatology, 12 (1990) 1216-1221.
[66] M.M. Fisher, R. Magnusson, K. Miyai, Bile acid metabolism in mammals. I. Bile acid-induced intrahepatic cholestasis, Lab Invest, 25 (1971) 88-91.
[67] I.M. Yousef, S.G. Barnwell, B. Tuchweber, A. Weber, C.C. Roy, Effect of complete sulfation of bile acids on bile formation in rats, Hepatology, 7 (1987) 535-542.
[68] E.J. Sanchez Pozzi, F.A. Crocenzi, J.M. Pellegrino, V.A. Catania, M.G. Luquita, M.G. Roma, E.A. Rodriguez Garay, A.D. Mottino, Ursodeoxycholate reduces ethinylestradiol glucuronidation in the rat: role in prevention of estrogen-induced cholestasis, J Pharmacol Exp Ther, 306 (2003) 279-286.
[69] R. Drew, B.G. Priestly, Choleretic and cholestatic effects of infused bile salts in the rat, Experientia, 35 (1979) 809-811.
[70] Y. Kawamata, R. Fujii, M. Hosoya, M. Harada, H. Yoshida, M. Miwa, S. Fukusumi, Y. Habata, T. Itoh, Y. Shintani, S. Hinuma, Y. Fujisawa, M. Fujino, A G protein-coupled receptor responsive to bile acids, J Biol Chem, 278 (2003) 9435-9440.

[71] M. Makishima, A.Y. Okamoto, J.J. Repa, H. Tu, R.M. Learned, A. Luk, M.V. Hull, K.D. Lustig, D.J. Mangelsdorf, B. Shan, Identification of a nuclear receptor for bile acids, Science, 284 (1999) 1362-1365.
[72] S.I. Sayin, A. Wahlstrom, J. Felin, S. Jantti, H.U. Marschall, K. Bamberg, B. Angelin, T. Hyotylainen, M. Oresic, F. Backhed, Gut microbiota regulates bile acid metabolism by reducing the levels of tauro-beta-muricholic acid, a naturally occurring FXR antagonist, Cell Metab, 17 (2013) 225-235.
[73] C. Jiang, C. Xie, Y. Lv, J. Li, K.W. Krausz, J. Shi, C.N. Brocker, D. Desai, S.G. Amin, W.H. Bisson, Y. Liu, O. Gavrilova, A.D. Patterson, F.J. Gonzalez, Intestine-selective farnesoid X receptor inhibition improves obesity-related metabolic dysfunction, Nat Commun, 6 (2015) 10166.
[74] T. Patel, S.F. Bronk, G.J. Gores, Increases of intracellular magnesium promote glycodeoxycholate-induced apoptosis in rat hepatocytes, J Clin Invest, 94 (1994) 2183-2192.
[75] N. Azarpira, F. Rastegar, M. Amiri, E. Esfandiari, B. Geramizadeh, Comparison of Cytotoxic Activity of Bile on HepG2 and CCRF-CEM Cell Lines: An in Vitro Study, Iran J Med Sci, 37 (2012) 266-270.
[76] D.M. Heuman, W.M. Pandak, P.B. Hylemon, Z.R. Vlahcevic, Conjugates of ursodeoxycholate protect against cytotoxicity of more hydrophobic bile salts: in vitro studies in rat hepatocytes and human erythrocytes, Hepatology, 14 (1991) 920-926.
[77] R.G. Quist, H.T. Ton-Nu, J. Lillienau, A.F. Hofmann, K.E. Barrett, Activation of mast cells by bile acids, Gastroenterology, 101 (1991) 446-456.
[78] A.I. Haza, B. Glinghammar, A. Grandien, J. Rafter, Effect of colonic luminal components on induction of apoptosis in human colonic cell lines, Nutr Cancer, 36 (2000) 79-89.
[79] A.A. Powell, J.M. LaRue, A.K. Batta, J.D. Martinez, Bile acid hydrophobicity is correlated with induction of apoptosis and/or growth arrest in HCT116 cells, Biochem J, 356 (2001) 481-486.
[80] C. Rust, K. Bauchmuller, P. Fickert, A. Fuchsbichler, U. Beuers, Phosphatidylinositol 3-kinase-dependent signaling modulates taurochenodeoxycholic acid-induced liver injury and cholestasis in perfused rat livers, Am J Physiol Gastrointest Liver Physiol, 289 (2005) G88-94.
[81] J. Sonoda, W. Xie, J.M. Rosenfeld, J.L. Barwick, P.S. Guzelian, R.M. Evans, Regulation of a xenobiotic sulfonation cascade by nuclear pregnane X receptor (PXR), Proc Natl Acad Sci U S A, 99 (2002) 13801-13806.
[82] B.W. Katona, S. Anant, D.F. Covey, W.F. Stenson, Characterization of enantiomeric bile acid-induced apoptosis in colon cancer cell lines, J Biol Chem, 284 (2009) 3354-3364.
[83] S.P. Bathena, S. Mukherjee, M. Olivera, Y. Alnouti, The profile of bile acids and their sulfate metabolites in human urine and serum, J Chromatogr B Analyt Technol Biomed Life Sci, 942-943 (2013) 53-62.
[84] L.R. Hagey, C.D. Schteingart, S.S. Rossi, H.T. Ton-Nu, A.F. Hofmann, An N-acyl glycyltaurine conjugate of deoxycholic acid in the biliary bile acids of the rabbit, J Lipid Res, 39 (1998) 2119-2124.
[85] E.M. Shonsey, M. Sfakianos, M. Johnson, D. He, C.N. Falany, J. Falany, D.J. Merkler, S. Barnes, Bile acid coenzyme A: amino acid N-acyltransferase in the amino acid conjugation of bile acids, Methods Enzymol, 400 (2005) 374-394.
[86] J.C. Garcia-Canaveras, M.T. Donato, J.V. Castell, A. Lahoz, Targeted profiling of circulating and hepatic bile acids in human, mouse, and rat using a UPLC-MRM-MS-validated method, J Lipid Res, 53 (2012) 2231-2241.

[87] J. Huang, S.P. Bathena, I.L. Csanaky, Y. Alnouti, Simultaneous characterization of bile acids and their sulfate metabolites in mouse liver, plasma, bile, and urine using LC-MS/MS, J Pharm Biomed Anal, 55 (2011) 1111-1119.
[88] Y. Alnouti, I.L. Csanaky, C.D. Klaassen, Quantitative-profiling of bile acids and their conjugates in mouse liver, bile, plasma, and urine using LC-MS/MS, J Chromatogr B Analyt Technol Biomed Life Sci, 873 (2008) 209-217.
[89] P.H. Kook, S. Schellenberg, K.M. Rentsch, C.E. Reusch, T.M. Glaus, Effect of twice-daily oral administration of hydrocortisone on the bile acids composition of gallbladder bile in dogs, Am J Vet Res, 72 (2011) 1607-1612.
[90] W. Taylor, The bile acid composition of rabbit and cat gall-bladder bile, J Steroid Biochem, 8 (1977) 1077-1084.
[91] T. Washizu, I. Tomoda, J.J. Kaneko, Serum bile acid composition of the dog, cow, horse and human, J Vet Med Sci, 53 (1991) 81-86.
[92] K. Lundell, Cloning and expression of two novel pig liver and kidney fatty acid hydroxylases [cytochrome P450 (CYP)4A24 and CYP4A25], Biochem J, 363 (2002) 297-303.
[93] J. Zhang, W. Huang, M. Qatanani, R.M. Evans, D.D. Moore, The constitutive androstane receptor and pregnane X receptor function coordinately to prevent bile acid-induced hepatotoxicity, J Biol Chem, 279 (2004) 49517-49522.
[94] T. Adachi, T. Kaminaga, H. Yasuda, T. Kamiya, H. Hara, The involvement of endoplasmic reticulum stress in bile acid-induced hepatocellular injury, J Clin Biochem Nutr, 54 (2014) 129-135.
[95] M. Schwenk, A.F. Hofmann, G.L. Carlson, J.A. Carter, F. Coulston, H. Greim, Bile acid conjugation in the chimpanzee: effective sulfation of lithocholic acid, Arch Toxicol, 40 (1978) 109-118.
[96] A.F. Hofmann, L.R. Hagey, M.D. Krasowski, Bile salts of vertebrates: structural variation and possible evolutionary significance, J Lipid Res, 51 (2010) 226-246.
[97] E. Ogimura, S. Sekine, T. Horie, Bile salt export pump inhibitors are associated with bile acid-dependent drug-induced toxicity in sandwich-cultured hepatocytes, Biochem Biophys Res Commun, 416 (2011) 313-317.
[98] T.L. Marion, C.H. Perry, R.L. St Claire, 3rd, K.L. Brouwer, Endogenous bile acid disposition in rat and human sandwich-cultured hepatocytes, Toxicol Appl Pharmacol, 261 (2012) 1-9.
[99] X. Chu, K. Bleasby, R. Evers, Species differences in drug transporters and implications for translating preclinical findings to humans, Expert Opin Drug Metab Toxicol, 9 (2013) 237-252.
[100] D. Keppler, Multidrug resistance proteins (MRPs, ABCCs): importance for pathophysiology and drug therapy, Handb Exp Pharmacol, DOI 10.1007/978-3-642-14541-4_8(2011) 299-323.
[101] H. Akita, H. Suzuki, T. Hirohashi, H. Takikawa, Y. Sugiyama, Transport activity of human MRP3 expressed in Sf9 cells: comparative studies with rat MRP3, Pharm Res, 19 (2002) 34-41.
[102] G. Ostapowicz, R.J. Fontana, F.V. Schiodt, A. Larson, T.J. Davern, S.H. Han, T.M. McCashland, A.O. Shakil, J.E. Hay, L. Hynan, J.S. Crippin, A.T. Blei, G. Samuel, J. Reisch, W.M. Lee, U.S.A.L.F.S. Group, Results of a prospective study of acute liver failure at 17 tertiary care centers in the United States, Ann Intern Med, 137 (2002) 947-954.
[103] A.M. Larson, J. Polson, R.J. Fontana, T.J. Davern, E. Lalani, L.S. Hynan, J.S. Reisch, F.V. Schiodt, G. Ostapowicz, A.O. Shakil, W.M. Lee, G. Acute Liver Failure Study, Acetaminophen-induced acute liver failure: results of a United States multicenter, prospective study, Hepatology, 42 (2005) 1364-1372.

[104] N. Mohankumar, P. Ranjan, A. Kumari, Drug-induced liver injury: Diagnosing (and treating) it early, J Fam Pract, 64 (2015) 634-644.
[105] H. Kawai, N. Kudo, Y. Kawashima, A. Mitsumoto, Efficacy of urine bile acid as a non-invasive indicator of liver damage in rats, J Toxicol Sci, 34 (2009) 27-38.
[106] C.E. Balkman, S.A. Center, J.F. Randolph, D. Trainor, K.L. Warner, M.A. Crawford, K. Adachi, H.N. Erb, Evaluation of urine sulfated and nonsulfated bile acids as a diagnostic test for liver disease in dogs, J Am Vet Med Assoc, 222 (2003) 1368-1375.
[107] D. Trainor, S.A. Center, F. Randolph, C.E. Balkman, K.L. Warner, M.A. Crawford, K. Adachi, H.N. Erb, Urine sulfated and nonsulfated bile acids as a diagnostic test for liver disease in cats, J Vet Intern Med, 17 (2003) 145-153.
[108] M.B. De Valle, V. Av Klinteberg, N. Alem, R. Olsson, E. Bjornsson, Drug-induced liver injury in a Swedish University hospital out-patient hepatology clinic, Aliment Pharmacol Ther, 24 (2006) 1187-1195.
[109] M. Wagner, G. Zollner, M. Trauner, New molecular insights into the mechanisms of cholestasis, J Hepatol, 51 (2009) 565-580.
[110] S. Dueland, J. Reichen, G.T. Everson, R.A. Davis, Regulation of cholesterol and bile acid homoeostasis in bile-obstructed rats, Biochem J, 280 (Pt 2) (1991) 373-377.
[111] F.A. Atienzar, E.A. Blomme, M. Chen, P. Hewitt, J.G. Kenna, G. Labbe, F. Moulin, F. Pognan, A.B. Roth, L. Suter-Dick, O. Ukairo, R.J. Weaver, Y. Will, D.M. Dambach, Key Challenges and Opportunities Associated with the Use of In Vitro Models to Detect Human DILI: Integrated Risk Assessment and Mitigation Plans, Biomed Res Int, 2016 (2016) 9737920.
[112] R.E. Morgan, M. Trauner, C.J. van Staden, P.H. Lee, B. Ramachandran, M. Eschenberg, C.A. Afshari, C.W. Qualls, Jr., R. Lightfoot-Dunn, H.K. Hamadeh, Interference with bile salt export pump function is a susceptibility factor for human liver injury in drug development, Toxicol Sci, 118 (2010) 485-500.
[113] S. Dawson, S. Stahl, N. Paul, J. Barber, J.G. Kenna, In vitro inhibition of the bile salt export pump correlates with risk of cholestatic drug-induced liver injury in humans, Drug Metab Dispos, 40 (2012) 130-138.
[114] R.W. Yucha, K. He, Q. Shi, L. Cai, Y. Nakashita, C.Q. Xia, M. Liao, In Vitro Drug-Induced Liver Injury Prediction: Criteria Optimization of Efflux Transporter IC50 and Physicochemical Properties, Toxicol Sci, 157 (2017) 487-499.
[115] K. Kock, B.C. Ferslew, I. Netterberg, K. Yang, T.J. Urban, P.W. Swaan, P.W. Stewart, K.L. Brouwer, Risk factors for development of cholestatic drug-induced liver injury: inhibition of hepatic basolateral bile acid transporters multidrug resistance-associated proteins 3 and 4, Drug Metab Dispos, 42 (2014) 665-674.
[116] R.E. Morgan, C.J. van Staden, Y. Chen, N. Kalyanaraman, J. Kalanzi, R.T. Dunn, 2nd, C.A. Afshari, H.K. Hamadeh, A multifactorial approach to hepatobiliary transporter assessment enables improved therapeutic compound development, Toxicol Sci, 136 (2013) 216-241.
[117] D. Smith, C. Broadhead, G. Descotes, R. Fosse, R. Hack, K. Krauser, R. Pfister, B. Phillips, Y. Rabemampianina, J. Sanders, S. Sparrow, M. Stephan-Gueldner, S.D. Jacobsen, Preclinical safety evaluation using nonrodent species: an industry/welfare project to minimize dog use, ILAR J, 43 Suppl (2002) S39-42.
[118] R. Dixit, U.A. Boelsterli, Healthy animals and animal models of human disease(s) in safety assessment of human pharmaceuticals, including therapeutic antibodies, Drug Discov Today, 12 (2007) 336-342.
[119] M. Chen, J. Borlak, W. Tong, Predicting idiosyncratic drug-induced liver injury: some recent advances, Expert Rev Gastroenterol Hepatol, 8 (2014) 721-723.

[120] H.S. Schadt, A. Wolf, F. Pognan, S.D. Chibout, M. Merz, G.A. Kullak-Ublick, Bile acids in drug induced liver injury: Key players and surrogate markers, Clin Res Hepatol Gastroenterol, 40 (2016) 257-266.
[121] M. Podell, H.A. Volk, M. Berendt, W. Loscher, K. Munana, E.E. Patterson, S.R. Platt, 2015 ACVIM Small Animal Consensus Statement on Seizure Management in Dogs, J Vet Intern Med, 30 (2016) 477-490.
[122] T.R. Gadacz, R.N. Allan, E. Mack, A.F. Hofmann, Impaired lithocholate sulfation in the rhesus monkey: a possible mechanism for chenodeoxycholate toxicity, Gastroenterology, 70 (1976) 1125-1129.
[123] H. Dyrszka, G. Salen, F.G. Zaki, T. Chen, E.H. Mosbach, Hepatic toxicity in the rhesus monkey treated with chenodeoxycholic acid for 6 months: biochemical and ultrastructural studies, Gastroenterology, 70 (1976) 93-104.
[124] C.D. Fischer, N.S. Cooper, M.A. Rothschild, E.H. Mosbach, Effect of dietary chenodeoxycholic acid and lithocholic acid in the rabbit, Am J Dig Dis, 19 (1974) 877-886.
[125] A.F. Hofmann, The enterohepatic circulation of bile acids in mammals: form and functions, Front Biosci (Landmark Ed), 14 (2009) 2584-2598.
[126] R. Okun, L.I. Goldstein, G.A. Van Gelder, E.I. Goldenthal, F.X. Wazeter, R.G. Giel, National Cooperative Gallstone Study: nonprimate toxicology of chenodeoxycholic acid, J Toxicol Environ Health, 9 (1982) 727-741.
[127] A.F. Hofmann, Detoxification of lithocholic acid, a toxic bile acid: relevance to drug hepatotoxicity, Drug Metab Rev, 36 (2004) 703-722.
[128] L.J. Schoenfield, J.M. Lachin, Chenodiol (chenodeoxycholic acid) for dissolution of gallstones: the National Cooperative Gallstone Study. A controlled trial of efficacy and safety, Ann Intern Med, 95 (1981) 257-282.
[129] M.J. Dew, K. James, D. Gatehouse, N.J. Dorricott, R.N. Allan, Lithocholate sulphation in the baboon, J Med Primatol, 11 (1982) 59-64.
[130] F. Stellaard, P.D. Klein, A.F. Hofmann, J.M. Lachin, Mass spectrometry identification of biliary bile acids in bile from patients with gallstones before and during treatment with chenodeoxycholic acid. An ancillary study of the National Cooperative Gallstone Study, J Lab Clin Med, 105 (1985) 504-513.
[131] S.A. Bagheri, M.G. Bolt, J.L. Boyer, R.H. Palmer, Stimulation of thymidine incorporation in mouse liver and biliary tract epithelium by lithocholate and deoxycholate, Gastroenterology, 74 (1978) 188-192.
[132] N.R. Pattinson, B.A. Chapman, Lithocholate detoxification and biliary secretion in the rat, Biochem Int, 9 (1984) 137-142.
[133] T. Susukida, S. Sekine, M. Nozaki, M. Tokizono, K. Ito, Prediction of the Clinical Risk of Drug-Induced Cholestatic Liver Injury Using an In Vitro Sandwich Cultured Hepatocyte Assay, Drug Metab Dispos, 43 (2015) 1760-1768.
[134] R. Wang, M. Salem, I.M. Yousef, B. Tuchweber, P. Lam, S.J. Childs, C.D. Helgason, C. Ackerley, M.J. Phillips, V. Ling, Targeted inactivation of sister of P-glycoprotein gene (spgp) in mice results in nonprogressive but persistent intrahepatic cholestasis, Proc Natl Acad Sci U S A, 98 (2001) 2011-2016.
[135] H.U. Marschall, M. Wagner, K. Bodin, G. Zollner, P. Fickert, J. Gumhold, D. Silbert, A. Fuchsbichler, J. Sjovall, M. Trauner, Fxr(-/-) mice adapt to biliary obstruction by enhanced phase I detoxification and renal elimination of bile acids, J Lipid Res, 47 (2006) 582-592.
[136] S.P.R. Bathena, S. Mukherjee, M. Olivera, Y. Alnouti, The profile of bile acids and their sulfate metabolites in human urine and serum, Journal of Chromatography B, 942–943 (2013) 53-62.

[137] E. Raschi, F. De Ponti, Drug-induced liver injury: Towards early prediction and risk stratification, World J Hepatol, 9 (2017) 30-37.
[138] Q. Wu, X. Zhang, M. Zhong, H. Han, S. Liu, T. Liu, M. Wei, W. Guo, H. Xie, S. Hu, G. Zhang, Effects of Bariatric Surgery on Serum Bile Acid Composition and Conjugation in a Diabetic Rat Model, Obes Surg, 26 (2016) 2384-2392.
[139] S.J. Tsai, Y.S. Zhong, J.F. Weng, H.H. Huang, P.Y. Hsieh, Determination of bile acids in pig liver, pig kidney and bovine liver by gas chromatography-chemical ionization tandem mass spectrometry with total ion chromatograms and extraction ion chromatograms, J Chromatogr A, 1218 (2011) 524-533.
[140] P. Gunness, B.A. Williams, W.J. Gerrits, A.R. Bird, O. Kravchuk, M.J. Gidley, Circulating triglycerides and bile acids are reduced by a soluble wheat arabinoxylan via modulation of bile concentration and lipid digestion rates in a pig model, Mol Nutr Food Res, 60 (2016) 642-651.
[141] V. Spinelli, F. Lalloyer, G. Baud, E. Osto, M. Kouach, M. Daoudi, E. Vallez, V. Raverdy, J.F. Goossens, A. Descat, P. Doytcheva, T. Hubert, T.A. Lutz, S. Lestavel, B. Staels, F. Pattou, A. Tailleux, Influence of Roux-en-Y gastric bypass on plasma bile acid profiles: a comparative study between rats, pigs and humans, Int J Obes (Lond), 40 (2016) 1260-1267.
[142] J. Han, Y. Liu, R. Wang, J. Yang, V. Ling, C.H. Borchers, Metabolic profiling of bile acids in human and mouse blood by LC-MS/MS in combination with phospholipid-depletion solid-phase extraction, Anal Chem, 87 (2015) 1127-1136.
[143] M. Ando, T. Kaneko, R. Watanabe, S. Kikuchi, T. Goto, T. Iida, T. Hishinuma, N. Mano, J. Goto, High sensitive analysis of rat serum bile acids by liquid chromatography/electrospray ionization tandem mass spectrometry, J Pharm Biomed Anal, 40 (2006) 1179-1186.
[144] T. Washizu, T. Ishida, M. Washizu, I. Tomoda, J.J. Kaneko, Changes in bile acid composition of serum and gallbladder bile in bile duct ligated dogs, J Vet Med Sci, 56 (1994) 299-303.
[145] C. Chen, B. Hu, T. Wu, Y. Zhang, Y. Xu, Y. Feng, H. Jiang, Bile acid profiles in diabetic (db/db) mice and their wild type littermates, J Pharm Biomed Anal, 131 (2016) 473-481.
[146] M. Aoki, Y. Konya, T. Takagaki, K. Umemura, Y. Sogame, T. Katsumata, S. Komuro, Metabolomic investigation of cholestasis in a rat model using ultra-performance liquid chromatography/tandem mass spectrometry, Rapid Commun Mass Spectrom, 25 (2011) 1847-1852.
[147] F.A. Bodewes, M. Wouthuyzen-Bakker, M.J. Bijvelds, R. Havinga, H.R. de Jonge, H.J. Verkade, Ursodeoxycholate modulates bile flow and bile salt pool independently from the cystic fibrosis transmembrane regulator (Cftr) in mice, Am J Physiol Gastrointest Liver Physiol, 302 (2012) G1035-1042.
[148] A.F. Attili, M. Angelico, A. Cantafora, D. Alvaro, L. Capocaccia, Bile acid-induced liver toxicity: relation to the hydrophobic-hydrophilic balance of bile acids, Med Hypotheses, 19 (1986) 57-69.
[149] S. Watanabe, K. Tsuneyama, Cattle bile but not bear bile or pig bile induces lipid profile changes and fatty liver injury in mice: mediation by cholic acid, J Toxicol Sci, 37 (2012) 105-121.
[150] J. Han, Y. Liu, R. Wang, J. Yang, V. Ling, C.H. Borchers, Metabolic profiling of bile acids in human and mouse blood by LC-MS/MS in combination with phospholipid-depletion solid-phase extraction, Analytical Chemistry, 87 (2015) 1127-1136.
[151] Y. Zhang, C.D. Klaassen, Effects of feeding bile acids and a bile acid sequestrant on hepatic bile acid composition in mice, J Lipid Res, 51 (2010) 3230-3242.

[152] B.I. Cohen, A.F. Hofmann, E.H. Mosbach, R.J. Stenger, M.A. Rothschild, L.R. Hagey, Y.B. Yoon, Differing effects of nor-ursodeoxycholic or ursodeoxycholic acid on hepatic histology and bile acid metabolism in the rabbit, Gastroenterology, 91 (1986) 189-197.
[153] G.L. Si, P. Yao, L. Shi, Rapid Determination of Bile Acids in Bile from Various Mammals by Reversed-Phase Ultra-Fast Liquid Chromatography, J Chromatogr Sci, 53 (2015) 1060-1065.
[154] P. Scanff, P. Monti, C. Joubert, S. Grison, P. Gourmelon, N.M. Griffiths, Modified bile acid profiles in mixed neutron and gamma-irradiated pigs, Int J Radiat Biol, 75 (1999) 209-216.
[155] J. Kasbo, M. Saleem, S. Perwaiz, D. Mignault, T. Lamireau, B. Tuchweber, I. Yousef, Biliary, fecal and plasma deoxycholic acid in rabbit, hamster, guinea pig, and rat: comparative study and implication in colon cancer, Biol Pharm Bull, 25 (2002) 1381-1384.
[156] J.B. Das, N.D. Poulos, G.G. Ansari, Biliary lipid composition and bile acid profiles during and after enteral fast of total parenteral nutrition in the rabbit, J Pediatr Gastroenterol Nutr, 22 (1996) 85-91.
[157] R. Coleman, S. Iqbal, P.P. Godfrey, D. Billington, Membranes and bile formation. Composition of several mammalian biles and their membrane-damaging properties, Biochem J, 178 (1979) 201-208.
[158] J. Scholmerich, M.S. Becher, K. Schmidt, R. Schubert, B. Kremer, S. Feldhaus, W. Gerok, Influence of hydroxylation and conjugation of bile salts on their membrane-damaging properties--studies on isolated hepatocytes and lipid membrane vesicles, Hepatology, 4 (1984) 661-666.
[159] P. Song, Y. Zhang, C.D. Klaassen, Dose-response of five bile acids on serum and liver bile Acid concentrations and hepatotoxicty in mice, Toxicol Sci, 123 (2011) 359-367.
[160] R.K. Latta, H. Fiander, N.W. Ross, C. Simpson, H. Schneider, Toxicity of bile acids to colon cancer cell lines, Cancer Lett, 70 (1993) 167-173.
[161] R.H. Palmer, Bile acid sulfates. II. Formation, metabolism, and excretion of lithocholic acid sulfates in the rat, J Lipid Res, 12 (1971) 680-687.
[162] R.T. Jensen, R.A. Davis, F. Kern, Jr., Increased sulfation and decreased 7alpha-hydroxylation of deoxycholic acid in ethinyl estradiol-induced cholestasis in rats, Gastroenterology, 73 (1977) 314-320.
[163] M. Takita, S. Ikawa, Y. Ogura, Effect of bile duct ligation on bile acid and cholesterol metabolism in rats, J Biochem, 103 (1988) 778-786.
[164] D.P. Cleland, T.C. Bartholomew, B.H. Billing, Hepatic transport of sulfated and nonsulfated bile acids in the rat following relief of bile duct obstruction, Hepatology, 4 (1984) 477-485.
[165] E. Purucker, H.U. Marschall, R. Winograd, S. Matern, Metabolism and effects on cholestasis of isoursodeoxycholic and ursodeoxycholic acids in bile duct ligated rats, Biochim Biophys Acta, 1526 (2001) 44-52.
[166] R.H. Palmer, C.K. McSherry, Lithocholate metabolism in baboons fed chenodeoxycholate, J Lab Clin Med, 99 (1982) 533-538.
[167] S. Barnes, P.G. Burhol, R. Zander, B.I. Hirschowitz, The effect of bile duct ligation on hepatic bile acid sulfotransferase activity in the hamster, Biochem Med, 22 (1979) 165-174.
[168] A.E. Cowen, M.G. Korman, A.F. Hofmann, O.W. Cass, Metabolism of lethocholate in healthy man. I. Biotransformation and biliary excretion of intravenously administered lithocholate, lithocholylglycine, and their sulfates, Gastroenterology, 69 (1975) 59-66.

[169] B. Alme, A. Bremmelgaard, J. Sjovall, P. Thomassen, Analysis of metabolic profiles of bile acids in urine using a lipophilic anion exchanger and computerized gas-liquid chromatorgaphy-mass spectrometry, J Lipid Res, 18 (1977) 339-362.
[170] I. Makino, H. Hashimoto, K. Shinozaki, K. Yoshino, S. Nakagawa, Sulfated and nonsulfated bile acids in urine, serum, and bile of patients with hepatobiliary diseases, Gastroenterology, 68 (1975) 545-553.
[171] L. Humbert, M.A. Maubert, C. Wolf, H. Duboc, M. Mahe, D. Farabos, P. Seksik, J.M. Mallet, G. Trugnan, J. Masliah, D. Rainteau, Bile acid profiling in human biological samples: comparison of extraction procedures and application to normal and cholestatic patients, J Chromatogr B Analyt Technol Biomed Life Sci, 899 (2012) 135-145.
[172] K.D. Setchell, A. Matsui, Serum bile acid analysis, Clin Chim Acta, 127 (1983) 1-17.
[173] H. Takikawa, H. Otsuka, T. Beppu, Y. Seyama, T. Yamakawa, Serum concentrations of bile acid glucuronides in hepatobiliary diseases, Digestion, 27 (1983) 189-195.
[174] J. Huang, S.P. Bathena, J. Tong, M. Roth, B. Hagenbuch, Y. Alnouti, Kinetic analysis of bile acid sulfation by stably expressed human sulfotransferase 2A1 (SULT2A1), Xenobiotica, 40 (2010) 184-194.
[175] L. Capocaccia, A.F. Attili, A. Cantafora, F. Bracci, L. Paciscopi, C. Puoti, U. Pieche, M. Angelico, Sulfated bile acids in serum, bile, and urine of cirrhotic patients before and after portacaval anastomosis, Dig Dis Sci, 26 (1981) 513-517.
[176] S. Krief, A. Jamart, C.M. Hladik, On the possible adaptive value of coprophagy in free-ranging chimpanzees, Primates, 45 (2004) 141-145.
[177] A. Groen, C. Kunne, R.P. Oude Elferink, Increased serum concentrations of secondary bile salts during cholate feeding are due to coprophagy. A study with wild-type and Atp8b1-deficient mice, Mol Pharm, 3 (2006) 756-761.
[178] M. Zhang, J.Y. Chiang, Transcriptional regulation of the human sterol 12alpha-hydroxylase gene (CYP8B1): roles of heaptocyte nuclear factor 4alpha in mediating bile acid repression, J Biol Chem, 276 (2001) 41690-41699.
[179] W.M. Pandak, P. Bohdan, C. Franklund, D.H. Mallonee, G. Eggertsen, I. Bjorkhem, G. Gil, Z.R. Vlahcevic, P.B. Hylemon, Expression of sterol 12alpha-hydroxylase alters bile acid pool composition in primary rat hepatocytes and in vivo, Gastroenterology, 120 (2001) 1801-1809.
[180] J. Trottier, A. Bialek, P. Caron, R.J. Straka, J. Heathcote, P. Milkiewicz, O. Barbier, Metabolomic profiling of 17 bile acids in serum from patients with primary biliary cirrhosis and primary sclerosing cholangitis: a pilot study, Dig Liver Dis, 44 (2012) 303-310.
[181] G. Xie, Y. Wang, X. Wang, A. Zhao, T. Chen, Y. Ni, L. Wong, H. Zhang, J. Zhang, C. Liu, P. Liu, W. Jia, Profiling of serum bile acids in a healthy Chinese population using UPLC-MS/MS, J Proteome Res, 14 (2015) 850-859.
[182] B.C. Ferslew, G. Xie, C.K. Johnston, M. Su, P.W. Stewart, W. Jia, K.L. Brouwer, A.S.t. Barritt, Altered Bile Acid Metabolome in Patients with Nonalcoholic Steatohepatitis, Dig Dis Sci, 60 (2015) 3318-3328.
[183] R.E. Roberts, C. Glicksman, J. Alaghband-Zadeh, R.A. Sherwood, N. Akuji, C.W. le Roux, The relationship between postprandial bile acid concentration, GLP-1, PYY and ghrelin, Clin Endocrinol (Oxf), 74 (2011) 67-72.
[184] G. Brufau, M.J. Bahr, B. Staels, T. Claudel, J. Ockenga, K.H. Boker, E.J. Murphy, K. Prado, F. Stellaard, M.P. Manns, F. Kuipers, U.J. Tietge, Plasma bile acids are not associated with energy metabolism in humans, Nutr Metab (Lond), 7 (2010) 73.
[185] M. Wewalka, M.E. Patti, C. Barbato, S.M. Houten, A.B. Goldfine, Fasting serum taurine-conjugated bile acids are elevated in type 2 diabetes and do not change with intensification of insulin, J Clin Endocrinol Metab, 99 (2014) 1442-1451.

[186] J. Huang, S.P.R. Bathena, I.L. Csanaky, Y. Alnouti, Simultaneous characterization of bile acids and their sulfate metabolites in mouse liver, plasma, bile, and urine using LC–MS/MS, Journal of pharmaceutical and biomedical analysis, 55 (2011) 1111-1119.
[187] H. Nittono, K. Obinata, N. Nakatsu, T. Watanabe, S. Niijima, H. Sasaki, O. Arisaka, H. Kato, K. Yabuta, T. Miyano, Sulfated and nonsulfated bile acids in urine of patients with biliary atresia: analysis of bile acids by high-performance liquid chromatography, J Pediatr Gastroenterol Nutr, 5 (1986) 23-29.
[188] J. Lee, F. Azzaroli, L. Wang, C.J. Soroka, A. Gigliozzi, K.D. Setchell, W. Kramer, J.L. Boyer, Adaptive regulation of bile salt transporters in kidney and liver in obstructive cholestasis in the rat, Gastroenterology, 121 (2001) 1473-1484.
[189] A. Stiehl, R. Raedsch, G. Rudolph, U. Gundert-Remy, M. Senn, Biliary and urinary excretion of sulfated, glucuronidated and tetrahydroxylated bile acids in cirrhotic patients, Hepatology, 5 (1985) 492-495.
[190] H. Takikawa, T. Beppu, Y. Seyama, Profiles of bile acids and their glucuronide and sulphate conjugates in the serum, urine and bile from patients undergoing bile drainage, Gut, 26 (1985) 38-42.
[191] K. Obinata, M. Hayashi, A. Tokita, N. Nakatsu, T. Watanabe, S. Niijima, O. Arisaka, H. Nittono, K. Yabuta, T. Miyano, Sulfated and nonsulfated urinary bile acids in cholestasis in children, Acta Paediatr Jpn, 30 (1988) 299-303.
[192] L.J. Meng, H. Reyes, J. Palma, I. Hernandez, J. Ribalta, J. Sjovall, Effects of ursodeoxycholic acid on conjugated bile acids and progesterone metabolites in serum and urine of patients with intrahepatic cholestasis of pregnancy, J Hepatol, 27 (1997) 1029-1040.
[193] S. Fischer, U. Beuers, F. Berr, G. Paumgartner, Deoxycholic acid is not reconverted to cholic acid in humans--a study by isotope ratio mass spectrometry, Clin Chim Acta, 203 (1991) 269-273.
[194] T.A. Mahowald, J.T. Matschiner, S.L. Hsia, R. Richter, E.A. Doisy, Jr., W.H. Elliott, E.A. Doisy, Bile acids. II. Metabolism of deoxycholic acid-24-C14 and chenodeoxycholic acid-24-C14 in the rat, J Biol Chem, 225 (1957) 781-793.
[195] A. Kiontke, A. Oliveira-Birkmeier, A. Opitz, C. Birkemeyer, Electrospray Ionization Efficiency Is Dependent on Different Molecular Descriptors with Respect to Solvent pH and Instrumental Configuration, PLoS One, 11 (2016) e0167502.
[196] E. Brewer, J. Henion, Atmospheric pressure ionization LC/MS/MS techniques for drug disposition studies, J Pharm Sci, 87 (1998) 395-402.
[197] J.S. Page, R.T. Kelly, K. Tang, R.D. Smith, Ionization and transmission efficiency in an electrospray ionization-mass spectrometry interface, J Am Soc Mass Spectrom, 18 (2007) 1582-1590.
[198] S. Schadt, L.Z. Chen, D. Bischoff, Evaluation of relative LC/MS response of metabolites to parent drug in LC/nanospray ionization mass spectrometry: potential implications in MIST assessment, J Mass Spectrom, 46 (2011) 1281-1286.
[199] S. Zhang, C.K. Van Pelt, Chip-based nanoelectrospray mass spectrometry for protein characterization, Expert Rev Proteomics, 1 (2004) 449-468.
[200] Y. Deng, J.T. Wu, H. Zhang, T.V. Olah, Quantitation of drug metabolites in the absence of pure metabolite standards by high-performance liquid chromatography coupled with a chemiluminescence nitrogen detector and mass spectrometer, Rapid Commun Mass Spectrom, 18 (2004) 1681-1685.
[201] D.A. Yurek, D.L. Branch, M.S. Kuo, Development of a system to evaluate compound identity, purity, and concentration in a single experiment and its application in quality assessment of combinatorial libraries and screening hits, J Comb Chem, 4 (2002) 138-148.

[202] D. Corens, M. Carpentier, M. Schroven, L. Meerpoel, Liquid chromatography-mass spectrometry with chemiluminescent nitrogen detection for on-line quantitative analysis of compound collections: advantages and limitations, J Chromatogr A, 1056 (2004) 67-75.
[203] H.E. Fries, C.A. Evans, K.W. Ward, Evaluation of evaporative light-scattering detection for metabolite quantification without authentic analytical standards or radiolabel, J Chromatogr B Analyt Technol Biomed Life Sci, 819 (2005) 339-344.
[204] S. Lane, B. Boughtflower, I. Mutton, C. Paterson, D. Farrant, N. Taylor, Z. Blaxill, C. Carmody, P. Borman, Toward single-calibrant quantification in HPLC. A comparison of three detection strategies: evaporative light scattering, chemiluminescent nitrogen, and proton NMR, Anal Chem, 77 (2005) 4354-4365.
[205] G. Lappin, M. Seymour, G. Gross, M. Jorgensen, M. Kall, L. Kvaerno, Meeting the MIST regulations: human metabolism in Phase I using AMS and a tiered bioanalytical approach, Bioanalysis, 4 (2012) 407-416.
[206] S. Almeling, D. Ilko, U. Holzgrabe, Charged aerosol detection in pharmaceutical analysis, J Pharm Biomed Anal, 69 (2012) 50-63.
[207] C. Yu, C.L. Chen, F.L. Gorycki, T.G. Neiss, A rapid method for quantitatively estimating metabolites in human plasma in the absence of synthetic standards using a combination of liquid chromatography/mass spectrometry and radiometric detection, Rapid Commun Mass Spectrom, 21 (2007) 497-502.
[208] Y. Yang, M.F. Grubb, C.E. Luk, W.G. Humphreys, J.L. Josephs, Quantitative estimation of circulating metabolites without synthetic standards by ultra-high-performance liquid chromatography/high resolution accurate mass spectrometry in combination with UV correction, Rapid Commun Mass Spectrom, 25 (2011) 3245-3251.
[209] R. Espina, L. Yu, J. Wang, Z. Tong, S. Vashishtha, R. Talaat, J. Scatina, A. Mutlib, Nuclear magnetic resonance spectroscopy as a quantitative tool to determine the concentrations of biologically produced metabolites: implications in metabolites in safety testing, Chem Res Toxicol, 22 (2009) 299-310.
[210] K. Vishwanathan, K. Babalola, J. Wang, R. Espina, L. Yu, A. Adedoyin, R. Talaat, A. Mutlib, J. Scatina, Obtaining exposures of metabolites in preclinical species through plasma pooling and quantitative NMR: addressing metabolites in safety testing (MIST) guidance without using radiolabeled compounds and chemically synthesized metabolite standards, Chem Res Toxicol, 22 (2009) 311-322.
[211] G.S. Walker, J.N. Bauman, T.F. Ryder, E.B. Smith, D.K. Spracklin, R.S. Obach, Biosynthesis of drug metabolites and quantitation using NMR spectroscopy for use in pharmacologic and drug metabolism studies, Drug Metab Dispos, 42 (2014) 1627-1639.
[212] R. Lucena, S. Cardenas, M. Valcarcel, Evaporative light scattering detection: trends in its analytical uses, Anal Bioanal Chem, 388 (2007) 1663-1672.
[213] E.F. Brandon, C.D. Raap, I. Meijerman, J.H. Beijnen, J.H. Schellens, An update on in vitro test methods in human hepatic drug biotransformation research: pros and cons, Toxicol Appl Pharmacol, 189 (2003) 233-246.
[214] R.B. Kirkpatrick, R.A. Belsaas, Formation and secretion of glycolithocholate-3-sulfate in primary hepatocyte cultures, J Lipid Res, 26 (1985) 1431-1437.
[215] P.R. Galle, L. Theilmann, R. Raedsch, G. Rudolph, B. Kommerell, A. Stiehl, Taurine and glycine conjugation and sulfation of lithocholate in primary hepatocyte cultures, Biochim Biophys Acta, 1003 (1989) 250-253.
[216] M. Lambiotte, N. Thierry, Hydroxylation, sulfation, and conjugation of bile acids in rat hepatoma and hepatocyte cultures under the influence of glucocorticoids, J Biol Chem, 255 (1980) 11324-11331.
[217] R.B. Kirkpatrick, M.D. Green, L.R. Hagey, A.F. Hofmann, T.R. Tephly, Effect of side chain length on bile acid conjugation: glucuronidation, sulfation and coenzyme A

formation of nor-bile acids and their natural C24 homologs by human and rat liver fractions, Hepatology, 8 (1988) 353-357.
[218] L.J. Chen, I.H. Segel, Purification and characterization of bile salt sulfotransferase from human liver, Arch Biochem Biophys, 241 (1985) 371-379.
[219] R.E. Kane, L.J. Chen, J.J. Herbst, M.M. Thaler, Sexual differentiation of rat hepatic bile salt sulfotransferase isoenzymes, Pediatr Res, 24 (1988) 247-253.
[220] M. Lambiotte, J. Sjovall, Hydroxylation and sulfation of bile acids in rat hepatoma cultures under the influence of a glucocorticoid, Biochem Biophys Res Commun, 86 (1979) 1089-1095.
[221] A.K. Deo, S.M. Bandiera, Biotransformation of lithocholic acid by rat hepatic microsomes: metabolite analysis by liquid chromatography/mass spectrometry, Drug Metab Dispos, 36 (2008) 442-451.
[222] A.K. Deo, S.M. Bandiera, 3-ketocholanoic acid is the major in vitro human hepatic microsomal metabolite of lithocholic acid, Drug Metab Dispos, 37 (2009) 1938-1947.
[223] D. Trulzsch, J. Roboz, H. Greim, P. Czygan, J. Rudick, F. Hutterer, F. Schaffner, H. Popper, Hydroxylation of taurolithocholate by isolated human liver microsomes. I. Identification of metabolic product, Biochem Med, 9 (1974) 158-166.
[224] P. Czygan, H. Greim, D. Trulzsch, J. Rudick, F. Hutterer, F. Schaffner, H. Popper, O. Rosenthal, D.Y. Cooper, Hydroxylation of taurolithocholate by isolated human liver microsomes. II. Cytochrome P-450 dependency, Biochim Biophys Acta, 354 (1974) 168-171.
[225] Z. Araya, K. Wikvall, 6alpha-hydroxylation of taurochenodeoxycholic acid and lithocholic acid by CYP3A4 in human liver microsomes, Biochim Biophys Acta, 1438 (1999) 47-54.
[226] S. Matern, H. Matern, E.H. Farthmann, W. Gerok, Hepatic and extrahepatic glucuronidation of bile acids in man. Characterization of bile acid uridine 5'-diphosphate-glucuronosyltransferase in hepatic, renal, and intestinal microsomes, J Clin Invest, 74 (1984) 402-410.
[227] R.B. Kirkpatrick, C.N. Falany, T.R. Tephly, Glucuronidation of bile acids by rat liver 3-OH androgen UDP-glucuronyltransferase, J Biol Chem, 259 (1984) 6176-6180.
[228] K. Mitamura, S. Watanabe, Y. Mitsumoto, T. Sakai, M. Sogabe, T. Wakamiya, S. Ikegawa, Formation and biliary excretion of glutathione conjugates of bile acids in the rat as shown by liquid chromatography/electrospray ionization-linear ion trap mass spectrometry, Anal Biochem, 384 (2009) 224-230.
[229] K. Mitamura, N. Hori, T. Iida, A.F. Hofmann, S. Ikegawa, Identification of bile acid S-acyl glutathione conjugates in rat bile by liquid chromatography/electrospray ionization-linear ion trap mass spectrometry, Steroids, 76 (2011) 68-77.
[230] A. Pellicoro, F.A. van den Heuvel, M. Geuken, H. Moshage, P.L. Jansen, K.N. Faber, Human and rat bile acid-CoA:amino acid N-acyltransferase are liver-specific peroxisomal enzymes: implications for intracellular bile salt transport, Hepatology, 45 (2007) 340-348.
[231] C.N. Falany, H. Fortinberry, E.H. Leiter, S. Barnes, Cloning, expression, and chromosomal localization of mouse liver bile acid CoA:amino acid N-acyltransferase, J Lipid Res, 38 (1997) 1139-1148.
[232] S. Ohkuma, J. Tamura, K. Kuriyama, Roles of endogenous and exogenous taurine and glycine in the formation of conjugated bile acids: analyses using freshly isolated and primary cultured rat hepatocytes, Jpn J Pharmacol, 35 (1984) 347-358.
[233] R. Lourenco, M.E. Camilo, Taurine: a conditionally essential amino acid in humans? An overview in health and disease, Nutr Hosp, 17 (2002) 262-270.
[234] J.A. Sturman, G.E. Gaull, Taurine in the brain and liver of the developing human and monkey, J Neurochem, 25 (1975) 831-835.

[235] H. Barle, B. Ahlman, B. Nyberg, K. Andersson, P. Essen, J. Wernerman, The concentrations of free amino acids in human liver tissue obtained during laparoscopic surgery, Clin Physiol, 16 (1996) 217-227.
[236] S. Itoh, S. Onishi, Hepatic taurine, glycine and individual bile acids in early human fetus, Early Hum Dev, 57 (2000) 71-77.
[237] K. Mohri, K. Okada, L.Z. Benet, Stereoselective taurine conjugation of (R)-benoxaprofen enantiomer in rats: in vivo and in vitro studies using rat hepatic mitochondria and microsomes, Pharm Res, 22 (2005) 79-85.
[238] C.P. Siegers, K.H. Bossen, M. Younes, R. Mahlke, D. Oltmanns, Glutathione and glutathione-S-transferases in the normal and diseased human liver, Pharmacol Res Commun, 14 (1982) 61-72.
[239] F. Michelet, R. Gueguen, P. Leroy, M. Wellman, A. Nicolas, G. Siest, Blood and plasma glutathione measured in healthy subjects by HPLC: relation to sex, aging, biological variables, and life habits, Clin Chem, 41 (1995) 1509-1517.
[240] W. Zhang, P. Li, Q. Geng, Y. Duan, M. Guo, Y. Cao, Simultaneous determination of glutathione, cysteine, homocysteine, and cysteinylglycine in biological fluids by ion-pairing high-performance liquid chromatography coupled with precolumn derivatization, J Agric Food Chem, 62 (2014) 5845-5852.
[241] Y. Ogasawara, M. Funakoshi, K. Ishii, Determination of reduced nicotinamide adenine dinucleotide phosphate concentration using high-performance liquid chromatography with fluorescence detection: ratio of the reduced form as a biomarker of oxidative stress, Biol Pharm Bull, 32 (2009) 1819-1823.
[242] E.M. van Lieshout, W.H. Peters, Age and gender dependent levels of glutathione and glutathione S-transferases in human lymphocytes, Carcinogenesis, 19 (1998) 1873-1875.
[243] N. Gautam, R. Thakare, S. Rana, A. Natarajan, Y. Alnouti, Irreversible binding of an anticancer compound (BI-94) to plasma proteins, Xenobiotica, 45 (2015) 858-873.
[244] X. Diao, X. Pang, C. Xie, Z. Guo, D. Zhong, X. Chen, Bioactivation of 3-n-butylphthalide via sulfation of its major metabolite 3-hydroxy-NBP: mediated mainly by sulfotransferase 1A1, Drug Metab Dispos, 42 (2014) 774-781.
[245] M.P. Grillo, C.G. Knutson, P.E. Sanders, D.J. Waldon, F. Hua, J.A. Ware, Studies on the chemical reactivity of diclofenac acyl glucuronide with glutathione: identification of diclofenac-S-acyl-glutathione in rat bile, Drug Metab Dispos, 31 (2003) 1327-1336.
[246] C.D. Klaassen, J.W. Boles, Sulfation and sulfotransferases 5: the importance of 3'-phosphoadenosine 5'-phosphosulfate (PAPS) in the regulation of sulfation, FASEB J, 11 (1997) 404-418.
[247] A.E. Schwaninger, M.R. Meyer, J. Zapp, H.H. Maurer, Sulfation of the 3,4-methylenedioxymethamphetamine (MDMA) metabolites 3,4-dihydroxymethamphetamine (DHMA) and 4-hydroxy-3-methoxymethamphetamine (HMMA) and their capability to inhibit human sulfotransferases, Toxicol Lett, 202 (2011) 120-128.
[248] C.H. Yang, L. Tang, C. Lv, L. Ye, B.J. Xia, M. Hu, Z.Q. Liu, Sulfation of selected mono-hydroxyflavones by sulfotransferases in vitro: a species and gender comparison, J Pharm Pharmacol, 63 (2011) 967-970.
[249] A.M. Furimsky, C.E. Green, L.E. Sharp, P. Catz, A.A. Adjei, T. Parman, I.M. Kapetanovic, R.M. Weinshilboum, L.V. Iyer, Effect of resveratrol on 17beta-estradiol sulfation by human hepatic and jejunal S9 and recombinant sulfotransferase 1E1, Drug Metab Dispos, 36 (2008) 129-136.
[250] Q. Wang, R. Jia, C. Ye, M. Garcia, J. Li, I.J. Hidalgo, Glucuronidation and sulfation of 7-hydroxycoumarin in liver matrices from human, dog, monkey, rat, and mouse, In Vitro Cell Dev Biol Anim, 41 (2005) 97-103.

[251] M. Cappiello, L. Giuliani, G.M. Pacifici, Distribution of UDP-glucuronosyltransferase and its endogenous substrate uridine 5'-diphosphoglucuronic acid in human tissues, Eur J Clin Pharmacol, 41 (1991) 345-350.
[252] C. King, W. Tang, J. Ngui, T. Tephly, M. Braun, Characterization of rat and human UDP-glucuronosyltransferases responsible for the in vitro glucuronidation of diclofenac, Toxicol Sci, 61 (2001) 49-53.
[253] S. Kumar, K. Samuel, R. Subramanian, M.P. Braun, R.A. Stearns, S.H. Chiu, D.C. Evans, T.A. Baillie, Extrapolation of diclofenac clearance from in vitro microsomal metabolism data: role of acyl glucuronidation and sequential oxidative metabolism of the acyl glucuronide, J Pharmacol Exp Ther, 303 (2002) 969-978.
[254] H. Liu, H. Sun, D. Lu, Y. Zhang, X. Zhang, Z. Ma, B. Wu, Identification of glucuronidation and biliary excretion as the main mechanisms for gossypol clearance: in vivo and in vitro evidence, Xenobiotica, 44 (2014) 696-707.
[255] B.T. Gufford, J.B. Lu, I.F. Metzger, D.R. Jones, Z. Desta, Stereoselective Glucuronidation of Bupropion Metabolites In Vitro and In Vivo, Drug Metab Dispos, 44 (2016) 544-553.
[256] K.M. Knights, R. Drew, A radioisotopic assay of picomolar concentrations of coenzyme A in liver tissue, Anal Biochem, 168 (1988) 94-99.
[257] K. Chijiiwa, A. Mizuta, J. Ueda, Y. Takamatsu, K. Nakamura, M. Watanabe, S. Kuroki, M. Tanaka, Relation of biliary bile acid output to hepatic adenosine triphosphate level and biliary indocyanine green excretion in humans, World J Surg, 26 (2002) 457-461.
[258] M.W. Gorman, E.O. Feigl, C.W. Buffington, Human plasma ATP concentration, Clin Chem, 53 (2007) 318-325.
[259] T.F. Slater, Oxidized and reduced nicotinamide-adenine dinucleotide phosphate in tissue suspensions of rat liver, Biochem J, 104 (1967) 833-842.
[260] J. Huang, S.P. Bathena, Y. Alnouti, Metabolite profiling of praziquantel and its analogs during the analysis of in vitro metabolic stability using information-dependent acquisition on a hybrid triple quadrupole linear ion trap mass spectrometer, Drug Metab Pharmacokinet, 25 (2010) 487-499.
[261] X. Yu, D. Cui, M.R. Davis, Identification of in vitro metabolites of Indinavir by "intelligent automated LC-MS/MS" (INTAMS) utilizing triple quadrupole tandem mass spectrometry, J Am Soc Mass Spectrom, 10 (1999) 175-183.
[262] L. Wang, L.J. Christopher, D. Cui, W. Li, R. Iyer, W.G. Humphreys, D. Zhang, Identification of the human enzymes involved in the oxidative metabolism of dasatinib: an effective approach for determining metabolite formation kinetics, Drug Metab Dispos, 36 (2008) 1828-1839.
[263] K. Chijiiwa, F. Nakayama, Simultaneous microanalysis of bile acids and cholesterol in bile by glass capillary column gas chromatography, J Chromatogr, 431 (1988) 17-25.
[264] M.M. Fisher, I.M. Yousef, Sex differences in the bile acid composition of human bile: studies in patients with and without gallstones, Can Med Assoc J, 109 (1973) 190-193.
[265] S. Perwaiz, B. Tuchweber, D. Mignault, T. Gilat, I.M. Yousef, Determination of bile acids in biological fluids by liquid chromatography-electrospray tandem mass spectrometry, J Lipid Res, 42 (2001) 114-119.
[266] D.Q. Wang, S. Tazuma, D.E. Cohen, M.C. Carey, Feeding natural hydrophilic bile acids inhibits intestinal cholesterol absorption: studies in the gallstone-susceptible mouse, Am J Physiol Gastrointest Liver Physiol, 285 (2003) G494-502.
[267] G. Lee, H. Lee, J. Hong, S.H. Lee, B.H. Jung, Quantitative profiling of bile acids in rat bile using ultrahigh-performance liquid chromatography-orbitrap mass spectrometry:

Alteration of the bile acid composition with aging, J Chromatogr B Analyt Technol Biomed Life Sci, 1031 (2016) 37-49.
[268] C. Cohen-Solal, M. Parquet, J. Ferezou, C. Serougne, C. Lutton, Effects of hyodeoxycholic acid and alpha-hyocholic acid, two 6 alpha-hydroxylated bile acids, on cholesterol and bile acid metabolism in the hamster, Biochim Biophys Acta, 1257 (1995) 189-197.
[269] R.L. Cowles, J.Y. Lee, D.D. Gallaher, C.L. Stuefer-Powell, T.P. Carr, Dietary stearic acid alters gallbladder bile acid composition in hamsters fed cereal-based diets, J Nutr, 132 (2002) 3119-3122.
[270] E.A. Trautwein, D. Rieckhoff, A. Kunath-Rau, H.F. Erbersdobler, Psyllium, not pectin or guar gum, alters lipoprotein and biliary bile acid composition and fecal sterol excretion in the hamster, Lipids, 33 (1998) 573-582.
[271] K.D. Setchell, C.M. Rodrigues, C. Clerici, A. Solinas, A. Morelli, C. Gartung, J. Boyer, Bile acid concentrations in human and rat liver tissue and in hepatocyte nuclei, Gastroenterology, 112 (1997) 226-235.
[272] Y. Suzuki, R. Kaneko, M. Nomura, H. Naito, K. Kitamori, T. Nakajima, T. Ogawa, H. Hattori, H. Seno, A. Ishii, Simple and rapid quantitation of 21 bile acids in rat serum and liver by UPLC-MS-MS: effect of high fat diet on glycine conjugates of rat bile acids, Nagoya J Med Sci, 75 (2013) 57-71.
[273] T. Iwaki, K. Ishizaki, S. Kinoshita, H. Tanaka, A. Fukunari, M. Tsurufuji, T. Imada, Protective effects of ursodeoxycholic acid on chenodeoxycholic acid-induced liver injury in hamsters, World J Gastroenterol, 13 (2007) 5003-5008.

CHAPTER 2

Bile Acids as Potential Novel Biomarkers for Organic Anion-Transporting Polypeptides

2.1 Introduction

It is now accepted that organic anion-transporting polypeptides (OATPs) mediate the active uptake of numerous drugs into hepatocytes and hence govern their pharmacokinetic profile and liver (free)-to-plasma (free) concentration ratio. OATPs can also serve as the loci of important drug-drug interactions (DDIs) leading to changes in systemic and local drug concentrations, possibly resulting in altered efficacy and toxicity profiles [1, 2]. Consequently, tools have been developed to facilitate OATP inhibition screening in vitro, drive model-based DDI in vitro-in vivo extrapolations, and support OATP DDI risk assessment prior to human dosing [3-6]. The latter is particularly important because OATP activity and expression is also known to be impacted by genotype and liver disease [7, 8].

More recently, it has been envisioned that OATP biomarkers will greatly facilitate clinical phenotyping and DDI studies, while possibly deferring more formal studies employing drug probes [9, 10]. For example, Lai et al (2016) recently evaluated plasma bilirubin, bilirubin glucuronide, and coproporphyrin isomers (I and III) as OATP biomarkers in human subjects following a single dose of rifampicin (RIF) [9]. The authors noted a 4.0- and 3.3-fold increase in the coproporphyrin I and III area under the plasma concentration-time curve (AUC), respectively, consistent with in vitro data [11, 12]. Likewise, Yee et al (2016) identified the 3-O-sulfate conjugates of glycochenodeoxycholic acid (GCDCA-S), glycodeoxycholic acid (GDCA-S),

and taurolithocholic acid (TLCA-S) as candidate OATP biomarkers after dosing of SLCO1B1 genotyped subjects with cyclosporine [10]. Because of the high sequence identity with human OATPs, the cynomolgus monkey has been used increasingly as a model to study OATP inhibition in vivo [13-15]. The utility of the cynomolgus monkey has extended also to the search for OATP biomarkers, which has involved the administration of a single RIF dose and reporting its impact on the plasma bilirubin, bilirubin glucuronide, coproporphyrins (I and III), non-sulfated bile acids (BAs) and dehydroepiandrosterone (DHEA) 3-O-sulfate [12, 16, 17].

As described, an attempt was made to extend the work of Chu et al by profiling 30 different BAs in cynomolgus monkey plasma following single oral doses of RIF (1, 3, 10 and 30 mg/kg) [16]. It was possible to prepare synthetic standards of numerous BA 3-O-sulfates and apply a liquid chromatography-tandem mass spectrometry (LC-MS/MS) method that has been used successfully to profile non-sulfated and sulfated BAs in human serum and urine [18]. It should be noted that at the time of the study, BA sulfation in the cynomolgus monkey was not well characterized, although the putative hydroxysteroid sulfotransferase (SULT2A1) that catalyses BA sulfation in humans was known to be expressed in monkey liver [19-21]. It was also known that DHEA 3-O-sulfate was detectable in cynomolgus monkeys following DHEA administration [22].

In the present study, animals also received a single i.v. dose of 2H4-pitavastatin to ensure that OATP was inhibited by RIF in a dose-dependent manner [14]. In addition, the plasma concentrations of RIF were determined at each of the four dose levels. Sulfated BAs are known to be cleared renally in humans [18, 21]; therefore BA profiling was extended to include urine of control and RIF-dosed cynomolgus monkeys. The different BAs were then assessed in terms of their utility as OATP biomarkers: (a) detectability in control animals; (b) magnitude of the RIF dose response; and (c) detectability in human serum. Based on these criteria, seven sulfated BAs (GCDCA-S,

GDCA-S, glycolithocholate 3-O-sulfate [GLCA-S], TLCA-S, taurochenodeoxycholate 3-O-sulfate [TCDCA-S], taurodeoxycholate 3-O-sulfate [TDCA-S], and deoxycholate 3-O-sulfate [DCA-S]) were identified as potential OATP biomarkers. For GCDCA-S, GDCA-S, and TLCA-S, the results are consistent with human plasma metabolomic data from a recent OATP1B1 (SLCO1B1) genome-wide association study and earlier reports describing TLCA-S as an OATP substrate in vitro [10, 23, 24]. The present study also included an in vitro assessment of BA sulfation by cynomolgus monkey liver cytosol, as well as uptake studies with GDCA-S, GCDCA-S, DCA-S, and TDCA-S (cynomolgus monkey plated primary hepatocytes) in order to phenotype both in terms of OATP- and sodium-taurocholate co-transporting polypeptide (NTCP)-mediated active uptake.

2.2 Materials and Methods

2.2.1 Chemicals and Reagents

3'-Phosphoadenosine-5'-phosphosulfate (PAPS), simvastatin, rifamycin SV (RIFsv), and rifampicin (RIF) were purchased from Sigma-Aldrich (St Louis, MO, USA). Deuterium labeled RIF ($^{2}H_{8}$-RIF) were obtained from ALSACHIM (Illkirch, Graffenstaden, France). Pitavastatin was purchased from Sequoia Research Products Ltd. (Oxford, UK). Deuterium labeled pitavastatin ($^{2}H_{4}$-pitavastatin) was purchased from Clearsynth (Ontario, Canada). InVitroGro-HT and CP hepatocyte media were purchased from Celsis IVT (Baltmore, MD). Collagen I coated 24-well plates were obtained from BD Biosciences (Franklin Lakes, NJ). Cryopreserved cynomolgus monkey hepatocytes were purchased from In vitro ADMET Laboratories, LLC (Columbia, Maryland). BCR protein assay kit was purchased from PIERCE (Rockford, IL). RIPA protein lysis buffer was purchased from TEKNOVA (Hollister, CA). Methanol, acetonitrile, water, ammonium hydroxide were obtained from Fisher Scientific (Fair Lawn, NJ, USA).

Cholic acid (CA), glycocholic acid (GCA), taurocholic acid (TCA), deuterium labeled taurocholic acid ($^{2}H_{4}$-TCA), chenodeoxycholic acid (CDCA), deuterium labeled

chenodeoxycholic acid ($^2H_4$-CDCA), taurochenodeoxycholic acid (TCDCA), deoxycholic acid (DCA), glycochenodeoxycholic acid (GCDCA), glycodeoxycholic acid (GDCA), taurodeoxycholic acid (TDCA), lithocholic acid (LCA), glycolithocholic acid (GLCA), taurolithocholic acid (TLCA), ursodeoxycholic acid (UDCA), tauroursodeoxycholic acid (TUDCA), glycoursodeoxycholic acid (GUDCA), and deuterium labeled glycodeoxycholic acid 3-O-sulfate ($^2H_4$-GDCA-S) were purchased from IsoSciences (King of Prussia, PA, USA). Lithocholic acid 3-O-sulfate (LCA-S), glycolithocholic acid 3-O-sulfate (GLCA-S), chenodeoxycholic acid 3-O-sulfate (CDCA-S), glycochenodeoxycholic acid 3-O-sulfate (GCDCA-S), and deuterium labeled glycochenodeoxycholic acid 3-O-sulfate ($^2H_5$-GCDCA-S) were purchased from Toronto Research Chemicals (Toronto, Ontario, Canada). Ursodeoxycholic acid 3-O-sulfate (UDCA-S) was obtained from ALSACHIM (Illkirch, Graffenstaden, France). Deuterium labeled glycochenodeoxycholic acid ($^2H_4$-GCDCA) was purchased from C/D/N isotopes, Inc. (Pointe-Claire, Quebec, Canada). Taurolithocholic acid 3-O-sulfate (TLCA-S) was purchased from Sigma-Aldrich (St Louis, MO, USA).

2.2.2 Animal Handling, Dosing, Plasma Draws, and Urine Collection

All experiments involving animals were conducted at the Pfizer Groton (Connecticut) facilities (Association for Assessment & Accreditation of Laboratory Animal Care-accredited) and were reviewed and approved by the Pfizer Institutional Animal Care and Use Committee. Male cynomolgus macaque Mauritian monkeys (approximately 6 to 8.5 years of age) were used for these studies. A cross-over study design was employed, where the same four animals were dosed over a series of five studies, following a minimum one-week wash-out period between each study. One exception was the 3 mg/kg RIF dose group, where one of four monkeys was dosed only in that single study.

Animals were provided a normal food schedule the day before the study (meals at 8:00 am and 11:00 am, with one treat daily) and were allowed free access to water. On the day of the study, monkeys were fed at approximately 1h and 3h post-dose and allowed water *ad libitum*. RIF was administered via oral gavage at 0 (blank vehicle), 1, 3, 10, and 30 mg/kg. RIF was given at a dose volume of 2 ml/kg in a 0.5% (w/v) methylcellulose (in water) suspension. Approximately one hour and 15 minutes following the oral RIF administration, 2H4-pitavastatin was administered via an intravenous (i.v.) bolus (cephalic vein), at dose of 0.2 mg/kg, in a dosing volume of 0.2 ml/kg; 2% DMSO (v/v) and 98% of TRIS-buffered saline (pH ~7.7). All i.v. formulations were sterile filtered prior to administration. Serial blood samples were collected via the femoral vein before dosing into K2EDTA tubes and then at 0.083, 0.25, 0.5, 0.75, 1, 2, 3, 5, 6, and 24 hours post i.v. dosing. Blood samples were stored on wet ice prior to being centrifuged to obtain plasma (3000 RPM, 10 minutes at 4 ◦C; Jouan BR4i refrigerated centrifuge). Urine was also collected (metabolism cages), on wet ice, pre-dose and at intervals of 0 to 6 hours and 6 to 24 hours post-dose. Due to instability and possible inter-conversion of lactone to pitavastatin, each plasma and urine sample was equally divided into two aliquots prior to being stored frozen. The first was untreated matrix, while the second was added to an equal volume of 0.1 M sodium acetate buffer (pH 4) to stabilize pitavastatin. All urine and plasma samples, treated and untreated, were kept cold during collection, after which they were stored frozen at -20°C. It is known that BAs undergo enterohepatic recirculation, but no attempt was made to collect portal vein blood from the different cynomolgus monkeys. Following LC-MS/MS analysis of femoral vein-derived plasma, it was apparent that the concentration (plasma total) of the various BA sulfates was low (≤ 30 nM). For some of the BA sulfates (TCDCA-S, GCDCA-S,TDCA-S, and GDCA-S), unbound fraction in cynomolgus monkey plasma was determined (~0.016); maximal free plasma concentration ~0.5 nM. It is assumed that

even if free BA sulfate concentrations were 100-fold higher in the portal vein, such concentrations would still likely be below the apparent Km for cynomolgus monkey OATPs. As described in *Results*, RIF dosing brought about robust (≥ 10-fold) dose-dependent increase in the area under the plasma concentration-time curve (AUC) for a number of BA sulfates (LCA-S, GLCA-S, TLCA-S, GCDCA-S, TCDCA-S, DCA-S, GDCA-S, TDCA-S). Such a result is consistent with low substrate concentration-to-OATP K_m ratios in vivo.

2.2.3 Liquid Chromatography-Tandem Mass Spectrometry (LC-MS/MS) Analysis

2.2.3.1 Analysis of BAs and their 3-O-sulfate conjugates

Plasma and urine concentrations of BAs and their 3-O-sulfate conjugates were measured in untreated matrices by LC-MS/MS, as described previously with some modifications (Bathena et al., 2013). Briefly, a Waters ACQUITY ultra performance liquid chromatography (UPLC) system (Waters, Milford, MA) coupled to an 5500 Q TRAP® quadrupole linear ion trap hybrid mass spectrometer (MS) with an electrospray ionization (ESI) source (Applied Biosystems, MDS Sciex, Foster City, CA) was used. Chromatographic separations were performed with an ACQUITY UPLC®BEH C18 column (1.7 µm, 150 × 2.1 mm) maintained at 25°C and equipped with an in-line pre-column filter. The mobile phase consisted of 7.5 mM ammonium bicarbonate, adjusted to pH 9.0 using ammonium hydroxide (mobile phase A), and 30% acetonitrile in methanol (mobile phase B), at a total flow rate of 0.2 ml/min. The gradient profile was held at 52.5% mobile phase B for 12.75 min, increased linearly to 68% in 0.25 min, held at 68% for 8.75 min, increased linearly to 90% in 0.25 min, held at 90% for 1 min, and finally brought back to 52.5% in 0.25 min followed by 4.75 min re-equilibration (total run time of 28 min per sample). Ten µl of sample was injected for analysis. Quantitative data were acquired in multiple reaction monitoring (MRM)-negative ESI mode. MRM

transitions and MS parameters for the different BAs and their respective 3-O-sulfate conjugates are shown in Supplemental Table 1.

For preparation of calibration curves blank plasma and urine were obtained by charcoal stripping as described previously [18]. Fourteen-point calibration curves were prepared in stripped matrices by spiking ten µl of appropriate standard solution at final concentrations ranging from 0.5 to 2500 ng/ml. For extraction of plasma samples, 1 ml of ice-cold alkaline ACN (5% NH4OH) containing 2H4-GCDCA and 2H4-CDCA as internal standards was added to 100 µl of samples. Samples were then vortex mixed and centrifuged at 16,000 × g for 10 min and the supernatants were aspirated, evaporated, and reconstituted in 100 µl of 50% MeOH solution. Urine samples were extracted similar to plasma samples except that Tween 20 was added (final concentration of 0.2% v/v) to reduce non-specific binding.

3.2.3.2 Analysis of $^{2}H_{4}$-pitavastatin and RIF

The plasma concentrations of RIF and $^{2}H_{4}$-pitavastatin were measured in plasma samples treated with 0.1 M sodium acetate buffer (pH 4) using the LC-MS/MS system listed above. All standards and QCs were made in blank monkey plasma mixed with an equal volume of 0.1 M sodium acetate buffer (pH 4). Standard and QC mixtures of the analytes were made to encompass a range of concentrations (0.1 to 500 ng/ml, 2H4-pitavastatin; 1 to 5,000 ng/ml, RIF). Samples were diluted to be measured in the linear range of the instrument responses; with the high specificity of MRM (no interference in the blank matrixes) and a wide dynamic range for each analyte, the dilution integrity was confirmed by independent analysis of the drugs in the samples in separate assays. Aliquots of 50 µl of standards, QCs and plasma samples were prepared by protein precipitation using 200 µl of acetonitrile containing an internal standard mixture of simvastatin and $^{2}H_{8}$-RIF (100 ng/ml). The plates were vortexed for 2 minutes, centrifuged at 3000 rpm for 10 minutes, and 100 µl supernatants of the mixture were

transferred for LC-MS/MS analysis. Chromatographic separation was accomplished on a Waters Acquity UPLC HSS T3 C18 column (1.8µm, 2.1 × 50 mm) maintained at 40 °C. The mobile phase consisted of two solvents, solvent A (0.1% formic acid in water) and solvent B (0.1% formic acid in acetonitrile). The total run time for each injection was 3 minutes. The flow rate was 0.6 ml/min. The gradient was maintained at 5% B for 0.3 min, followed by a linear increase to 95% B in 1.8 minutes, and kept at 95% B for 0.3 min then a linear decrease to 5% in 0.3 minutes. The column was equilibrated at 5% B for 0.3 min. A Valco VICI valve (Valco Instruments Co., Houston, TX) was used to divert the first 0.3 min and the last 0.5 minutes of HPLC effluent to waste. The injection volume was 2 µl. The analytes were monitored using MRM with settings listed in Supplemental Table 2.

2.2.4 Determination of Uptake Clearance in the Presence of Cynomolgus Monkey Plated Primary Hepatocytes

Thawing and seeding procedure for cynomolgus monkey hepatocytes was the same as that described previously for human hepatocytes [25]. In brief, cryopreserved cynomolgus monkey primary hepatocytes (male animal; Lot number 10106012; In vitro ADMET Laboratories, LLC. Columbia, Maryland) were thawed and seeded into 24-well collagen coated plates using In Vitro-HT and In Vitro-CP hepatocyte media at a density of 0.35 x 106 cells/well (0.5 ml/well). After culturing for 6 hours, the uptake study was conducted. To assess the rate of uptake and passive diffusion, the cells were pre-incubated with and without (DMSO only) RIFsv (1 mM) or RIF (5 µM) at 37 °C for 10 minutes. The uptake was initiated by the addition of 0.5 ml containing $^{2}H_{4}$-TCDCA-S (0.1 µM), $^{2}H_{4}$-TDCA-S (0.1 µM), $^{2}H_{4}$-DCA-S (0.1 µM), $^{2}H_{5}$-GCDCA-S (0.1 and 0.5 µM), $^{2}H_{4}$-GDCA-S (0.1 and 0.5 µM), $^{2}H_{4}$-TCA (0.1 and 0.5 µM), and non-labeled pitavastatin (0.1 µM). To determine the effect of sodium on substrate uptake, the cells were pre-incubated in Krebs-Henseleit buffer (KHB) without sodium (NaCl and NaHCO3 replaced

with choline chloride and choline bicarbonate, respectively) at 37 °C for 10 minutes [26]. In all cases, incubations were terminated at 0.5, 1, 2 and 5 minutes by washing the cells three times with ice-cold HBSS buffer. The cells were then lysed with 100% methanol containing internal standard (diclofenac), centrifuged, and dried down under nitrogen and reconstituted in 50/50 methanol/water. Chromatography was performed on a Waters Acquity UPLC System (Milford, MA). The autosampler and column were kept at 10°C and 50°C, respectively. Separation was achieved with a Waters BEH C18 column (2.1x50mm, 1.7 µm), and a gradient of 7.5 mM ammonium bicarbonate (Mobile Phase A) and 70/30 methanol/acetonitrile (Mobile Phase B) at a flow rate of 0.2 ml/min. An initial mobile phase composition of 50% B was held for 2 minutes, then ramped to 95% in 1.5 minutes, held at 95% for 1 minute, and then returned to initial 50% B for 0.5 minute re-equilibration. The total analysis time for each sample was 5 minutes. Data were collected on an AB Sciex API5500 (QTRAP) mass spectrometer (Foster City, CA, USA) using negative Turbo IonSpray™ electrospray ionization (ESI) and multiple reaction monitoring (MRM) mode with the following transitions: 290.6/96.8 ($^2H_4$-TDCA-S), 475.2/96.8 ($^2H_4$-DCA-S), 533.3/453.4 ($^2H_5$-GCDCA-S), 532.3/452.3 ($^2H_4$-GDCA-S), and 514.2/79.8 ($^2H_4$-TCA). Data acquisition and processing was carried out with Analyst software version 1.6.2. (Applied Biosystems/MDS Sciex, Canada) Analysis of pitavastatin was performed as described above. Stability of the various sulfated BA substrates was confirmed after their addition to assay buffer and incubation for 5 mins at 37 °C.

2.2.5 Pharmacokinetics Analysis

2.2.5.1 BAs

For each BA, the plasma AUC from 0 to 24 hour ($AUC_{0\text{-}24,plasma}$) was derived from the concentration-time profile for each individual animal (trapezoidal rule, Microsoft Office Excel). Renal clearance (CL_{renal}) was calculated by dividing the amount excreted

in urine from 0 to 24 hour ($Ae_{0\text{-}24,urine}$) by the $AUC_{0\text{-}24,plasma}$. $AUC_{0\text{-}24,plasma}$ ratios (AUCRplasma) were determined by dividing the AUC0-24,plasma after RIF treatment by the vehicle alone $AUC_{0\text{-}24,plasma}$. The CL_{renal} ratio was determined by dividing the CL_{renal} after RIF treatment by the vehicle alone CL_{renal}.

2.2.5.2 RIF and pitavastatin

The non-compartmental analyses of 2H4-pitavastatin and RIF plasma concentration-time data were performed using Watson LIMSTM version 7.4.1 (Thermo Fisher Scientific Inc, Waltham, MA), which supported the generation of the various pharmacokinetic parameters; AUC, $T_{1/2}$ (half-life), CL (clearance), Vd_{ss} (volume of distribution), Cmax (peak plasma concentration), and Tmax (time to peak plasma concentration). As for the different BAs, 2H4-pitavastatin AUCRplasma values were determined by dividing the $AUC_{0\text{-}24,plasma}$ after RIF treatment by the vehicle alone $AUC_{0\text{-}24,plasma}$. For RIF, it was possible to calculate RIF plasma free C_{max} based on a plasma unbound fraction of 0.265.

In turn, in vitro IC50s for RIF with cynomolgus monkey OATP and NTCP [13, 16] were used to calculate % inhibition; % inhibition = 100 * {[I]/([I] + IC50)}. It is assumed that IC_{50} ~ Ki (when substrate concentration < Km). [I] represents plasma C_{max} of RIF (total or free). Consideration of free and total plasma Cmax is consistent with [5]; in the absence of i.v. RIF pharmacokinetic data, it was not possible to derive an absorption rate constant for RIF and estimate its liver inlet (portal) concentration in the cynomolgus monkey.

2.2.6 Statistical Analysis of RIF Dose Response

Plasma: Plasma profiles over time for each animal were collapsed into an AUC using the trapezoidal rule and a C_{max} score. The analyses were then conducted using a linear mixed model, such that the within-animal correlations were accounted for in the model. The R computing language was used for these calculations (R Core Team,

2014). Outcomes were analyzed on the log (base 2) scale to make the residuals more normal. Concentrations were entered into the model on the same scale and the p-value for the linear trend is based on an F-statistic using Satterthwaite's approximation (Burghoff, 2016). False discovery rate (FDR) estimates were computed using the Benjamini and Hochberg procedure (Benjamini and Hochberg, 1995).

Urine: Renal clearance (CL_{renal}) values (ml/min/kg) of zero were treated as missing and analytes with greater than five missing values were excluded. As such, 18 of the 30 BAs were analyzed. As described for plasma, the analysis was conducted using a linear mixed model such that the within-animal correlations were accounted for in the model. The BAs were analyzed on the natural log scale to make the residuals more normal. Similar to plasma, the p-value for the linear trend is based on an F-statistic using Satterthwaite's approximation and FDR estimates were computed using the Benjamini and Hochberg procedure.

2.3 Results

2.3.1 Pharmacokinetics of RIF in Cynomolgus Monkeys

As expected, a dose-dependent increase in RIF $AUC_{0\text{-}24,plasma}$, and plasma C_{max} was observed over the dose range of 1 to 30 mg/kg **(Table 2.1 and Supplemental Fig. 1).** However, at the RIF doses of 3, 10 and 30 mg/kg, there was evidence for a greater than proportional increase in $AUC_{0\text{-}24,plasma}$ (11-, 71- and 243-fold versus AUC at 1 mg/kg) and plasma C_{max} (12-, 45-, and 137-fold versus C_{max} at 1 mg/kg). For RIF, plasma unbound fraction was 0.265 and so the calculated free C_{max} was 0.057, 0.659, 2.57 and 7.79 μM at 1, 3, 10 and 30 mg/kg, respectively. Such concentrations exceed the reported in vitro IC_{50} values (0.14 to 1.7 μM) for RIF with cynomolgus monkey OATP1B1 and OATP1B3 [13, 16].

2.3.2 Impact of RIF on 2H4-Pitavastatin Pharmacokinetics

The pharmacokinetic parameters of $^{2}H_{4}$-pitavastatin, an accepted cynomolgus monkey OATP probe drug [14], were determined after dosing of an i.v. bolus (0.2 mg/kg) to vehicle control and RIF-dosed cynomolgus monkeys (**Table 2.2, Supplemental Fig. 1**). Compared with the vehicle control, $^{2}H_{4}$-pitavastatin CL was decreased 21%, 58%, 73%, and 76% with RIF treatment at 1, 3, 10, and 30 mg/kg dose levels, respectively. However, the change was only statistically significant at the 3 top RIF doses. Furthermore, $^{2}H_{4}$-pitavastatin $AUC_{0\text{-}24,plasma}$ was increased 1.2-, 2.4-, 3.8-, and 4.5-fold at 1, 3, 10 and 30 mg/kg RIF, respectively. Both the Vd_{ss} and $T_{1/2}$ of 2H4-pitavastatin were decreased (~70 %) at the three highest RIF doses. At all the RIF dose levels, recovery of unchanged $^{2}H_{4}$-pitavastatin in urine was less than 5% of the dose. Overall, the impact of the lowest RIF dose on $^{2}H_{4}$-pitavastatin pharmacokinetics was not statistically significant.

2.3.3 Profiling of Plasma BAs at Different Doses of RIF

As with $^{2}H_{4}$-pitavastatin, the plasma levels of various BAs, as well as their corresponding 3-O-sulfate conjugates, were measured in cynomolgus monkeys following increasing doses of RIF. In total, 30 different BAs were monitored. Sulfated BAs, in particular GDCA-S, TDCA-S, GCDCA-S, TCDCA-S, GLCA-S, and TLCA-S, presented a marked dose-dependent increase in their plasma concentration-time profile **(Figure1.1, Supplemental Table 3).** In contrast, the plasma concentration-time profile of non-sulfated BAs, particularly DCA, GDCA, TDCA, GCDCA, TCDCA, UDCA, GUDCA, TUDCA, CA, GCA, and TCA, showed a relatively weak increase at the RIF doses of 10 and 30 mg/kg **(Supplemental Figure 2)**. Chu et al. have also reported a weak increase in non-sulfated BAs after an oral RIF dose of 18 mg/kg [16]. RIF treatment did not cause significant changes in LCA, GLCA and TLCA. Unfortunately, GUDCA-S, TUDCA-S, CA-S, TCA-S, and GCA-S plasma levels were low and remained undetectable even after RIF treatment. Overall, the presence of various sulfo-conjugates in plasma was

indicative of BA sulfation in the cynomolgus monkey. However, the pool of cynomolgus monkey BAs in circulation was distinct from that reported for human subjects; the percentages of sulfated (1.3% versus 28.4%) and amidated (21.5% versus 75.4%) BAs were low for monkey versus human, respectively **(Supplemental Table 4).** To complement the in vivo studies, the sulfation of six representative BAs (GCDCA, GUDCA, LCA, GLCA, GCA, and TLCA) was investigated after incubation with cynomolgus monkey liver cytosol (Supplemental Figure 3); the availability of authentic standards supported the identification of the 3-O-sulfate as the major product of PAPS-fortified monkey liver cytosol. Although a good correlation was obtained between human and cynomolgus monkey (R2 = 0.905), a low activity ratio (cynomolgus monkey-to-human) was obtained for the formation of LCA-S, GLCA-S, TLCA-S, and GUDCA-S (0.20, 0.25, 0.36, and 0.37, respectively). In comparison, GCDCA-S (activity ratio = 0.89) and GCA-S (activity ratio = 3.0) rendered higher activity ratios comparable to those of DHEA 3-O-sulfate (activity ratio of 1.3). Importantly, RIF (up to 100 μM) was shown not to inhibit cynomolgus monkey liver cytosol-catalyzed BA sulfation **(Supplemental Fig. 4).**

2.3.4 Assessment of RIF Dose Response

$AUCR_{plasma}$ values for the various BAs after RIF treatment are shown in **Figure 2.2.** The highest $AUCR_{plasma}$ (≥ 78) was observed for GDCA-S and GCDCA-S, followed by TDCA-S, DCA-S and TCDCA-S (~50) and GLCA-S and TLCA-S (~30). A relatively modest $AUCR_{plasma}$ (5 to 10) was observed for CA, GCA and TCA. The remaining non-sulfated BAs presented low $AUCR_{plasma}$ values (2 to 5). Fold changes in plasma C_{max} after RIF treatment are shown in Figure 3. Similar to the AUC changes, the highest (50- to 80-) fold increase was observed for DCA-S, GDCA-S, TCDCA-S, TDCA-S, and GCDCA-S followed by a 20-fold increase for GLCA-S and TLCA-S at RIF dose of 30

mg/kg. $AUC_{0\text{-}24,plasma}$ and plasma C_{max} values at each RIF dose and vehicle control are shown in **Supplemental Table 3.**

Statistical analysis for linear trend in $AUC_{0\text{-}24,plasma,}$ and C_{max} and FDR for each BA are shown in **Table 2.3.** Overall, with the exception of CA-S, all BA 3-O-sulfates were characterized by a significant linear trend (p-value < 0.01) with a slope of more than 0.6700 and a FDR less than 10% for $AUC_{0\text{-}24,plasma.}$ GDCA-S, GCDCA-S, TDCA-S, TCDCA-S, GLCA-S, and TLCA-S were the most significant sulfate conjugates with a p-value for the linear trend of less than 0.001, a slope of more than 0.7500 and FDR less than 1% for $AUC_{0\text{-}24,plasma}$ as well as C_{max}. In contrast, most of the non-sulfated bile acids did not show a statistically significant linear trend and FDR was more than 10% for $AUC_{0\text{-}24,plasma}$ and C_{max}. Only TCA and TDCA showed a p-value less than 0.01 and ~ 10% FDR.

Importantly, the plasma $AUCR_{plasma}$ values showed a good linear correlation (R^2 > 0.7000) between pitavastatin and GDCA-S, TDCA-S, GCDCA-S, TCDCA-S, GLCA-S, and TLCA-S **(Figure 2.4)**. Similarly, a good linear correlation (R2 > 0.7500) between RIF plasma free Cmax and 2H4-pitavastatin, GDCA-S, TDCA-S, GCDCA-S, TCDCA-S, GLCA-S, and TLCA-S $AUCR_{plasma}$ was observed **(Figure 2.5).**

As described previously, an effort was made to administer RIF over a dose range that generated a wide range of plasma total (0.2 to 29 μM) and free (0.06 to 7.8 μM) C_{max} values (**Table 2.1**). In so doing, it was possible to investigate the dose-dependent inhibition of OATPs and NTCP. Based on in vitro IC50 data, dose-dependent inhibition of OATP1B1 (16% to ≥ 96%) and OATP1B3 (<10% to ≥ 85%) was expected, with less inhibition of OATP2B1 (<10% to 31%) and NTCP (<10% to 29%) anticipated (Supplemental Table 5 and 6). Despite the effort to ensure dose-dependent inhibition, however, the $AUCR_{plasma}$ values for the various BA sulfates differed markedly. The highest maximal $AUCR_{plasma}$ values (≥ 78) were obtained with GDCA-S and GCDCA-S,

followed by TDCA-S, DCA-S and TCDCA-S ($AUCR_{plasma}$ ~ 50) and GLCA-S and TLCA-S ($AUCR_{plasma}$ ~ 30).

2.3.5 Impact of RIF on BA Renal Clearance

Because the 3-O-sulfate conjugates of the various BAs are recovered in human urine [18, 27, 28], the present study was extended to include the profiling of urine of control and RIF-dosed cynomolgus monkeys. In this regard, a dose-dependent increase in the amounts of GDCA-S, TDCA-S, GCDCA-S, TCDCA-S, GLCA-S, and TLCA-S excreted in urine was observed (Supplemental Table 3). CL_{renal} ratios and statistical analysis for each BA are shown in **Figure 2.6** and **Table 2.3**, respectively. A weak dose-dependent increase in CL_{renal} was observed for UDCA, GDCA, and DCA. However, there was no statistically significant effect of RIF treatment on the CL_{renal} of sulfated and non-sulfated bile acids. For the former, this is in marked contrast to the changes in plasma AUC and C_{max} following RIF treatment.

2.3.6 Incubation of GCDCA-S, GDCA-S, DCA-S, TDCA-S, TCA and Pitavastatin with Cynomolgus Monkey Plated Hepatocytes

Based on the availability of deuterium-labeled material and RIF-dependent $AUCR_{plasma}$ values in vivo, four sulfated BAs (GCDCA-S, GDCA-S, DCA-S, and TDCA-S) were chosen for study as solute carrier (SLC) substrates in vitro after incubation with plated cynomolgus monkey primary hepatocytes (Figures 7 and 8). TCA and pitavastatin were also incubated as representative cynomolgus monkey NTCP (> OATP) and OATP (>NTCP) substrates, respectively [14, 16]. To discern the role of NTCP versus OATPs, incubations were performed in the presence and absence of sodium (NTCP is sodium-dependent). In addition, RIF (5 μM) and RIFsv (1 mM) were deployed as cynomolgus monkey OATP-selective and pan-SLC inhibitors, respectively (Supplemental Table 5; [13, 16]).

When incubated with RIFsv, the uptake of TCA, GDCA-S, GCDCA-S, and pitavastatin was markedly inhibited (≥ 92%). For the four substrates, such a result is consistent with relatively high rates of active (versus passive; ≤ 8%) uptake **(Figure 2.7A)**. As shown in **Figure 2.7B**, the uptake of GCDCA-S and GDCA-S was minimally impacted by the removal of sodium. By contrast, uptake of TCA (74%) and pitavastatin (~44%) was decreased in the presence of sodium-free buffer. As expected, RIF elicited relatively weak inhibition of TCA uptake when compared to pitavastatin (14% versus 58%). Uptake of both GCDCA-S (69% inhibition) and GDCA-S (82% inhibition) was sensitive to RIF. Although the exact contribution of OATP1B1 and OATP1B3 was not determine, in the absence of selective inhibitors and established relative activity factors for cynomolgus monkey transporters, it is concluded that uptake of both GCDCA-S and GDCA-S (0.5 μM) in the presence of cynomolgus monkey hepatocytes is dominated by OATPs and that their profile is distinct from that of TCA. Based on the results presented in **Figure 2.8**, the same can be said for two additional BA sulfates (TDCA-S and DCA-S). In this instance, RIF (5 μM) was shown to inhibit the uptake of TCA, pitavastatin, GCDCA-S, GDCA-S, TDCA-S and DCA-S (0.1 μM) by 21%, 73%, 92%, 83%, 95% and 80%, respectively.

2.4 Discussion and Conclusion

Metabolism of various BAs is complex and involves oxidation, amidation, glucuronidation, and sulfation. Once conjugated, BAs are also subjected to transporter-mediated uptake (e.g., OATP and NTCP) and efflux [23, 28-32]. Therefore, the BA pool of most species is complex, and subject to enterohepatic recirculation and renal clearance. This means that the BA profiling requires robust LC-MS/MS methods with access to a large number of authentic standards [18]. To support the present study, therefore, authentic standards of a number of non-commercially available BA 3-O-

sulfates were prepared and 30 different BAs were profiled in cynomolgus monkey plasma and urine.

Although in vivo sulfation of DHEA has been reported in cynomolgus monkeys [22], and SULT2A1 (human sulfotransferase involved in BA 3-O-sulfation) is known to be expressed in cynomolgus monkey liver [19-21], there have been no reports describing the BA sulfation in the cynomolgus monkey. For the first time, it was possible to report that DHEA and various BAs undergo sulfation in vitro (Supplemental Figure 3). Importantly, the presence of BA sulfates in cynomolgus monkey urine is consistent with human data [18, 28]. However, the fraction of the BA pool in circulation as the sulfated species was low in cynomolgus monkey versus human (28.4% versus 1.3%; Supplemental Table 4), and likely reflects species differences in CL_{renal} and formation clearance. In agreement, the CL_{renal} of GCDCA-S is lower in humans (31 versus 0.05 ml/min per kg) (Supplemental Table 3; [28]) and the rate of BA sulfation in vitro was lower in the presence of cynomolgus monkey cytosol (Supplemental Figure 3). A species difference in OATP-mediated hepatic uptake clearance is also a possibility.

GCDCA-S has been shown to undergo active renal secretion and has been proposed as a biomarker for human organic anion transporter 3 (OAT3) [28]. Although the cynomolgus monkey OAT3 has been expressed and characterized, nothing is known of its ability to transport BA sulfates and its inhibition by RIF [33]. Therefore, as part of the present study, it was important to assess the impact of RIF on BA sulfation and renal clearance. This ensured that any observed changes in BA $AUC_{0\text{-}24,plasma}$ were reflective of hepatic transporter inhibition. In vitro data indicated that RIF (up to 100 μM) did not inhibit liver cytosol-catalyzed BA sulfation (Supplemental Figure 4). Likewise, profiling of cynomolgus monkey urine supported calculation of CL_{renal} for the different BAs and it was determined that the impact of RIF was minimal (Table 2.3; Supplemental Table 3). Importantly, there is evidence indicating that BA sulfates also serve as substrates of

human canalicular multidrug resistance-associated protein (MRP) MRP2 and basolateral MRP3 and MRP4 [23, 29-31]. The possibility that single dose RIF can inhibit cynomolgus monkey MRP2 has already been considered by Chu et al (2015). In this instance, the authors showed that RIF is a relatively weak inhibitor of cynomolgus monkey MRP2 (IC_{50} = 118 μM) and argued for relatively minimal inhibition based on estimated free RIF liver levels (~10 μM). Although no RIF inhibition data are available for monkey MRP3 and MRP4, given that robust $AUCR_{plasma}$ values for the various BA sulfates it is assumed that neither transporter is inhibited. Alternatively, RIF could induce MRP3 and MRP4 and compromise the interpretation of the data [34, 35]. However, it can be argued that significant and sustained induction of both MRP proteins is unlikely following a single RIF dose. Importantly, BA sulfate plasma concentration-time profiles were consistent with relatively rapid (within 6 hr) dose-dependent inhibition of hepatic uptake. Moreover, plasma concentrations for five of the six BA sulfates were trending towards pre-RIF dose levels by 24 hr **(Figure 2.1).**

To date, efforts to inhibit cynomolgus monkey OATP in vivo have involved oral administration of a single RIF dose that generates a plasma total C_{max} of ~10 μM [13, 14, 16]. As described, it was possible to administer RIF at four dose levels of 1, 3, 10, and 30 mg/kg and obtain mean plasma total C_{max} values of 0.2, 2.5, 9.7, and 29 μM, respectively; corresponding to a plasma free C_{max} of 0.06, 0.67, 2.57 and 7.79 μM, respectively **(Table 2.1).** Evidently, the pharmacokinetic profile of RIF in the cynomolgus monkey was non-linear, likely reflecting saturation of first pass, and consistent with human data [36]. Despite the non-linearity, there was a good linear correlation (R^2 > 0.9332) between RIF plasma C_{max} and $AUCR_{plasma}$ for a number of BA sulfates (Fig. 5) and, because expression of hepatic OATP2B1 is relatively low in cynomolgus monkey, such a dose response is more likely reflective of OATP1B1 and OATP1B3 inhibition [37]. Based on the in vitro IC50s reported for both OATPs (≤ 1.7 μM; Supplemental Table 5),

and assuming that RIF plasma concentrations support estimates of inhibition [5], up to >85% (RIF free C_{max}) and >96% (RIF total C_{max}) inhibition is anticipated (Supplemental Table 6). In agreement, a clear RIF dose-dependent increase in 2H4-pitavastatin $AUCR_{plasma}$ (1.2, 2.4, 3.8 and 4.5) was evident **(Figure 2.5).** Because of weaker inhibition by RIF (IC_{50} ≥ 35.1 μM, **Supplemental Table 5**), less NTCP inhibition (10% to 29%) is expected **(Supplemental Table 6).** This is an important consideration, because certain BAs are known to favor NTCP over OATPs [38-41]. For example, the uptake of TCA by primary cynomolgus monkey hepatocytes was shown to be highly sodium dependent and relatively refractory to RIF (Figures 7 and 8). Although no formal in vitro-in vivo exercise was attempted, it assumed that the RIF dose-dependent $AUCR_{plasma}$ values for TCA (1.2, 2.0, 1.8 and 5.4) are largely reflective of NTCP inhibition (Supplemental Tables 3 and 6). On the other hand, GCDCA-S, GDCA-S, TDCA-S and DCA-S behaved as OATP substrates in the presence of cynomolgus monkey hepatocytes **(Figures 2.7 and 2.8),** consistent with reports of a fifth sulphated BA (TLCA-S) presenting as an OATP substrate in vitro [23, 24].

As described, five sulfated BAs in plasma responded robustly to RIF in a dose-dependent manner (maximal $AUCR_{plasma}$ ≥ 50). Two additional BA sulfates, GLCA-S and TLCA-S, were also found to respond to RIF (maximal $AUCR_{plasma}$ ~ 30) **(Figure 2.2).** From the standpoint of detectability in control animals, magnitude of the RIF dose response, and detectability in human plasma, these seven BA sulfates (GCDCA-S, TCDCA-S, DCA-S, GDCA-S, TDCA-S, GLCA-S and TLCA-S) all present as potential sensitive OATP biomarkers. Importantly, the RIF dose-response obtained was far greater than the increases (<10-fold) reported for cynomolgus monkey plasma bilirubin, bilirubin glucuronide, coproporphyrin (I and III), non-sulfated BAs, and DHEA sulfate [12, 16, 17].

Although the results presented herein showcase various BA sulfates as sensitive cynomolgus monkey OATP biomarkers, it cannot be assumed that the results translate directly to human subjects. For example, the balance of OATP- versus NTCP-mediated liver uptake, and the contributions of individual OATPs, may not be the same across species. Despite the caveats, the results of the present work are consistent with plasma metabolomic data from a recent OATP1B1 (SLCO1B1) genome-wide association study that identified GCDCA-S, GDCA-S and TLCA-S as potential OATP1B1 biomarkers [10]. Such BA sulfates could potentially serve as sensitive human OATP biomarkers and provide the necessary dynamic range to support perpetrator differentiation (weak, moderate, versus potent inhibition), enable the study of OATP genotype-phenotype associations, and facilitate phenotyping of hepatobiliary diseased subjects [7, 8]. In this regard, sulfated BAs could be superior human OATP biomarkers when compared to plasma coproporphyrin I and III ($AUCR_{plasma}$ ~4.0) [9]. As discussed previously, because circulating sulfated BAs are substrates of renal transporters also, they may serve as dual liver OATP and renal OAT3 biomarkers. In agreement, an increase in “urinary sulfated bile acids” has been reported in patients with various hepatobiliary diseases, which may in part reflect altered liver OATP function [27, 42, 43]. Consistent with human data, the amount of sulfated BAs in cynomolgus monkey urine increased with RIF dose **(Supplemental Table 3).**

Based on the results of the present study, it is concluded that the cynomolgus monkey can form BA sulfates that comprise only ~1% of the plasma BA pool and present as sensitive hepatic OATP biomarkers. Given the number of similarly sulfated BAs that are detectable in human serum [18], it is envisioned that they will be increasingly studied as human OATP substrates and compared to other biomarkers such as coproporphyrin I and III.

Figure 2.1 Plasma concentration-time profile of (A) GDCA-S, (B) TDCA-S, (C) GCDCA-S, (D) TCDCA-S, (E) GLCA-S and (F) TLCA-S in male cynomolgus monkeys after oral administration of vehicle alone (open squares), and RIF 1 mg/kg (open circles), 3 mg/kg (closed triangles), 10 mg/kg (closed circles) and 30 mg/kg (closed squares). Data are presented as mean ± SD of n = 4 animals.

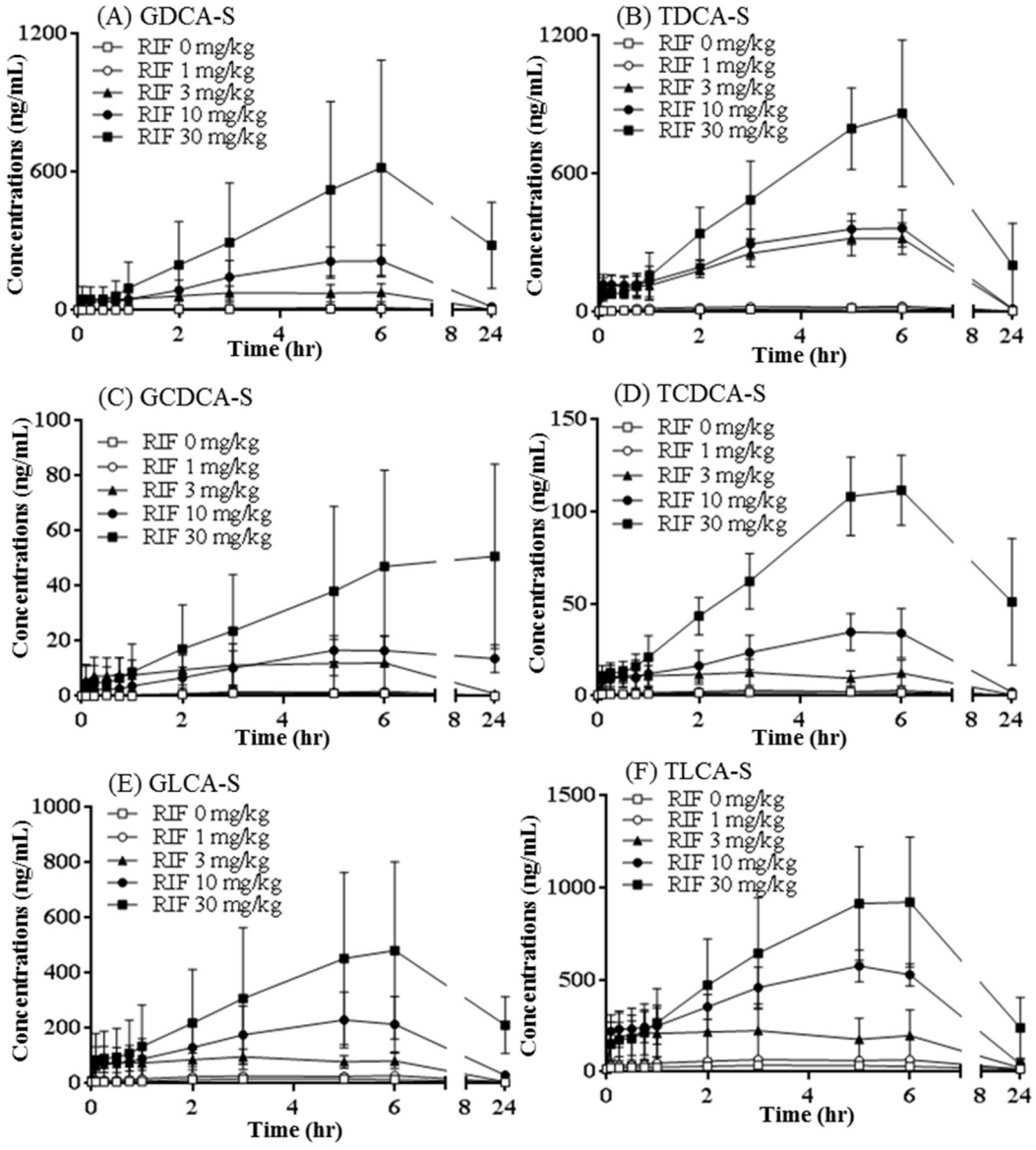

Figure 2.2 Fold change in $AUC_{0\text{-}24,plasma}$ of (A) un-sulfated bile acids and (B) bile acid 3-O-sulfates at increasing doses of RIF in male cynomolgus monkeys.

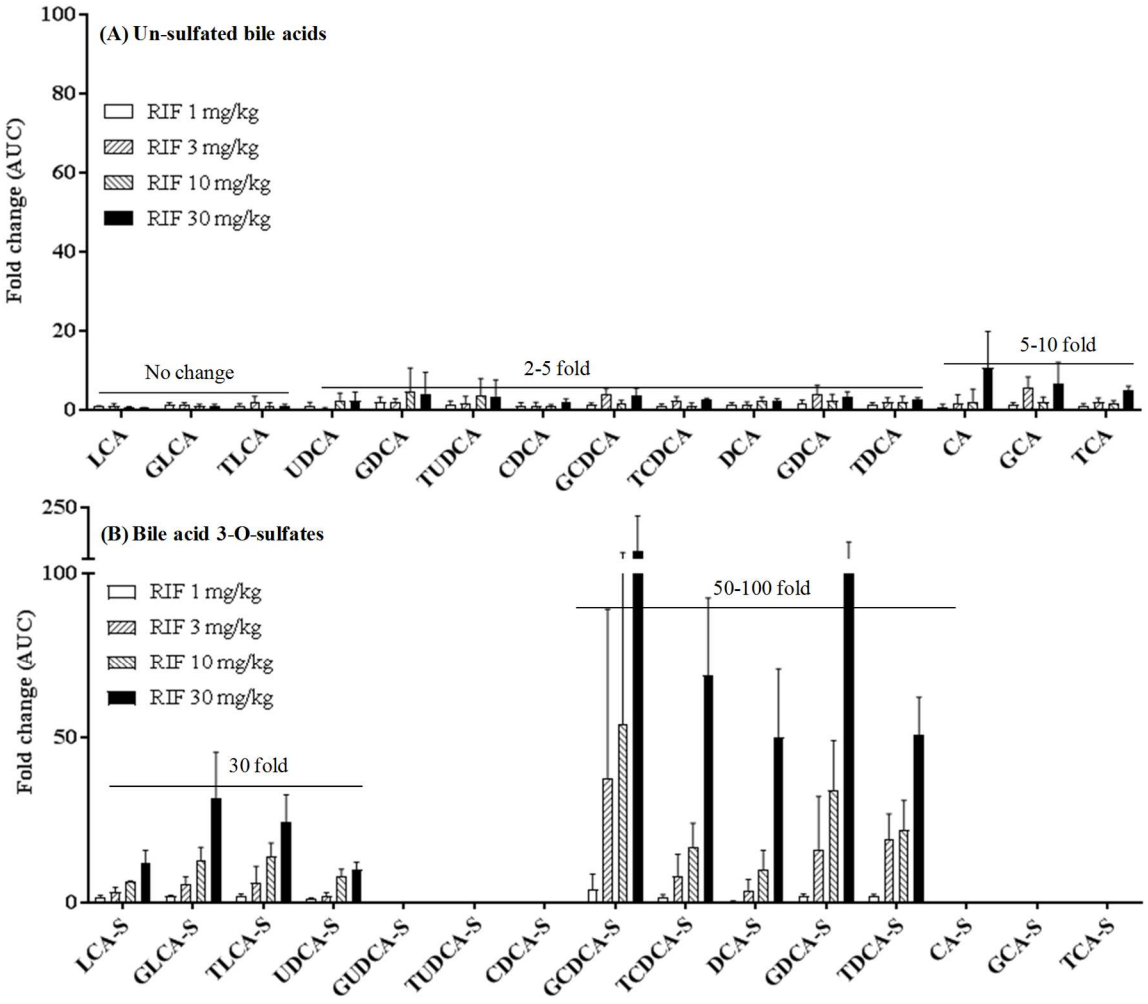

Figure 2.3 Fold change in plasma C_{max} of (A) un-sulfated bile acids and (B) bile acid 3-O-sulfates at increasing doses of RIF in male cynomolgus monkeys.

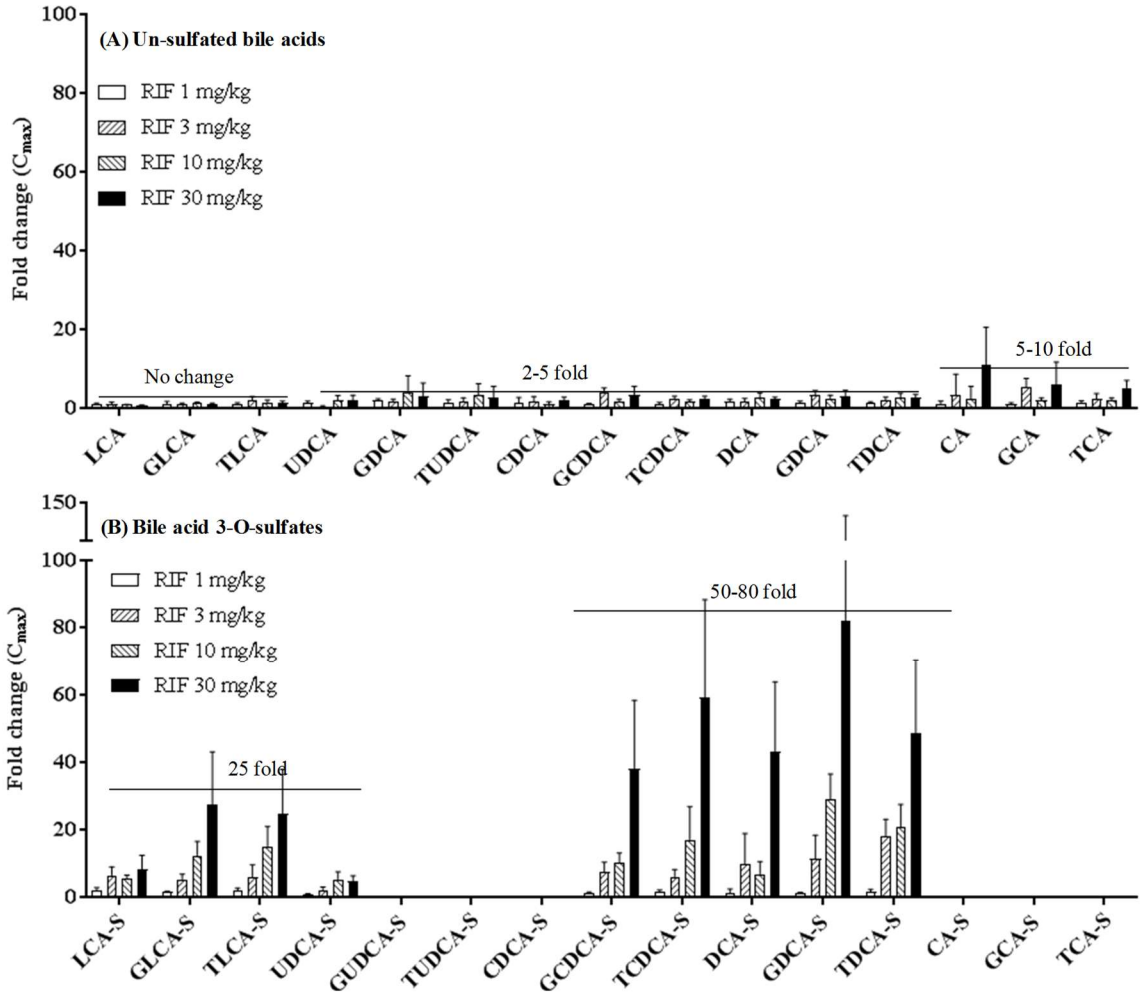

Figure 2.4 Linear regression of plasma AUC ratio ($AUCR_{plasma}$) between pitavastatin and bile acid 3-O-sulfates for (A) GDCA-S, (B) TDCA-S, (C) GCDCA-S, (D) TCDCA-S, (E) GLCA-S and (F) TLCA-S. For pitavastatin and bile acids, $AUCR_{plasma}$ is calculated by dividing $AUC_{0\text{-}24,plasma}$ obtained with RIF (1, 3, 10 and 30 mg/kg) by the $AUC_{0\text{-}24,plasma}$ for vehicle control.

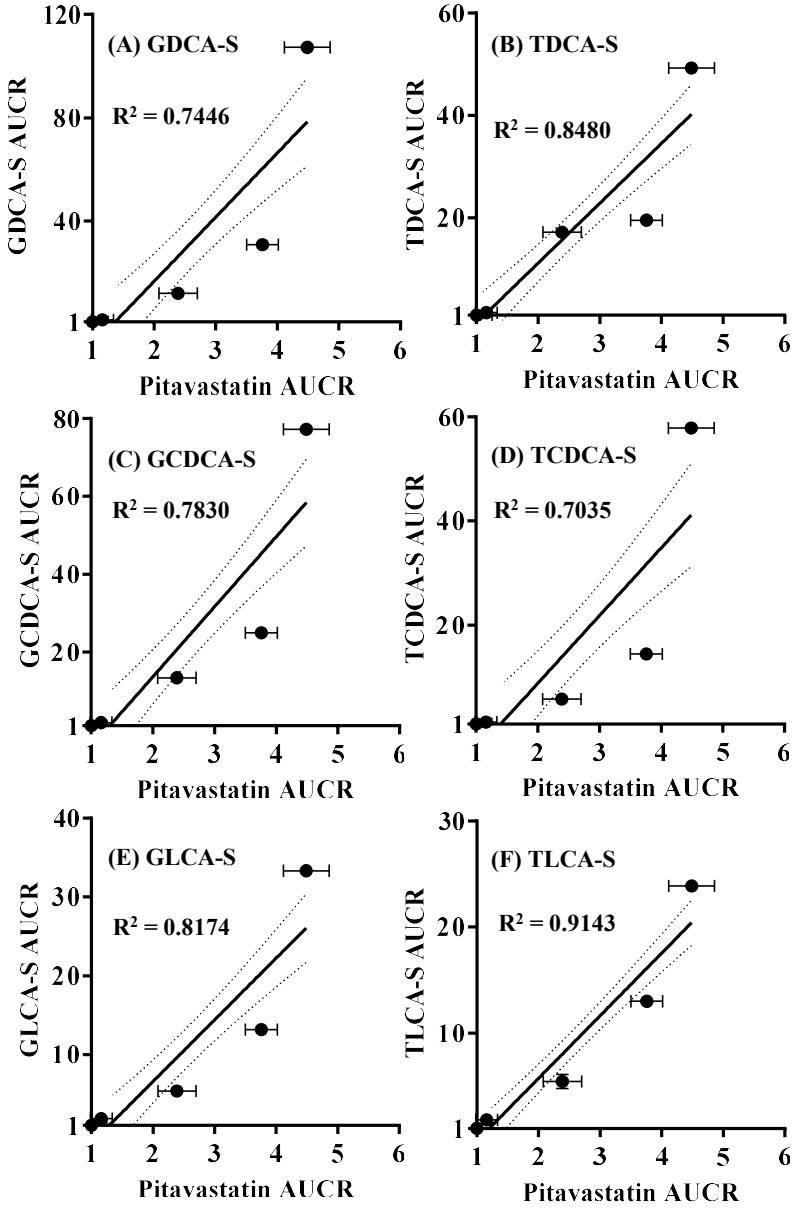

Figure 2.5 Linear regression between free RIF plasma C_{max} (μM) at 1, 3, 10 and 30 mg/kg and bile acid 3-O-sulfate $AUCR_{plasma}$ for (A) GDCA-S, (B) TDCA-S, (C) GCDCA-S, (D) TCDCA-S, (E) GLCA-S, (F) TLCA-S, and (G) pitavastatin. $AUCR_{plasma}$ as defined in the legend to Figure 2.4.

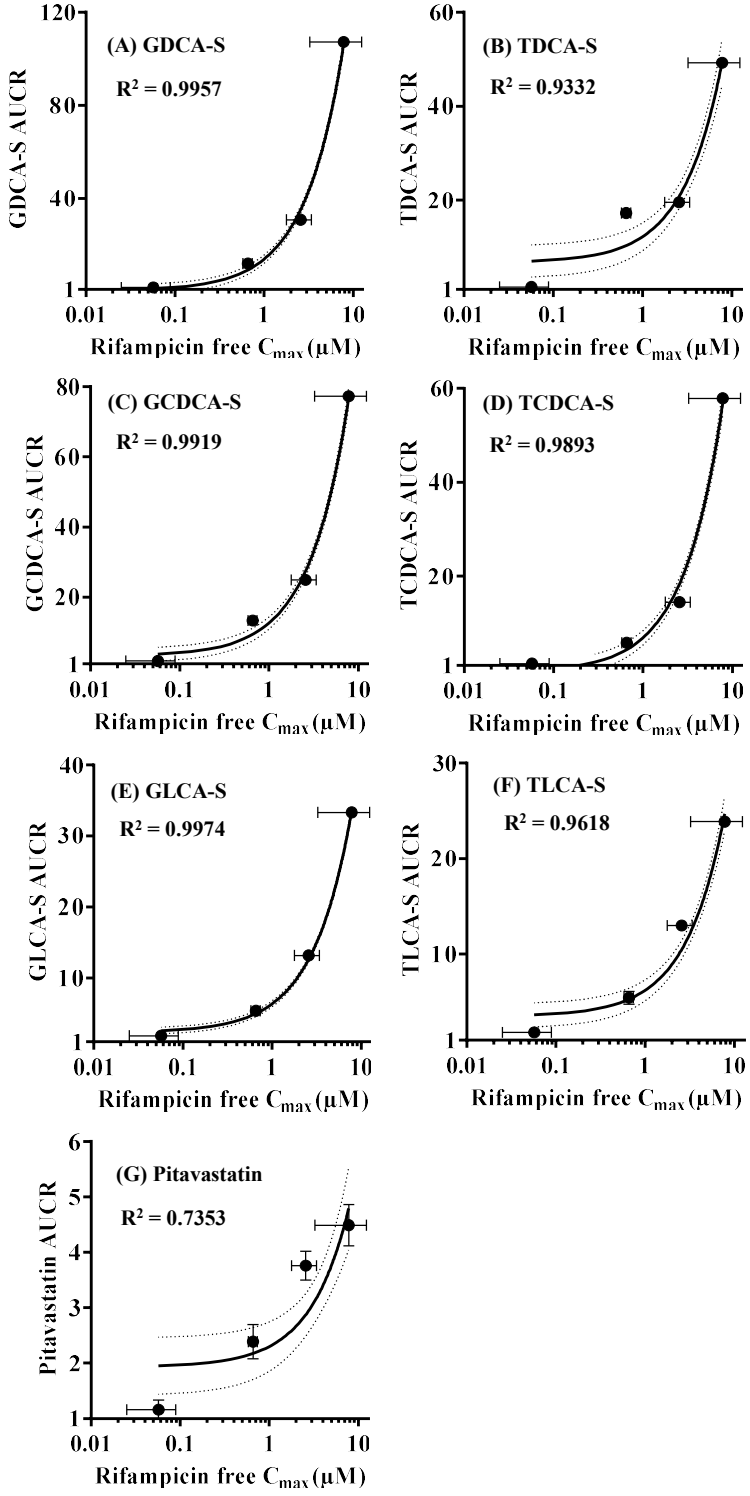

Figure 2.6 Fold change in CL_{renal} of (A) un-sulfated bile acids and (B) bile acid 3-O-sulfates at increasing doses of RIF in male cynomolgus monkeys.

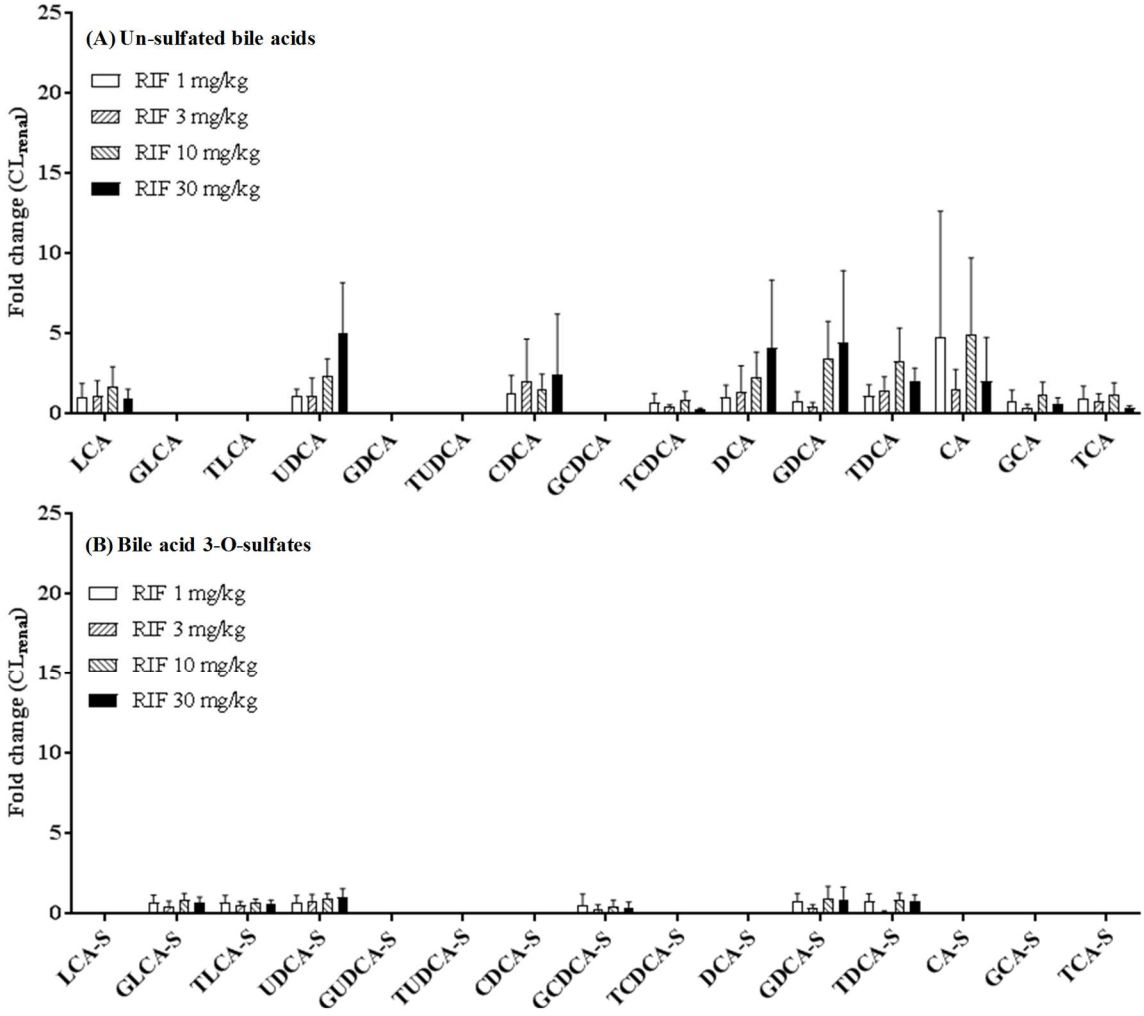

Figure 2.7 Impact of RIF and RIFsv (A) and sodium removal (B) on the uptake of $^{2}H_{5}$-GCDCA-S (0.5 mM), $^{2}H_{4}$-GDCA-S (0.5 mM), $^{2}H_{4}$-TCA (0.5 mM), and non-labeled pitavastatin (0.1 mM) by plated cynomolgus monkey primary hepatocytes. RIF and RIFsv were added at a final concentration of 5 mM and 1 mM, respectively. Data for individual duplicates are shown. The mean % decrease is shown also and calculated as $(V_{DMSO}-V_i/ V_{DMSO})*100$. V_{DMSO} and V_i is the mean uptake rate in the presence of DMSO alone (plus sodium) and inhibitor (or minus sodium) respectively.

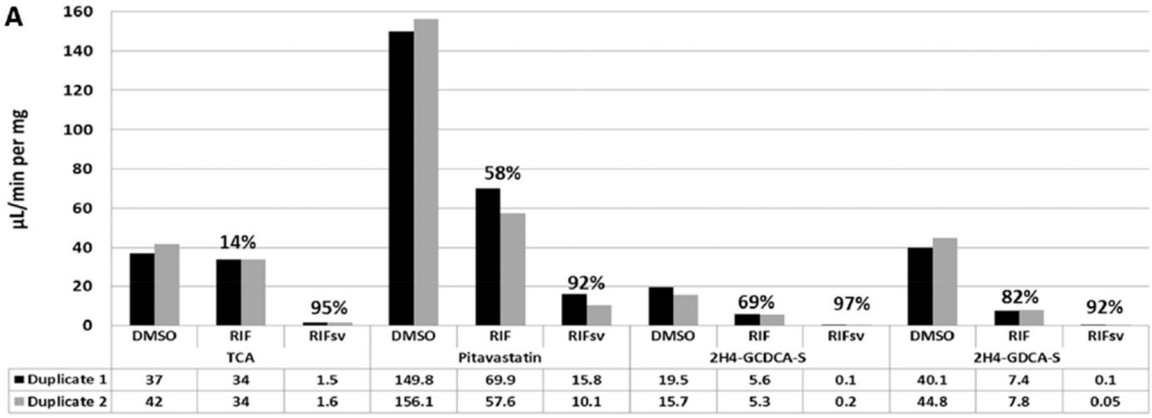

	DMSO	RIF	RIFsv	DMSO	RIF	RIFsv	DMSO	RIF	RIFsv	DMSO	RIF	RIFsv
	TCA			Pitavastatin			2H4-GCDCA-S			2H4-GDCA-S		
Duplicate 1	37	34	1.5	149.8	69.9	15.8	19.5	5.6	0.1	40.1	7.4	0.1
Duplicate 2	42	34	1.6	156.1	57.6	10.1	15.7	5.3	0.2	44.8	7.8	0.05

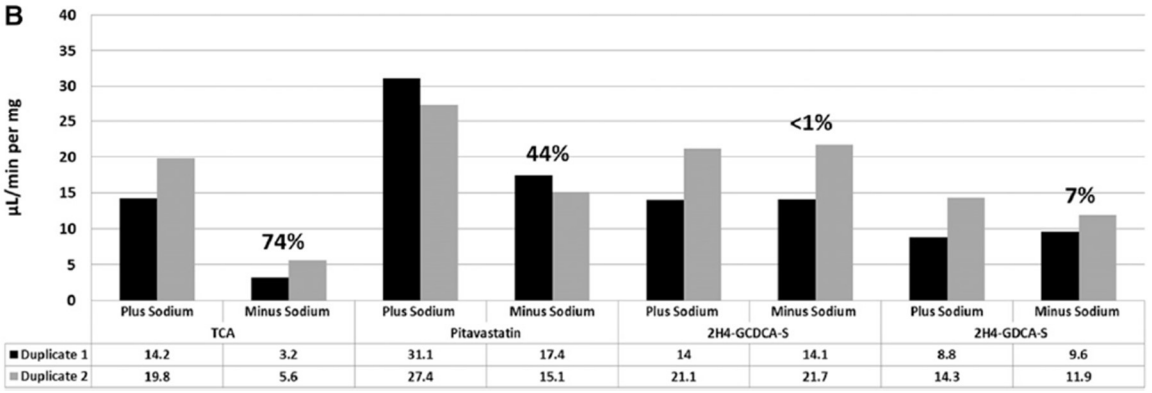

	Plus Sodium	Minus Sodium	Plus Sodium	Minus Sodium	Plus Sodium	Minus Sodium	Plus Sodium	Minus Sodium
	TCA		Pitavastatin		2H4-GCDCA-S		2H4-GDCA-S	
Duplicate 1	14.2	3.2	31.1	17.4	14	14.1	8.8	9.6
Duplicate 2	19.8	5.6	27.4	15.1	21.1	21.7	14.3	11.9

Figure 2.8 Impact of RIF on the uptake of $^{2}H_5$-GCDCA-S (0.1 mM), $^{2}H_4$-GDCA-S (0.1 mM), $^{2}H_4$-TCA (0.1 mM), $^{2}H_4$-TDCA-S (0.1 mM), $^{2}H_4$-DCA-S (0.1 mM), and nonlabeled pitavastatin (0.1 mM) by plated cynomolgus monkey primary hepatocytes. RIF was added at a final concentration of 5 mM. Data for individual duplicates are shown. The mean % decrease is shown and was calculated as described in the legend to Figure 2.7.

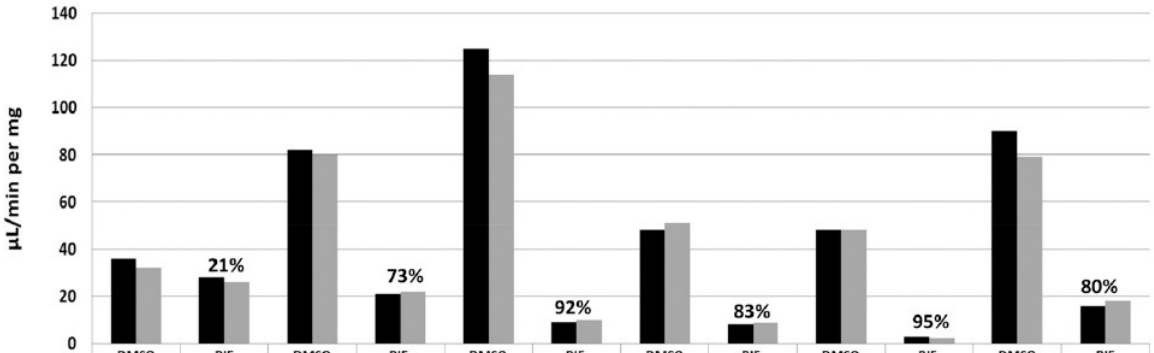

	2H4-TCA		Pitavastatin		2H5-GCDCA-S		2H4-GDCA-S		2H4-TDCA-S		2H4-DCA-S	
	DMSO	RIF	DMSO	RIF	DMSO	RIF	DMSO	RIF	DMSO	RIF	DMSO	RIF
Duplicate 1	36	28	82	21	125	9.2	48	8.3	48	2.9	90	16
Duplicate 2	32	26	80	22	114	9.9	51	8.9	48	2.3	79	18

Table 2.1 Pharmacokinetic parameters of pitavastatin in male cynomolgus monkeys after i.v. administration (0.2 mg/kg) with increasing doses of RIF

Parameter	Oral RIF Dose				
	0 mg/kg	1 mg/kg	3 mg/kg	10 mg/kg	30 mg/kg
$AUC_{0\text{-}Tlast}$ (ng.hr/ml)	192 ± 48.8	223 ± 40.5	459 ± 141	722 ± 190	862 ± 319
$AUC_{0\text{-}inf}$ (ng.hr/ml)	194 ± 48.2	228 ± 44.3	469 ± 139	724 ± 190	871 ± 325
C_0 (ng/ml)	1200 ± 628	925 ± 278	1840 ± 579	1660 ± 355	1570 ± 577
$T_{1/2}$ (hr)	5.95 ± 0.854	7.21 ± 1.74	2.95 ± 1.86	3.77 ± 0.679	4.55 ± 0.594
CL (ml/min/kg)	18 ± 4.62	14.2 ± 2.22	7.55 ± 2.0	4.80 ± 1.36	4.27 ± 1.61
V_{dSS} (l/kg)	1.79 ± 0.723	1.97 ± 0.498	0.466 ± 0.2	0.521 ± 0.164	0.546 ± 0.201
% Dose in urine[a]	1.77 ± 2.02	1.17 ± 0.595	1.23 ± 1.29	4.00 ± 2.02	2.89 ± 0.38

[a]% of Total dose (as pitavastatin) recovered in urine over 24h.

Data are presented as mean ± SD, n = 4 animals.

Table 2.2 Pharmacokinetic parameters of RIF after oral administration to male cynomolgus monkeys

	RIF Dose			
Parameter	1 mg/kg	3 mg/kg	10 mg/kg	30 mg/kg
$AUC_{0\text{-}Tlast}$ (ng.hr/ml)	985 ± 396	11300 ± 3260	70100 ± 10800	240000 ± 73900
$AUC_{0\text{-}inf}$ (ng.hr/ml)	1010 ± 389	11400 ± 3300	72400 ± 8550	304000 ± 79100
C_{max}(ng/ml)	176 ± 98.7	2050 ± 245	7980 ± 2480	24200 ± 14100
Free C_{max} (uM)[a]	0.057 ± 0.032	0.659 ± 0.079	2.57 ± 0.80	7.79 ± 4.54
T_{max}(hr)	2.70 ± 0.86	1.80 ± 0.36	1.70 ± 0.43	2.70 ± 0.58
$T_{1/2}$(hr)	5.18 ± 1.52	2.84 ± 0.202	4.56 ± 2.18	11.5 ± 6.26

[a]Total C_{max} converted to μM and corrected for RIF plasma free fraction (0.265). RIF plasma protein binding was determined using equilibrium dialysis with ascorbic acid as a stabilizer.

Data are presented as mean ± SD, n = 4 animals.

Table 2.3 The p-value for the linear trend with RIF dose and false discovery rate (FDR) estimates for area under the plasma concentration-time curve ($AUC_{0\text{-}24,plasma}$), maximum plasma concentration ($C_{max,plasma}$) and renal clearance (CL_{renal}) for various bile acids and their respective 3-O-sulfate conjugates.

	$AUC_{0\text{-}24,plasma}$			$C_{max,plasma}$			CL_{renal}		
Bile Acid	Slope[a]	p-value	FDR	Slope	p-value	FDR	Slope	p-value	FDR
CA-S	2.08	0.0218	0.2395	1.06	0.0589	0.5889	NA[b]	NA	NA
DCA-S[c]	1.44	< 0.0001	< 0.0001	0.9	< 0.0001	< 0.0001	-0.005	0.798	1
TCA-S	1.2	0.0004	0.0067	1.07	0.0011	0.0193	NA	NA	NA
GDCA-S[c]	1.13	< 0.0001	< 0.0001	1.11	< 0.0001	0.0001	0.003	0.767	1
GCA-S	1.1	0.0021	0.0373	0.89	0.0067	0.1067	NA	NA	NA
TCDCA-S[c]	1.09	< 0.0001	< 0.0001	1.04	< 0.0001	< 0.0001	0.01	0.2517	1
GCDCA-S[c]	1.07	< 0.0001	< 0.0001	0.97	< 0.0001	< 0.0001	-0.02	0.3157	1
CDCA-S	0.99	0.0036	0.0619	0.61	0.094	0.6907	NA	NA	NA
TDCA-S[c]	0.91	< 0.0001	< 0.0001	0.89	< 0.0001	0.0001	0.01	0.4206	1
GLCA-S[c]	0.81	< 0.0001	< 0.0001	0.78	< 0.0001	< 0.0001	-0.003	0.7155	1
TLCA-S[c]	0.78	< 0.0001	< 0.0001	0.76	< 0.0001	< 0.0001	-0.003	0.7002	1
UDCA-S	0.77	< 0.0001	< 0.0001	0.56	< 0.0001	0.0009	0.003	0.6382	1
CA	0.72	0.0049	0.0737	0.49	0.0251	0.3264	-0.006	0.7236	1
LCA-S	0.68	< 0.0001	< 0.0001	0.35	0.0013	0.0219	NA[b]	NA	NA

TCA	0.35	0.0071	0.092	0.35	0.0006	0.012	-0.03	0.0162	0.2434
GCA	0.3	0.0971	0.8231	0.31	0.0767	0.6907	-0.005	0.6641	1
DCA	0.25	0.0049	0.0737	0.18	0.0222	0.3107	0.04	0.0086	0.1369
UDCA	0.24	0.0112	0.1343	0.19	0.0829	0.6907	0.04	0.004	0.0685
TDCA	0.23	0.0045	0.0724	0.26	0.0004	0.0075	0.02	0.0485	0.6303
GDCA	0.21	0.0622	0.6218	0.23	0.0346	0.4152	0.05	0.0027	0.0478
GCDCA	0.17	0.2221	0.8884	0.18	0.1857	1	NA	NA	NA
TCDCA	0.16	0.0915	0.8231	0.19	0.0073	0.1088	-0.03	0.0226	0.3161
CDCA	0.16	0.1127	0.8231	0.09	0.3571	1	0.003	0.7522	1
TUDCA	0.15	0.1343	0.8231	0.11	0.3341	1	NA	NA	NA
GUDCA	0.1	0.2289	0.8884	0.05	0.5432	1	NA	NA	NA
GLCA	-0.06	0.413	0.8884	-0.03	0.669	1	NA	NA	NA
LCA	-0.1	0.1097	0.8231	-0.13	0.0434	0.4771	-0.009	0.5259	1

[a]Results ranked in terms of slope ($AUC_{0\text{-}24,plasma}$).
[b]No baseline (vehicle control) levels; NA: not applicable.
[c]Considered candidate OATP biomarkers (See Figure 3.2 and 3.3).

Figure S1 Plasma concentration-time profile of (A) $^{2}H_{4}$-pitavastatin administered, intravenously (0.2 mg/kg), approximately one hour and 15 minutes after oral administration of vehicle (open circles), and rifampicin at 1 mg/kg (closed triangles), 3 mg/kg (open triangles), 10 mg/kg (open square) and 30 mg/kg (closed circles) and (B) rifampicin after oral administration at a dose of 1 mg/kg (open circles), 3 mg/kg (closed triangles), 10 mg/kg (open triangles) and 30 mg/kg (closed circles). Data are presented as the mean ± SD (n = 4 different cynomolgus monkeys).

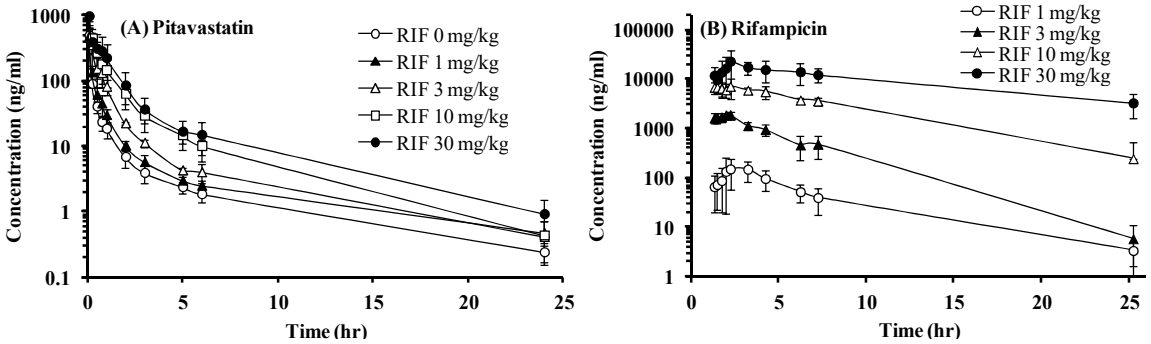

Figure S2. Plasma concentration-time profile of (A) LCA, (B) GLCA, (C) TLCA, (D) LCA-S, (E) UDCA, (F) GUDCA, (G) TUDCA, (H) UDCA-S, (I) GUDCA-S, (J) TUDCA-S, (K) CDCA, (L) GCDCA, (M) TCDCA, (N) CDCA-S, (O) DCA, (P) GDCA, (Q) TDCA, (R) DCA-S, (S) CA, (T) GCA, (U) TCA, (V) CA-S, (W) GCA-S, and (X) TCA-S in cynomolgus monkeys (mean ± SD, n = 4 animals) after oral administration of dose vehicle (open squares), and RIF at 1 mg/kg (open circles), 3 mg/kg (closed triangles), 10 mg/kg (closed circles), and 30 mg/kg (closed squares).

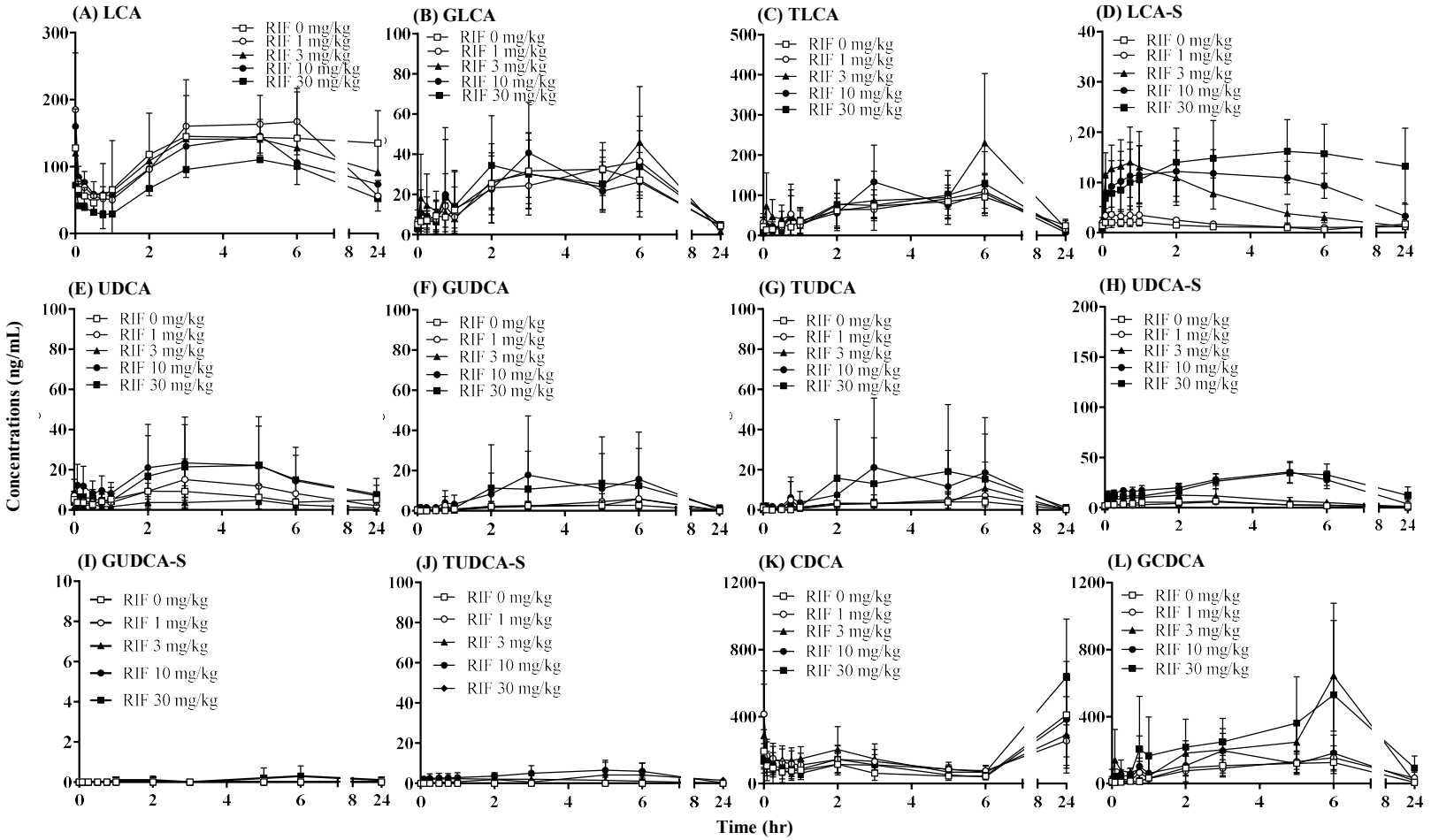

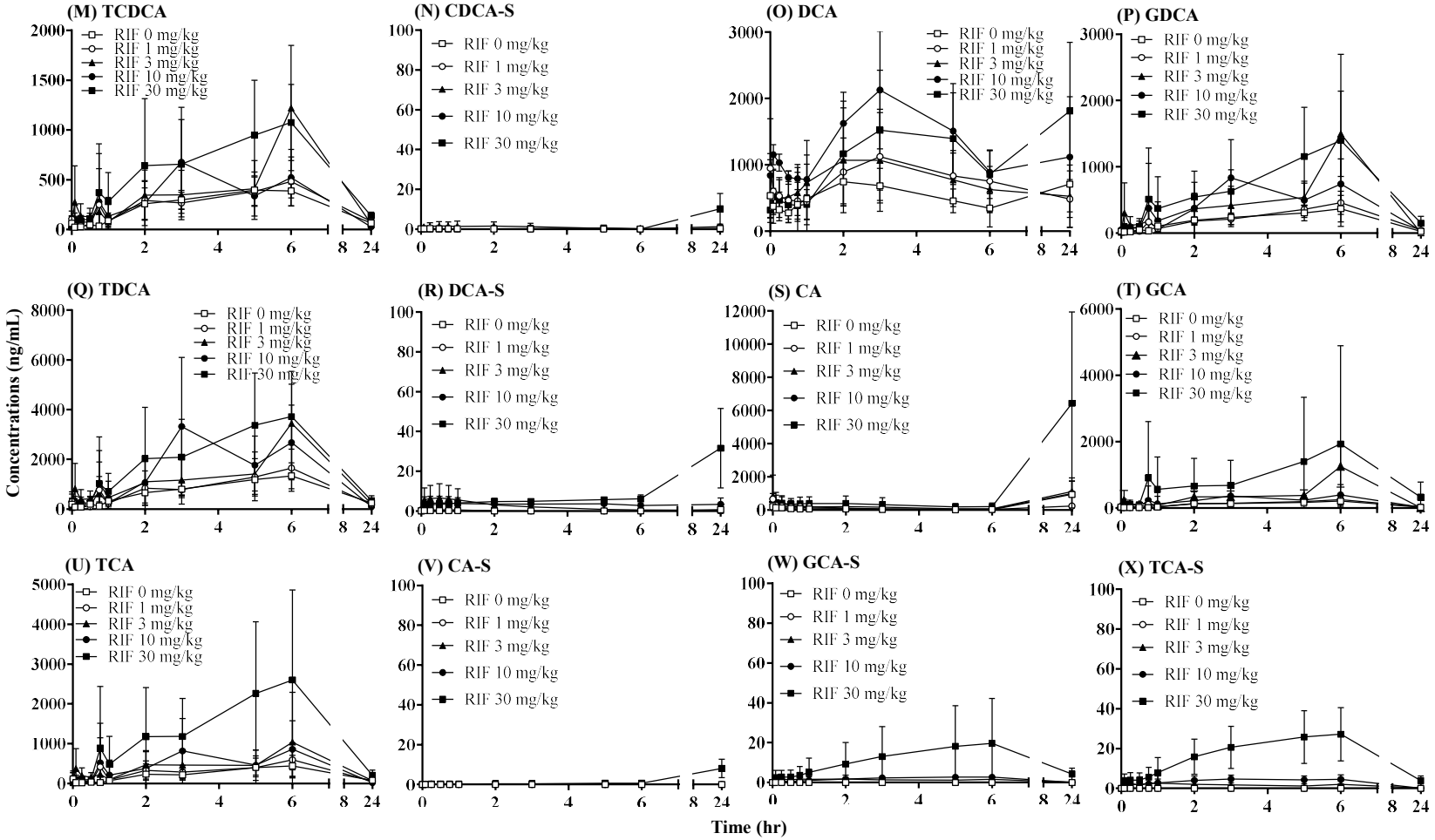
(M) TCDCA
(N) CDCA-S
(O) DCA
(P) GDCA
(Q) TDCA
(R) DCA-S
(S) CA
(T) GCA
(U) TCA
(V) CA-S
(W) GCA-S
(X) TCA-S
RIF 0 mg/kg
RIF 1 mg/kg
RIF 3 mg/kg
RIF 10 mg/kg
RIF 30 mg/kg
Concentrations (ng/mL)
Time (hr)

Figure S3 Correlation of sulfation rate (pmol of bile acid sulfate formed per pmol of parent bile acid) between PAPS-fortified human liver and cynomolgus monkey liver cytosol (six different bile acids are considered). Dotted line represents the line of identity. Under the same incubation conditions, the rate of DHEA sulfation in the presence of cynomolgus liver cytosol (0.35 pmol sulfate per pmol DHEA) was similar to that of PAPS-fortified human liver cytosol (0.27 pmol sulfate per pmol DHEA). The ratio of sulfation (cynomolgus monkey-to-human) is 0.20, 0.25, 0.36, 0.37, 0.89 and 3.0 for LCA-S, GLCA-S, TLCA-S, GUDCA-S, GCDCA-S, and GCA-S, respectively.

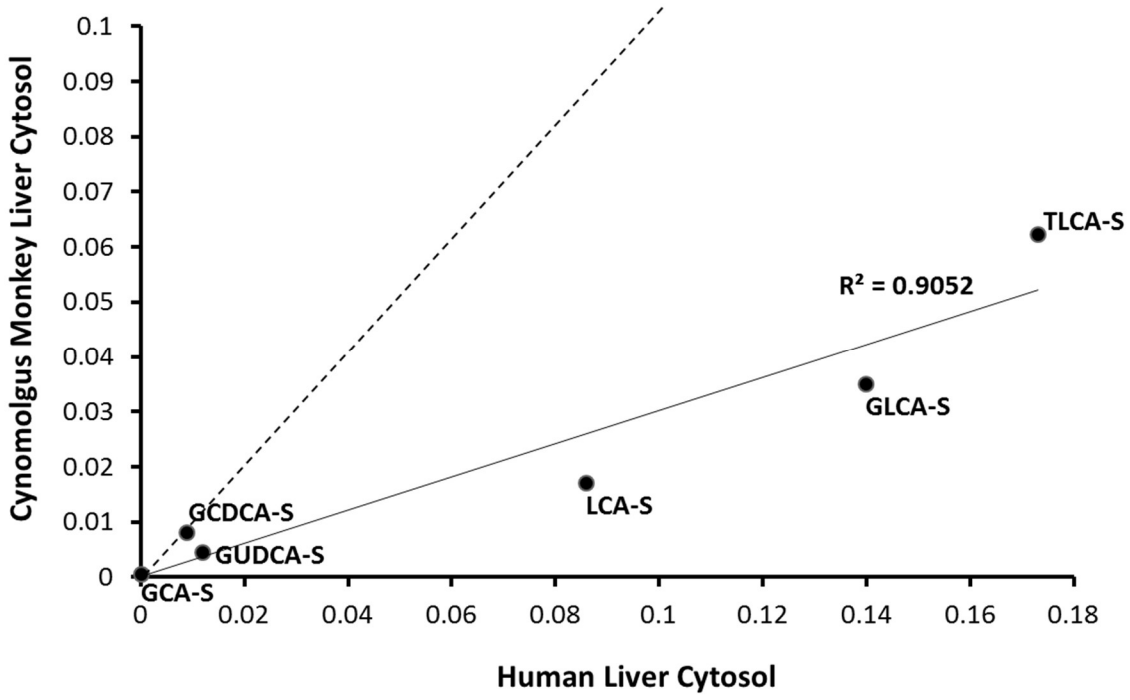

Figure S4. Assessment of rifampicin as inhibitor of GDCA and GCDCA sulfation catalysed by PAPS-fortified cynomolgus monkey liver cytosol. Substrate concentrations were 5 µM GDCA (A and B), 50 µM GDCA (C and D), 5 µM GCDCA (E and F), and 50 µM GCDCA (G and H). Inhibitors (rifampicin and danazol) were studied at concentrations between 0.13 and 100 µM. Danazol was used as positive control, assuming inhibition similar to that reported for human SULT2A1; IC_{50} = 4.2 µM. Rate of sulfation (mean ± SD; n = 6 determinations) for GDCA and GCDCA was 0.043 ± 0.018 and 0.045 ± 0.0051 pmol/min per mg (at 5 µM) and 0.34 ± 0.15, 0.26 ± 0.015 pmol/min per mg (at 50 µM), respectively.

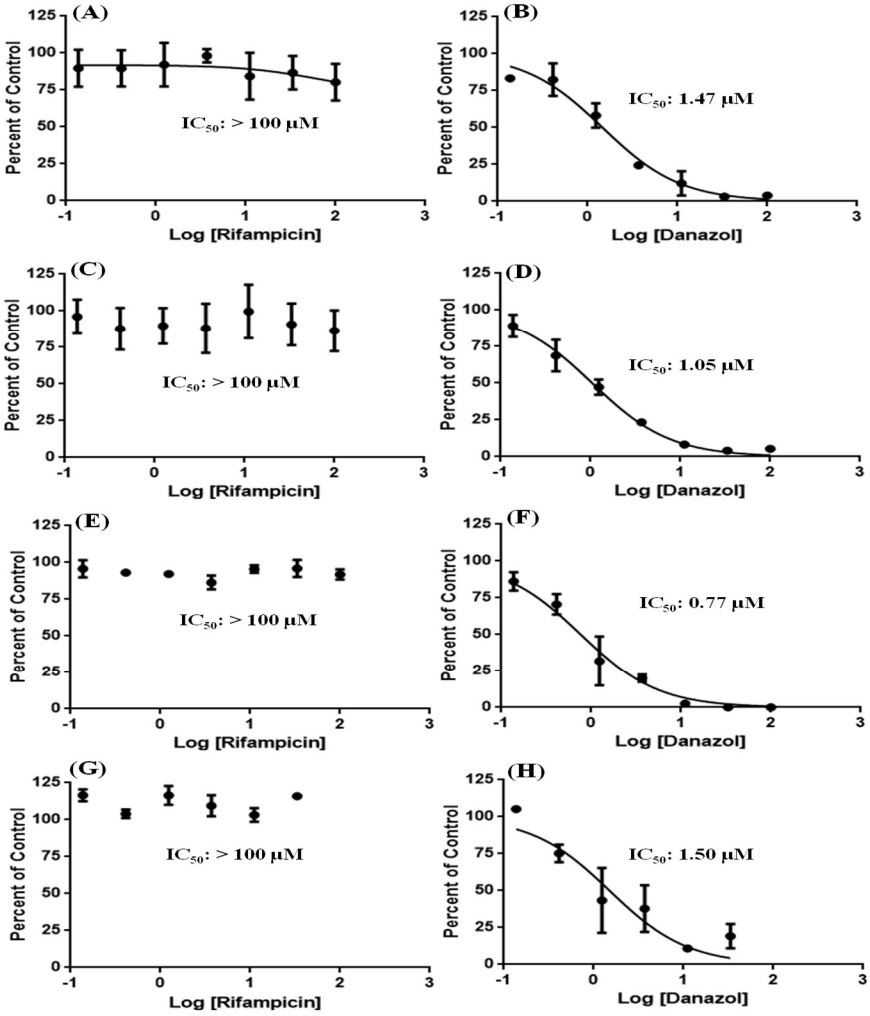

Table S1 MRM transitions and MS parameters for bile acids and their 3-O-sulfate conjugates

Analyte	MRM transition	DP (V)	CE (eV)	CXP (V)
$^{2}H_4$-GCDCA	452.2/74	-125	-75	-11
$^{2}H_4$-CDCA	395.2/395.2	-175	-20	-11
LCA	375.2/375.2	-200	-20	-11
GLCA	432.2/74	-130	-65	-7
TLCA	482.2/79.8	-130	-105	-13
LCA-S	455.2/96.8	-120	-90	-8
GLCA-S	512.2/432.2	-120	-44	-13
TLCA-S	280.6/96.8	-80	-37	-11
UDCA	391.2/391.2	-200	-20	-11
CDCA	391.2/391.2	-200	-20	-11
DCA	391.2/391.2	-200	-20	-11
GUDCA	448.2/74	-130	-65	-7
GCDCA	448.2/74	-130	-65	-7
GDCA	448.2/74	-130	-65	-7
TUDCA	498.2/79.8	-130	-105	-13
TCDCA	498.2/79.8	-130	-105	-13
TDCA	498.2/79.8	-130	-105	-13
UDCA-S	471.2/96.8	-120	-71	-13
CDCA-S	471.2/96.8	-120	-71	-13
DCA-S	471.2/96.8	-120	-71	-13
GUDCA-S	528.2/448.2	-120	-44	-13
GCDCA-S	528.2/448.2	-120	-44	-13
GDCA-S	528.2/448.2	-120	-44	-13
TUDCA-S	288.6/96.8	-70	-35	-7
TCDCA-S	288.6/96.8	-70	-35	-7
TDCA-S	288.6/96.8	-70	-35	-7
CA	407.2/407.2	-200	-20	-11
GCA	464.2/74	-130	-65	-7
TCA	514.2/79.8	-130	-105	-13
CA-S	487.2/96.8	-120	-80	-8
GCA-S	544.2/464.2	-120	-45	-13
TCA-S	296.6/96.8	-70	-35	-7

Table S2 MRM transitions and MS parameters for $^{2}H_{4}$-pitavastatin, rifampicin, and internal standards

Analyte	MRM transition	DP (V)	CE (eV)	CXP (V)
$^{2}H_{4}$-Pitavastatin	426.2/294.2	100	40	11
Rifampicin	823.4/791.7	100	17	7
$^{2}H_{8}$-Rifampicin	831.4/799.7	100	17	13
Simvastatin	419.2/285.2	80	15	8

Table S3 Plasma AUC ($AUC_{0\text{-}24,plasma}$), maximum concentration in plasma ($C_{max,plasma}$), amount recovered in urine, and renal clearance (CL_{renal}) of bile acids in male cynomolgus monkeys (mean ± SD, N = 4 animals) following the oral administration of dose vehicle and rifampicin (1, 3, 10, and 30 mg/kg)

Bile acid	RIF dose (mg/kg)	$AUC_{0\text{-}24,plasma}$ (ng.h/ml)	$C_{max,plasma}$ (ng/ml)	Amount recovered in urine (ng)	CL_{renal} (ml/min/kg)
LCA	Vehicle	3211 ± 1120	183 ± 31	4768 ± 3892	0.20 ± 0.18
	1	2767 ± 830	205 ± 80	5406 ± 5825	0.31 ± 0.40
	3	2665 ± 1400	174 ± 91	3880 ± 3881	0.18 ± 0.18
	10	2276 ± 472	162 ±30	6708 ± 6261	0.43 ± 0.42
	30	1847 ± 537	117 ± 36	2745 ± 2385	0.20 ± 0.16
GLCA	Vehicle	434 ± 139	39 ± 17	-[b]	-
	1	511 ± 164	40 ± 14	-	-
	3	574 ± 346	46 ± 28	-	-
	10	424 ± 221	49 ± 29	-	-
	30	502 ± 326	39 ± 23	-	-
TLCA	Vehicle	1473 ± 627	114 ± 41	-	-
	1	1521 ± 453	119 ± 42	-	-
	3	2765 ± 2088	230 ± 173	-	-
	10	1489 ± 656	161 ± 77	-	-
	30	1715 ± 870	143 ± 78	-	-
UDCA	Vehicle	123 ± 51	12 ± 3.4	296 ± 228	0.35 ± 0.31
	1	150 ± 116	16 ± 10	455 ± 391	0.37 ± 0.35
	3	53 ± 11	6 ± 2	205 ± 297	0.52 ± 0.72
	10	304 ± 256	27 ± 19	2304 ± 1066	1.41 ± 0.97
	30	301 ± 316	25 ± 23	3062 ± 2012	1.79 ± 1.24
GUDCA	Vehicle	37 ± 25	3.7 ± 2.7	-	-
	1	73± 66	7 ± 6	-	-
	3	78 ± 66	6 ± 6	-	-
	10	208 ± 311	20 ± 28	-	-
	30	181 ± 277	15 ± 23	-	-
TUDCA	Vehicle	57 ± 38	5.7 ± 4.0	-	-
	1	90 ± 81	10 ± 9	-	-
	3	106 ± 150	11 ± 13	-	-
	10	241 ± 350	26 ± 33	-	-
	30	225 ± 339	20 ± 33	38[a]	0.1
CDCA	Vehicle	4514 ± 3164	424 ± 304	4980 ± 1137	0.22 ± 0.14
	1	3692 ± 1242	435 ± 236	4411 ± 2526	0.16 ± 0.06
	3	4041 ± 2030	428 ± 203	6598 ± 3383	0.21 ± 0.07
	10	4308 ± 2655	390 ± 266	7226 ± 3532	0.24 ± 0.11
	30	6961 ± 3290	617 ± 372	10389 ± 5957	0.21 ± 0.13
GCDCA	Vehicle	1734 ± 845	157 ± 65	-	-
	1	2228 ± 1116	167 ± 73	-	-
	3	7148 ± 3525	644 ± 330	914	0.01
	10	2555 ± 1434	262 ± 144	203 ± 406	0.01 ± 0.03
	30	7196 ± 6668	549 ± 537	1960 ± 2255	0.05 ± 0.07
TCDCA	Vehicle	5669 ± 1245	508 ± 204	2642 ± 1385	0.07 ± 0.06
	1	6730 ± 2826	582 ± 278	2195 ± 2224	0.07 ± 0.10

	3	13775 ± 7288	1220 ± 629	2517 ± 1116	0.03 ± 0.03
	10	7203 ± 3780	881 ± 457	2591 ± 1806	0.08 ± 0.10
	30	14850 ± 4525	1233 ± 497	2056 ± 1005	0.02 ± 0.01
	Vehicle	12777 ± 7593	908 ± 439	62899 ± 36723	0.80 ± 0.54
	1	16146 ± 10141	1299 ± 631	61438 ± 26188	0.74 ± 0.56
DCA	3	15484 ± 8200	1273 ± 724	48696 ± 28035	0.64 ± 0.76
	10	26893 ± 13094	2220 ± 799	237524 ± 143178	1.32 ± 0.94
	30	30651 ± 14452	2018 ± 926	414830 ± 283148	2.10 ± 1.85
	Vehicle	4847 ±2410	441 ± 165	2289 ± 902	0.07 ± 0.02
	1	5911 ±1655	484 ± 168	2067 ± 988	0.05 ± 0.03
GDCA	3	16280 ±7205	1498 ± 644	3368 ± 273	0.03 ± 0.01
	10	10026 ± 4738	1089 ± 525	11959 ± 2612	0.20 ± 0.13
	30	18284 ± 15428	1517 ± 1233	22601 ± 10219	0.26 ± 0.24
	Vehicle	18868 ± 7292	1621 ± 705	5539 ± 2075	0.04 ±0.02
	1	21692 ± 10093	1881 ± 1000	6402 ± 2843	0.04 ±0.02
TDCA	3	40155 ± 25256	3453 ± 2092	14107 ± 9158	0.06 ± 0.03
	10	35730 ± 19425	4108 ± 2161	28213 ±11709	0.12 ± 0.05
	30	49375 ± 16320	4330 ± 1832	30438 ±16376	0.08 ± 0.03
	Vehicle	8917 ± 7730	938 ± 823	55637 ± 33210	1.28 ± 1.15
	1	3021 ± 950	689 ± 297	49732 ± 51921	2.48 ± 3.00
CA	3	11728 ± 8234	1570 ± 1099	102863 ± 96773	1.43 ± 0.98
	10	9845 ± 6534	993 ± 745	259726 ± 250421	3.96 ± 3.80
	30	61457 ± 53811	6430 ± 5519	604915 ± 653179	1.25 ± 0.96
	Vehicle	2769 ± 1961	258 ± 150	29273 ± 19499	1.39 ± 0.33
	1	3379 ± 1713	263 ± 134	21676 ± 9412	1.04 ± 0.57
GCA	3	13643 ± 6665	1258 ± 629	45482 ± 37342	0.44 ± 0.26
	10	5261 ± 3918	523 ± 359	51524 ± 46370	1.58 ± 0.86
	30	25737 ± 38285	1993 ± 2934	100389 ± 94136	0.91 ± 0.55
	Vehicle	6208 ± 3826	579 ± 394	14751 ± 5320	0.43 ± 0.36
	1	7745 ± 5022	801 ± 643	15075 ± 9524	0.60 ± 0.91
TCA	3	12639 ± 12969	1281 ± 1073	17752 ± 4358	0.33 ± 0.25
	10	10995 ± 8702	1235 ± 925	24217 ± 11243	0.65 ± 0.90
	30	33488 ± 26203	3038 ± 2347	28313 ± 15852	0.13 ± 0.07
	Vehicle	29 ± 9.3	2.3 ± 0.9	-	-
	1	32 ± 10	4.4 ± 1.1	-	-
LCA-S	3	87 ± 38	15 ± 6.6	352 ± 587	0.55 ± 0.90
	10	179 ± 64	13 ± 5	511 ± 430	0.34 ± 0.30
	30	342 ± 133	18 ± 7.1	1353 ± 1248	0.43 ± 0.41
	Vehicle	241 ± 43	18 ± 3.0	3875 ± 2302	2.27 ± 1.73
	1	449 ± 93	30 ± 6	4328 ± 2647	1.38 ± 0.93
GLCA-S	3	1293 ± 415	99 ± 28	7213 ± 2329	0.78 ± 0.46
	10	3169 ± 1500	230 ± 101	33847 ± 15961	1.45 ± 0.58
	30	8010 ± 4792	495 ± 307	67379 ± 34578	1.31 ± 0.65
	Vehicle	588 ± 163	41 ± 13	16638 ± 4659	4.05 ± 2.01
	1	1066 ± 220	77 ± 20	20673 ± 10353	2.72 ± 1.54
TLCA-S	3	3189 ± 2206	238 ± 149	36305 ± 13151	1.76 ± 0.82
	10	7643 ± 867	576 ± 86	144452 ± 20699	2.52 ± 0.34
	30	14035 ± 5468	954 ± 350	240905 ± 39793	2.48 ± 0.72
UDCA-S	Vehicle	59 ± 29	7.7 ± 4.2	3463 ± 1245	8.71 ± 4.45
	1	49 ± 17	5.9 ± 1.6	2489 ± 2299	5.76 ± 5.18

	3	111 ± 60	15 ± 10	5026 ± 2110	5.91 ± 1.17
	10	437 ± 131	37 ± 9	23974 ± 5952	7.55 ± 1.66
	30	547 ± 202	35 ± 11	33129 ± 15294	8.06 ± 2.00
	Vehicle	-	-	-	-
	1	-	-	-	-
GUDCA-S	3	1.0 ± 1.6	0.6 ± 0.7	-	-
	10	-	-	-	-
	30	3.8 ± 6.0	0.3 ± 0.5	47 ± 68	1.92 ± 0.37
	Vehicle	-	-	-	-
	1	-	-	-	-
TUDCA-S	3	23 ± 25	2.7 ± 2.8	-	-
	10	83 ± 54	6.5 ± 4.9	628 ± 500	1.02 ± 0.54
	30	64 ± 75	4.7 ± 6.1	1087 ± 914	3.15 ± 2.11
	Vehicle	16	1.6	380	3.15
	1	-	-	478	-
CDCA-S	3	9.1 ± 15	3.7 ± 2.6	1911	7.25
	10	14 ± 17	0.6 ± 0.6	4100	14
	30	93 ± 71	8.1 ± 9.0	2982 ± 3994	2.73 ± 2.69
	Vehicle	13 ± 15	1.4 ± 1.2	1044 ± 621	31 ± 40
	1	24 ± 13	1.8 ± 0.8	1138 ± 1115	6.59 ± 3.53
GCDCA-S	3	177 ± 118	13 ± 7.6	3996 ± 4059	2.51 ± 1.08
	10	331 ± 100	17 ± 4.5	10920 ± 6717	4.04 ± 1.45
	30	1024 ± 654	60 ± 32	30009 ± 19298	3.99 ± 1.48
	Vehicle	32 ± 21	2.5 ± 1.3	1153	2.39
	1	44 ± 15	3.4 ± 0.9	503 ± 630	1.34 ± 1.23
TCDCA-S	3	184 ± 101	14 ± 6.4	1333 ± 1247	0.79 ± 0.75
	10	460 ± 162	36 ± 11	5474 ± 2767	1.56 ± 0.40
	30	1844 ± 373	119 ± 12	24431 ± 9946	1.76 ± 0.51
	Vehicle	6.5 ± 4.5	0.9 ± 0.1	2883 ± 1774	32 ± 31
	1	2.4 ± 2.4	1.2 ± 0.9	2908± 3641	320 ± 585
DCA-S	3	25 ± 21	7.2 ± 6.8	3624 ± 2907	32 ± 35
	10	79 ± 41	5.7 ± 2.9	54541 ± 54904	100 ± 80
	30	368 ± 172	32 ± 20	127109 ± 108964	43 ± 22
	Vehicle	93 ± 31	7.6 ± 1.1	10422 ± 4527	18 ± 13
	1	167 ± 27	12 ± 1.4	12513 ± 6656	10 ± 5.1
GDCA-S	3	1117 ± 543	83 ± 38	35843 ± 12340	4.30 ± 1.71
	10	2864 ± 956	221 ± 66	247858 ± 123183	12 ± 5.89
	30	9958 ± 6998	640 ± 449	735541 ± 427431	12 ± 6.93
	Vehicle	253 ± 102	20 ± 6.9	22234 ± 7734	13 ± 7.52
	1	388 ± 91	30 ± 6.4	26579 ± 13785	8.91 ± 4.38
TDCA-S	3	4360 ± 736	332 ± 70	55389 ± 27684	1.51 ± 0.51
	10	4952 ± 822	376 ± 66	328392 ± 95393	8.84 ± 2.27
	30	12474 ± 4811	882 ± 307	811253 ± 222741	9.63 ± 4.86
	Vehicle	-	-	-	-
	1	-	-	-	-
CA-S	3	3	0.89	-	-
	10	-	-	318 ± 397	-
	30	81 ± 43	8.0 ± 4.6	1746 ± 2024	1.91 ± 2.20
GCA-S	Vehicle	-	-	238	-
	1	-	-	196	-

	3	23 ± 20	2.2 ± 1.7	699 ± 1124	1.95 ± 2.89
	10	37 ± 20	2.8 ± 1.3	2853 ± 1892	9.98 ± 3.40
	30	289 ± 303	20 ± 22	17186 ± 13469	9.38 ± 4.60
	Vehicle	-	-	263	-
	1	-	-	196	-
TCA-S	3	31 ± 22	3.1 ± 2.5	481 ± 572	1.62 ± 2.07
	10	64 ± 32	5.4 ± 2.6	3673 ± 1699	7.94 ± 2.26
	30	388 ± 171	28 ± 13	20401 ± 7389	7.61 ± 3.60

[a]Data from one animal only.

[b]Not detectable.

Table S4 Concentration (nM) of circulating bile acids in human and cynomolgus monkey (mean ± SEM)

Bile acid	Human Serum[a]	Monkey Plasma[b]
LCA	7.50 ± 0.38 (0.21%)[c]	353.9 ± 26.7 (7.62%)
GLCA	10.7 ± 0.8 (0.29%)	12.5 ± 4.4 (0.27%)
TLCA	1.64 ± 0.15 (0.05%)	43.4 ± 6.7 (0.93%)
DCA	395.0 ± 19.9 (10.9%)	1627 ± 46.6 (35%)
GDCA	283.1 ± 22.1 (7.78%)	71.4 ± 7.3 (1.54%)
TDCA	79.3±16.9 (2.18%)	412.9 ± 18 (8.89%)
CDCA	191.9 ± 21.0 (5.28%)	607.5 ± 26.8 (13.1%)
GCDCA	580.3 ± 45.2 (16.0%)	41.3 ± 5.5 (0.89%)
TCDCA	223.6 ± 22.3 (6.15%)	121.6 ± 10.7 (2.62%)
UDCA	77.3 ± 7.7 (2.13%)	12.5 ± 3.7 (0.27%)
GUDCA	106.1 ± 10.4 (2.92%)	0.9 ± 0.7 (0.02%)
TUDCA	6.18 ± 0.90 (0.17%)	1.7 ± 0.90 (0.04%)
CA	193.7 ± 26.6 (5.33%)	1039.6 ± 26.8 (22.4%)
GCA	322.7 ± 50.3 (8.87%)	80 ± 7.8 (1.72%)
TCA	126.9 ± 35.1 (3.49%)	159.4 ± 10 (3.43%)
LCA-S	5.36 ± 0.54 (0.15%)	3.5 ± 2.1 (0.08%)
GLCA-S	275.5 ± 15.0 (7.57%)	13.6 ± 4.5 (0.29%)
TLCA-S	83.0 ± 5.1 (2.28%)	29.3 ± 9.0 (0.63%)
DCA-S	0.82 ± 0.08 (0.02%)	0.7 ± 0.6 (0.02%)
GDCA-S	203.0 ± 10.4 (5.58%)	3 ± 1.8 (0.06%)
TDCA-S	29.3 ± 1.9 (0.81%)	6 ± 3.6 (0.13%)
CDCA-S	5.10 ± 0.42 (0.14%)	0.3 ± 0.3 (0.01%)
GCDCA-S	247.8 ± 12.9 (6.81%)	0.2 ± 0.3 (0.01%)
TCDCA-S	13.9 ± 0.9 (0.38%)	0.5 ± 0.6 (0.01%)
UDCA-S	18.2 ± 1.0 (0.50%)	3.9 ± 2.8 (0.08%)
GUDCA-S	134.8 ± 7.3 (3.71%)	-[c]
TUDCA-S	3.15 ± 0.18 (0.09%)	-
CA-S	0.23 ± 0.03 (0.01%)	-

GCA-S	1.35 ± 0.15 (0.04%)	-
TCA-S	10.1 ± 0.7 (0.28%)	-
% Sulfated	28.4%[d]	1.3%
% Non-sulfated	71.6%	98.7%
% Amidated	75.4%	21.5%
% Non-amidated	24.6%	78.5%
% Amidated + sulfated	27.2%	1.1%
% Non-amidated + sulfated	0.8%	0.2%
% Amidated + non-sulfated	47.8%	20.3%
% Non-amidated + non-sulfated	23.8%	78.3%
% Glycine amidated	59.5%	4.8%
% Taurine amidated	15.9%	16.7%
% Glycine amidated + sulfated	23.7%	0.4%
% Glycine amidated + non-sulfated	35.8%	4.4%
% Taurine amidated + sulfated	3.8%	0.8%
% Taurine amidated + non-sulfated	12.0%	15.9%

[a]Bathena SP, Mukherjee S, Olivera M, and Alnouti Y (2013) The profile of bile acids and their sulfate metabolites in human urine and serum. *J Chromatogr B Analyt Technol Biomed Life Sci* 942-943:53-62.
[b]Present study.
[c]Not detectable
[d]Percent of circulating bile acids analysed.

Table S5 RIF and RIFsv as inhibitors of cynomolgus monkey OATPs and NTCP expressed in HEK293 cells

Inhibitor	Substrate (μM)	Reported IC_{50} (μM)[a]				Reference
		OATP1B1	OATP1B3	OATP2B1	NTCP	
RIFsv	RSV (0.1)	0.05 ± 0.02 (100%)	0.45 ± 0.03 (100%)	-[b]	-	
	TCA (0.1)	-	-	-	32.7 ± 0.9 (97%)	
RIF	RSV (0.1)	0.42 ± 0.09 (92%)	1.7 ± 0.28 (75%)	69.1 ± 7.7 (7%)	-	(Shen et al., 2013)
	RSV (0.1)	0.25 ± 0.03 (95%)	1.3 ± 0.1 (79%)	61.7 ± 3.6 (7%)	83.5 ± 7.6 (6%)	(Chu et al., 2015)
	ATV (0.01)	0.14 ± 0.01 (97%)	0.75 ± 0.08 (87%)	62.7 ± 10.7 (7%)	93.4 ± 10.4 (5%)	
	E17G (1.0)	0.38 ± 0.02 (93%)	1.6 ± 0.1 (76%)	-	-	
	TCA (1.0)	-	-	-	35.1 ± 6.3 (13%)	
Mean (all substrates)		0.3	1.3	64.5	70.7	

RSV, rosuvastatin; RIFsv, rifamycin SV; RIF, rifampicin; TCA, taurocholic acid; E17G, estradiol 17β-D-glucuronide; ATV, atorvastatin.

[a]Mean ± SD. Data in parentheses represent % inhibition based on the reported IC_{50} and a final RIF and RIFsv inhibitor concentration [I] of 5 μM and 1 mM, respectively.

% inhibition = 100 * {[I]/([I] + IC_{50})}, assuming $IC_{50} \sim K_i$ (where substrate concentration < K_m).

[b]Not reported.

Chu X, Shih SJ, Shaw R, Hentze H, Chan GH, Owens K, Wang S, Cai X, Newton D, Castro-Perez J, Salituro G, Palamanda J, Fernandis A, Ng CK, Liaw A, Savage MJ, and Evers R (2015) Evaluation of cynomolgus monkeys for the identification of endogenous biomarkers for hepatic transporter inhibition and as a translatable model to predict pharmacokinetic interactions with statins in humans. *Drug Metab Dispos* **43:**851-863.

Shen H, Yang Z, Mintier G, Han YH, Chen C, Balimane P, Jemal M, Zhao W, Zhang R, Kallipatti S, Selvam S, Sukrutharaj S, Krishnamurthy P, Marathe P, and Rodrigues AD (2013) Cynomolgus monkey as a potential model to assess drug interactions involving hepatic organic anion transporting polypeptides: in vitro, in vivo, and in vitro-to-in vivo extrapolation. *J Pharmacol Exp Ther* **344:**673-685.

Table S6 Estimation of cynomolgus monkey OATP and NTCP inhibition at increasing doses of rifampicin (RIF)

RIF Dose (mg/kg)	RIF Free C_{max} (μM)	Predicted % Inhibition[a]			
		OATP1B1	OATP1B3	OATP2B1	NTCP
1	0.057	16	4	0.1	0.1
3	0.659	69	33	1	1
10	2.57	90	66	4	4
30	7.79	96	85	11	10

RIF Dose (mg/kg)	RIF Total C_{max} (μM)	Predicted % Inhibition[a]			
		OATP1B1	OATP1B3	OATP2B1	NTCP
1	0.2	40	13	0.3	0.3
3	2.5	89	65	4	3
10	9.7	97	88	13	12
30	29	99	96	31	29

[a]Based on the mean IC_{50} (across substrates) determined in vitro (Supplemental Table 5); % inhibition = 100 * {[I]/([I] + IC_{50})}, assuming IC_{50} ~ K_i (where substrate concentration < K_m). [I] represents plasma C_{max} of RIF (total or free). In the absence of i.v. RIF pharmacokinetic data, it was not possible to derive an absorption rate constant for RIF and estimate its liver inlet (portal) concentration.

2.5 References

[1] K.M. Giacomini, S.M. Huang, D.J. Tweedie, L.Z. Benet, K.L. Brouwer, X. Chu, A. Dahlin, R. Evers, V. Fischer, K.M. Hillgren, K.A. Hoffmaster, T. Ishikawa, D. Keppler, R.B. Kim, C.A. Lee, M. Niemi, J.W. Polli, Y. Sugiyama, P.W. Swaan, J.A. Ware, S.H. Wright, S.W. Yee, M.J. Zamek-Gliszczynski, L. Zhang, Membrane transporters in drug development, Nat Rev Drug Discov, 9 (2010) 215-236.
[2] K. Yoshida, K. Maeda, Y. Sugiyama, Transporter-mediated drug--drug interactions involving OATP substrates: predictions based on in vitro inhibition studies, Clin Pharmacol Ther, 91 (2012) 1053-1064.
[3] A. Poirier, C. Funk, T. Lave, J. Noe, New strategies to address drug-drug interactions involving OATPs, Curr Opin Drug Discov Devel, 10 (2007) 74-83.
[4] M. Jamei, F. Bajot, S. Neuhoff, Z. Barter, J. Yang, A. Rostami-Hodjegan, K. Rowland-Yeo, A mechanistic framework for in vitro-in vivo extrapolation of liver membrane transporters: prediction of drug-drug interaction between rosuvastatin and cyclosporine, Clin Pharmacokinet, 53 (2014) 73-87.
[5] J. Vaidyanathan, K. Yoshida, V. Arya, L. Zhang, Comparing Various In Vitro Prediction Criteria to Assess the Potential of a New Molecular Entity to Inhibit Organic Anion Transporting Polypeptide 1B1, J Clin Pharmacol, 56 Suppl 7 (2016) S59-72.
[6] T. Yoshikado, K. Yoshida, N. Kotani, T. Nakada, R. Asaumi, K. Toshimoto, K. Maeda, H. Kusuhara, Y. Sugiyama, Quantitative Analyses of Hepatic OATP-Mediated Interactions Between Statins and Inhibitors Using PBPK Modeling With a Parameter Optimization Method, Clin Pharmacol Ther, (2016).
[7] I.Y. Gong, R.B. Kim, Impact of genetic variation in OATP transporters to drug disposition and response, Drug Metab Pharmacokinet, 28 (2013) 4-18.
[8] J.D. Clarke, R.N. Hardwick, A.D. Lake, A.J. Lickteig, M.J. Goedken, C.D. Klaassen, N.J. Cherrington, Synergistic interaction between genetics and disease on pravastatin disposition, J Hepatol, 61 (2014) 139-147.
[9] Y. Lai, S. Mandlekar, H. Shen, V.K. Holenarsipur, R. Langish, P. Rajanna, S. Murugesan, N. Gaud, S. Selvam, O. Date, Y. Cheng, P. Shipkova, J. Dai, W.G. Humphreys, P. Marathe, Coproporphyrins in Plasma and Urine Can Be Appropriate Clinical Biomarkers to Recapitulate Drug-Drug Interactions Mediated by Organic Anion Transporting Polypeptide Inhibition, J Pharmacol Exp Ther, 358 (2016) 397-404.
[10] S.W. Yee, M.M. Giacomini, C.H. Hsueh, D. Weitz, X. Liang, S. Goswami, J.M. Kinchen, A. Coelho, A.A. Zur, K. Mertsch, W. Brian, D.L. Kroetz, K.M. Giacomini, Metabolomic and Genome-wide Association Studies Reveal Potential Endogenous Biomarkers for OATP1B1, Clin Pharmacol Ther, (2016).
[11] D. Bednarczyk, C. Boiselle, Organic anion transporting polypeptide (OATP)-mediated transport of coproporphyrins I and III, Xenobiotica, 46 (2016) 457-466.
[12] H. Shen, J. Dai, T. Liu, Y. Cheng, W. Chen, C. Freeden, Y. Zhang, W.G. Humphreys, P. Marathe, Y. Lai, Coproporphyrins I and III as Functional Markers of OATP1B Activity: In Vitro and In Vivo Evaluation in Preclinical Species, J Pharmacol Exp Ther, 357 (2016) 382-393.
[13] H. Shen, Z. Yang, G. Mintier, Y.H. Han, C. Chen, P. Balimane, M. Jemal, W. Zhao, R. Zhang, S. Kallipatti, S. Selvam, S. Sukrutharaj, P. Krishnamurthy, P. Marathe, A.D. Rodrigues, Cynomolgus monkey as a potential model to assess drug interactions involving hepatic organic anion transporting polypeptides: in vitro, in vivo, and in vitro-to-in vivo extrapolation, J Pharmacol Exp Ther, 344 (2013) 673-685.
[14] T. Takahashi, T. Ohtsuka, T. Yoshikawa, I. Tatekawa, Y. Uno, M. Utoh, H. Yamazaki, T. Kume, Pitavastatin as an in vivo probe for studying hepatic organic anion

transporting polypeptide-mediated drug-drug interactions in cynomolgus monkeys, Drug Metab Dispos, 41 (2013) 1875-1882.
[15] H. Shen, H. Su, T. Liu, M. Yao, G. Mintier, L. Li, R.M. Fancher, R. Iyer, P. Marathe, Y. Lai, A.D. Rodrigues, Evaluation of rosuvastatin as an organic anion transporting polypeptide (OATP) probe substrate: in vitro transport and in vivo disposition in cynomolgus monkeys, J Pharmacol Exp Ther, 353 (2015) 380-391.
[16] X. Chu, S.J. Shih, R. Shaw, H. Hentze, G.H. Chan, K. Owens, S. Wang, X. Cai, D. Newton, J. Castro-Perez, G. Salituro, J. Palamanda, A. Fernandis, C.K. Ng, A. Liaw, M.J. Savage, R. Evers, Evaluation of cynomolgus monkeys for the identification of endogenous biomarkers for hepatic transporter inhibition and as a translatable model to predict pharmacokinetic interactions with statins in humans, Drug Metab Dispos, 43 (2015) 851-863.
[17] M. Watanabe, T. Watanabe, M. Yabuki, I. Tamai, Dehydroepiandrosterone sulfate, a useful endogenous probe for evaluation of drug-drug interaction on hepatic organic anion transporting polypeptide (OATP) in cynomolgus monkeys, Drug Metab Pharmacokinet, 30 (2015) 198-204.
[18] S.P. Bathena, S. Mukherjee, M. Olivera, Y. Alnouti, The profile of bile acids and their sulfate metabolites in human urine and serum, J Chromatogr B Analyt Technol Biomed Life Sci, 942-943 (2013) 53-62.
[19] M. Nishimura, A. Koeda, H. Morikawa, T. Satoh, S. Narimatsu, S. Naito, Tissue-specific mRNA expression profiles of drug-metabolizing enzymes and transporters in the cynomolgus monkey, Drug Metab Pharmacokinet, 24 (2009) 139-144.
[20] M. Nishimura, A. Koeda, T. Shimizu, M. Nakayama, T. Satoh, S. Narimatsu, S. Naito, Comparison of inducibility of sulfotransferase and UDP-glucuronosyltransferase mRNAs by prototypical microsomal enzyme inducers in primary cultures of human and cynomolgus monkey hepatocytes, Drug Metab Pharmacokinet, 23 (2008) 45-53.
[21] Y. Alnouti, Bile Acid sulfation: a pathway of bile acid elimination and detoxification, Toxicol Sci, 108 (2009) 225-246.
[22] M. Leblanc, C. Labrie, A. Belanger, B. Candas, F. Labrie, Bioavailability and pharmacokinetics of dehydroepiandrosterone in the cynomolgus monkey, J Clin Endocrinol Metab, 88 (2003) 4293-4302.
[23] M. Sasaki, H. Suzuki, K. Ito, T. Abe, Y. Sugiyama, Transcellular transport of organic anions across a double-transfected Madin-Darby canine kidney II cell monolayer expressing both human organic anion-transporting polypeptide (OATP2/SLC21A6) and Multidrug resistance-associated protein 2 (MRP2/ABCC2), J Biol Chem, 277 (2002) 6497-6503.
[24] L.J. Meng, P. Wang, A.W. Wolkoff, R.B. Kim, R.G. Tirona, A.F. Hofmann, K.S. Pang, Transport of the sulfated, amidated bile acid, sulfolithocholyltaurine, into rat hepatocytes is mediated by Oatp1 and Oatp2, Hepatology, 35 (2002) 1031-1040.
[25] Y.A. Bi, D. Kazolias, D.B. Duignan, Use of cryopreserved human hepatocytes in sandwich culture to measure hepatobiliary transport, Drug Metab Dispos, 34 (2006) 1658-1665.
[26] R.H. Ho, B.F. Leake, R.L. Roberts, W. Lee, R.B. Kim, Ethnicity-dependent polymorphism in Na+-taurocholate cotransporting polypeptide (SLC10A1) reveals a domain critical for bile acid substrate recognition, J Biol Chem, 279 (2004) 7213-7222.
[27] S.P. Bathena, R. Thakare, N. Gautam, S. Mukherjee, M. Olivera, J. Meza, Y. Alnouti, Urinary bile acids as biomarkers for liver diseases I. Stability of the baseline profile in healthy subjects, Toxicol Sci, 143 (2015) 296-307.
[28] Y. Tsuruya, K. Kato, Y. Sano, Y. Imamura, K. Maeda, Y. Kumagai, Y. Sugiyama, H. Kusuhara, Investigation of Endogenous Compounds Applicable to Drug-Drug Interaction

Studies Involving the Renal Organic Anion Transporters, OAT1 and OAT3, in Humans, Drug Metab Dispos, 44 (2016) 1925-1933.
[29] H. Akita, H. Suzuki, K. Ito, S. Kinoshita, N. Sato, H. Takikawa, Y. Sugiyama, Characterization of bile acid transport mediated by multidrug resistance associated protein 2 and bile salt export pump, Biochim Biophys Acta, 1511 (2001) 7-16.
[30] N. Zelcer, T. Saeki, I. Bot, A. Kuil, P. Borst, Transport of bile acids in multidrug-resistance-protein 3-overexpressing cells co-transfected with the ileal Na+-dependent bile-acid transporter, Biochem J, 369 (2003) 23-30.
[31] N. Zelcer, G. Reid, P. Wielinga, A. Kuil, I. van der Heijden, J.D. Schuetz, P. Borst, Steroid and bile acid conjugates are substrates of human multidrug-resistance protein (MRP) 4 (ATP-binding cassette C4), Biochem J, 371 (2003) 361-367.
[32] A.D. Rodrigues, Y. Lai, M.E. Cvijic, L.L. Elkin, T. Zvyaga, M.G. Soars, Drug-induced perturbations of the bile acid pool, cholestasis, and hepatotoxicity: mechanistic considerations beyond the direct inhibition of the bile salt export pump, Drug Metab Dispos, 42 (2014) 566-574.
[33] H. Tahara, M. Shono, H. Kusuhara, H. Kinoshita, E. Fuse, A. Takadate, M. Otagiri, Y. Sugiyama, Molecular cloning and functional analyses of OAT1 and OAT3 from cynomolgus monkey kidney, Pharm Res, 22 (2005) 647-660.
[34] H.U. Marschall, M. Wagner, G. Zollner, P. Fickert, U. Diczfalusy, J. Gumhold, D. Silbert, A. Fuchsbichler, L. Benthin, R. Grundstrom, U. Gustafsson, S. Sahlin, C. Einarsson, M. Trauner, Complementary stimulation of hepatobiliary transport and detoxification systems by rifampicin and ursodeoxycholic acid in humans, Gastroenterology, 129 (2005) 476-485.
[35] L. Badolo, B. Jensen, C. Sall, U. Norinder, P. Kallunki, D. Montanari, Evaluation of 309 molecules as inducers of CYP3A4, CYP2B6, CYP1A2, OATP1B1, OCT1, MDR1, MRP2, MRP3 and BCRP in cryopreserved human hepatocytes in sandwich culture, Xenobiotica, 45 (2015) 177-187.
[36] G. Acocella, Clinical pharmacokinetics of rifampicin, Clin Pharmacokinet, 3 (1978) 108-127.
[37] L. Wang, B. Prasad, L. Salphati, X. Chu, A. Gupta, C.E. Hop, R. Evers, J.D. Unadkat, Interspecies variability in expression of hepatobiliary transporters across human, dog, monkey, and rat as determined by quantitative proteomics, Drug Metab Dispos, 43 (2015) 367-374.
[38] P.J. Meier, U. Eckhardt, A. Schroeder, B. Hagenbuch, B. Stieger, Substrate specificity of sinusoidal bile acid and organic anion uptake systems in rat and human liver, Hepatology, 26 (1997) 1667-1677.
[39] K. Maeda, M. Kambara, Y. Tian, A.F. Hofmann, Y. Sugiyama, Uptake of ursodeoxycholate and its conjugates by human hepatocytes: role of Na(+)-taurocholate cotransporting polypeptide (NTCP), organic anion transporting polypeptide (OATP) 1B1 (OATP-C), and oatp1B3 (OATP8), Mol Pharm, 3 (2006) 70-77.
[40] Z. Dong, S. Ekins, J.E. Polli, A substrate pharmacophore for the human sodium taurocholate co-transporting polypeptide, Int J Pharm, 478 (2015) 88-95.
[41] T. Suga, H. Yamaguchi, T. Sato, M. Maekawa, J. Goto, N. Mano, Preference of Conjugated Bile Acids over Unconjugated Bile Acids as Substrates for OATP1B1 and OATP1B3, PLoS One, 12 (2017) e0169719.
[42] N. Kobayashi, H. Katsumata, Y. Uto, J. Goto, T. Niwa, K. Kobayashi, Y. Mizuuchi, A monoclonal antibody-based enzyme-linked immunosorbent assay of glycolithocholic acid sulfate in human urine for liver function test, Steroids, 67 (2002) 827-833.
[43] A. Nanashima, M. Obatake, Y. Sumida, T. Abo, Y. Yamane, M. Nomura, I. Yuhio, T. Sawai, H. Takeshita, S. Hidaka, T. Yasutake, T. Nagayasu, Clinical significance of

measuring urinary sulfated bile acids in adult patients with hepatobiliary diseases, Hepatogastroenterology, 56 (2009) 299-302.

CHAPTER 3

QUANTITATIVE ANALYSIS OF ENDOGENOUS COMPOUNDS

3.1 Introduction

Metabolomics is a field of science, which involves the comprehensive quantitative and qualitative profiling of multiple metabolites and their interaction with environmental variables of interest such as diet, disease, environment, or exposure to chemicals. In a simplistic view, a metabolomics experiment is a comparative analysis of samples to identify if these samples can be distinguished on the basis of quantitative and/or qualitative differences in their metabolic profiles. In general, two strategies can be followed in metabolite profiling. The first strategy targets limited number of metabolites or a subset of known metabolites that either have similar structure or involved in a specific metabolic pathway. The metabolites of interest are already selected and their absolute concentrations are measured usually to prove a hypothesis based on a priori information about the targeted metabolites. This approach is referred to as “targeted” metabolomics [1, 2]. The second strategy relies on a holistic approach towards the profiling of as many metabolites as possible without a prior knowledge of the identity of these metabolites. This “non-targeted approach” produces comprehensive lists of metabolites of potential interest with relative quantification. These metabolic changes then can then be mapped to specific pathways and provide biomarkers and/or mechanistic information [3].

Eicosanoid, bile acids, and steroid hormones represent examples of classes of endogenous compounds (metabolites) that are extensively characterized via various metabolomics approaches. Comprehensive analysis of the eicosanoids metabolome helps understand their role in cell proliferation, inflammatory diseases, tissue repair, coagulation, and the immune system [4, 5]. Bile acids have both pathological and

physiological roles in liver diseases, regulating lipid, glucose, energy, and their own homeostasis. Due to the wide variation of the physicochemical, pathological, and physiological roles of individual BAs, quantitative metabolomics is the best approach to elucidate the mechanisms underlying the various BA functions [6-11]. Quantitative analyses of steroid hormones are used clinically for the diagnosis of cushing's syndrome, congenital steroid enzyme deficiency, and other endocrine disorders [12]. In addition, metabolomics is also widely used in agricultural applications to study plant responses to environmental factors, including drought, salt, low oxygen caused by waterlogging or flooding of the soil, temperature, light and oxidative stress [13].

The quantitative component of metabolomics analyses can be classified into relative, semi-quantitative, or absolute quantification [14, 15]. In relative quantification, the effect of treatment(s) on the analytes of interest is measured by comparing the detector responses of these analytes in samples from treatment groups relative to reference or control groups. Semi-quantitative analyses are used when reference standards for the analytes of interest are not readily available; therefore, available standards of other molecules related to these analytes are used as surrogate standards to translate the detector responses into concentrations. For example, parent compounds are sometimes used as standards to quantify their metabolites [16]. The assumption is that both the analytes and the surrogate molecules have similar detector responses. In absolute quantification, however, concentrations of analytes are measured with predetermined levels of accuracy and precision using standards of the same analytes.

3.2 Quantitative Liquid Chromatography-Tandem Mass Spectrometry (LC-MS/MS) Analysis

Liquid chromatography-tandem mass spectrometry (LC-MS/MS) has become the technique of choice for quantitative analyses because of its sensitivity, selectivity, and

speed [17, 18]. In LC-MS, the effluent from the LC system enters the ionization source, where analytes are ionized before mass-separation by the MS analyzer. Atmospheric pressure ionization (API) sources, allow direct coupling of the LC system to the MS, where LC effluent flows directly into the ionization source. However, due to differences in ionization efficiencies in the MS source, different analytes of the same concentrations may produce different MS responses. Therefore, authentic standards are always required for the absolute quantification of analytes using LC-MS/MS.

Any components of biological matrices, primarily salts and phsphospholipids that co-elute from the chromatographic column with the analytes of interest, do compete over the same charges with the analytes in the MS source, which may suppress/enhance the signal intensity of these analytes. Therefore, the same analyte with the same concentration can produce different MS responses, when exist in different matrices. This phenomenon is known as matrix effect [19].

Typically; biological samples are prepared before analyses to extract the analytes of interest from as much as possible of the irrelevant endogenous sample components. The most popular extraction techniques used are protein precipitation (PP), liquid-liquid extraction (LLE), and solid-phase extraction (SPE). PP can be achieved by (i) decreasing the dielectric constant with the addition of an organic reagent such as methanol or acetonitrile, (ii) increasing the ionic strength, i.e. salting out effect by the addition of high concentrations of ammonium sulfate, or (iii) changing the sample pH with the addition of concentrated acids such as perchloric acid or trichloroacetic acid, or concentrated alkaline reagents like sodium or potassium hydroxide. In LLE, an organic solvent is used in which analytes have higher solubility in comparison to their solubility in the aqueous phase. The pH of the sample is adjusted so that the drug to be extracted is unionized, thus facilitating partitioning into the organic solvent. The upper organic layer is then aspirated, evaporated, and reconstituted in a solvent compatible

with the buffer system. Trimethylbutylether, chloroform, diethylether, dichloromethane, and diethyl acetate are the commonly used organic solvents in LLE of biological samples. SPE is the most popular sample preparation method. In SPE, the analytes are selectively retained to a special adsorbent via different mechanisms of interaction, such as hydrophobic, electrostatic, or size exclusion. The tremendous advances in SPE technology, which produces sorbents with a very wide diversity in selectivity, allow SPE to be suitable for the extraction of a wide spectrum of compounds with different physicochemical properties. These sorbents are commercially available in different formats such as columns, cartridges, or syringes.

Extraction recovery is then calculated to quantify the efficiency of the sample preparation method in the extraction of analytes from the matrix [20, 21]. Overall absolute extraction recovery is calculated as the ratio of the analyte peak area in samples spiked before extraction compared to the corresponding peak area in untreated samples prepared in neat solution (assuming no loss of analyte due to degradation by matrix components). In LC-MS/MS, however, absolute extraction recovery does not only represent extraction efficiency of the sample preparation procedure, but also includes the matrix effect on the MS signal. Matrix effect is calculated as the ratio of analyte peak area in samples spiked after extraction compared to the corresponding peak area in untreated samples prepared in neat solution. On the other hand extraction efficiency can be quantified via the relative extraction recovery, which is the ratio of analyte peak areas in samples spiked before extraction compared to the corresponding peak area in samples spiked after extraction. Therefore, Overall absolute extraction recovery = matrix effect × relative extraction recovery (extraction efficiency). For example, as shown in **Figure 3.1-A**, extraction of two different matrices spiked with one analyte at the same concentration (before extraction) resulted in absolute extraction recovery of 60% and 30% in plasma and liver, respectively. In contrast, spiking of the same analyte at the

same concentrations into the same matrices after extraction, showed 80% and 40% matrix effect in plasma and liver, respectively compared to neat solution **(Figure 3.1-B)**, whereas, extraction efficiency is 75% for both plasma and liver. Even though, the extraction method was equally efficient in extracting the analyte from both matrices, total extraction recovery was smaller in liver compared to plasma due to a stronger matrix effect. The stronger matrix effect is expected given the complexity, diversity, and higher concentrations of endogenous components of liver compared to plasma.

Standard curves should ideally be prepared in the same matrix as the test samples, to ensure that the same MS response is produced for an analyte existing in both the standard and study samples at equal concentrations. However, by definition, analyte-free biological matrices do not exist for endogenous compounds. Furthermore, blank matrices may not be available or can be difficult to obtain, even for some exogenous compounds, because they are rare matrices such as tears, seminal, and vaginal fluid [22, 23], or due to contamination with analytes such as antibiotics in wastewaters [24], or presence of identical matrix components with the same MS and chromatography properties as the analytes of interest such as erlotinib [25].

3.3 Approaches for Quantification of Endogenous Analytes

Various approaches **(Figure 3.2)** are followed to address the lack of blank matrices for the quantification of endogenous compounds by LC-MS/MS including, background subtraction [26-31], the standard addition method [24, 25, 32-44], neat solutions [45-52], artificial matrices of biological fluids [23, 53-73], stripped matrices [8, 10, 11, 74-91], and surrogate analytes [66, 92-98].

3.3.1 Method of Background Subtraction

In background subtraction, the endogenous background concentrations of analytes in a pooled/representative matrix are subtracted from the concentrations of the added standards, subsequently the subtracted concentrations are used to construct the

calibration curve **(Figure 3.2-C)**. This approach allows the use of the same matrix for the calibration curve as the one to be analyzed, so that recovery and matrix effect are the same between samples and calibration curves. However, for this method to be reproducible, the increase in background peak area after spiking with standards has to be significantly higher than the reproducibility limits of the method at best, i.e. 15-20% of the background peak areas. Therefore, the lower limits of quantification (LLOQ) of these methods are limited by the endogenous background concentrations in the particular batches used as blanks in building the calibration curves, rather than by the analytical sensitivity. LLOQ is defined as the concentration at which the signal-to-noise ratio is 10 [27]. A statistical *t* test can also be used to define the LLOQ as the minimum concentration that results in the lowest statistically-significant increase in background concentration [30]. For example, if the concentration of an endogenous analyte in the matrix to be used as a blank is a 100 ng/ml, the LLOQ of this method is limited to 20 ng/ml despite the fact that the limit of detection for this analyte could be in the pg/ml range. Subtraction of peak areas after spiking with standards of concentrations lower than 20 ng/ml will likely result into negative values or irreproducible positive values, which does not allow the quantification of this analyte at concentrations lower than 20 ng/ml. In contrast, for an exogenous analyte with the same sensitivity as the abovementioned endogenous analyte, LLOQ is defined by the detection sensitivity of the MS, which is in the pg/ml range, because no background subtraction is performed.

Another drawback of this method is that the different batches of pooled bio-fluids that are used as blank matrices will have different background levels of endogenous analyte to subtract, which makes it an irreproducible process over time or between different labs [27, 29]. Furthermore, it is difficult to quantify multiple analytes if they have variable endogenous levels [27, 43].

When lower LLOQ of endogenous compounds are required, the background concentrations in the blank matrices can be lowered by dilution of the blank matrices before spiking with standards, to facilitate subtraction from low-concentration standards. However, this means that the composition of the matrices in the study samples vs. calibration curve is different, which may lead to different recoveries of analytes from the study samples vs. calibration standards. Therefore, before this approach is used, extraction recoveries of analytes between the matrix and diluted-matrix should be determined to be similar. **Table 3.1** summarizes representative examples of compounds quantified by the method of background subtraction. For example, our group used three-fold diluted brain homogenates compared to actual study samples, to construct calibration curves for the quantitation of amino acids in mice. However, it was demonstrated that extraction recoveries of amino acids from the diluted (calibration standards) and undiluted (study samples) were similar [29]. In another example background subtraction was applied for the quantification of amino acids in human plasma [43]. The endogenous levels of arginine, citrulline, and ornithine in the human plasma serving as the blank matrix were 154.4, 17.0, and 63.1 μM, respectively and the linear ranges using the background subtraction method were 25–200, 4–200, and 10–200 μM, respectively. As described above the high LLOQs were not because of the lack of sensitivity of the method but rather because of the high and variable endogenous levels of amino acids in plasma. In another example, Gachet et al. developed a method for the measurement of arachidonic acid, prostanoids, endocannabinoids, N-acylethanolamines, and steroids in human plasma by background subtraction [27]. The authors observed high inter-day variability at low concentration (1.3 ng/ml) by the method of background subtraction. However, this could be avoided by increasing the LLOQ level of the calibration curve.

3.3.2 Method of Standard Addition

In the standard addition method, every study sample is divided into aliquots of equal volumes. All aliquots, but one, are separately spiked with known and varying amounts of the analyte standards to construct a calibration curve for every study sample **(Figure 3.2-D)**. The study sample concentration is then determined as the negative x-intercept of the standard calibration curve prepared in that particular study sample [99]. In the background subtraction method, a pooled matrix is used as a surrogate for the matrices of all study samples, which may not be the case due to variability of the matrix components from sample to sample or batch to batch. In contrast, the standard addition method has the advantage of the use of the exact same matrix of every study sample for the construction of its own calibration curve. Furthermore, this approach allows direct quantitation of endogenous analytes without manual subtraction of background peak areas. However, this process generally requires a large amount of sample and can be markedly time-consuming and labor intensive. **Table 3.2** summarizes representative examples of compounds quantified by the method of standard addition. This method is usually followed to eliminate matrix effects when analyte free matrices are not available [32-37, 43]. For example, abscisic acid, a phytohormone, from plant leaves [33] and the emission of polycyclinc aromatic hydrocarbons from petroleum refineries [37] were quantified using the method of standard addition because blank matrices are not available for these analytes. The standard addition method is also used for the quantitation of exogenous analytes, when different matrix effects are observed for different samples [24, 38-42]. For example, antibiotics quantified in the effluents from wastewater-treatment plants had different recoveries and detection limits in at least two different wastewater effluents [39]. Similarly, matrix effect of diarrhetic shellfish poisoning toxins (DSPs) in scallop varied markedly between scallop samples [41]. Standard addition can also be used if some matrix components produce MS signals that interfere with the analytes of interest. For example, erlotinib was quantified in rat liver,

muscles, and spleen using the standard addition method because an unknown endogenous component of these matrices produced the same MS signal and had the same retention time as erlotinib [25].

3.3.3 Surrogate Matrices

It is often difficult to obtain biological matrix free of endogenous analyte to prepare calibration standards. Hence, various matrices are used as surrogate matrices for the actual matrix of study samples. Surrogate matrices can vary widely in complexity.

3.3.3.1 Neat solutions

In its simplest form, mobile-phase solvents (neat) [48, 49, 51] or pure water [45, 47, 50, 52] can be used as a surrogate matrix. To use neat solutions as surrogate matrices, it is required to demonstrate that extraction recovery and matrix effect are comparable with the original matrix. **Table 3.3** summarizes representative examples of compounds quantified using neat solutions as surrogate matrices. For example, thromboxane B_2 and 12(S)-hydroxyeicosatetraenoic acid were quantified in human serum using mixture of water/methanol/acetonitrile (80:10:10, v/v/v) as a surrogate matrix [51]. Authors demonstrated comparable matrix effect between neat solution and the original serum matrix.

3.3.3.2 Artificial matrices

Various biological matrices including cerebrospinal fluid, tears, vaginal fluid, and sputum are scarce and are difficult to obtain. However, if the composition of the study matrix is known, an artificial matrix can be prepared [100-105]. Artificial matrices are analyte-free, and are typically made to simulate the authentic matrices in terms of composition, salts content, analyte solubility, extraction recovery, and matrix effect. Phosphate-buffered saline (PBS) is frequently used for plasma and serum sample analyses because of its pH (7.4) and ionic strength. Often, bovine (BSA) or human

serum albumin (HSA) is added to PBS at a concentration of 20–80 g/l to take the protein content of the biological matrix into account and to increase the solubility of hydrophobic analytes. **Table 3.4** shows more complex artificial solutions that are prepared as surrogates for urine, cerebrospinal fluid, vaginal fluid, semen, tears and saliva. **Table 3.5** show representative examples of analytes quantitated using calibration curves prepared in in artificial matrices. For example, isotonic saline solution was used as an artificial matrix for the quantitation of polyunsaturated fatty acids and ecosanoids in human plasma [55]. Similar recoveries were found for these analytes in saline solution and human plasma. In addition, artificial tear fluid was used as a matrix for the characterization of ocular pharmacokinetics of amphotericin B and natamycin in rabbits. Authors demonstrated that QCs of amphotericin B and natamycin prepared in both real and artificial tear fluids showed similar accuracy and precision [23, 57].

3.3.3.3 Stripped matrices

Biological matrices are stripped from particular endogenous components to generate analyte-free surrogate matrices that can be used as blanks for the construction of calibration curves [74, 77, 78]. Activated-charcoal is an efficient adsorbent; therefore, it is most commonly used for this purpose. Other methods such as heating to decompose the analytes of interest can also be used. For example, plasma can be depleted of ascorbic acid by leaving it on the bench for 96 h [106]. During charcoal stripping, special care should be taken so that all charcoal particles are effectively removed from the matrix after stripping and before spiking with analytes, because the added analytes can readily bind to the remaining traces of charcoal, which can falsely decrease the measured analyte concentrations in study samples. Furthermore, not all endogenous analytes are efficiently removed by charcoal. Importantly, the composition of resulting stripped matrices may be drastically altered, which may lead to completely different extraction recoveries and matrix effects compared to the original matrices. In

addition, batch-to-batch variations may occur in the efficiency of stripping due to the differences in the levels of endogenous compounds to be stripped in blank matrices. Examples of analytes quantitated using stripping of matrices are given in **Table 3.6.** For example, our group quantified bile acids in mouse liver, bile, plasma and urine, as well as human plasma and urine using charcoal stripping after demonstrating similar extraction recoveries from stripped matrices and original matrices for two stable-labeled isotope internal standards [8, 10]. Similarly, we used charcoal-stripped human saliva for the quantification of four lysophosphatidic acids in saliva and gingival cervical fluids [82].

Overall, the various surrogate matrix approaches allow direct and sensitive quantification of analytes due to the lack of endogenous background in the surrogate matrix. However, analytes may have low solubility in the surrogate matrix, which could lead to precipitation of the analyte, nonspecific binding to the surfaces of tubes and vials, which will result in biased and irreproducible results. For proper assay performance, it is important to demonstrate similar matrix effect and extraction recovery of all internal standards and analytes over the entire intended concentration range in both surrogate and original matrices. Background subtraction, standard addition [53, 54, 56, 80], or labeled internal standards or analytes methods [8, 10, 11] can be used to determine extraction recovery of endogenous compounds in the original matrices.

3.3.4 Surrogate Analytes

In the surrogate analyte method, stable-isotope labeled analytes are used as surrogate standards to construct the calibration curves for the quantification of endogenous analytes **(Figure 3.2-F)**. This method allows direct and sensitive quantification of analytes due to the lack of any endogenous background. In this method it is assumed that the physico-chemical properties of the authentic and surrogate analytes are the same with the exception of molecular weight; therefore, extraction recovery, chromatographic retention, and signal intensity are identical or have minimal

differences. However, these assumptions are not always met, and isotope standards may differ in retention time and MS sensitivity compared to the unlabeled analytes. Therefore, before the application of this approach, the ratio of the labeled to unlabeled analyte MS responses (the response factor (RF)), should be close to unity and should be constant over the entire calibration range. If the RF does not equal one, it should be incorporated into the regression equation of the calibration curve [34]. To determine matrix effect and recovery of the authentic endogenous analytes, the background subtraction method as described above can be used. The labeled and unlabeled standards may have slightly different retention times as well as ionization efficiencies in the MS source, especially with larger number of labeled deuterium atoms. Furthermore, the mass difference between surrogate and authentic analytes should be sufficient, so that the naturally-occurring ^{13}C isotopes of the unlabeled analyte do not overlap with the labeled analyte [34]. In addition, contamination of the labeled standards with trace amount of unlabeled analytes is common, which may also exacerbate over time under storage conditions due to the degradation of labeled standards into unlabeled analytes. Stabled-labeled surrogate standards can only be used with methods using MS detectors because separation of the labeled and unlabeled compounds is based only on mass difference. Finally, this method is limited by the availability of expensive labeled standards.

Table 3.7 summarizes representative examples of compounds quantified by the surrogate analyte method. For example, the deuterium-labeled $^{2}H_{6}$-γ-hydroxybutyrate was used as a surrogate analyte for the quantitation of γ-hydroxybutyrate in human urine [92]. To examine the suitability of the surrogate analyte approach, calibration curves were prepared using both the surrogate analyte and standard addition methods. The slopes of both calibration curves were similar and resulted in the same concentrations of tested samples. In another example, $^{2}H_{3}$-ketoisocaproate was used as a surrogate

analyte for the quantitation of ketoisocaproate in rat plasma, brain, and cerebrospinal fluid [93]. In this method authors demonstrated similar MS response for the surrogate and authentic analyte in neat solution, but the matrix effect and extraction recovery were not compared.

3.4 Regulatory Guidelines

Validation of bioanalytical methods is required to ensure that these methods are accurate, reproducible, robust, and reliable for their various applications. United States Food and Drug Administration (USFDA) and European Medicines Agency (EMA, European authority) issued the most recent drafts of their guidelines for acceptance criteria and strategies on bioanalytical method validation in 2013 [107] and 2012 [108], respectively. For sensitivity and selectivity, blank samples of the biological matrix to be analyzed should be obtained from at least six sources and the responses of any interfering components with analytes and IS should be less than 20% of the response at the LLOQ of the analytes and less than 5% of the response of the internal standard (IS). Accuracy and precision should be measured at LLOQ, low quality control (LQC- within three times the LLOQ), middle QC (in the midrange), and high QC (approaching the high end) using a minimum of five determinations per concentration, and they should be within 15%, except for the LLOQ that can be up to 20%. A calibration curve should consist of a blank matrix, a zero standard, and at least six non-zero standards covering the expected dynamic range. Accuracy for these standards should also follow the same criteria as the QCs. Additional criteria regarding stability, recovery, matrix effect, and incurred sample analysis are also discussed in the guidelines.

These guidelines are primarily designed to address validation of exogenous compounds and following their validation criteria for the quantification of endogenous compounds is a challenge, because of the lack of blank matrix needed to make all the standards and QCs that are used to obtain all these validation parameters. This has

recently triggered the FDA to dedicate a section for the quantification of endogenous compounds in its most recent (2013) draft [107], which was not addressed in the previous 2001 version [109]. The FDA guidelines stated that "the biological matrix used to prepare calibration standards should be the same as the study samples and should be free of the endogenous analytes. The suitability of analyte-free biological matrices needs to be assured, by demonstrating no measurable endogenous analytes and no matrix effect or interference when compared to the biological matrices of the study samples". The guidelines recommended that the quality control samples (QCs) should be prepared in the same biological matrix as study samples and that the concentrations of these QCs should account for the background endogenous concentrations in the biological matrix, i.e. using the method of background subtraction. The guidelines also referred to the use of alternate (surrogate) matrices such as buffers and dialyzed serum, but did not recommend this approach unless an analyte-free biological matrix is not readily available or cannot be prepared. If this approach is used, justification and evidence of similar matrix effect to the original matrix are required.

3.5 Conclusions

In summary, various methods are available for the quantitative analyses of endogenous compounds. Background subtraction and standard addition methods use the same biological matrix as the study samples to prepare the calibration standards, hence recovery and matrix effect for the study samples are identical to those of the calibration standards. However, the sensitivity of the background subtraction method is limited by the endogenous levels of the analytes rather than by the sensitivity of the detector. On the other hand, the standard addition method requires large sample volumes as calibration curves are built in each individual sample. In contrast the surrogate matrix approach uses matrices devoid of endogenous analytes for preparing calibration standards and it allows direct and sensitive quantification of analytes.

Surrogate matrices include neat solutions, artificial matrices, and stripped matrices. However, for this method it is required to demonstrate similar matrix effect and extraction recovery in both the surrogate and original matrix. Finally, similar to the background subtraction and standard addition methods, the surrogate analyte approach use the same biological matrix as the study samples to prepare the calibration standards. However, stable-isotope labeled analytes are used as surrogate standards to construct the calibration curves for the quantification of endogenous analytes. Hence, utility of this method is limited by the use of MS detectors and by the availability of expensive and pure labeled standards. Furthermore, it is required to demonstrate similarity in matrix effect and recovery between surrogate and authentic endogenous analytes. Finally, all these methods represent indirect approaches to quantify endogenous compounds and regardless of what approach is followed, it has to be shown that none of the validation criteria have been compromised due to the indirect analyses. Addressing endogenous compounds in the most recent version of FDA guidelines reflect the growing need for quantitative analysis of endogenous analytes. However, the guidelines did not specify the different approaches of how to obtain analyte-free biological matrices for endogenous compounds.

Figure 3.1 A LC-MS/MS chromatograms showing differences in MS response of one analyte spiked pre- extraction (A) and post-extraction (B) into plasma, liver, as well as neat matrices at the same concentration.

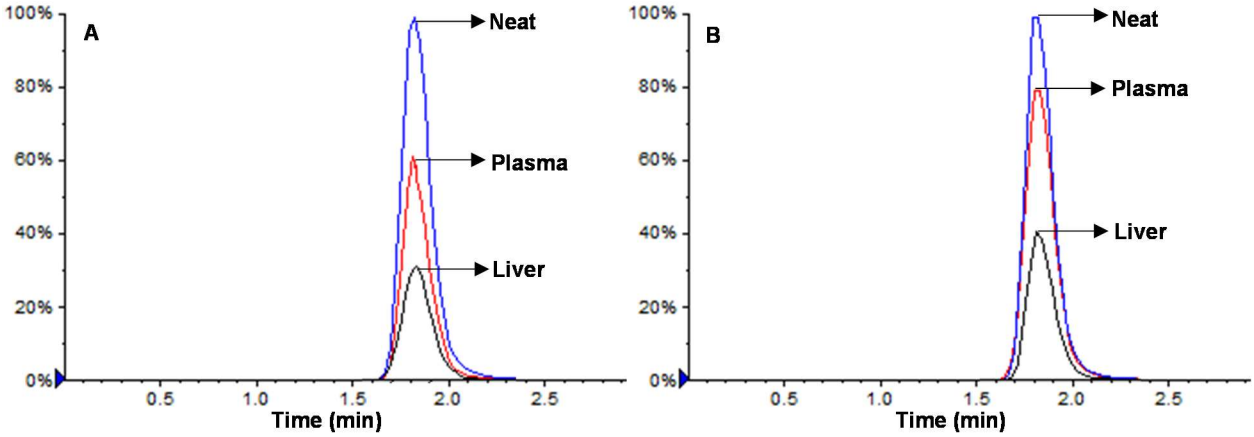

Figure 3.2 LC-MS/MS chromatograms showing (A) background peak of endogenous analyte in blank matrix, (B) a neat standard with known concentration of the same analyte, (C) the same matrix after spiking with a standard of a known concentration (method of background subtraction), (D) one study sample is split into several aliquots, each spiked with a standard (Std.) of different concentration (method of standard addition), (E) analyte standard spiked into a surrogate matrix that contains no background (surrogate matrix method), (F) a standard of a surrogate analyte spiked into the same original matrix (surrogate analyte method).

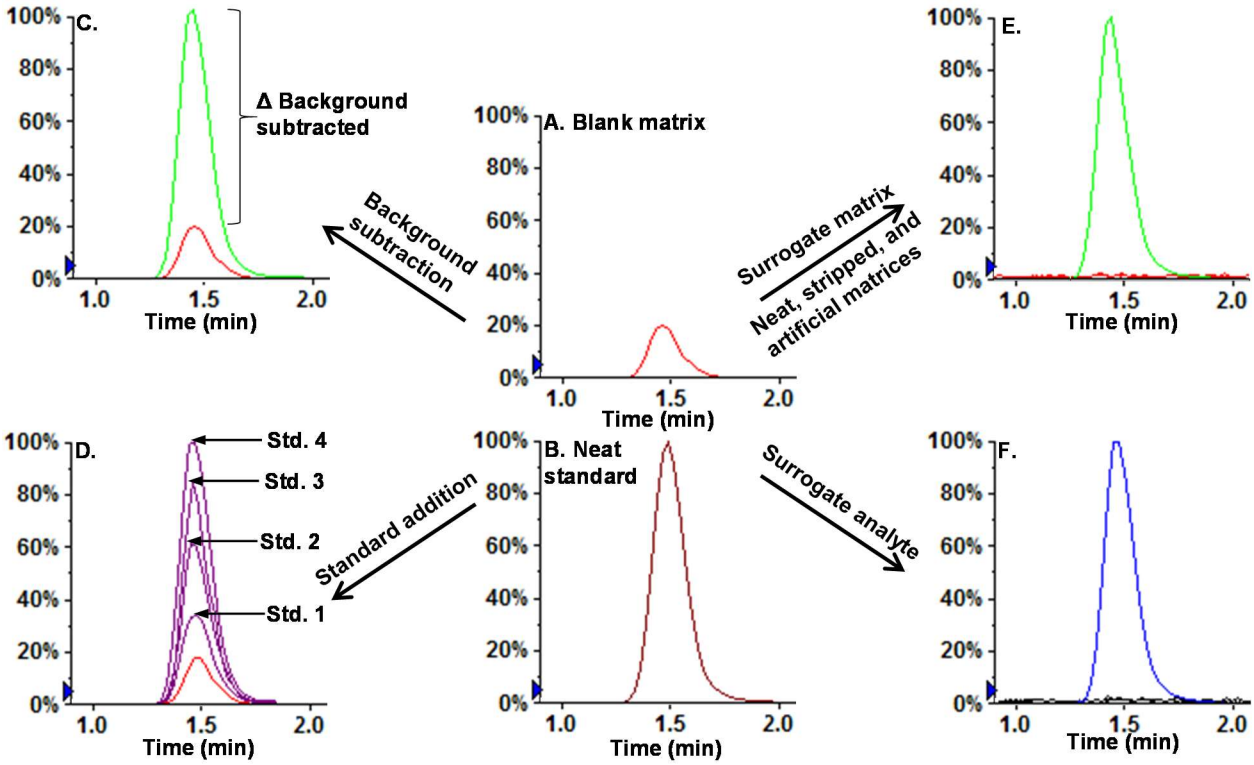

Figure 3.3 A LC-MS/MS chromatogram showing the subtraction of the background (blank) peak area of endogenous compound (A) from the peak area of the same compound after spiking with a 500 ng/ml standard. (B) is an exogenous compound and no background exists in the blank matrix.

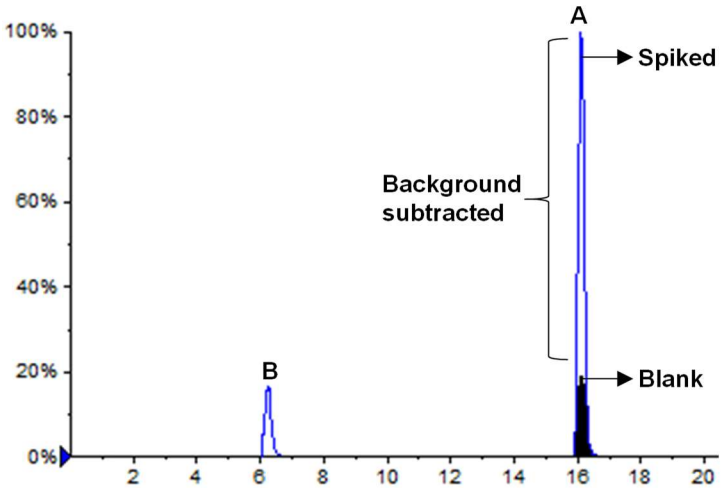

Table 3.1 Applications of the background subtraction method.

Class	Application	Matrix	Analytical technique	Reason[a]	References
Amino acids	Biomarkers for cardiovascular diseases	Human plasma	LC-MS/MS	Blank matrix not available	[26]
Amino acids	Biomarkers for diabetic complications	Human plasma and urine	LC-MS/MS	Blank matrix not available	[28]
Amino acids	Biomarkers for neurodegenerative diseases	Mouse brain	LC-MS/MS	Blank matrix not available.	[29]
Eicosanoids	Biomarkers for cardiovascular diseases	Human plasma	LC-MS/MS	Blank matrix not available.	[30]
Eicosanoids and steroids	Biomarkers for inflammatory, neuropsychiatric and cardiovascular diseases	Human plasma	LC-MS/MS	Blank matrix not available.	[27]
Cobalt mesoporphyrin (Antiobesity)	Pharmacokinetics	Rat plasma	Atomic absorption spectroscopy	Blank matrix not available.	[31]

[a]Reason why background subtraction method was required.

Table 3.2 Applications of the method of standard addition.

Class	Application	Matrix	Analytical technique	Reason[a]	References
Sphingosine 1-phosphate (Sphingolipids)	Biomarker for atherosclerosis	Human plasma	LC- Fluorescence	Blank matrix not available	[32]
Abscisic acid (Plant hormone)	Biomarkers for plant growth	Plant leaves	LC-MS/MS	Blank matrix not available	[33]
Androgens	Biomarkers for endocrine disorders	human urine	GC-MS	Blank matrix not available	[34]
Purines and Pyrimidines	Estimation of protein supply in animals	Bovine and ovine urine	HPLC-UV	Blank matrix not available	[35]
Bile acids	Biomarkers for vascular and metabolic disorders	Human serum	LC-MS/MS	Blank matrix not available	[36]
Polycyclic aromatic hydrocarbons	Monitoring of pollutant from petroleum refinery	Flame	TOF	Blank matrix not available	[37]
Erlotinib (Anticancer)	Pharmacokinetics	Rat liver, spleen and muscles	MALDI-TOF	Interference from matrix components	[25]
Antibiotics	Monitoring of antibiotics residues in feeding stuffs	Animal feeds	LC-MS/MS	variable matrix effect between samples	[38]
Trimethoprim (Antibiotics)	Monitoring of drug residues in wastewater	Wastewater	LC-MS/MS	variable matrix effect between samples	[39]
Antibiotics	Monitoring of antibiotics residues in wastewater	Wastewater	LC-MS/MS	variable matrix effect between samples	[24]
Flavoring additives	Monitoring aroma in food products	Wheat flour doughs	GC-FID	variable matrix effect between samples	[40]
Seafood poisons	Monitoring shellfish poisons in scallop	Scallops	LC-MS/MS	variable matrix effect between samples	[41]
N-carboxymethyl lysine (Amino acid)	Biomarker for diabetes	Human plasma	LC- Fluorescence	variable matrix effect between samples	[42]
Amino acids	Biomarkers for pulmonary diseases	Human plasma	LC-MS/MS	Blank matrix not available	[43]
Steroids	Forensic	Wood	LC-MS/MS	Blank matrix not available	[44]

[a]Reason why standard addition method was required.

Table 3.3 Applications of the use of neat solutions as surrogate matrices.

Class	Application	Matrix	Analytical technique	Neat composition	Validation[a]	References
Amino Acids	Biomarkers for pelvic organ prolapse	Human pelvic connective tissues	LC-MS/MS	Water	Similar recovery in surrogate and original matrices for all analytes at three QCs	[45]
Amino acids	Biomarkers for metabolic disorders.	Human plasma, urine and cerebrospinal fluid	LC-MS/MS	0.1% HCL	-	[46]
Amino Acids and neurotransmitters	Biomarkers for central nervous system disorders	Rat plasma and PC12 cells	LC-MS/MS	Water	Similar recovery in surrogate and original matrices for all analytes at three QCs	[47]
Bile acids	Biomarkers for hepatobiliary diseases	Mouse plasma and human serum	LC-MS/MS	50 % methanol	Similar recovery in surrogate and original matrices for all analytes at one QC	[48]
Bile acids	Biomarkers for hepatobiliary diseases	Human plasma, human urine and mouse liver	LC-MS/MS	Methanol	Similar recovery in surrogate and original matrices for all analytes at one QC	[49]
LTB_4 (Eicosanoids)	Biomarkers for inflammatory diseases	Human exhaled breath condensate	LC-MS/MS	Water	-	[50]
Eicosanoids	Biomarkers for platelet activity	Human serum	LC-MS/MS	Water/methanol/acetonitrile	Similar calibration coefficient for surrogate and original matrices	[51]
Small organic acids	Biomarkers for acidosis in malaria	Human plasma and urine	LC-MS	Water	Similar recovery in surrogate and original matrices for all analytes at three QCs	[52]

[a]Validation: How similarity of recoveries/matrix effect for original and surrogate matrices were demonstrated.

Table 3.4 Typical composition of commonly used artificial matrices[a].

vaginal fluid [100]	Semen [101]	Urine [102]	Tears [103]	Cerebrospinal fluid [104]	Saliva [105]
Glucose - 5.0	Glucose - 1.02	NaCl - 14.1	Lysozyme - 1.9	NaCl - 7.592	NaCl - 8.0
Glycerol - 0.16	Sodium citrate - 8.13	KCl - 2.8	Lactoferrin - 1.8	KCl - 0.146	KH_2PO_4 - 0.19
Lactic acid - 2.0	KOH - 0.881	Urea - 17.3	α-acid glycoprotein - 0.5	$MgCl_2.6H_2O$ - 0.24	Na_2HPO_4 - 2.38
Acetic acid - 1.0	KCl - 0.908	25% ammonia water-0.19%	albumin - 0.2	$CaCl_2.2H_2O$ - 0.174	
Albumin - 0.018	Fructose - 2.72	$CaCl_2$ - 0.6	mucin - 0.15	KH_2PO_4 - 0.154	
Urea - 0.40	Lactic acid - 0.62	$MgSO_4$ - 0.43	γ-globulins - 0.1	Sodium lactate - 1.69	
NaCl - 3.51	Urea - 0.42	HCl - 0.02 M	NaCl- 6.626, KCl - 1.716	glucose - 0.719	
KOH - 1.40	BSA - 50.4		$NaHCO_3$ -1.376	$NaHCO_3$ - 0.924	
$Ca(OH)_2$ - 0.222	$NaH_2PO_4 \cdot H_2O$ - 0.0927		Lactic acid - 0.27		
pH - 4.2	Na_2HPO_4 - 0.858		$CaCl_2$ - 0.147		
			$NaH_2PO_4.H_2O$ - 0.1		
			Lipids - 0.0798		

[a]Values are in grams per liter.

Table 3.5 Applications of the use of artificial matrices as surrogate matrices.

Class	Application	Matrix	Analytical technique	Surrogate matrix	Validation[a]	Reference
Eicosanoids	Biomarkers for asthma and COPD	Human sputum	LC-MS/MS	Human serum albumin (HAS) in phosphate buffer saline (PBS)	No matrix effect and ~ 100% recovery in original matrix for all analytes at one QC	[53]
Eicosanoids	Biomarkers for asthma and COPD	Human urine	LC-MS/MS	Artificial urine	No matrix effect in original and surrogate matrix for all analytes at one QC	[54]
Eicosanoids	Biomarkers for Inflammatory, respiratory, and cancer diseases	Human plasma	LC-MS/MS	Saline solution	Similar recovery in surrogate and original matrices for all analytes at one QC	[55]
8-iso-PGF2α (Eicosanoid)	Biomarker for hypertension	Human urine	LC-MS/MS	Phosphate buffer saline	No matrix effect in original matrix for analyte at one QC	[56]
Natamycin (Antibiotics)	Pharmacokinetics	Rabbit lachrymal fluid	LC-MS/MS	Artificial tear fluid	No matrix effect in original and surrogate matrix for analyte at three QCs	[57]
Amphotericin B (Antibiotics)	Pharmacokinetics	Rabbit lachrymal fluid	LC-MS/MS	Artificial tear fluid	No matrix effect in original and surrogate matrix for analyte and IS at one QC	[23]
Sphingolipids	Biomarkers for cancer and immune system disorder	Human plasma	LC-MS/MS	5 % bovine serum albumin (BSA) in PBS	No matrix effect and similar recovery in original and surrogate matrix for all analytes at two QCs	[58]
Pyridoxal-5'-phosphate (Vitamins)	Biomarkers for neurological disorders	Human blood	LC-MS/MS	2% BSA in PBS	No matrix effect and similar recovery in original and surrogate matrix for analyte at two QCs	[59]
Vitamin D	Biomarkers for cancer, cardiovascular and autoimmune diseases	Human serum and plasma	LC-MS/MS	5% BSA in PBS	No matrix effect in original matrix for analytes at three QCs	[60]
Ceramides	Biomarkers for type 2 diabetes	Human plasma	LC-MS/MS	5 % BSA in water	Similar matrix effect and recovery in original and surrogate matrix for all analytes and IS at one QC	[61]
homocysteine (Amino acid)	Biomarkers for vascular diseases	Human serum	LC-MS/MS	2% BSA in water	No matrix effect and similar recovery in original and surrogate matrix for analyte and IS at two QCs	[62]
Amino acids	Biomarkers for immune system functions	Rat plasma	LC-MS/MS	BSA (79g/L)	-	[63]
Androgens	Biomarkers for prostate	Mouse lung,	LC-MS/MS	1 g/L of PBS/BSA	-	[64]

	cancer	brain, liver, heart, kidney, prostate, testis, bladder				
24(S)-hydroxycholesterol	Biomarkers for Niemann-Pick type C disease	Human plasma and cerebrospinal fluid (CSF)	LC-MS/MS	5% BSA in water for plasma and 2.5% HP-β-CD for CSF	No matrix effect and ~100% recovery in original and surrogate matrix	[65]
Steroids	Endogenous biomarker for drug–drug interactions	human and mouse plasma	LC-MS/MS	4.2% HSA in PBS	-	[73]
Polypeptides	Biomarkers for chronic obstructive pulmonary disease	Human urine	LC-MS/MS	PBS	Similar calibration coefficient for surrogate and original matrices	[66]
Amyloid peptides	Biomarkers for Alzheimer's disease	Human CSF	LC-MS	Artificial CSF	Similar calibration coefficient for surrogate and original matrices	[67]
N-terminal natriuretic peptide	Biomarkers for cardiac hypertrophy	Rat serum	LC-MS/MS	Human serum	Similar calibration coefficient for surrogate and original matrices	[68]
Insulin-like growth factor-1	Anti-doping test	Human and chicken dried-blood spot	LC-MS/MS	HSA (1 mg/mL)	-	[69]
Purine metabolites	Biomarkers for hyperuricemia	Human serum	LC-UV	Phosphate buffer	~ 100% recovery in original matrix for analytes and IS at one QC	[70]
Acetylcholine (Neurotransmitter)	Biomarker for Alzheimer's disease and schizophrenia	Rat CSF	LC-MS/MS	Artificial CSF	No matrix effect in original matrix	[71]
Neurotransmitters	Biomarkers for diabetes, heart diseases, and anxiety	Human plasma	LC-MS/MS	Heated human plasma	Similar matrix effect and recovery between original and surrogate matrix at three QCs	[72]

[a]Validation: How similarity of recoveries/matrix effect for original and surrogate matrices were demonstrated.

Table 3.6 Applications of the use of stripped matrices as surrogate matrices.

Class	Application	Matrix	Analytical technique	Validation[a]	Reference
Amino acids	Biomarkers for hypotension and hypovolemia	Human plasma and urine	LC-MS/MS	No matrix effect in original matrix for analyte at three QCs	[60]
Amino Acids	Biomarkers for acute porphyrias	Human serum and Urine	LC-MS/MS	No matrix effect in original matrix for analytes at one QC	[75]
Estradiol	Biomarkers for endocrine disorder	Human plasma	LC-MS/MS	No matrix effect in original matrix for analytes at four QCs	[76]
Testosterone	Biomarkers for endocrine disorder	Human serum	LC-MS/MS	-	[88]
Steroids	Biomarkers for endocrine disorder	Human serum	LC-MS/MS	No matrix effect in stripped and original matrix for analytes for calibration curve	[89]
Steroids	Biomarkers for endocrine disorder	Human CSF	LC-MS/MS	-	[90]
Cortisol	Biomarkers for endocrine disorder	Human plasma	LC-MS/MS	No matrix effect and 100% recovery in stripped matrix at 3 QCs	[91]
Bile acids	Biomarkers for hepatobiliary diseases	Human plasma	LC-MS/MS	No matrix effect in original matrix for analytes at two QCs	[77]
Bile acids	Biomarkers for hepatobiliary diseases	Human urine	LC-MS/MS	-	[78]
Bile acids	Biomarkers for hepatobiliary diseases	Human plasma	LC-MS/MS	Matrix effect and recovery is similar for stripped and original matrix for all analytes one QC	[79]
Bile Acids	Biomarkers for hepatobiliary diseases	Mouse liver, bile, plasma, and urine	LC-MS/MS	Similar recovery for stripped and original matrix for stable isotope labeled internal standards at one QC	[8]
Bile Acids	Biomarkers for hepatobiliary diseases	Mouse liver, bile, plasma, and urine	LC-MS/MS	Similar recovery for stripped and original matrix for stable isotope labeled internal standards at one QC	[11]
Bile acids	Biomarkers for hepatobiliary diseases	Human urine and serum	LC-MS/MS	Similar recovery for stripped and original matrix for stable isotope labeled internal standards at one QC	[10]
Bile Acid	Biomarkers for hepatobiliary diseases	Rat plasma	LC-MS/MS	No matrix effect in stripped and original matrix for analytes for calibration curve	[80]
Bile Acid	Biomarkers for hepatobiliary diseases	Sea Lamprey plasma and tissues	LC-MS/MS	Similar matrix effect between original and stripped matrix for all analytes and IS at one QC	[81]
Phospholipids	Biomarker for periodontal diseases	Human saliva and gingival cervicular fluid	LC-MS/MS	-	[82]
Fatty acids	Bimarker for drug addiction, obesity, inflammation and cancer	Human plasma	LC-MS/MS	No matrix effect in original matrix for analytes at one QC	[83]

poly saccharides	Biomarkers for Crohn's, nonalcoholic fatty liver diseases, and diarrhea	Human plasma	LC-MS/MS	Similar matrix effect and recovery for stripped and original matrix for all analytes and IS for 2 QCs	[84]
human serum albumin	Biomarker for renal disorder	Human urine	LC-MS/MS	-	[85]
Nucleotides	Biomarker for cellular biochemical processes	peripheral blood mononuclear cells	LC-MS/MS	Similar matrix effect in stripped and original matrix for IS at three QCs	[86]
Eicosanoids	Biomarkers for cardiovascular diseases	Human Sputum	LC-MS/MS	No matrix effect in original matrix for all analytes at two QCs	[87]

[a]Validation: How similarity of recoveries/matrix effect for original and surrogate matrices were demonstrated.

Table 3.7 Applications of the surrogate analytes method.

Class	Application	Matrix	Analytical technique	Isotope labels	Validation[a]	References
Peptide	biomarkers for lung disease	Human urine	LC-MS/MS	^{2}H and ^{18}O	Similar calibration coefficient for authentic analyte surrogate and surrogate analyte original matrices	[66]
γ-hydroxybutyrate (neurotransmitter)	Forensic analysis	Human urine	LC-MS/MS	^{2}H	-	[92]
α-ketoisocaproic acid	Biomarker for chronic uremia	Plasma, Brain homogenate, and Cerebrospinal fluid	LC-MS/MS	^{2}H	Compared MS response between labeled and unlabeled in neat solution	[93]
Mevalonic acid	Biomarker for cholesterol lowering drugs	Human plasma	LC-MS/MS	^{2}H	Compared MS response between labeled and unlabeled in matrix	[94]
Monosaccharides	Biomarker for uremia and diabetes	Human red blood cells (RBCs)	LC-MS/MS	$^{13}C_6$	-	[95]
Monosaccharides	Biomarker for uremia and diabetes	Human nerve tissues	LC-MS/MS	$^{13}C_6$	-	[96]
Amino Acids	Biomarker for metabolic disorder.	Human plasma	LC-MS/MS	^{2}H	Similar calibration coefficient for authentic analyte surrogate and surrogate analyte original matrices	[97]
4β-hydroxycholesterol	Endogenous biomarker for drug–drug interactions	Human plasma	LC-MS/MS	^{2}H	Compared MS response between labeled and unlabeled in neat solution	[98]

[a]Validation: How similarity of MS response for original and surrogate analytes were demonstrated.

3.6 References

[1] M. Breier, S. Wahl, C. Prehn, M. Fugmann, U. Ferrari, M. Weise, F. Banning, J. Seissler, H. Grallert, J. Adamski, A. Lechner, Targeted metabolomics identifies reliable and stable metabolites in human serum and plasma samples, PLoS One, 9 (2014) e89728.
[2] E.J. Want, M. Coen, P. Masson, H.C. Keun, J.T. Pearce, M.D. Reily, D.G. Robertson, C.M. Rohde, E. Holmes, J.C. Lindon, R.S. Plumb, J.K. Nicholson, Ultra performance liquid chromatography-mass spectrometry profiling of bile acid metabolites in biofluids: application to experimental toxicology studies, Anal Chem, 82 (2010) 5282-5289.
[3] W.B. Dunn, I.D. Wilson, A.W. Nicholls, D. Broadhurst, The importance of experimental design and QC samples in large-scale and MS-driven untargeted metabolomic studies of humans, Bioanalysis, 4 (2012) 2249-2264.
[4] R. Yang, N. Chiang, S.F. Oh, C.N. Serhan, Metabolomics-lipidomics of eicosanoids and docosanoids generated by phagocytes, Curr Protoc Immunol, Chapter 14 (2011) Unit 14 26.
[5] V.A. Blaho, M.W. Buczynski, C.R. Brown, E.A. Dennis, Lipidomic analysis of dynamic eicosanoid responses during the induction and resolution of Lyme arthritis, J Biol Chem, 284 (2009) 21599-21612.
[6] Y. Qi, C. Jiang, J. Cheng, K.W. Krausz, T. Li, J.M. Ferrell, F.J. Gonzalez, J.Y. Chiang, Bile acid signaling in lipid metabolism: metabolomic and lipidomic analysis of lipid and bile acid markers linked to anti-obesity and anti-diabetes in mice, Biochim Biophys Acta, 1851 (2015) 19-29.
[7] S.P. Bathena, R. Thakare, N. Gautam, S. Mukherjee, M. Olivera, J. Meza, Y. Alnouti, Urinary bile acids as biomarkers for liver diseases I. Stability of the baseline profile in healthy subjects, Toxicol Sci, 143 (2015) 296-307.
[8] Y. Alnouti, I.L. Csanaky, C.D. Klaassen, Quantitative-profiling of bile acids and their conjugates in mouse liver, bile, plasma, and urine using LC–MS/MS, Journal of Chromatography B, 873 (2008) 209-217.
[9] S.P. Bathena, R. Thakare, N. Gautam, S. Mukherjee, M. Olivera, J. Meza, Y. Alnouti, Urinary bile acids as biomarkers for liver diseases II. Signature profiles in patients, Toxicol Sci, 143 (2015) 308-318.
[10] S.P.R. Bathena, S. Mukherjee, M. Olivera, Y. Alnouti, The profile of bile acids and their sulfate metabolites in human urine and serum, Journal of Chromatography B, 942–943 (2013) 53-62.
[11] J. Huang, S.P.R. Bathena, I.L. Csanaky, Y. Alnouti, Simultaneous characterization of bile acids and their sulfate metabolites in mouse liver, plasma, bile, and urine using LC–MS/MS, Journal of pharmaceutical and biomedical analysis, 55 (2011) 1111-1119.
[12] A. Kotłowska, Application of Steroid Hormone Metabolomics in Search of Biomarkers in Clinical Research, Drug Development Research, 73 (2012) 381-389.
[13] T.F. Jorge, J.A. Rodrigues, C. Caldana, R. Schmidt, J.T. van Dongen, J. Thomas-Oates, C. Antonio, Mass spectrometry-based plant metabolomics: Metabolite responses to abiotic stress, Mass Spectrom Rev, (2015).
[14] Z. Lei, D.V. Huhman, L.W. Sumner, Mass spectrometry strategies in metabolomics, J Biol Chem, 286 (2011) 25435-25442.
[15] L.D. Roberts, A.L. Souza, R.E. Gerszten, C.B. Clish, Targeted metabolomics, Curr Protoc Mol Biol, Chapter 30 (2012) Unit 30 32 31-24.
[16] K. Vishwanathan, K. Babalola, J. Wang, R. Espina, L. Yu, A. Adedoyin, R. Talaat, A. Mutlib, J. Scatina, Obtaining exposures of metabolites in preclinical species through plasma pooling and quantitative NMR: addressing metabolites in safety testing (MIST)

guidance without using radiolabeled compounds and chemically synthesized metabolite standards, Chem Res Toxicol, 22 (2009) 311-322.
[17] J.F. Xiao, B. Zhou, H.W. Ressom, Metabolite identification and quantitation in LC-MS/MS-based metabolomics, Trends Analyt Chem, 32 (2012) 1-14.
[18] E. Brewer, J. Henion, Atmospheric pressure ionization LC/MS/MS techniques for drug disposition studies, J Pharm Sci, 87 (1998) 395-402.
[19] P.J. Taylor, Matrix effects: the Achilles heel of quantitative high-performance liquid chromatography-electrospray-tandem mass spectrometry, Clin Biochem, 38 (2005) 328-334.
[20] B.K. Matuszewski, M.L. Constanzer, C.M. Chavez-Eng, Strategies for the assessment of matrix effect in quantitative bioanalytical methods based on HPLC-MS/MS, Anal Chem, 75 (2003) 3019-3030.
[21] Y. Huang, R. Shi, W. Gee, R. Bonderud, Matrix effect and recovery terminology issues in regulated drug bioanalysis, Bioanalysis, 4 (2012) 271-279.
[22] J.B. Bulitta, M. Kinzig, C.K. Naber, F.M. Wagenlehner, C. Sauber, C.B. Landersdorfer, F. Sorgel, K.G. Naber, Population pharmacokinetics and penetration into prostatic, seminal, and vaginal fluid for ciprofloxacin, levofloxacin, and their combination, Chemotherapy, 57 (2011) 402-416.
[23] R. Bhatta, C. Rathi, H. Chandasana, D. Kumar, Y. Chhonker, G. Jain, LC–MS Method for Determination of Amphotericin B in Rabbit Tears and Its Application to Ocular Pharmacokinetic Study, Chromatographia, 73 (2011) 487-493.
[24] J. Rossmann, S. Schubert, R. Gurke, R. Oertel, W. Kirch, Simultaneous determination of most prescribed antibiotics in multiple urban wastewater by SPE-LC-MS/MS, J Chromatogr B Analyt Technol Biomed Life Sci, 969 (2014) 162-170.
[25] L. Signor, E. Varesio, R.F. Staack, V. Starke, W.F. Richter, G. Hopfgartner, Analysis of erlotinib and its metabolites in rat tissue sections by MALDI quadrupole time-of-flight mass spectrometry, J Mass Spectrom, 42 (2007) 900-909.
[26] K. Vishwanathan, R.L. Tackett, J.T. Stewart, M.G. Bartlett, Determination of arginine and methylated arginines in human plasma by liquid chromatography-tandem mass spectrometry, J Chromatogr B Biomed Sci Appl, 748 (2000) 157-166.
[27] M.S. Gachet, P. Rhyn, O.G. Bosch, B.B. Quednow, J. Gertsch, A quantitiative LC-MS/MS method for the measurement of arachidonic acid, prostanoids, endocannabinoids, N-acylethanolamines and steroids in human plasma, J Chromatogr B Analyt Technol Biomed Life Sci, 976-977 (2015) 6-18.
[28] Z. Jing, L. Kuang, N. Liu, J. Yang, LC-MS/MS for the simultaneous determination of polar endogenous ADMA and CML in plasma and urine from diabetics, Bioanalysis, 7 (2015) 1261-1271.
[29] S.P. Bathena, J. Huang, A.A. Epstein, H.E. Gendelman, M.D. Boska, Y. Alnouti, Rapid and reliable quantitation of amino acids and myo-inositol in mouse brain by high performance liquid chromatography and tandem mass spectrometry, J Chromatogr B Analyt Technol Biomed Life Sci, 893-894 (2012) 15-20.
[30] K. Strassburg, A.M. Huijbrechts, K.A. Kortekaas, J.H. Lindeman, T.L. Pedersen, A. Dane, R. Berger, A. Brenkman, T. Hankemeier, J. van Duynhoven, E. Kalkhoven, J.W. Newman, R.J. Vreeken, Quantitative profiling of oxylipins through comprehensive LC-MS/MS analysis: application in cardiac surgery, Anal Bioanal Chem, 404 (2012) 1413-1426.
[31] K.L. Hoffman, M.R. Feng, D.T. Rossi, Quantitation of a novel metalloporphyrin drug in plasma by atomic absorption spectroscopy, J Pharm Biomed Anal, 19 (1999) 319-326.
[32] J.J. Butter, R.P. Koopmans, M.C. Michel, A rapid and validated HPLC method to quantify sphingosine 1-phosphate in human plasma using solid-phase extraction

followed by derivatization with fluorescence detection, J Chromatogr B Analyt Technol Biomed Life Sci, 824 (2005) 65-70.
[33] M. Lopez-Carbonell, O. Jauregui, A rapid method for analysis of abscisic acid (ABA) in crude extracts of water stressed Arabidopsis thaliana plants by liquid chromatography--mass spectrometry in tandem mode, Plant Physiol Biochem, 43 (2005) 407-411.
[34] R. Ahmadkhaniha, A. Shafiee, N. Rastkari, M.R. Khoshayand, F. Kobarfard, Quantification of endogenous steroids in human urine by gas chromatography mass spectrometry using a surrogate analyte approach, J Chromatogr B Analyt Technol Biomed Life Sci, 878 (2010) 845-852.
[35] K.J. Shingfield, N.W. Offer, Simultaneous determination of purine metabolites, creatinine and pseudouridine in ruminant urine by reversed-phase high-performance liquid chromatography, J Chromatogr B Biomed Sci Appl, 723 (1999) 81-94.
[36] M. Scherer, C. Gnewuch, G. Schmitz, G. Liebisch, Rapid quantification of bile acids and their conjugates in serum by liquid chromatography-tandem mass spectrometry, J Chromatogr B Analyt Technol Biomed Life Sci, 877 (2009) 3920-3925.
[37] C.M. Gittins, M.J. Castaldi, S.M. Senkan, E.A. Rohlfing, Real-Time Quantitative Analysis of Combustion-Generated Polycyclic Aromatic Hydrocarbons by Resonance-Enhanced Multiphoton Ionization Time-of-Flight Mass Spectrometry, Anal Chem, 69 (1997) 286-293.
[38] A. Boscher, C. Guignard, T. Pellet, L. Hoffmann, T. Bohn, Development of a multi-class method for the quantification of veterinary drug residues in feedingstuffs by liquid chromatography-tandem mass spectrometry, J Chromatogr A, 1217 (2010) 6394-6404.
[39] J.E. Renew, C.H. Huang, Simultaneous determination of fluoroquinolone, sulfonamide, and trimethoprim antibiotics in wastewater using tandem solid phase extraction and liquid chromatography-electrospray mass spectrometry, J Chromatogr A, 1042 (2004) 113-121.
[40] M.A. Pozo-Bayo´ n, E. Guichard, N. Cayot, Feasibility and application of solvent assisted flavour evaporation and standard addition method to quantify the aroma compounds in flavoured baked matrices, Food Chemistry, 99 (2006) 416-423.
[41] S. Ito, K. Tsukada, Matrix effect and correction by standard addition in quantitative liquid chromatographic-mass spectrometric analysis of diarrhetic shellfish poisoning toxins, J Chromatogr A, 943 (2002) 39-46.
[42] N.C. van de Merbel, C.J. Mentink, G. Hendriks, B.H. Wolffenbuttel, Liquid chromatographic method for the quantitative determination of Nepsilon-carboxymethyllysine in human plasma proteins, J Chromatogr B Analyt Technol Biomed Life Sci, 808 (2004) 163-168.
[43] X. Lai, J.A. Kline, M. Wang, Development, validation, and comparison of four methods to simultaneously quantify l-arginine, citrulline, and ornithine in human plasma using hydrophilic interaction liquid chromatography and electrospray tandem mass spectrometry, J Chromatogr B Analyt Technol Biomed Life Sci, 1005 (2015) 47-55.
[44] K. Verheyden, H. Noppe, J. Vanden Bussche, K. Wille, K. Bekaert, L. De Boever, J. Van Acker, C.R. Janssen, H.F. De Brabander, L. Vanhaecke, Characterisation of steroids in wooden crates of veal calves by accelerated solvent extraction (ASE) and ultra-high performance liquid chromatography coupled to triple quadrupole mass spectrometry (U-HPLC-QqQ-MS-MS), Anal Bioanal Chem, 397 (2010) 345-355.
[45] N. Shama, S.W. Bai, B.C. Chung, B.H. Jung, Quantitative analysis of 17 amino acids in the connective tissue of patients with pelvic organ prolapse using capillary electrophoresis-tandem mass spectrometry, J Chromatogr B Analyt Technol Biomed Life Sci, 865 (2008) 18-24.
[46] A. Le, A. Ng, T. Kwan, K. Cusmano-Ozog, T.M. Cowan, A rapid, sensitive method for quantitative analysis of underivatized amino acids by liquid chromatography-tandem

mass spectrometry (LC-MS/MS), Journal of chromatography. B, Analytical technologies in the biomedical and life sciences, 944 (2014) 166-174.
[47] X.E. Zhao, S. Zhu, H. Yang, J. You, F. Song, Z. Liu, S. Liu, Simultaneous determination of amino acid and monoamine neurotransmitters in PC12 cells and rats models of Parkinson's disease using a sensitizing derivatization reagent by UHPLC-MS/MS, Journal of chromatography. B, Analytical technologies in the biomedical and life sciences, 995-996 (2015) 15-23.
[48] J. Han, Y. Liu, R. Wang, J. Yang, V. Ling, C.H. Borchers, Metabolic profiling of bile acids in human and mouse blood by LC-MS/MS in combination with phospholipid-depletion solid-phase extraction, Analytical chemistry, 87 (2015) 1127-1136.
[49] I. Bobeldijk, M. Hekman, J. de Vries-van der Weij, L. Coulier, R. Ramaker, R. Kleemann, T. Kooistra, C. Rubingh, A. Freidig, E. Verheij, Quantitative profiling of bile acids in biofluids and tissues based on accurate mass high resolution LC-FT-MS: compound class targeting in a metabolomics workflow, Journal of chromatography. B, Analytical technologies in the biomedical and life sciences, 871 (2008) 306-313.
[50] P. Montuschi, S. Martello, M. Felli, C. Mondino, M. Chiarotti, Ion trap liquid chromatography/tandem mass spectrometry analysis of leukotriene B4 in exhaled breath condensate, Rapid communications in mass spectrometry : RCM, 18 (2004) 2723-2729.
[51] I. Squellerio, B. Porro, P. Songia, F. Veglia, D. Caruso, E. Tremoli, V. Cavalca, Liquid chromatography-tandem mass spectrometry for simultaneous measurement of thromboxane B2 and 12(S)-hydroxyeicosatetraenoic acid in serum, J Pharm Biomed Anal, 96 (2014) 256-262.
[52] N. Sriboonvorakul, N. Leepipatpiboon, A.M. Dondorp, T. Pouplin, N.J. White, J. Tarning, N. Lindegardh, Liquid chromatographic-mass spectrometric method for simultaneous determination of small organic acids potentially contributing to acidosis in severe malaria, J Chromatogr B Analyt Technol Biomed Life Sci, 941 (2013) 116-122.
[53] W. Jian, R.W. Edom, X. Xue, M.Q. Huang, A. Fourie, N. Weng, Quantitation of leukotriene B4 in human sputum as a biomarker using UPLC-MS/MS, Journal of Chromatography B: Analytical Technologies in the Biomedical and Life Sciences, 932 (2013) 59-65.
[54] Y. Zhang, G. Zhang, P.A. Clarke, J.T.J. Huang, E. Takahashi, D. Muirhead, R.C. Steenwyk, Z. Lin, Simultaneous and high-throughput quantitation of urinary tetranor PGDM and tetranor PGEM by online SPE-LC–MS/MS as inflammatory biomarkers, Journal of Mass Spectrometry, 46 (2011) 705-711.
[55] L. Kortz, J. Dorow, S. Becker, J. Thiery, U. Ceglarek, Fast liquid chromatography-quadrupole linear ion trap-mass spectrometry analysis of polyunsaturated fatty acids and eicosanoids in human plasma, Journal of chromatography. B, Analytical technologies in the biomedical and life sciences, 927 (2013) 209-213.
[56] S. Noble, D. Neville, R. Houghton, Determination of 8-iso-prostaglandin F2α (8-iso-PGF2α) in human urine by ultra-performance liquid chromatography–tandem mass spectrometry, Journal of Chromatography B, 947–948 (2014) 173-178.
[57] R.S. Bhatta, H. Chandasana, C. Rathi, D. Kumar, Y.S. Chhonker, G.K. Jain, Bioanalytical method development and validation of natamycin in rabbit tears and its application to ocular pharmacokinetic studies, J Pharm Biomed Anal, 54 (2011) 1096-1100.
[58] A. Basit, D. Piomelli, A. Armirotti, Rapid evaluation of 25 key sphingolipids and phosphosphingolipids in human plasma by LC-MS/MS, Anal Bioanal Chem, 407 (2015) 5189-5198.
[59] S. Ghassabian, L. Griffiths, M.T. Smith, A novel fully validated LC–MS/MS method for quantification of pyridoxal-5′-phosphate concentrations in samples of human whole blood, Journal of Chromatography B, 1000 (2015) 77-83.

[60] S. Zhang, W. Jian, S. Sullivan, B. Sankaran, R.W. Edom, N. Weng, D. Sharkey, Development and validation of an LC–MS/MS based method for quantification of 25 hydroxyvitamin D2 and 25 hydroxyvitamin D3 in human serum and plasma, Journal of Chromatography B, 961 (2014) 62-70.
[61] H. Jiang, F.-F. Hsu, M. Farmer, L. Peterson, J. Schaffer, D. Ory, X. Jiang, Development and validation of LC-MS/MS method for determination of very long acyl chain (C22:0 and C24:0) ceramides in human plasma, Analytical and bioanalytical chemistry, 405 (2013) 7357-7365.
[62] S. Ghassabian, N.S.A. Rethwan, L. Griffiths, M.T. Smith, Fully validated LC–MS/MS method for quantification of homocysteine concentrations in samples of human serum: A new approach, Journal of Chromatography B, 972 (2014) 14-21.
[63] J. Galba, A. Michalicova, V. Parrak, M. Novak, A. Kovac, Quantitative analysis of phenylalanine, tyrosine, tryptophan and kynurenine in rat model for tauopathies by ultra-high performance liquid chromatography with fluorescence and mass spectrometry detection, J Pharm Biomed Anal, 117 (2016) 85-90.
[64] S.F. Soh, X. Yin, J. Sun, J. Li, E.L. Yong, Q. Wei, Y. Gong, Simultaneous determination of multiple androgens in mice organs with liquid chromatography tandem mass spectrometry, J Pharm Biomed Anal, 115 (2015) 457-466.
[65] R. Sidhu, H. Jiang, N.Y. Farhat, N. Carrillo-Carrasco, M. Woolery, E. Ottinger, F.D. Porter, J.E. Schaffer, D.S. Ory, X. Jiang, A validated LC-MS/MS assay for quantification of 24(S)-hydroxycholesterol in plasma and cerebrospinal fluid, Journal of lipid research, 56 (2015) 1222-1233.
[66] S. Ongay, G. Hendriks, J. Hermans, M. van den Berge, N.H. ten Hacken, N.C. van de Merbel, R. Bischoff, Quantification of free and total desmosine and isodesmosine in human urine by liquid chromatography tandem mass spectrometry: a comparison of the surrogate-analyte and the surrogate-matrix approach for quantitation, J Chromatogr A, 1326 (2014) 13-19.
[67] M.E. Lame, E.E. Chambers, M. Blatnik, Quantitation of amyloid beta peptides Abeta(1-38), Abeta(1-40), and Abeta(1-42) in human cerebrospinal fluid by ultra-performance liquid chromatography-tandem mass spectrometry, Anal Biochem, 419 (2011) 133-139.
[68] M. Berna, L. Ott, S. Engle, D. Watson, P. Solter, B. Ackermann, Quantification of NTproBNP in rat serum using immunoprecipitation and LC/MS/MS: a biomarker of drug-induced cardiac hypertrophy, Anal Chem, 80 (2008) 561-566.
[69] H.D. Cox, J. Rampton, D. Eichner, Quantification of insulin-like growth factor-1 in dried blood spots for detection of growth hormone abuse in sport, Anal Bioanal Chem, 405 (2013) 1949-1958.
[70] N. Cooper, R. Khosravan, C. Erdmann, J. Fiene, J.W. Lee, Quantification of uric acid, xanthine and hypoxanthine in human serum by HPLC for pharmacodynamic studies, J Chromatogr B Analyt Technol Biomed Life Sci, 837 (2006) 1-10.
[71] P. Keski-Rahkonen, M. Lehtonen, J. Ihalainen, T. Sarajarvi, S. Auriola, Quantitative determination of acetylcholine in microdialysis samples using liquid chromatography/atmospheric pressure spray ionization mass spectrometry, Rapid Commun Mass Spectrom, 21 (2007) 2933-2943.
[72] G. Zhang, Y. Zhang, C. Ji, T. McDonald, J. Walton, E.A. Groeber, R.C. Steenwyk, Z. Lin, Ultra sensitive measurement of endogenous epinephrine and norepinephrine in human plasma by semi-automated SPE-LC–MS/MS, Journal of Chromatography B, 895–896 (2012) 186-190.
[73] Y. Xu, Y. Yuan, L. Smith, R. Edom, N. Weng, R. Mamidi, J. Silva, D.C. Evans, H.K. Lim, LC-ESI-MS/MS quantification of 4beta-hydroxycholesterol and cholesterol in plasma samples of limited volume, J Pharm Biomed Anal, 85 (2013) 145-154.

[74] D. Zhang, D.R. Rios, V.H. Tam, D.S.L. Chow, Development and validation of a highly sensitive LC–MS/MS assay for the quantification of arginine vasopressin in human plasma and urine: Application in preterm neonates and child, Journal of pharmaceutical and biomedical analysis, 99 (2014) 67-73.
[75] J. Zhang, M. Yasuda, R.J. Desnick, M. Balwani, D. Bishop, C. Yu, A LC–MS/MS method for the specific, sensitive, and simultaneous quantification of 5-aminolevulinic acid and porphobilinogen, Journal of Chromatography B, 879 (2011) 2389-2396.
[76] P. Keski-Rahkonen, R. Desai, M. Jimenez, D.T. Harwood, D.J. Handelsman, Measurement of Estradiol in Human Serum by LC-MS/MS Using a Novel Estrogen-Specific Derivatization Reagent, Analytical Chemistry, (2015).
[77] C. Steiner, A. von Eckardstein, K.M. Rentsch, Quantification of the 15 major human bile acids and their precursor 7α-hydroxy-4-cholesten-3-one in serum by liquid chromatography–tandem mass spectrometry, Journal of Chromatography B, 878 (2010) 2870-2880.
[78] T. Goto, K.T. Myint, K. Sato, O. Wada, G. Kakiyama, T. Iida, T. Hishinuma, N. Mano, J. Goto, LC/ESI-tandem mass spectrometric determination of bile acid 3-sulfates in human urine: 3β-Sulfooxy-12α-hydroxy-5β-cholanoic acid is an abundant nonamidated sulfate, Journal of Chromatography B, 846 (2007) 69-77.
[79] X. Xiang, Y. Han, M. Neuvonen, J. Laitila, P.J. Neuvonen, M. Niemi, High performance liquid chromatography–tandem mass spectrometry for the determination of bile acid concentrations in human plasma, Journal of Chromatography B, 878 (2010) 51-60.
[80] K. Minato, M. Suzuki, H. Nagao, R. Suzuki, H. Ochiai, Development of analytical method for simultaneous determination of five rodent unique bile acids in rat plasma using ultra-performance liquid chromatography coupled with time-of-flight mass spectrometry, J Chromatogr B Analyt Technol Biomed Life Sci, 1002 (2015) 399-410.
[81] H. Wang, C.-Y. Yeh, K. Li, Y.-W. Chung-Davidson, W. Li, An UPLC–MS/MS method for quantitative profiling of bile acids in sea lamprey plasma and tissues, Journal of Chromatography B, 980 (2015) 72-78.
[82] S.P. Bathena, J. Huang, M.E. Nunn, T. Miyamoto, L.C. Parrish, M.S. Lang, T.P. McVaney, M.L. Toews, D.R. Cerutis, Y. Alnouti, Quantitative determination of lysophosphatidic acids (LPAs) in human saliva and gingival crevicular fluid (GCF) by LC–MS/MS, Journal of pharmaceutical and biomedical analysis, 56 (2011) 402-407.
[83] J. Palandra, J. Prusakiewicz, J.S. Ozer, Y. Zhang, T.G. Heath, Endogenous ethanolamide analysis in human plasma using HPLC tandem MS with electrospray ionization, J Chromatogr B Analyt Technol Biomed Life Sci, 877 (2009) 2052-2060.
[84] B. Zhu, F. Liu, X. Li, Y. Wang, X. Gu, J. Dai, G. Wang, Y. Cheng, C. Yan, Fast quantification of endogenous carbohydrates in plasma using hydrophilic interaction liquid chromatography coupled with tandem mass spectrometry, Journal of separation science, 38 (2015) 34-41.
[85] J.C. Seegmiller, D.R. Barnidge, B.E. Burns, T.S. Larson, J.C. Lieske, R. Kumar, Quantification of Urinary Albumin by Using Protein Cleavage and LC-MS/MS, Clinical Chemistry, 55 (2009) 1100-1107.
[86] T. Kamceva, T. Bjanes, A. Svardal, B. Riedel, J. Schjott, T. Eide, Liquid chromatography/tandem mass spectrometry method for simultaneous quantification of eight endogenous nucleotides and the intracellular gemcitabine metabolite dFdCTP in human peripheral blood mononuclear cells, J Chromatogr B Analyt Technol Biomed Life Sci, 1001 (2015) 212-220.
[87] S. Ogawa, K. Tomaru, N. Matsumoto, S. Watanabe, T. Higashi, LC/ESI-MS/MS method for determination of salivary eicosapentaenoic acid concentration to arachidonic acid concentration ratio, Biomedical Chromatography, (2015) n/a-n/a.

[88] D. French, Development and validation of a serum total testosterone liquid chromatography-tandem mass spectrometry (LC-MS/MS) assay calibrated to NIST SRM 971, Clin Chim Acta, 415 (2013) 109-117.
[89] T. Soeborg, H. Frederiksen, P. Fruekilde, T.H. Johannsen, A. Juul, A.M. Andersson, Serum concentrations of DHEA, DHEAS, 17alpha-hydroxyprogesterone, Delta4-androstenedione and testosterone in children determined by TurboFlow-LC-MS/MS, Clin Chim Acta, 419 (2013) 95-101.
[90] H.P. Nguyen, L. Li, J.W. Gatson, D. Maass, J.G. Wigginton, J.W. Simpkins, K.A. Schug, Simultaneous quantification of four native estrogen hormones at trace levels in human cerebrospinal fluid using liquid chromatography-tandem mass spectrometry, J Pharm Biomed Anal, 54 (2011) 830-837.
[91] A. Szeitz, J. Manji, K.W. Riggs, A. Thamboo, A.R. Javer, Validated assay for the simultaneous determination of cortisol and budesonide in human plasma using ultra high performance liquid chromatography-tandem mass spectrometry, J Pharm Biomed Anal, 90 (2014) 198-206.
[92] S. Kang, S.M. Oh, K.H. Chung, S. Lee, A surrogate analyte-based LC-MS/MS method for the determination of gamma-hydroxybutyrate (GHB) in human urine and variation of endogenous urinary concentrations of GHB, J Pharm Biomed Anal, 98 (2014) 193-200.
[93] W. Li, L.H. Cohen, Quantitation of endogenous analytes in biofluid without a true blank matrix, Anal Chem, 75 (2003) 5854-5859.
[94] M. Jemal, A. Schuster, D.B. Whigan, Liquid chromatography/tandem mass spectrometry methods for quantitation of mevalonic acid in human plasma and urine: method validation, demonstration of using a surrogate analyte, and demonstration of unacceptable matrix effect in spite of use of a stable isotope analog internal standard, Rapid Commun Mass Spectrom, 17 (2003) 1723-1734.
[95] H.R. Liang, T. Takagaki, R.L. Foltz, P. Bennett, Quantitative determination of endogenous sorbitol and fructose in human nerve tissues by atmospheric-pressure chemical ionization liquid chromatography/tandem mass spectrometry, Rapid Commun Mass Spectrom, 19 (2005) 2284-2294.
[96] H.R. Liang, T. Takagaki, R.L. Foltz, P. Bennett, Quantitative determination of endogenous sorbitol and fructose in human erythrocytes by atmospheric-pressure chemical ionization LC tandem mass spectrometry, J Chromatogr B Analyt Technol Biomed Life Sci, 824 (2005) 36-44.
[97] B.R. Jones, G.A. Schultz, J.A. Eckstein, B.L. Ackermann, Surrogate matrix and surrogate analyte approaches for definitive quantitation of endogenous biomolecules, Bioanalysis, 4 (2012) 2343-2356.
[98] A.K. Goodenough, J.M. Onorato, Z. Ouyang, S. Chang, A.D. Rodrigues, S. Kasichayanula, S.P. Huang, W. Turley, R. Burrell, M. Bifano, M. Jemal, F. LaCreta, A. Tymiak, D. Wang-Iverson, Quantification of 4-beta-hydroxycholesterol in human plasma using automated sample preparation and LC-ESI-MS/MS analysis, Chem Res Toxicol, 24 (2011) 1575-1585.
[99] M. Bader, A systematic approach to standard addition methods in instrumental analysis, Journal of Chemical Education, 57 (1980) 703.
[100] D.H. Owen, D.F. Katz, A vaginal fluid simulant, Contraception, 59 (1999) 91-95.
[101] D.H. Owen, D.F. Katz, A review of the physical and chemical properties of human semen and the formulation of a semen simulant, J Androl, 26 (2005) 459-469.
[102] T. Tanaka, Y. Hayashi, Determination of silicon, calcium, magnesium and phosphorus in urine using inductively-coupled plasma emission spectrometry and a matrix-matching technique, Clin Chim Acta, 156 (1986) 109-113.

[103] D. Mirejovsky, A.S. Patel, D.D. Rodriguez, T.J. Hunt, Lipid adsorption onto hydrogel contact lens materials. Advantages of Nile red over oil red O in visualization of lipids, Optom Vis Sci, 68 (1991) 858-864.
[104] K. Oka, M. Yamamoto, T. Nonaka, M. Tomonaga, The significance of artificial cerebrospinal fluid as perfusate and endoneurosurgery, Neurosurgery, 38 (1996) 733-736.
[105] R.C. Mashru, V.B. Sutariya, M.G. Sankalia, P.P. Parikh, Development and evaluation of fast-dissolving film of salbutamol sulphate, Drug Dev Ind Pharm, 31 (2005) 25-34.
[106] A. Karlsen, R. Blomhoff, T.E. Gundersen, High-throughput analysis of vitamin C in human plasma with the use of HPLC with monolithic column and UV-detection, J Chromatogr B Analyt Technol Biomed Life Sci, 824 (2005) 132-138.
[107] U.S. Department of Health and Human Services, Food and Drug Administration, Guidance for Industry, Bioanalytical Method Validation, Draft Guidance, September 2013 (http://www.fda.gov/downloads/drugs/guidancecomplianceregulatoryinformation/guidances/ucm368107.pdf).
[108] European Medicines Agency, Comittee for Medicinal Product for Human Use, Guideline on bioanalytical method validation, July 2011 (http://www.ema.europa.eu/docs/en_GB/document_library/Scientific_guideline/2011/08/WC500109686.pdf).
[109] U.S. Department of Health and Human Services, Food and Drug Administration, Guidance for Industry, Bioanalytical Method Validation, May 2001 (http://www.fda.gov/downloads/Drugs/Guidance/ucm070107.pdf).

CHAPTER 4

SIMULTANEOUS LC-MS/MS ANALYSIS OF EICOSANOIDS AND RELATED METABOLITES IN HUMAN SERUM, SPUTUM, AND BALF

4.1 Introduction

Polyunsaturated fatty acids (PUFAs) are precursors of oxylipins, a large family of metabolites involved in various physiological roles such as regulation of cell proliferation, tissue repair, coagulation, and immune functions. The eicosanoids are a large subclass of oxylipins, which includes over 100 lipid mediators such as prostaglandins (PG), thromboxanes (TX), leukotrienes (LT), hydroxyeicosatetraenoic acids (HETEs), dihydroxy-eicosatetraenoic acids (DHETs), hydroxyeicosapentaenoic acids (HEPEs), lipoxins (LXs), reolvins (RvEs) and epoxyeicosatrienoic acids (EET) [1, 2]. Eicosanoids are synthesized from dihomo gamma-linolenic acid (DGLA), arachidonic acid (AA), and eicosapentaenoic acid (EPA) via different enzymes such as cyclooxygenase enzymes (COX), lipoxygenase enzymes (LOX), cytochrome P450, as well as by non-enzymatic oxidation [3, 4].

Disruption of the homeostasis of eicosanoids is closely related to a range of inflammatory pathological conditions including asthma and chronic obstructive pulmonary disease (COPD), fever, pain, nephritis, cardiovascular diseases, Crohn's disease, and cancer [5-9]. PGE2 regulates tumor angiogenesis in prostate cancer [10], whereas LTs and LXs regulate vasoconstriction and vascular permeability [11, 12]. 20-HETE regulates cerebral microvessel constriction [13], conversely, EET metabolites increase cerebral blood flow [14].

Given the clinical interest in eicosanoids and the complexity of their responses to biological stimuli, it is necessary to systematically monitor the changes in their concentrations in various tissues and biological fluids. This requires sensitive, selective,

and reproducible methods for their quantification. Quantification of eicosanoids in biological matrices is associated with numerous challenges including their low concentrations (pM-nM range) in biological fluids. Some eicosanoids are unstable and can also be formed artificially *ex vivo* after sample collection and during sample preparation. This could be overcome by measuring more stable metabolites as surrogates for their unstable parent compounds. For example, TxB2 and 6-keto-PGF1α are measured as surrogates for TxA2 and PGI2, respectively [15-17]. Other challenges include the presence of multiple isomeric forms that share the same mass and fragmentation pattern, which makes it difficult to resolve them by mass spectrometry and by chromatography [18].

A broad range of techniques have been employed for the separation, detection, and quantification of eicosanoids, including HPLC-UV [19-23], enzyme immunoassays [24, 25], LC–fluorescence detection [26, 27], electrophoresis [28, 29], immuno-affinity chromatography (IAC) [30], gas chromatography–mass spectrometry (GC-MS) [18, 31-33] and liquid chromatography–mass spectrometry (LC–MS) [34-40]. HPLC-UV requires active chromophore to quantify eicosanoids. The main disadvantages of HPLC-UV are the limited sensitivity and specificity of UV detection in complex biological matrices, which typically require long run times [19-23]. Moreover, not all eicosanoids have active chromophores that absorb UV light at appropriate wavelengths [23, 41]. Disadvantages of UV detection can be overcome by using fluorescence detection. However, eicosanoids does not have inherent fluorescence signal and requires derivatization with fluorescent agents. This process is labor intensive, expensive, time consuming, and produce interfering peaks from side reactions [27, 42]. Immunoassays were also used to quantify eicosanoids, but they are limited to one analyte per assay and they suffer from high cross reactivity between the numerous eicosanoid isomers [24, 25]. GC-MS/MS provide high sensitivity and resolution of isomeric eicosanoids but this

technique is limited by complex sample preparation and derivatization [18, 42, 43]. The high sensitivity and selectivity of LC-MS/MS can overcome most of the above mentioned limitations, which makes it the method of choice for the quantification of eicosanoids in biological matrices. Many LC-MS/MS methods, which have been reviewed recently [18, 42, 44, 45], have been reported for the quantification of a variety of eicosanoids in plasma [34-36], serum [37, 46], blood [40], urine [38, 39, 47], tissues [26, 48, 49], lung cells [50], cell culture media [51], sputum [52, 53], and bronchial alveolar lavage fluid (BALF) [54]. The long-term goal of this project is to support a clinical study that aims to identify eicosanoids-based biomarkers for the prognosis of COPD. Despite, the plethora of available eicosanoid LC-MS methods as cited above, we needed a sensitive method for the simultaneous quantification of specific eicosanoids in several matrices of interest to support our biomarker study. Therefore, we have developed and validated a sensitive and simple LC–MS/MS method for the simultaneous quantification of 34 eicosanoids in human serum, sputum, and BALF.

4.2 Experimental

4.2.1 Chemicals and Reagents

Prostaglandin J2 (PGJ2), 20-hydroxy prostaglandin E2 (20-OH-PGE2), prostaglandin B2 (PGB2), prostaglandin D2 (PGD2), prostaglandin E2 (PGE2), arachidonic acid (AA), 15-hydroxyeicosatetraenoic acid (15-HETE), 12-hydroxyeicosatetraenoic acid (12-HETE), 11-hydroxyeicosatetraenoic acid (11-HETE), 8-hydroxyeicosatetraenoic acid (8-HETE), 5-hydroxyeicosatetraenoic acid (5-HETE), leukotriene E4 (LTE4), leukotriene D4 (LTD4), leukotriene C4 (LTC4), leukotriene B4 (LTB4), 13,14-dihydro-15-keto-prostaglandin E2 (13,14-dihydro-15-keto-PGE2), 11-Beta prostaglandin F2α (11-β-PGF2α), 8-iso prostaglandin F2α (8-iso-PGF2α), prostaglandin F2α (PGF2α), 15-keto-prostaglandin E2 (15-keto-PGE2), 6-keto-prostaglandin F1α (6-keto-PGF1α), thromboxane B2 (TXB2), 13,14-dihydro-prostaglandin F2α (13,14-DiOH-

PGF2α), prostaglandin F1α (PGF1α), 13,14-dihydro-15-keto-prostaglandin F2α (13,14-DiOH-15-keto-PGF2α), 13,14-dihydro-15-keto-prostaglandin E1 (13,14-DiOH-15-k-PGE1), prostaglandin D1 (PGD1), 13,14-dihydro-prostaglandin E1 (13,14-DiOH-PGE1), thromboxane B3 (TXB3), 15- deoxy-delta 12,14 Prostaglandin J2 (15- deoxy-delta 12,14 PGJ2), prostaglandin E1 (PGE1), prostaglandin E3 (PGE3), prostaglandin D3 (PGD3), prostaglandin F3 α (PGF3α), 13,14-leukotriene C4 (13,14 LTC4), tetranor-prostaglandin E metabolite (tetranor-PGEM), tetranor-prostaglandin F metabolite (tetranor- PGFM), 11-dehydro-thromboxane B3 (11-dehydro-TXB3), 2,3-dinor-8-iso prostaglandin F2α (2,3-dinor-8-iso PGF2α), and deuterated compounds (PGE2 -d4, TXB2-d4, AA-d8, 15-HETE-d8,and LTB4-d8) were purchased from Cayman Chemicals (Ann Arbor, MI, USA). HPLC-grade methanol (MeOH), acetonitrile (ACN), water, ammonium acetate, aqueous ammonia, formic acid, and acetic acid were obtained from Fisher Scientific (Fair Lawn, NJ).

4.2.2 Instrumentation

A Waters ACQUITY ultra performance liquid chromatography (UPLC) system (Waters, Milford, MA) coupled to an Applied Biosystem 6500 Q TRAP® quadrupole linear ion trap hybrid mass spectrometer with an electrospray ionization (ESI) source (Applied Biosystems, MDS Sciex, Foster City, CA) was used throughout. The UPLC and MS systems were controlled by Empower 3.0 and Analyst 1.6.2 software, respectively. All chromatographic separations were performed with an Acquity UPLC®BEH shield RP18 column (1.7µm, 150 x 2.1 mm) equipped with an Acquity UPLC C_{18} guard column (Waters, Milford, MA).

4.2.3 Liquid chromatographic and Mass spectrometric Conditions

The mobile phase consisted of 0.1% acetic acid in water (mobile phase A) and 0.1% acetic acid in ACN: MeOH (90:10) (mobile phase B), at total flow rate of 0.3 ml/min. The chromatographic separation was achieved using 25 min gradient elution.

The initial mobile phase composition was 20 % B for the first 3.0 min, gradually increased to 65% B in 13 min, gradually increased to 95% B in 3.0 min, then held constant at 95% B for 4.0 min, and finally brought back to initial condition of 20 % B in 0.20 min followed by 2-min re-equilibration. The injection volume of all samples was 10µl.

The mass spectrometer parameters, such as temperature, voltage, gas pressure, etc., were optimized by infusing each analyte and the internal standard (IS) using a 5 µg/ml solution in 50% MeOH via a Harvard '22' standard infusion syringe pump (Harvard Apparatus, South Natick, MA, USA) at 10 µl/min. All eicosanoids were detected in the negative ionization mode and deprotonated molecules were used as the precursors for selected reaction monitoring (SRM) with the following mass spectrometer source settings: ion spray voltage, -4000 V; source temperature, 500 °C, curtain gas, 15 AU; gas-1, 40 AU, gas-2, 40 AU, collision gas pressure, high; Q1/Q3 resolution, high; and interface heater, on. SRM transitions for each analyte and IS, as well as their respective optimum MS parameters, such as declustering potential (DP), and collision energy (CE), are shown in **Table 4.1**.

4.2.4. Preparation of Charcoal-stripped Serum for Calibration Curves

Serum was stripped with activated charcoal to remove endogenous eicosanoids. Twelve mL charcoal suspension (0.66 g of dextran-coated charcoal in 100 ml of Dulbecco's Phosphate buffered saline (DPBS)) was transferred into a glass tube, centrifuged at 4000 g for 15 minutes at 4°C, and the supernatant DPBS was discarded. Serum (6.0 ml) was then added on to the charcoal pellet under continuous stirring at 37 ± 1°C for two hours, centrifuged at 13,000 g for 15 min, and the supernatant was collected. The process was repeated a second time for maximal removal of endogenous eicosanoids. This stripped serum was used to construct serum calibration curves.

4.2.5 Preparation of Standard Solutions and Calibration Curves

Aliquots from original stock solutions of every analyte were mixed to prepare spiking solution mixtures, which were stored in -80 °C. Blank serum (pooled, n=10) was purchased from Equitech Enterprises, Inc, (Kerriville, Texas, USA) and stripped from endogenous eicosanoids as described above. Blank sputum and BALF were collected from healthy control subjects. Stripped serum was used to construct serum calibration curves, whereas sputum and BALF calibration curves were prepared in untreated matrices.

The calibration ranges of the various eicosanoids were divided in to three categories: 0.2- 500 ng/mL, 1-500 ng/mL and 3-500 ng/mL. Five hundred □l of stripped blank serum, 10x-diluted stripped blank serum, untreated blank sputum, and BALF were spiked with spiking analyte (10X) and IS (10X) solutions, 10□□l each, and vortexed for 30 seconds. Samples were then extracted as described below and reconstituted in a 100 µl of 50% ACN in deionized water. Five stable-labeled eicosanoids were used as internal standards (IS) for the different analytes as described in **table 4.1**. The final concentration of all five ISs was 100 ng/ml and the final concentration of analytes in standards and QC samples are listed in **table 4.2**.

4.2.6 Sample preparation

For serum, sputum, and BALF samples, Oasis® HLB 3cc (60mg) SPE cartridges (Waters, Milford, MA) were used for sample extraction. A 500 µL samples were spiked with 10 µl IS, and diluted with 1500 µL 5% acetic acid in water, vortexed, and loaded onto SPE cartridges pre-conditioned with two ml MeOH, followed by two ml 0.1% acetic acid in H_2O. Loaded cartridges were washed with two ml 0.1% acetic acid in H_2O and eluted with 2 ml MeOH. Eluates were evaporated under vacuum at room temperature and reconstituted in 100 µL of 50% ACN in water i.e. samples were concentrated by 5 folds after evaporation and reconstitution.

4.2.7 Extraction Recovery

Recoveries of analytes and labeled ISs from charcoal-stripped serum, 10-x diluted charcoal-stripped serum, original serum, 10-x diluted serum, sputum and BALF were determined by dividing the peak area ratio of analyte to IS (after subtracting any endogenous background) from blank samples spiked before extraction to those from neat un-extracted standards for both the low and high QCs (n = 5).

4.2.8 Method Validation

The ratios of analyte to IS and the $1/x^2$ weighting scheme was used in all calibration curves. The method was validated using five QC points for each calibration curve and the concentrations of the QC points are shown in **table 4.2**. Five replicates of each QC point were analyzed each day to determine the intra- and inter-day accuracy and precision. This process was repeated three times over three days in order to determine the inter-day accuracy and precision using freshly prepared calibration curves. Intra-day accuracy and precision were calculated from the % bias [% (measured – theoretical)/measured concentrations] and relative standard deviation [%RSD = %standard deviation/mean], respectively, for the five replicates of each QC point. Inter-day accuracy and precision were calculated similarly using the 15 replicates of each QC point from the three validation runs.

4.2.9 Stability Studies

Stability experiments were carried out to examine the analyte stability in stock solutions, original matrices (samples spiked, stored at different conditions, then extracted before analysis), and extracted matrices (samples spiked, extracted, then stored at different conditions after extraction) under different conditions. Stability studies included auto-sampler stability (at 4 °C for 48 hr), bench-top stability (at room temperature for 8 hr), freeze-thaw stability (three freeze-thaw cycles), and long-term stability (at -20 °C and at -80 °C for 6 months), for both the low and high QCs (n = 3).

4.2.10 Human Subjects

This work was performed as a part of a clinical trial that aims to determine the role of the inhibition of prostaglandin E (PGE) production in restoring lung repair processes and thus improve outcomes of COPD. This study was approved by the institutional review board (IRB) at the clinical sites where the samples were collected and written informed consent was obtained from all individuals. In the healthy control arm of this study, control healthy subjects, age >45, who have no medical conditions that place them at untoward risk for bronchoscopy and broncho alveolar lavage were recruited after obtaining written consents. Healthy non-smoking controls were recruited locally either from prior study participants or de novo and, other than smoking history, they met the same criteria as smoking controls and had no emphysema defined as less than 3% of lung voxels with density less than -950 Hounsfield units on quantitative CT scan. In addition, control subjects had post bronchodilator forced expiratory volume in one second (FEV_1) greater than or equal to 80% predicted and an FEV_1/Forced Vital Capacity (FVE) ratio of at least 0.7. Serum, BALF, and sputum samples were collected and stored in -80 °C until the time of LC-MS/MS analysis.

4.3 Results

4.3.1 LC-MS/MS Method Development

In this study, a LC-MS/MS method for the quantification of eicosanoids from different classes including PGs, TBXs, HETE, AA, and LTs in human serum, sputum, and BALF was developed and validated. All eicosanoids have a free carboxylic acid functional group, which ionized efficiently in the negative ionization mode. **Table 4.1** summarizes the MS/MS conditions used to quantify all 34 eicosanoids. **Figure 1** shows a representative LC-MS/MS chromatogram of all eicosanoid standards. Mass spectrometer parameters were optimized during method development to maximize not only sensitivity but also selectivity. For example, several HETEs shared the same

precursor as well as fragment masses; therefore, the most selective rather than the most sensitive SRM transitions were used for the quantification of these analytes (**Figure 4.2**).

LC conditions were optimized to separate all eicosanoids of interest with a desirable peak shape and signal intensity using an Acquity UPLC®BEH shield RP18 column (1.7µm, 150 × 2.1 mm). Different mobile phases with a pH range of 3-9, were screened to optimize LC conditions. The less hydrophobic eicosanoids including PGs, TXs and LTs eluted earlier and largely independent of the mobile phase pH. In contrast, acidic pH mobile phases resulted in better peak shape and longer retention of the more hydrophobic eicosanoids including HETEs and AA. Therefore, acetic acid was used as an aqueous and organic mobile phase modifier.

Many eicosanoids are isobaric compounds that share the same parent mass and also the same fragmentation pattern such as PGE2, PGD2 and, 13, 14-dihydro-15-k-PGE2. Therefore, these compounds have to be chromatographically resolved (**Figure 4.3**). Moreover, eicosanoids can undergo in-source fragmentation into other eicosanoids; therefore, even some analytes with different masses have to be resolved chromatographically to distinguish in-source fragments from other analytes (**Figure 4.3**). Therefore, both chromatographic separation and MS/MS specificity were required to quantify all eicosanoids of interest. Under final chromatography conditions, more than 34 eicosanoids in human serum, sputum, and BALF were separated in 25 min.

Some eicosanoids (HETEs) had residual peak areas in serum after charcoal stripping. Therefore, calibration curves for these eicosanoids were constructed using 10x diluted charcoal stripped serum to decrease the residual peak areas after matrix stripping. Extraction recoveries were similar (90-115%) for these eicosanoids in diluted and undiluted serum and subsequently the method was validated with two sets of calibration curves, with and without 10-x diluted stripped serum.

4.3.2 Method Validation

The method was validated for each analyte using three calibration curves prepared on three days. **Table 4.2** shows the validation results in human serum including dynamic ranges and inter-day accuracy and precision values. Three dynamic ranges were used to cover all eicosanoids at relevant physiological concentrations in the various matrices, namely 0.2-500 ng/mL, 1-500 ng/mL, and 3-500 ng/mL.

The method of background subtraction was used to account for the background/endogenous concentrations in blank matrices before spiking with analyte standards. Therefore, the differences in the lower limit of quantification of the various eicosanoids are not necessarily due to differences in the sensitivity of the analytes, but rather due to the differences in the endogenous background levels in the blanks used for building the calibration curves. R^2 was higher than 0.998 for all eicosanoids in all matrices, confirming the linearity of the assay in the selected calibration ranges.

Intra-day and inter-day accuracy and precision were determined to evaluate the reliability and reproducibility of this method. **Table 4.2** shows the inter-day accuracy and precision of standards prepared in human serum. Validation data for all other matrices are shown in supplementary tables S1-3. Accuracy and precision were ≤20% at LLOQ and ≤15% at the other four QC concentrations for all eicosanoids in serum, sputum, and BALF.

4.3.3 Recovery

Several protein precipitation and SPE methods were investigated to increase extraction recovery and decrease matrix effect. The large variation in the physicochemical properties between different classes of eicosanoids resulted in different extraction recoveries of these compounds. The average extraction recovery of all analytes ranged from 57 to 115% in serum, 69 to 115% in 10-x dilute serum, 41 to 115% in BALF, 34 to 115% in sputum (data not shown). Our result confirms charcoal stripped

serum to mimic human serum with similar recovery rates using analyte/IS peak area ratios.

4.3.4 Stability Studies

Stability of eicosanoids in stocks and biological matrices were studied under various conditions as outlined in section 2.10. **Table 4.3** lists unstable analytes with >20% loss in peak area under the different storage conditions. Eicosanoids not listed in **Table 4.3** were stable under all storage conditions. All eicosanoids were stable in stock solutions and extracted serum in auto sampler at 4° C up to 24 h except compounds 8 and 27. However, by 48 hours the peak area of some eicosanoids decreased markedly (52-97%). Eicosanoids were also stable in stock solution, original matrix, and extracted matrix samples at room temperature on the bench up to 8 h except, 3, 18, 22, 27, 33, 39, 41, 42, 43, and 44 in serum which were stable only for 2 hours on the bench. In addition, compounds 15, 16, and 41 were stable in serum only for few minutes after spiking.

Under long-term storage conditions, eicosanoids were stable in stock solution and original matrices at -20 °C for up to 6 months except compounds 18, 22, 33, 38, 43 and 44 in serum. In addition, compounds 15, 16, 41 and 42 in serum, were stable only for seven days after spiking. In contrast, in extracted matrices, all eicosanoids except compounds 15 and 16 were stable only for 3 days at -20 °C and many started degrading after 7 days. In the -80 °C, all eicosanoid stocks were stable up to 6 months except for compounds 16 and 41, which were stable up to 2 months.

4.3.5 Human eicosanoids profiles

Eicosanoids profiles in serum, sputum and BALF of healthy human subjects were characterized using this LC-MS/MS method **(Table 4.4).** In accordance with previous reports, 12-HETE (22 ng/ml) and 8-HETE (0.6 ng/ml) were the HETEs with highest and lowest concentrations in serum, respectively [55, 56]. Among serum prostaglandins,

PGD2 and PGE2 have the highest concentrations (0.4 ng/ml), whereas PGJ2 (0.06 ng/ml) showed the lowest concentration. Among the three thromboxanes of interest, only TXB2 (6.4 ng/ml) was detected in serum. Eicosanoids concentrations in sputum and BALF were on average more than 10-x lower than serum. In sputum and BALF, highest concentrations were observed for HETEs (0.5-2 ng/ml). The concentrations reported in this manuscript were comparable with recent reports from healthy human subjects using LC-MS/MS analyses in serum [40, 55, 56] and sputum [52].

4.4 Discussion

Due to matrix effects on the ionization of analytes in the ESI MS source, it is critical to prepare calibration curves in the same or equivalent matrices as the study samples. This becomes a problem for endogenous analytes including eicosanoids, where analyte-free blank matrices are not available to spike with analyte standards of known concentrations for the construction of calibration curves. Various approaches are followed to solve the problem of endogenous background in blank matrices for the construction of calibration curves, which were reviewed recently [57]. These approaches including method of background subtraction [34], method of standard addition [36, 54, 58], surrogate analytes [59-61], and surrogate matrix [52, 62-69] were used for the quantification of eicosanoids in various biological matrices.

As we discussed previously [57], every one of these approaches has advantages and disadvantages. Therefore, we applied and compared the various approaches for the quantification of eicosanoids in serum and found that activated charcoal was the most accurate and convenient method for this application. Activated charcoal is an efficient adsorbent; consequently, blank serum free of eicosanoids was prepared by stripping serum from endogenous eicosanoids using activated charcoal. This eicosanoid-free serum was used to construct the calibration curves for the analyses of serum samples. The charcoal stripping conditions were optimized to maximize

eicosanoids depletion from serum. Most eicosanoids were completely depleted, but some eicosanoids (HETEs and LTB4) had trace residual peaks in serum after stripping with charcoal. For these eicosanoids, the background peak area of the remaining trace levels was subtracted from the peak area of the calibration curve standards, which allowed the construction of calibration curves with high accuracy and precision. Using analyte/IS peak area ratios, the recoveries of eicosanoids in the charcoal-stripped serum were similar to those in unstripped serum (data not shown), which indicates that matrix effect was the same for the study samples (unstripped serum) and calibration curve (stripped serum).

Three dynamic ranges were used to cover all analytes in serum, BALF, and sputum at relevant physiological concentrations, namely 0.2-500 ng/mL, 1-500 ng/mL, and 3-500 ng/mL. The different dynamic ranges were used because the various eicosanoids had different sensitivity, endogenous concentrations, and/or signal linearity. For example, the LLOQ of 5-HETE, 8-HETE, 11-HETE, 13-HETE, and 15-HETE was 3 ng/mL in serum, not due to limitations in detection sensitivity (limit of detection 0.1 ng/ml), but rather due to the relatively high residual background of these eicosanoids in the blank matrix used to construct the calibration curve after matrix stripping, which did not allow consistent subtraction from the peak areas of spiked-standards below 3 ng/ml. To quantify levels below 3 ng/ml, calibration curves were constructed using 10-fold diluted charcoal stripped serum to decrease the residual peak areas after matrix stripping. Consequently, the method was validated with two sets of calibration curves, one set in 10-x diluted stripped plasma and another in stripped undiluted plasma. Recoveries of these eicosanoids in undiluted and 10-x diluted serum were similar.

On the other hand, no matrix stripping was applied for BALF and sputum because we were able to obtain batches of blank matrices ranging from undetectable to

trace levels for most eicosanoids of interest, and this background was subtracted from the peak areas of calibration standards.

Eicosanoids comprise a large family of endogenous compounds, and many members of this family are isobaric with very similar physio-chemical properties including isomers and stereoisomers. Many eicosanoids, not only share the same mass, but also have the same fragmentation pattern, resulting into the same SRM transitions. Moreover, many eicosanoids undergo insource fragmentation, which results into fragments with similar masses to other eicosanoids. In addition, interfering peaks could arise from other unknown endogenous components of the matrix. Therefore, MS/MS specificity by itself is not always adequate to separate all eicosanoids, and chromatographic resolution is required for their separation in time. For example, the isobaric compounds PGE2, PGD2, and 13, 14-dihydro-15-k-PGE2 are identified through the same 351→333 SRM transition, but were separated chromatographically (retention time (RT) = 11.39, 11.77, and, 12.5 min, respectively) (Figure 3). Similarly, the isobaric compounds PGF2□, 11-□ PGF2□□ and 8-iso-PGF2□ are identified through the same 353.2→309.1 SRM transition but were separated chromatographically (RT = 11.7, 12.0, and, 13.0 min, respectively) (**Figure 4.1**). Variation in RT over the period of 12 months of utilization of this method for all analytes was less than 10%.

Under our final LC-MS/MS conditions, all eicosanoids of interest were resolved from each other in less than 25 min and all standards produced single peaks. One exception was TXB2 and TXB3 and their d4-labeled IS (TXB2-d4), each of which produced two peaks (completely chromatographically-resolved) that belonged to their anomers. Both anomers for both compounds were detected in standards as well biological samples. The peak areas for both anomers were summed together.

Moreover, eicosanoids can undergo in-source fragmentation into other eicosanoids, which means that, sometimes, even analytes with different masses have to

be resolved chromatographically to distinguish in-source fragments from other analytes. For example, PGJ2 (333.1→315.2) and 15-dexoxy-delta 12, 14-PGJ2 (315.2→271.2) have different parent as well as fragment masses, yet PGJ2 produces a shadow peak with the same SRM of 15-dexoxy-delta 12, 14-PGJ2, i.e. 315.2→271.2. Therefore, PGJ2 and 15-dexoxy-delta 12 14-PGJ2 had to be chromatographically resolved (**Figure 4.3**).

In addition to chromatographic resolution, isobaric compounds with similar SRMs can be distinguished if they produce specific SRMs, which may not be the most sensitive ones. For example, isobaric HETEs such as 8-HETE, 11-HETE, 5-HETE, and 12-HETE were not resolved chromatographically, but every isomer produced unique fragments that were not produced by the other isomers, namely 319→154.8, 319→167.2, 319→114.7, and 319→179, respectively, which was also shown previously [36, 45, 70, 71]. However, these specific SRMs were less sensitive than common SRMs such as 319→301.1 (**Figure 4.2**).

Although the detection and quantification of eicosanoids concentrations have become a routine analysis in many biomedical laboratories, only few reports have addressed eicosanoid stability under different storage and analysis conditions [35, 39, 64, 72-74]. Most of these studies have reported issues related to eicosanoid instability in original matrices or stock solutions for some eicosanoids. In this report, stability studies were carried out in stock solution, original matrices (serum), and extracted matrices. In autosampler, by 48 hours the peak area of some eicosanoids decreased markedly (52-97%). This could be a result of degradation and/or precipitation due to evaporation of organic solvent over time. Therefore, all samples were not stored in the auto-sampler longer than 24 hours. In contrast, in extracted matrices, all eicosanoids except compounds 15 and 16 were stable only for 3 days at -20 °C and many started degrading after 7 days. Therefore, extracted samples should be run or re-run within

three days from the time of sample preparation. Sample preparation, analyses, and storage conditions were adjusted in this method to ensure eicosanoid stability under these conditions.

Accordingly, we have excluded some eicosanoids from this method because they were not stable on the bench or in long-term (3, 15, 16, 41 and 42), in the autosampler (8, 27), storage for longer than 2 hours.

For valid quantitative analysis, analytical standards of high purity are always required. Some commercially available standards of eicosanoids contained impurities that were detected by LC-MS/MS at the time of purchase. For example, PGJ2 (1) contained 15-Keto-PGE2 (22) (0.28%), 15-deoxy-delta 12, 14 PGJ2 (36) (3.87%), PGE3 (38) (0.60%), unknown component (SRM = 222/123) (0.11%). Similarly, PGE3 (38) contained unknown component 1 (0.60%), component 2 (0.65%), and PGF3 (40) (5.67%). Another example is LTC4 (16), which contains an unknown component at SRM similar to that of 15-HETE (9) (0.11%) but with a different retention time, and LTD4 (15) (0.15%). These components could be impurities formed during the synthesis process, or degradants that formed after synthesis, during shipping, or during the 3 days' stocks were stored in the -80°from the time standards arrived to the time they were analyzed. Carry over and/or LC-MS system contamination was excluded by the lack of any of these impurities in injected blanks. The analytes were still included in the method because none of the validation criteria were compromised.

4.5 Conclusions

In summary, a LC-MS/MS method was developed for the simultaneous quantification of eicosanoids in human serum, BALF, and sputum. The method was sensitive, selective, accurate, and precise with a wide dynamic range. This method was successfully applied to the study of eicosanoid in healthy human subjects. The characterization of the detailed eicosanoids profile in healthy and COPD subjects will

facilitate a better understanding of the pathological and physiological role of eicosanoids in humans.

Figure 4.1 Representative chromatograms of all eicosanoid standards at 10 ng/ml under final chromatography and detection conditions in negative ESI mode. Peaks are labeled with analytes IDs and retention time as given in table 4.1

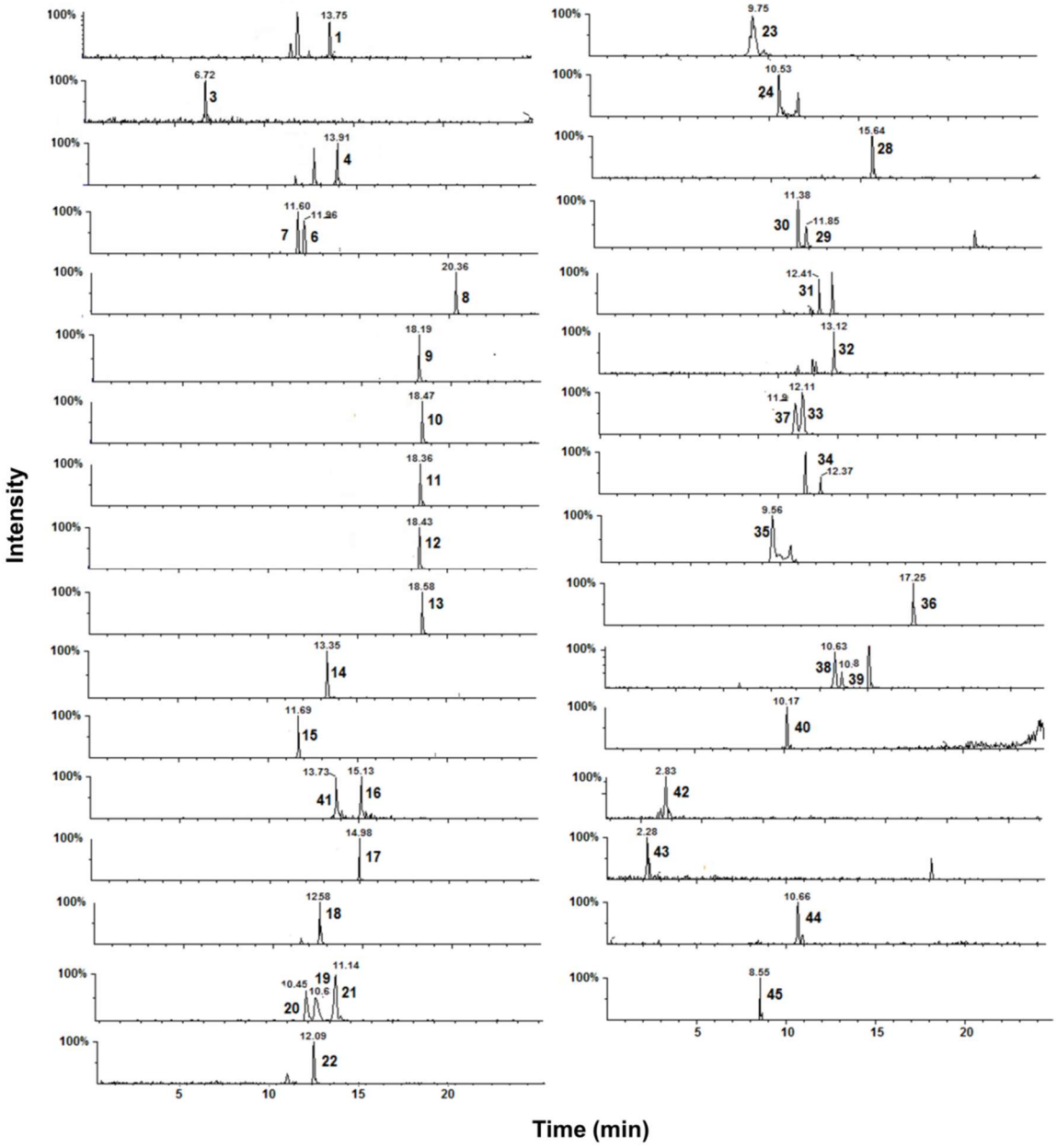

Figure 4.2 Isobaric compounds that also share fragmentation patterns as well as retention times were distinguished via specific MRMs. LC-MS/MS chromatograms of various HETEs after the injection of a 5-HETE standard at 500 ng/ml. Isobaric HETEs including 5-HETE (13), 8-HETE (12), 11-HETE (11), and, 12-HETE (10), were not resolved chromatographically, and they produced both common and selective fragments in MS/MS. The 319/301 transition was the most sensitive but was shared by all HETEs (a, c, e, g). In contrast, the less sensitive but more selective transitions of HETEs were used including 319/114.7 for 5-HETE (b), 319/154.8 for 8-HETE (d), 319/167.2 for 11-HETE (f) and 319/179 for 12-HETE (h).

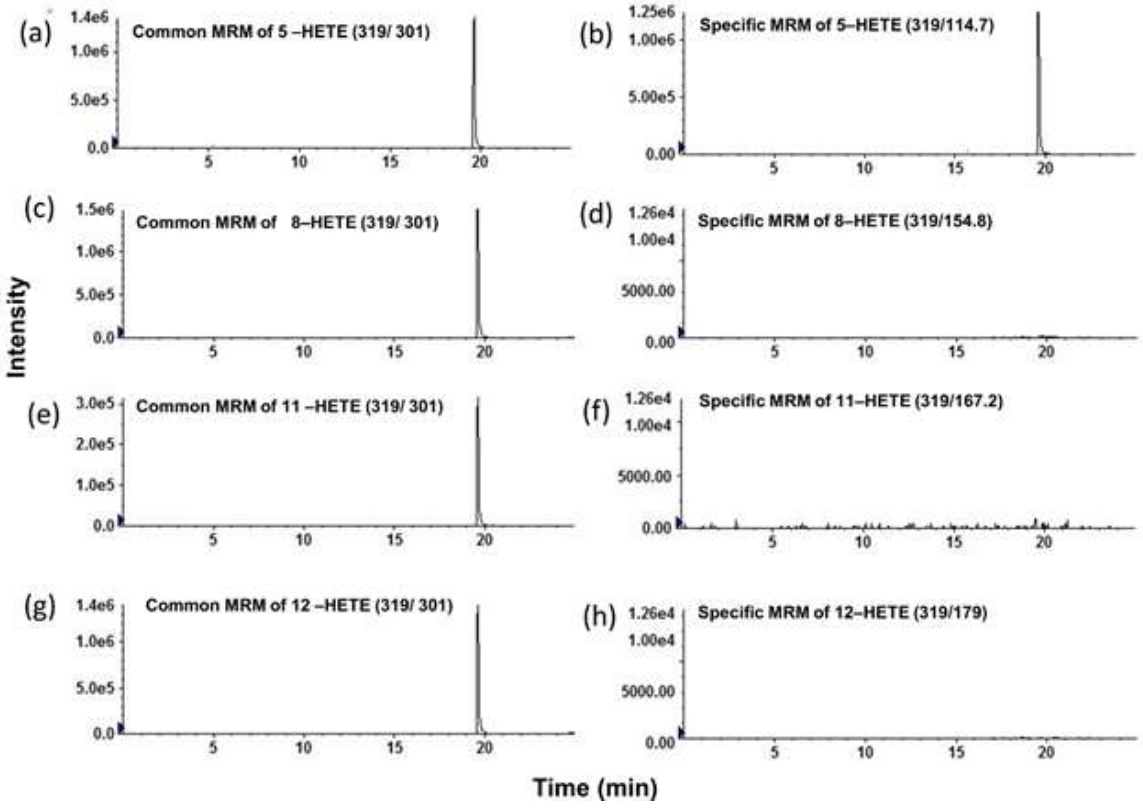

Figure 4.3 Isobaric and that undergo in-source fragmentation eicosanoids were separated chromatographically. (a) The isobaric compounds PGE2 (7), PGD2 (6), and 13, 14-dihydro-15-k-PGE2 (18) share the same MRM transition of 351→333 and had to be separated chromatographically (retention time (RT) = 11.58, 11.77, and, 12.5 min, respectively). (b) PGJ2 (333.1→315.2) and (c) 15-dexoxy-delta 12, 14-PGJ2 (315.2→271.2) have different precursor as well as fragment masses. However, PGJ2 produces an in-source fragment (315.2) with the same mass as the parent 15-dexoxy-delta 12, 14-PGJ2. Therefore, the two compounds had to be separated chromatographically.

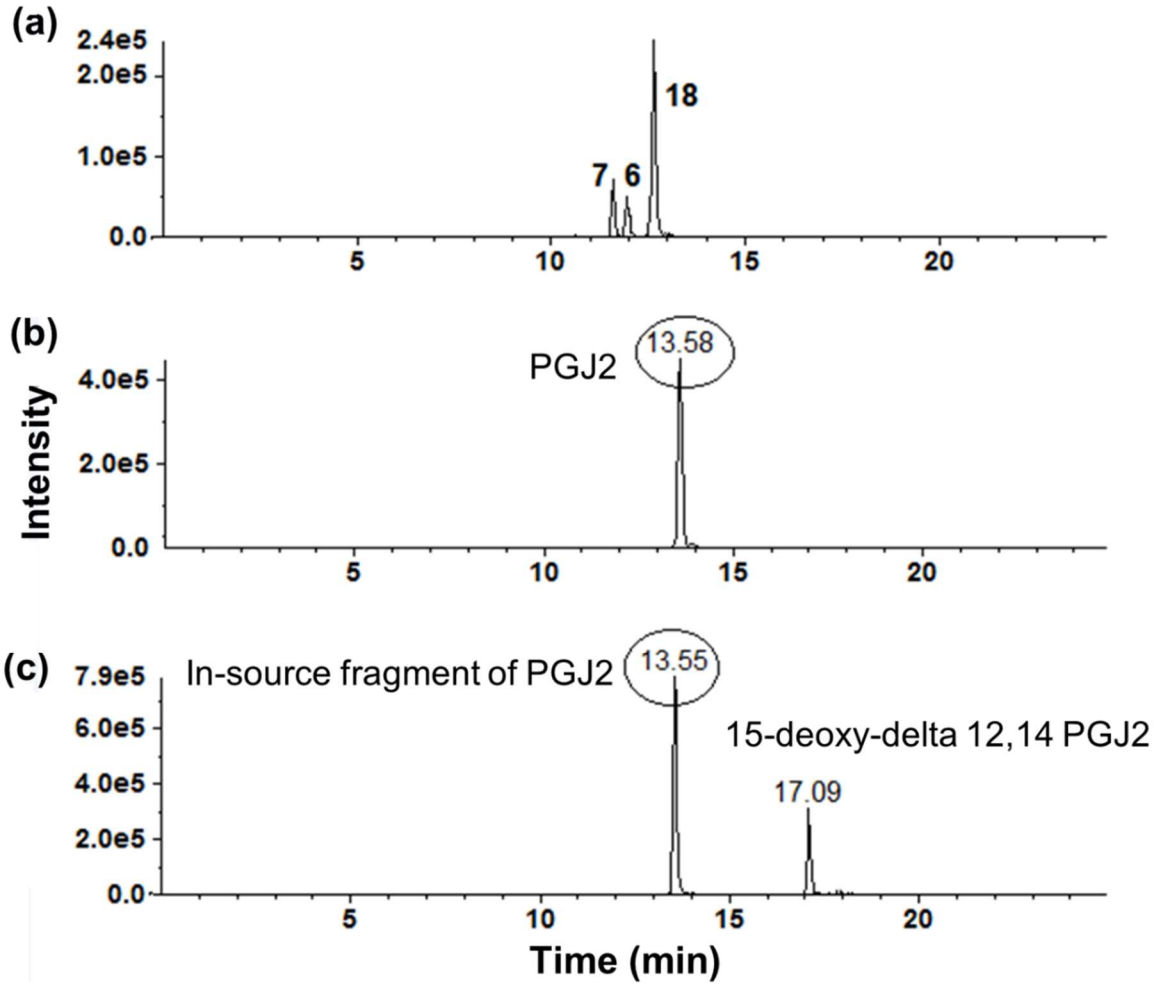

Table 4.1 Summary of SRM, precursor and product ions (Q1, Q3), internal standard (IS), declustering potential (DP), collision energy (CE), and retention time (RT) used for eicosanoids in negative ESI mode.

Analytes ID	Analytes	IS used	SRM (Q1/Q3)	DP	CE	RT
1	PGJ2	PGE2-d4	333.1/315.2	-60	-12	13.60
3	20-OH-PGE2	PGE2-d4	367.1/349.3	-58	-16	6.68
4	PGB2	PGE2-d4	333.0/235.0	-90	-28	13.85
6	PGD2	PGE2-d4	351.1/271.0	-60	-20	11.77
7	PGE2	PGE2-d4	351.1/271.0	-60	-20	11.39
8	AA	AA-d8	303.0/258.9	-75	-18	20.30
9	15-HETE	15-HETE-d8	319.0/175.1	-80	-20	18.10
10	12-HETE	15-HETE-d8	319.0/179.0	-80	-20	18.40
11	11-HETE	15-HETE-d8	319.0/167.2	-95	-22	18.30
12	8-HETE	15-HETE-d8	319.0/154.8	-80	-22	18.30
13	5-HETE	15-HETE-d8	319.0/114.7	-65	-20	18.50
14	LTE4	LTB4-d4	438.1/333.0	-70	-26	13.20
15	LTD4	LTB4-d4	495.1/176.8	-80	-28	11.50
16	LTC4	LTB4-d4	624.1/271.8	-110	-32	15.10
17	LTB4	LTB4-d4	335.0/194.8	-75	-22	14.90
18	13,14-DiOH-15-Keto-PGE2	PGE2-d4	351.0/333.0	-75	-20	12.50
19	11-B-PGF2α	PGE2-d4	353.2/309.1	-95	-28	10.50
20	8-iso-PGF2α	PGE2-d4	353.2/309.1	-95	-28	10.31
21	PGF2α	PGE2-d4	353.2/309.1	-95	-28	10.97
22	15-Keto-PGE2	PGE2-d4	349.0/331.1	-45	-14	12.00
23	6-Keto-PGF1α	PGE2-d4	369.0/163.0	-95	-38	8.89
24	TXB2	TXB2-d4	369.0/168.8	-75	-26	10.50
28	Ibuprofen	PGE2-d4	205.0/161.0	-30	-10	15.50
29	13,14-DiOH-PGF2α	PGE2-d4	355.0/311.3	-94	-34	11.80
30	PGF1α	PGE2-d4	355.0/311.3	-94	-34	11.23
31	13,14-DiOH-15-Keto-PGF2α	PGE2-d4	353.2/112.8	-102	-38	12.30
32	13,14-DiOH-15-Keto-PGE1	PGE2-d4	353.2/335.1	-47	-17	13.00
33	PGD1	PGE2-d4	353.2/317.1	-55	-18	12.00
34	13,14-DiOH-PGE1	PGE2-d4	355.2/337.1	-30	-20	12.3
35	TXB3	TXB2-d4	367.1/168.6	-90	-24	9.48
36	15-deoxy-delta 12,14 PGJ2	PGE2-d4	315.1/271.2	-40	-18	17.20
37	PGE1	PGE2-d4	353.2/317.1	-55	-18	11.77
38	PGE3	PGE2-d4	349.1/331.2	-30	-13	10.47
39	PGD3	PGE2-d4	349.1/331.2	-30	-13	10.77
40	PGF3α	PGE2-d4	351.2/307.0	-120	-26	10.07
41	14,15-LTC4	LTB4-d4	624.1/272.1	-50	-30	13.58
42	Tetranor-PGEM	PGE2-d4	327.1/309.1	-50	-15	2.49
43	Tetranor-PGFM	PGE2-d4	329.0/311.1	-50	-18	2.25
44	11-De TXB3	TXB2-d4	365.1/303.2	-100	-22	10.60
45	2,3 Dinor 8-iso PGF2	PGE2-d4	325.1/237.2	-50	-15	8.51
25	TXB2-d4	NA	373.1/172.8	-27	-22	10.45
26	PGE2-d4	NA	355.1/192.9	-46	-27	11.40

27	AA-d8	NA	311.0/267.1	-75	-20	20.20
46	15 -HETE-d8	NA	327.2/226.2	-60	-18	18.05
47	LTB4-d4	NA	339.1/197.1	-85	-10	14.80

NA: Not Applicable.

Table 4.2 Dynamic range, linearity, accuracy, and precision of eicosanoids in human serum.

Analytes ID	Dynamic Range (ng/mL)	LLOQ (0.2 ng/mL)		LQC (1ng/mL)		MQC (30ng/mL)		HQC (100ng/mL)		ULOQ (500ng/mL)	
		Accuracy	% RSD	Accuracy	% RSD	Accuracy	% RSD	Accuracy	% RSD	Accuracy	% RSD
1	0.2-500	111	9	95	15	90	1	98	4	112	4
4	0.2-500	101	10	98	4	91	3	92	4	90	3
6	0.2-500	99	14	101	10	94	3	94	4	94	4
7	0.2-500	109	12	94	6	101	2	104	3	113	2
14	0.2-500	104	10	88	9	92	6	94	5	114	3
17	0.2-500	110	8	105	11	97	5	99	6	115	5
18	0.2-500	110	8	87	3	85	1	87	9	100	2
20	0.2-500	99	6	103	9	92	3	97	4	97	1
21	0.2-500	105	9	101	13	99	4	109	4	115	1
22	0.2-500	103	13	88	7	91	6	103	5	116	1
24	0.2-500	94	11	109	3	100	1	99	1	106	1
28	0.2-500	106	12	92	13	91	4	95	2	103	4
29	0.2-500	104	12	100	10	103	5	108	3	108	3
30	0.2-500	105	8	101	11	96	2	101	2	108	2
31	0.2-500	90	11	90	10	93	5	89	6	85	1
32	0.2-500	103	7	86	5	86	3	86	5	115	3
33	0.2-500	103	11	97	11	96	3	97	8	93	3
34	0.2-500	107	14	79	6	88	3	85	5	90	3
35	0.2-500	93	12	92	9	100	3	103	11	96	10
36	0.2-500	110	9	96	14	88	3	90	2	114	3
37	0.2-500	105	15	90	5	94	4	99	3	98	1
38	0.2-500	105	13	94	8	90	3	97	1	104	3
39	0.2-500	96	14	103	5	95	4	95	6	107	2
44	0.2-500	103	5	102	7	102	4	100	2	112	2
45	0.2-500	96	13	105	10	90	1	94	3	113	2

Analytes ID	Dynamic Range (ng/mL)	LLOQ (1ng/mL)		LQC (3ng/mL)		MQC (30ng/mL)		HQC (100ng/mL)		ULOQ (500ng/mL)	
19	1-500	104	13	10.2	10	90	2	93	4	85	1
23	1-500	105	11	6.0	6	97	8	96	8	107	3
40	1-500	102	7	2.4	2	89	4	100	4	89	3
Analytes ID	Dynamic Range (ng/mL)	LLOQ (3ng/mL)		LQC (10ng/mL)		MQC (100 ng/mL)		HQC (350 ng/mL)		ULOQ (500ng/mL)	
9	3-500	115	4	4.7	5	115	4	103	3	100	5
10	3-500	110	10	6.5	6	115	3	105	7	99	6
11	3-500	112	6	5.4	5	107	3	103	7	102	5
12	3-500	97	15	6.2	6	114	7	106	9	99	5
13	3-500	110	12	7.4	7	105	5	98	5	94	4
43	3-500	95	12	11.6	12	105	9	110	11	106	12

Table 4.3 Unstable eicosanoids in different matrices under various storage conditions*.

Storage Condition	Auto sampler at 4 °C	Freeze-thaw three cycles at -20 °C	Bench top at room temperature			Long term stability at-20 ºC			Long term stability at-80 ºC
Matrix	Extracted Matrix	Original Matrix	Original Matrix		Extracted Matrix	Original Matrix	Extracted Matrix		Original Matrix
Time	up to 24 h	up to 3 cycles	up to 2 h	up to 8 h	up to 4 h	up to 180 days	up to 3 days	up to 7 days	up to 180 days
Stock solution	8 and 27	17 and 42	All stable	16 and 41	NA	16 and 41	NA	NA	16 and 41
Serum	8 and 27	3, 15, 16, 18, 33, 36, 41, 42, 43 and 44	3, 15, 16, 41, and 42	3,15, 16, 18, 22, 33, 39, 41, 42, 43, 27 and 44	All stable	15,16, 18, 22, 33, 36, 38, 41, 42, 43 and 44	15, 16	1, 14, 15, 16, 33, 34, and 41	NA

*Analytes with more than 20% loss by the reported time intervals under different storage conditions are presented.
NA: Not Applicable.

Table 4.4 Concentrations (ng/ml) of eicosanoids in serum (n=5), sputum (n =2), bronchial and alveolar fluids (n =5) of healthy human subjects.

Matrix		PGJ2	PGB2	PGD2	PGE2	15-HETE	12-HETE	11-HETE	8-HETE	5-HETE	LTE4	LTB4	PGF2α	13,14-DiOH-PGF2α	TXB2	TXB3
Serum	Mean	0.06	0.1	0.39	0.43	1.35	22	1.3	0.55	9.4	0.3	0.44	-	0.10	6.4	0.05
	SD	0.03	0.03	0.19	0.32	0.63	14	0.6	0.28	5.5	0.16	0.10	-	0.02	5.2	0.08
Sputum	Mean	-	-	-	0.09	1.05	2.13	0.29	0.27	2.71	-	0.72	0.04	-	0.23	-
	SD	-	-	-	0.01	0.09	0.3	0.03	0.01	0.27	-	0.65	0.0	-	0.01	-
Bronchial	Mean	-	-	-	-	0.43	0.32	0.24	0.18	0.48	-	0.09	0.04	-	-	-
fluid	SD	-	-	-	-	0.25	0.18	0.17	0.19	0.24	-	0.13	0.06	-	-	-
alveolar	Mean	-	-	-	-	-	-	-	-	0.18	-	0.1	0.08	-	-	-
fluid	SD	-	-	-	-	-	-	-	-	0.09	-	0.09	0.03	-	-	-

- not detected

Table S1. Dynamic range, linearity, accuracy, and precision of eicosanoids in human BALF.

Analytes ID	Dynamic Range (ng/mL)	LLOQ (0.2 ng/mL)		LQC (1ng/mL)		MQC (30ng/mL)		HQC (100ng/mL)		ULOQ (500ng/mL)	
		Accuracy	% RSD	Accuracy	% RSD	Accuracy	% RSD	Accuracy	% RSD	Accuracy	% RSD
1	0.2-500	93	18	102	15	104	4	113	7	107	5
3	0.2-500	114	5	113	4	106	5	108	3	90	4
4	0.2-500	107	15	98	5	103	4	97	3	95	5
6	0.2-500	95	8	96	11	103	2	101	2	107	6
7	0.2-500	96	9	94	13	97	8	89	6	86	4
14	0.2-500	97	8	85	10	94	6	92	3	96	2
17	0.2-500	101	10	93	5	103	2	100	4	104	4
18	0.2-500	98	6	100	12	104	4	95	2	86	5
19	0.2-500	93	10	97	7	104	3	96	3	95	4
20	0.2-500	97	7	99	8	99	4	92	3	86	4
21	0.2-500	98	15	105	8	110	3	91	2	91	5
22	0.2-500	112	7	97	9	98	3	91	3	97	5
23	0.2-500	111	4	105	3	100	2	94	1	97	1
24	0.2-500	109	13	107	8	115	3	114	6	106	4
28	0.2-500	113	13	100	7	97	2	91	2	85	3
29	0.2-500	104	15	94	6	99	3	92	3	91	5
30	0.2-500	109	6	105	7	110	2	92	4	70	4
31	0.2-500	103	9	86	3	88	4	93	4	108	6
32	0.2-500	103	5	92	6	96	4	88	4	85	2
33	0.2-500	111	5	89	3	102	3	96	1	86	5
34	0.2-500	100	4	94	14	94	1	90	1	101	2
35	0.2-500	107	17	92	8	95	3	107	5	115	4
36	0.2-500	110	6	98	4	103	4	97	2	85	3
37	0.2-500	92	9	99	5	104	3	107	4	109	5
38	0.2-500	105	12	105	7	101	6	110	4	115	1

39	0.2-500	103	13	100	7	99	3	102	3	109	4
40	0.2-500	110	15	102	13	95	2	99	3	113	2
44	0.2-500	92	12	98	6	95	2	90	3	107	3
45	0.2-500	93	18	102	15	104	4	113	7	107	5
	Dynamic Range	LLOQ (1ng/mL)		LQC (3ng/mL)		MQC (30ng/mL)		HQC (100ng/mL)		ULOQ (500ng/mL)	
9	1-500	90	7	112	9	109	6	94	5	85	6
10	1-500	93	14	115	2	112	3	98	2	85	7
11	1-500	95	8	106	10	101	5	115	8	114	4
12	1-500	93	11	103	6	104	5	120	5	109	7
13	1-500	106	9	108	5	97	8	114	8	115	4

Table S2. Dynamic range, linearity, accuracy, and precision of eicosanoids in human sputum.

Analytes ID	Dynamic Range (ng/mL)	LLOQ (0.2 ng/mL)		LQC (1ng/mL)		MQC (30ng/mL)		HQC (100ng/mL)		ULOQ (500ng/mL)	
		Accuracy	% RSD	Accuracy	% RSD	Accuracy	% RSD	Accuracy	% RSD	Accuracy	% RSD
1	0.2-500	95	15	108	5	100	3	103	1	94	3
3	0.2-500	112	12	111	4	96	3	95	3	87	5
4	0.2-500	103	10	101	6	93	5	95	3	95	4
6	0.2-500	113	6	103	6	92	2	96	2	107	1
7	0.2-500	95	12	97	11	93	4	92	2	107	3
17	0.2-500	112	8	100	4	89	3	93	2	109	3
18	0.2-500	92	27	103	15	104	3	102	2	88	3
19	0.2-500	109	6	110	5	99	2	97	3	99	3
20	0.2-500	111	5	106	5	96	2	98	2	102	3
21	0.2-500	115	9	94	6	85	3	105	6	112	4
22	0.2-500	112	11	100	12	97	3	98	1	111	2
23	0.2-500	93	9	112	3	96	11	92	1	96	2
24	0.2-500	112	16	98	4	100	4	94	3	106	2
28	0.2-500	106	4	102	11	97	1	97	3	99	3
29	0.2-500	102	5	98	3	94	2	97	2	107	2
30	0.2-500	95	9	105	5	101	3	96	2	85	1
31	0.2-500	100	10	87	4	87	3	92	1	110	3
32	0.2-500	114	5	102	7	93	6	94	3	94	4
33	0.2-500	112	2	100	2	99	3	100	2	93	4
34	0.2-500	92	80	90	6	102	12	99	2	112	2
35	0.2-500	115	3	103	2	96	2	97	1	91	2
37	0.2-500	111	7	101	6	93	2	96	1	106	2
38	0.2-500	111	10	100	4	100	12	98	3	104	1
39	0.2-500	95	9	98	5	99	3	104	2	106	1
40	0.2-500	99	7	98	11	96	10	98	2	110	1

44	0.2-500	99	10	93	4	93	1	92	2	115	4
45	0.2-500	95	15	108	5	100	3	103	1	94	3
	Dynamic Range (ng/mL)	LLOQ (1ng/mL)		LQC (3ng/mL)		MQC (30ng/mL)		HQC (100ng/mL)		ULOQ (500ng/mL)	
14	1-500	102	13	114	4	115	4	92	6	93	2
36	1-500	88	12	105	11	92	4	98	7	112	3
9	1-500	92	12	114	6	112	4	99	5	88	3
10	1-500	105	7	101	5	112	2	97	4	86	1
11	1-500	103	5	100	3	107	5	102	5	93	2
12	1-500	106	5	108	5	115	4	102	5	85	4
13	1-500	109	4	104	5	110	3	103	4	94	3

Table S3. Dynamic range, linearity, accuracy, and precision of eicosanoids in 10x diluted charcoal stripped serum.

Analytes ID	Dynamic Range (ng/mL)	LLOQ (0.2 ng/mL)		LQC (1ng/mL)		MQC (30ng/mL)		HQC (100ng/mL)		ULOQ (500ng/mL)	
		Accuracy	% RSD	Accuracy	% RSD	Accuracy	% RSD	Accuracy	% RSD	Accuracy	% RSD
1	0.2-500	89	11	90	6	93	3	103	4	107	5
4	0.2-500	105	14	100	4	103	4	98	3	87	3
6	0.2-500	93	11	101	9	98	4	100	4	101	3
7	0.2-500	106	6	99	3	101	2	104	3	111	3
14	0.2-500	105	6	95	10	85	3	107	6	110	10
17	0.2-500	109	9	100	8	93	3	94	3	108	3
18	0.2-500	93	12	96	6	96	2	100	3	115	3
20	0.2-500	98	9	94	8	100	4	97	3	98	3
21	0.2-500	95	15	91	10	98	2	99	4	103	4
22	0.2-500	103	9	89	4	92	3	100	2	109	4
24	0.2-500	96	12	101	3	100	2	100	1	106	1
28	0.2-500	104	8	85	8	99	3	100	2	106	4
29	0.2-500	93	9	94	11	102	3	99	5	103	3
30	0.2-500	110	9	99	4	96	3	97	2	105	4
31	0.2-500	102	13	115	3	103	2	96	3	78	8
32	0.2-500	106	10	89	3	94	2	103	3	113	5
33	0.2-500	104	10	104	7	96	6	102	3	89	6
34	0.2-500	99	9	94	4	100	4	101	2	96	3
35	0.2-500	105	12	89	14	95	3	95	2	107	2
36	0.2-500	106	9	94	11	87	7	101	9	95	4
37	0.2-500	107	5	96	6	98	3	100	3	97	3
38	0.2-500	113	11	97	6	93	2	96	1	107	1
39	0.2-500	113	9	104	6	94	5	102	3	111	3
44	0.2-500	100	10	93	8	94	4	97	2	107	3
45	0.2-500	102	10	98	8	99	2	101	2	115	2

	Dynamic Range (ng/mL)	LLOQ (1ng/mL)		LQC (3ng/mL)		MQC (30ng/mL)		HQC (100ng/mL)		ULOQ (500ng/mL)	
9	1-500	104	7	98	4	98	3	92	3	85	4
10	1-500	98	4	100	6	101	6	84	2	77	4
11	1-500	104	6	96	5	98	3	95	2	85	5
12	1-500	114	4	98	5	97	4	85	3	88	7
13	1-500	110	7	99	2	102	4	92	4	85	4
19	1-500	90	12	115	3	105	3	99	3	89	3
23	1-500	103	9	99	8	92	2	91	2	102	2
40	1-500	97	12	98	6	97	4	98	4	102	3

4.6 References

[1] D. Wang, R.N. DuBois, Measurement of Eicosanoids in Cancer Tissues, Methods in Enzymology, 2007, pp. 27-50.
[2] T. Shimizu, Lipid mediators in health and disease: Enzymes and receptors as therapeutic targets for the regulation of immunity and inflammation, Annual Review of Pharmacology and Toxicology, 2009, pp. 123-150.
[3] G.L. Milne, H. Yin, K.D. Hardy, S.S. Davies, L.J. Roberts, Isoprostane generation and function, Chemical Reviews, 111 (2011) 5973-5996.
[4] R.J. Roman, P-450 metabolites of arachidonic acid in the control of cardiovascular function, Physiological Reviews, 82 (2002) 131-185.
[5] L.M. Dong, X.O. Shu, Y.T. Gao, G. Milne, B.T. Ji, G. Yang, H.L. Li, N. Rothman, W. Zheng, W.H. Chow, C.C. Abnet, Urinary prostaglandin E2 metabolite and gastric cancer risk in the Shanghai women's health study, Cancer Epidemiology Biomarkers and Prevention, 18 (2009) 3075-3078.
[6] J.W. Eikelboom, J. Hirsh, J.I. Weitz, M. Johnston, Q. Yi, S. Yusuf, Aspirin-resistant thromboxane biosynthesis and the risk of myocardial infarction, stroke, or cardiovascular death in patients at high risk for cardiovascular events, Circulation, 105 (2002) 1650-1655.
[7] J.V. Gainer, A. Bellamine, E.P. Dawson, K.E. Womble, S.W. Grant, Y. Wang, L.A. Cupples, C.Y. Guo, S. Demissie, C.J. O'Donnell, N.J. Brown, M.R. Waterman, J.H. Capdevila, Functional variant of CYP4A11 20-hydroxyeicosatetraenoic acid synthase is associated with essential hypertension, Circulation, 111 (2005) 63-69.
[8] J.C. Johnson, C.R. Schmidt, M.J. Shrubsole, D.D. Billheimer, P.R. Joshi, J.D. Morrow, M.J. Heslin, M.K. Washington, R.M. Ness, W. Zheng, D.A. Schwartz, R.J. Coffey, R.D. Beauchamp, N.B. Merchant, Urine PGE-M: A Metabolite of Prostaglandin E2 as a Potential Biomarker of Advanced Colorectal Neoplasia, Clinical Gastroenterology and Hepatology, 4 (2006) 1358-1365.
[9] S.L.H. Ong, Y. Zhang, J.A. Whitworth, Reactive oxygen species and glucocorticoid-induced hypertension, Clinical and Experimental Pharmacology and Physiology, 35 (2008) 477-482.
[10] S. Jain, G. Chakraborty, R. Raja, S. Kale, G.C. Kundu, Prostaglandin E2 regulates tumor angiogenesis in prostate cancer, Cancer Research, 68 (2008) 7750-7759.
[11] A.H. Stephenson, A.J. Lonigro, T.M. Hyers, R.O. Webster, A.A. Fowler, Increased concentrations of leukotrienes in bronchoalveolar lavage fluid of patients with ARDS or at risk for ARDS, American Review of Respiratory Disease, 138 (1988) 714-719.
[12] J.W. Weiss, J.M. Drazen, E.R. McFadden Jr, P. Weller, E.J. Corey, R.A. Lewis, K.F. Austen, Airway constriction in normal humans produced by inhalation of leukotriene D. Potency, time course, and effect of aspirin therapy, Journal of the American Medical Association, 249 (1983) 2814-2817.
[13] N. Miyata, R.J. Roman, Role of 20-hydroxyeicosatetraenoic acid (20-HETE) in vascular system, Journal of Smooth Muscle Research, 41 (2005) 175-193.
[14] A.A. Spector, X. Fang, G.D. Snyder, N.L. Weintraub, Epoxyeicosatrienoic acids (EETs): Metabolism and biochemical function, Progress in Lipid Research, 43 (2004) 55-90.
[15] S. Virtue, M. Masoodi, B.A. de Weijer, M. van Eijk, C.Y. Mok, M. Eiden, M. Dale, A. Pirraco, M.J. Serlie, J.L. Griffin, A. Vidal-Puig, Prostaglandin profiling reveals a role for haematopoietic prostaglandin D synthase in adipose tissue macrophage polarisation in mice and humans, Int J Obes (Lond), 39 (2015) 1151-1160.

[16] J. Liu, T.I. Pestina, M.C. Berndt, S.A. Steward, C.W. Jackson, T.K. Gartner, The roles of ADP and TXA in botrocetin/VWF-induced aggregation of washed platelets, J Thromb Haemost, 2 (2004) 2213-2222.
[17] O. Aprikian, D. Reynaud, C. Pace-Asciak, P. Leone, F. Blancher, I. Monnard, C. Darimont, K. Mace, Neonatal dietary supplementation of arachidonic acid increases prostaglandin levels in adipose tissue but does not promote fat mass development in guinea pigs, Am J Physiol Regul Integr Comp Physiol, 293 (2007) R2006-2012.
[18] D. Tsikas, A.A. Zoerner, Analysis of eicosanoids by LC-MS/MS and GC-MS/MS: a historical retrospect and a discussion, J Chromatogr B Analyt Technol Biomed Life Sci, 964 (2014) 79-88.
[19] D.J. Carrier, T. Bogri, G.P. Cosentino, I. Guse, S. Rakhit, K. Singh, HPLC studies on leukotriene A4 obtained from the hydrolysis of its methyl ester, Prostaglandins Leukot Essent Fatty Acids, 34 (1988) 27-30.
[20] J. Huwyler, J. Gut, Single-step organic extraction of leukotrienes and related compounds and their simultaneous analysis by high-performance liquid chromatography, Anal Biochem, 188 (1990) 374-382.
[21] K.C. Lee, P.P. DeLuca, Simultaneous determination of prostaglandins E1, A1, and B1 by reversed-phase high-performance liquid chromatography for the kinetic studies of prostaglandin E1 in solution, J Chromatogr, 555 (1991) 73-80.
[22] C. Chavis, L. Fraissinet, P. Chanez, E. Thomas, J. Bousquet, A method for the measurement of plasma hydroxyeicosatetraenoic acid levels, Anal Biochem, 271 (1999) 105-108.
[23] A. Terragno, R. Rydzik, N.A. Terragno, High performance liquid chromatography and UV detection for the separation and quantitation of prostaglandins, Prostaglandins, 21 (1981) 101-112.
[24] F. Shono, K. Yokota, K. Horie, S. Yamamoto, K. Yamashita, K. Watanabe, H. Miyazaki, A heterologous enzyme immunoassay of prostaglandin E2 using a stable enzyme-labeled hapten mimic, Anal Biochem, 168 (1988) 284-291.
[25] A.S. Gandhi, D. Budac, T. Khayrullina, R. Staal, G. Chandrasena, Quantitative analysis of lipids: a higher-throughput LC-MS/MS-based method and its comparison to ELISA, Future Sci OA, 3 (2017) FSO157.
[26] H. Yue, K.I. Strauss, M.R. Borenstein, M.F. Barbe, L.J. Rossi, S.A. Jansen, Determination of bioactive eicosanoids in brain tissue by a sensitive reversed-phase liquid chromatographic method with fluorescence detection, J Chromatogr B Analyt Technol Biomed Life Sci, 803 (2004) 267-277.
[27] A. Aghazadeh-Habashi, W. Asghar, F. Jamali, Simultaneous determination of selected eicosanoids by reversed-phase HPLC method using fluorescence detection and application to rat and human plasma, and rat heart and kidney samples, J Pharm Biomed Anal, 110 (2015) 12-19.
[28] V.A. VanderNoot, M. VanRollins, Capillary Electrophoresis of Cytochrome P-450 Epoxygenase Metabolites of Arachidonic Acid. 1. Resolution of Regioisomers, Analytical Chemistry, 74 (2002) 5859-5865.
[29] T. Herrmann, D. Steinhilber, H.J. Roth, Determination of leukotriene B4 by high-performance liquid chromatography with electrochemical detection, Journal of Chromatography B: Biomedical Sciences and Applications, 416 (1987) 170-175.
[30] D. Tsikas, M.-T. Suchy, K. Tödter, J. Heeren, L. Scheja, Utilizing immunoaffinity chromatography (IAC) cross-reactivity in GC–MS/MS exemplified at the measurement of prostaglandin E1 in human plasma using prostaglandin E2-specific IAC columns, Journal of Chromatography B.

[31] J. Rivera, N. Ward, J. Hodgson, I.B. Puddey, J.R. Falck, K.D. Croft, Measurement of 20-hydroxyeicosatetraenoic acid in human urine by gas chromatography-mass spectrometry, Clin Chem, 50 (2004) 224-226.
[32] B. Watzer, S. Reinalter, H.W. Seyberth, H. Schweer, Determination of free and glucuronide conjugated 20-hydroxyarachidonic acid (20-HETE) in urine by gas chromatography/negative ion chemical ionization mass spectrometry, Prostaglandins Leukot Essent Fatty Acids, 62 (2000) 175-181.
[33] K. Nithipatikom, R.F. DiCamelli, S. Kohler, R.J. Gumina, J.R. Falck, W.B. Campbell, G.J. Gross, Determination of cytochrome P450 metabolites of arachidonic acid in coronary venous plasma during ischemia and reperfusion in dogs, Anal Biochem, 292 (2001) 115-124.
[34] M.S. Gachet, P. Rhyn, O.G. Bosch, B.B. Quednow, J. Gertsch, A quantitiative LC-MS/MS method for the measurement of arachidonic acid, prostanoids, endocannabinoids, N-acylethanolamines and steroids in human plasma, J Chromatogr B Analyt Technol Biomed Life Sci, 976-977 (2015) 6-18.
[35] Y. Wang, A.M. Armando, O. Quehenberger, C. Yan, E.A. Dennis, Comprehensive ultra-performance liquid chromatographic separation and mass spectrometric analysis of eicosanoid metabolites in human samples, J Chromatogr A, 1359 (2014) 60-69.
[36] K. Strassburg, A.M. Huijbrechts, K.A. Kortekaas, J.H. Lindeman, T.L. Pedersen, A. Dane, R. Berger, A. Brenkman, T. Hankemeier, J. van Duynhoven, E. Kalkhoven, J.W. Newman, R.J. Vreeken, Quantitative profiling of oxylipins through comprehensive LC-MS/MS analysis: application in cardiac surgery, Anal Bioanal Chem, 404 (2012) 1413-1426.
[37] A. Long, G. Zhong, Q. Li, N. Lin, X. Zhan, S. Lu, Y. Zhu, L. Jiang, L. Tan, Detection of 19 types of para-arachidonic acids in five types of plasma/serum by ultra performance liquid chromatography-tandem mass spectrometry, Int J Clin Exp Med, 8 (2015) 9248-9256.
[38] J. Fu, J.C. Schoeman, A.C. Harms, H.A. van Wietmarschen, R.J. Vreeken, R. Berger, B.V. Cuppen, F.P. Lafeber, J. van der Greef, T. Hankemeier, Metabolomics profiling of the free and total oxidised lipids in urine by LC-MS/MS: application in patients with rheumatoid arthritis, Anal Bioanal Chem, 408 (2016) 6307-6319.
[39] K. Sterz, G. Scherer, J. Ecker, A simple and robust UPLC-SRM/MS method to quantify urinary eicosanoids, J Lipid Res, 53 (2012) 1026-1036.
[40] J. Song, X. Liu, J. Wu, M.J. Meehan, J.M. Blevitt, P.C. Dorrestein, M.E. Milla, A highly efficient, high-throughput lipidomics platform for the quantitative detection of eicosanoids in human whole blood, Anal Biochem, 433 (2013) 181-188.
[41] M. Masoodi, A. Nicolaou, Lipidomic analysis of twenty-seven prostanoids and isoprostanes by liquid chromatography/electrospray tandem mass spectrometry, Rapid Commun Mass Spectrom, 20 (2006) 3023-3029.
[42] M. Puppolo, D. Varma, S.A. Jansen, A review of analytical methods for eicosanoids in brain tissue, J Chromatogr B Analyt Technol Biomed Life Sci, 964 (2014) 50-64.
[43] R. Yang, N. Chiang, S.F. Oh, C.N. Serhan, Metabolomics-lipidomics of eicosanoids and docosanoids generated by phagocytes, Curr Protoc Immunol, Chapter 14 (2011) Unit 14 26.
[44] L. Kortz, J. Dorow, U. Ceglarek, Liquid chromatography-tandem mass spectrometry for the analysis of eicosanoids and related lipids in human biological matrices: a review, J Chromatogr B Analyt Technol Biomed Life Sci, 964 (2014) 1-11.
[45] I. Willenberg, A.I. Ostermann, N.H. Schebb, Targeted metabolomics of the arachidonic acid cascade: current state and challenges of LC-MS analysis of oxylipins, Anal Bioanal Chem, 407 (2015) 2675-2683.

[46] C. Ferreiro-Vera, J.M. Mata-Granados, F. Priego-Capote, J.M. Quesada-Gomez, M.D. Luque de Castro, Automated targeting analysis of eicosanoid inflammation biomarkers in human serum and in the exometabolome of stem cells by SPE-LC-MS/MS, Anal Bioanal Chem, 399 (2011) 1093-1103.
[47] S. Medina, R. Dominguez-Perles, J.I. Gil, F. Ferreres, C. Garcia-Viguera, J.M. Martinez-Sanz, A. Gil-Izquierdo, A ultra-pressure liquid chromatography/triple quadrupole tandem mass spectrometry method for the analysis of 13 eicosanoids in human urine and quantitative 24 hour values in healthy volunteers in a controlled constant diet, Rapid Commun Mass Spectrom, 26 (2012) 1249-1257.
[48] A.J. Blewett, D. Varma, T. Gilles, J.R. Libonati, S.A. Jansen, Development and validation of a high-performance liquid chromatography-electrospray mass spectrometry method for the simultaneous determination of 23 eicosanoids, J Pharm Biomed Anal, 46 (2008) 653-662.
[49] H. Yue, S.A. Jansen, K.I. Strauss, M.R. Borenstein, M.F. Barbe, L.J. Rossi, E. Murphy, A liquid chromatography/mass spectrometric method for simultaneous analysis of arachidonic acid and its endogenous eicosanoid metabolites prostaglandins, dihydroxyeicosatrienoic acids, hydroxyeicosatetraenoic acids, and epoxyeicosatrienoic acids in rat brain tissue, J Pharm Biomed Anal, 43 (2007) 1122-1134.
[50] J.W. Lee, H.J. Mok, D.Y. Lee, S.C. Park, M.S. Ban, J. Choi, C.G. Park, Y.S. Ahn, K.P. Kim, H.D. Kim, UPLC-MS/MS-Based Profiling of Eicosanoids in RAW264.7 Cells Treated with Lipopolysaccharide, Int J Mol Sci, 17 (2016) 508.
[51] A. Furugen, H. Yamaguchi, N. Mano, Simultaneous quantification of leukotrienes and hydroxyeicosatetraenoic acids in cell culture medium using liquid chromatography/tandem mass spectrometry, Biomed Chromatogr, 29 (2015) 1084-1093.
[52] W. Jian, R.W. Edom, X. Xue, M.Q. Huang, A. Fourie, N. Weng, Quantitation of leukotriene B4 in human sputum as a biomarker using UPLC-MS/MS, Journal of Chromatography B: Analytical Technologies in the Biomedical and Life Sciences, 932 (2013) 59-65.
[53] J. Yang, J.P. Eiserich, C.E. Cross, B.M. Morrissey, B.D. Hammock, Metabolomic profiling of regulatory lipid mediators in sputum from adult cystic fibrosis patients, Free Radic Biol Med, 53 (2012) 160-171.
[54] J. Yang, K. Schmelzer, K. Georgi, B.D. Hammock, Quantitative profiling method for oxylipin metabolome by liquid chromatography electrospray ionization tandem mass spectrometry, Anal Chem, 81 (2009) 8085-8093.
[55] E. Hennessy, A. Rakovac Tisdall, N. Murphy, A. Carroll, D. O'Gorman, L. Breen, C. Clarke, M. Clynes, P. Dowling, S. Sreenan, Elevated 12-hydroxyeicosatetraenoic acid (12-HETE) levels in serum of individuals with newly diagnosed Type 1 diabetes, Diabet Med, 34 (2017) 292-294.
[56] J.P. Schuchardt, S. Schmidt, G. Kressel, H. Dong, I. Willenberg, B.D. Hammock, A. Hahn, N.H. Schebb, Comparison of free serum oxylipin concentrations in hyper- vs. normolipidemic men, Prostaglandins Leukot Essent Fatty Acids, 89 (2013) 19-29.
[57] R. Thakare, Y.S. Chhonker, N. Gautam, J.A. Alamoudi, Y. Alnouti, Quantitative analysis of endogenous compounds, J Pharm Biomed Anal, 128 (2016) 426-437.
[58] J.K. Prasain, A. Arabshahi, P.R. Taub, S. Sweeney, R. Moore, J.D. Sharer, S. Barnes, Simultaneous quantification of F2-isoprostanes and prostaglandins in human urine by liquid chromatography tandem-mass spectrometry, J Chromatogr B Analyt Technol Biomed Life Sci, 913-914 (2013) 161-168.
[59] R. Deems, M.W. Buczynski, R. Bowers-Gentry, R. Harkewicz, E.A. Dennis, Detection and Quantitation of Eicosanoids via High Performance Liquid Chromatography-Electrospray Ionization-Mass Spectrometry, in: H.A. Brown (Ed.) Methods in Enzymology, Academic Press2007, pp. 59-82.

[60] B.S. Levison, R. Zhang, Z. Wang, X. Fu, J.A. Didonato, S.L. Hazen, Quantification of fatty acid oxidation products using online high-performance liquid chromatography tandem mass spectrometry, Free Radical Biology and Medicine, 59 (2013) 2-13.
[61] S. Gouveia-Figueira, M.L. Nording, Validation of a tandem mass spectrometry method using combined extraction of 42 oxylipins and 15 endocannabinoid-related compounds including prostamides from biological matrices, Prostaglandins & other lipid mediators.
[62] P. Montuschi, S. Martello, M. Felli, C. Mondino, M. Chiarotti, Ion trap liquid chromatography/tandem mass spectrometry analysis of leukotriene B4 in exhaled breath condensate, Rapid communications in mass spectrometry : RCM, 18 (2004) 2723-2729.
[63] H. Idborg, S.C. Pawelzik, M. Perez-Manso, L. Bjork, J. Hamrin, E. Herlenius, P.J. Jakobsson, Evaluation of urinary prostaglandin E2 metabolite as a biomarker in infants with fever due to viral infection, Prostaglandins Leukot Essent Fatty Acids, 91 (2014) 269-275.
[64] I. Squellerio, B. Porro, P. Songia, F. Veglia, D. Caruso, E. Tremoli, V. Cavalca, Liquid chromatography-tandem mass spectrometry for simultaneous measurement of thromboxane B2 and 12(S)-hydroxyeicosatetraenoic acid in serum, J Pharm Biomed Anal, 96 (2014) 256-262.
[65] K.A. Massey, A. Nicolaou, Lipidomics of oxidized polyunsaturated fatty acids, Free Radic Biol Med, 59 (2013) 45-55.
[66] L. Kortz, J. Dorow, S. Becker, J. Thiery, U. Ceglarek, Fast liquid chromatography-quadrupole linear ion trap-mass spectrometry analysis of polyunsaturated fatty acids and eicosanoids in human plasma, Journal of chromatography. B, Analytical technologies in the biomedical and life sciences, 927 (2013) 209-213.
[67] Y. Yoshida, S. Kodai, S. Takemura, Y. Minamiyama, E. Niki, Simultaneous measurement of F2-isoprostane, hydroxyoctadecadienoic acid, hydroxyeicosatetraenoic acid, and hydroxycholesterols from physiological samples, Anal Biochem, 379 (2008) 105-115.
[68] Y. Zhang, G. Zhang, P.A. Clarke, J.T.J. Huang, E. Takahashi, D. Muirhead, R.C. Steenwyk, Z. Lin, Simultaneous and high-throughput quantitation of urinary tetranor PGDM and tetranor PGEM by online SPE-LC–MS/MS as inflammatory biomarkers, Journal of Mass Spectrometry, 46 (2011) 705-711.
[69] S. Ogawa, K. Tomaru, N. Matsumoto, S. Watanabe, T. Higashi, LC/ESI-MS/MS method for determination of salivary eicosapentaenoic acid concentration to arachidonic acid concentration ratio, Biomed Chromatogr, 30 (2016) 29-34.
[70] E.C. Kempen, P. Yang, E. Felix, T. Madden, R.A. Newman, Simultaneous quantification of arachidonic acid metabolites in cultured tumor cells using high-performance liquid chromatography/electrospray ionization tandem mass spectrometry, Anal Biochem, 297 (2001) 183-190.
[71] B. Gomolka, E. Siegert, K. Blossey, W.H. Schunck, M. Rothe, K.H. Weylandt, Analysis of omega-3 and omega-6 fatty acid-derived lipid metabolite formation in human and mouse blood samples, Prostaglandins Other Lipid Mediat, 94 (2011) 81-87.
[72] S. Gouveia-Figueira, M.L. Nording, Development and validation of a sensitive UPLC-ESI-MS/MS method for the simultaneous quantification of 15 endocannabinoids and related compounds in milk and other biofluids, Anal Chem, 86 (2014) 1186-1195.
[73] X. Zhang, N. Yang, D. Ai, Y. Zhu, Systematic metabolomic analysis of eicosanoids after omega-3 polyunsaturated fatty acid supplementation by a highly specific liquid chromatography-tandem mass spectrometry-based method, J Proteome Res, 14 (2015) 1843-1853.
[74] K.R. Maddipati, S.L. Zhou, Stability and analysis of eicosanoids and docosanoids in tissue culture media, Prostaglandins Other Lipid Mediat, 94 (2011) 59-72.